DANIEL GOMES COELHO

METALLIC ELEMENTS IN PLANTS: BIOACCUMULATION, PHYTOREMEDIATION POTENTIAL AND PHYSIOLOGICAL RESPONSES

Thesis presented to the Graduate Program in Plant Physiology as part of the requirements for the degree of *Doctor Scientiae* at Universidade Federal de Viçosa.

Adviser: Juraci Alves de Oliveira
Co-Advisers: Wagner Luiz Araújo
Fernanda dos Santos Farnese

VIÇOSA – MINAS GERAIS
2022

Ficha catalográfica elaborada pela Biblioteca Central da Universidade Federal de Viçosa - Campus Viçosa

T
C372m
2022

Coelho, Daniel Gomes, 1993-
Metallic elements in plants: bioaccumulation, phytoremediation potential and physiological responses / Daniel Gomes Coelho. – Viçosa, MG, 2022.
1 tese eletrônica (190 f.): il. (algumas color.).

Texto em inglês.
Orientador: Juraci Alves de Oliveira.
Tese (doutorado) - Universidade Federal de Viçosa, Departamento de Biologia Geral, 2022.
Inclui bibliografia.
DOI: https://doi.org/10.47328/ufvbbt.2022.515
Modo de acesso: World Wide Web.

1. Plantas aquáticas - Efeito da poluição. 2. Plantas aquáticas - Efeito dos metais pesados. 3. *Pistia stratiotes*. 4. Metais pesados. 5. Plantas aquáticas - Metabolismo. I. Oliveira, Juraci Alves de, 1965-. II. Universidade Federal de Viçosa. Departamento de Biologia Geral. Programa de Pós-Graduação em Fisiologia Vegetal. III. Título.

CDD 22. ed. 581.76

Bibliotecário(a) responsável: Alice Regina Pinto Pires CRB-6/2523

DANIEL GOMES COELHO

METALLIC ELEMENTS IN PLANTS: BIOACCUMULATION, PHYTOREMEDIATION POTENTIAL AND PHYSIOLOGICAL RESPONSES

Thesis presented to the Graduate Program in Plant Physiology as part of the requirements for the degree of *Doctor Scientiae* at Universidade Federal de Viçosa.

APPROVED: 20th July, 2022

Assent:

Daniel Gomes Coelho
Author

Juraci Alves de Oliveira
Adviser

Aos meus pais, por todo o amor e sacrifício,

Dedico.

ACKNOWLEDGEMENTS

To God, Lord of all things.

To the Universidade Federal de Viçosa, for the opportunity to become a member of a welcoming community, in this institution of recognized quality.

To the Postgraduate Program in Plant Physiology, for providing access to a course of excellence in the country.

This study was financed in part by the Coordenação de Aperfeiçoamento de Pessoal de Nível Superior - Brasil (CAPES) - Finance Code 001.

To the Conselho Nacional de Desenvolvimento Científico e Tecnológico (CNPq) for granting a scholarship.

À minha família, especialmente meus pais Agostinha e Geraldo e minha irmã, Natália, por todo o amor, compreensão por esses anos de ausência, de visitas corridas e despedidas tristonhas. Aos meus avós, tios e tias, por sempre torcerem e me apoiarem. Uma menção especial e saudosa ao meu tio e padrinho Raimundo Braga (*in memorian*) que sempre me incentivou e foi um exemplo de vida honrada.

À minha namorada e companheira Jéssica, por ser minha inspiração, minha amiga e minha incentivadora durante esses anos de distância, mas acima de tudo, de muito amor.

Aos familiares de Jéssica, Dona Neuma, Sr. Cláudio, Kyhara, Claudinho, Adriana, Natércia, Alana, Sandrinha e Alana, que sempre me recebem com todo carinho e se tornaram também a minha família.

Aos companheiros de República, queridos amigos que fiz em Viçosa: Bruno Codó, Ari e Bruno Nerso, por dividirmos mais que um teto e os boletos, como também as angústias, alegrias e muitas pizzas.

Aos amigos de uma vida, Jandelson, Gracinha, Rivânia, Valter, Juninho, Deoclecio, Francielho, Domingos e Moab, este último com quem tive a satisfação de continuar convivendo de perto durante o Doutorado.

Aos amigos do Laboratório de Biofísica Ambiental: Vinícius, Pedro, Letícia, Claúdio, Heloisa, Fernando, Angela, Laís, Darlielva, Dielle e Taline, pelo companheirismo, pelo entusiasmo pela ciência, pelo ambiente de trabalho incrível e, claro, pelos muitos e felizes momentos tomando um bom cafezinho.

Aos amigos Leo, Talita, Marcelle, Hugo, Marlon, Jonatas, Fred, Maria, Patrícia, Aline e Juliene, pela ajuda em momentos cruciais, pela inspiração como profissionais e pelos ótimos "rolês".

Aos amigos do futebol, pelas resenhas e pelas oportunidades de fazer raiva a eles jogando bola.

Aos amigos João Antônio, Jéssica, Paula, Dora, Marcelo, Jean, Sandy e Rita da UCP, pela parceria e acolhimento.

Aos amigos brasileiros na Alemanha, Toshik, Lauane, Renata, Vinícius e Amanda, por me fazerem sair um pouco da rotina de trabalho e pela oportunidade de conhecer lugares incríveis com eles.

To my friends Franz, Salome, Gabriel, Cordula, Ke, Marianna, Lena, Jan-Ole, Jan, Christopher, Sonja, Sophie, Dennis, Elias, and Betti from Münster and at the Plant Energy Biology Lab, which made my stay in Germany very fruitful and welcoming.

To Professor Markus Schwarzländer, who welcomed me and guided me through the development of the research together with his group and made me realize how exciting science can be.

To my Supervisor and friend, Professor Juraci Alves de Oliveira, for all the teachings, for the continuous encouragement and for all the efforts to make our projects and this thesis work possible, even sometimes in the midst of commitments and adversities.

To Professor Fabio DaMatta, one of the great names of Plant Physiology in our country, and with whom I had the honor of building a good friendship and sharing great moments of relaxation.

To my co-supervisors, Professor Fernanda Farnese and Professor Wagner Araújo, to whom I have great admiration, always helpful and providing valuable contributions during my training.

To Professor Rafael Miranda and Dr. Elias Feitosa Araújo, who, in addition to contributing substantially to this work and to my training, were also great supporters at important moments.

To the Professors of PPG Plant Physiology, great masters and scientific inspirations.

Thanks to everyone who somehow contributed to make this step possible.

ABSTRACT

COELHO, Daniel Gomes, D.Sc., Universidade Federal de Viçosa, July, 2022. **Metallic elements in plants: Bioaccumulation, phytoremediation potential and physiological responses.** Adviser: Juraci Alves de Oliveira. Co-advisers: Wagner Luiz Araújo and Fernanda dos Santos Farnese.

Pollution caused by metallic elements in the environment is becoming increasingly problematic worldwide. In the current work, several aspects of the metallic elements in plants were investigated, including the accumulation in species affected by an environmental disaster involving the disruption of a mining tailing dam; the physiological responses and phytoremediation potential of the aquatic macrophyte water lettuce (*Pistia stratiotes*) subjected to excess iron (Fe) and manganese (Mn), and combinations of Fe, Mn, and arsenic (As); and, finally, the *in vivo* monitoring of As-induced responses in *Arabidopsis thaliana* plants. We found a concerning enrichment of metal accumulation, especially for Fe and Mn, in the plant species evaluated in affected areas by mining tailings. Considering the spreading potential of contamination in aquatic environments, water lettuce plants, which are often used in phytoremediation studies, were tested for removal of excess Fe and Mn, along with the association with As. The plants displayed a great accumulation of Fe, mainly trapped in roots, whereas Mn was hyperaccumulated in shoots and roots. Accumulation of Mn was observed especially in the apoplast, avoiding major impairments of physiological processes. In presence of As, the plants displayed root loss as an acclimation response, followed by re-emission of the organs. Nonetheless, the specimens were able to maintain a high accumulation of the pollutants, supplied isolated or in association, demonstrating phytoremediation potential in multi-contaminated environments. Furthermore, the *in vivo* measurements using genetically-encoded biosensors showed intriguing stability of Mg-ATP^{2-} levels upon short-term arsenate (AsV) exposure. We also observed that the depletion of the GSH pool is the most likely cause of glutathione redox potential (E_{GSH}) oxidation. The findings presented here emphasize the importance of continuing to monitor metal-contaminated areas, as well as exposing alternatives for phytoremediation of aquatic environments and providing new insights into plant metabolism in response to pollutants.

Keywords: Aquatic plants – Pollution effect. Aquatic plants – Heavy metal effects. *Pistia stratiotes*. Heavy metals. Aquatic plants – Metabolism.

RESUMO

COELHO, Daniel Gomes, D.Sc., Universidade Federal de Viçosa, julho de 2022. **Elementos metálicos em plantas: Bioacumulação, potencial fitorremediador e respostas fisiológicas.** Orientador: Juraci Alves de Oliveira. Coorientadores: Wagner Luiz Araújo e Fernanda dos Santos Farnese.

A poluição causada por elementos metálicos tem se tornado uma problemática crescente ao redor do mundo. No presente trabalho, vários aspectos de elementos metálicos em plantas foram investigados, incluindo a acumulação em espécies afetadas pelo desastre ambiental envolvendo o rompimento de uma barragem de rejeitos de mineração; as respostas fisiológicas e o potencial de fitorremediação de alface d'água (*Pistia stratiotes*) submetida ao excesso de ferro (Fe), manganês (Mn) e às combinações de Fe, Mn e arsênio (As); bem como, o monitoramento *in vivo* das respostas induzidas por As em *Arabidopsis thaliana*. Nós observamos um preocupante enriquecimento do acúmulo de metais, especialmente para Fe e Mn nas áreas afetadas pelos rejeitos de mineração. Considerando o potencial de avanço da contaminação em ambientes aquáticos, plantas de alface d'água, as quais geralmente são usadas em estudos para fitorremediação, foram testadas na remoção do excesso de Fe e Mn, bem como na associação com As. Observou-se um acúmulo de Fe surpreendente, principalmente aprisionado na raiz, enquanto o Mn foi acumulado em elevadas concentrações tanto na raiz quanto na parte aérea. O acúmulo de Mn foi observado especialmente no apoplasto, evitando potenciais danos aos processos fisiológicos. Na presença de As, as plantas apresentaram perda de raízes como uma resposta de aclimatação, seguida de re-emissão dos órgãos. Apesar disso, os espécimes foram capazes de manter elevada acumulação dos poluentes, fornecidos de maneira isolada ou associada, demonstrando potencial para fitorremediação em ambientes com múltiplos contaminantes. Além disso, as análises *in vivo* usando biossensores mostraram estabilidade intrigante dos níveis de Mg-ATP^{2-} após exposição de curto prazo a arsenato (AsV). Nós também observamos que a depleção do pool de GSH é a causa mais provável da oxidação do potencial redox da glutationa (E_{GSH}). Os resultados apresentados aqui enfatizam a importância de continuar monitorando áreas contaminadas por metais, além de expor alternativas para fitorremediação de ambientes aquáticos e fornecem novos percepções sobre o metabolismo das plantas em resposta aos poluentes.

Palavras-chave: Plantas aquáticas – Efeito da poluição. Plantas aquáticas – Efeito dos metais pesados. *Pistia stratiotes*. Metais pesados. Plantas aquáticas – Metabolismo.

FIGURE LIST

CHAPTER 1

CHAPTER 2

CHAPTER 3

TABLE LIST

CHAPTER 1

CHAPTER 2

CHAPTER 3

CHAPTER 4

TABLE OF CONTENTS

1. INTRODUCTION

Environmental pollution has become a serious problem to be faced by the modern world, which has been exacerbated in the last years due to the accelerated industrialization (GAUTAM *et al.*, 2016). By definition, pollution occurs when an unwanted substance causes harm or deleterious effects or in processes by which natural or man-made resources become useless (RAMAKRISHNAN *et al.*, 2011). Among potential pollutants, metallic elements, such as arsenic (As), cadmium (Cd), lead (Pb), and mercury (Hg), have been included on the top of hazardous substances lists due to their adverse biological effects on living organisms, including serious problems caused to human health (BRIFFA; SINAGRA; BLUNDELL, 2020; FAY; MUMTAZ, 1996).

Other metallic elements, including iron (Fe) and manganese (Mn), are essential for the growth and development of most organisms. Nonetheless, toxicity may occur when concentrations exceed threshold levels (ARIF *et al.*, 2016; MUSZYŃSKA; LABUDDA, 2019). For instance, Fe overaccumulation has been pointed out as a risk factor for developing human diseases associated with ageing, such as atherosclerosis and Alzheimer's disease (BREWER, 2010), whereas excess Mn leads to reproductive and neurological disorders (BUDINGER *et al.*, 2021; ROELS *et al.*, 2012).

Although metallic elements are found naturally on the Earth's crust as mineral components of rocks, and therefore, several sites have a background of contamination, metal pollution has become prominent and widespread as a result of anthropogenic activity, due to metal mining, foundries, smelting, and other metal-based industries, and also leaching of metals from various sources (BRIFFA; SINAGRA; BLUNDELL, 2020).

Furthermore, contamination by metallic elements in Brazil in recent years has been exponentially magnified due to the failure of two iron ore tailings dams (QUARESMA *et al.*, 2021; VERGILIO *et al.*, 2020). These disasters caused irreparable losses, ranging from human lives to substantial environmental impacts, especially in the watersheds of the affected rivers, where the mud spread for hundreds of kilometers (GUERRA *et al.*, 2017; SEGURA *et al.*, 2016). The exposure of ecosystems to high concentrations of Fe and Mn in tailings, as well as the disturbance and solubilization of other pollutants in river sediments, such as arsenic (As) and chromium (Cr), are among the negative consequences of these events (QUADRA *et al.*, 2019). These effects were also observed in the first part of the current work, which looked at metal accumulation and enrichment in soil and plant species in areas affected by the Fundão dam disaster (COELHO *et al.*, 2020).

Faced with the global dilemma regarding metal pollution, it is imperative to deploy innovative, efficient and feasible methodologies to clean-up contaminated environments (KHALID *et al.*, 2017). All remediation technologies display shortcomings, including financial and technical limitations and complexity (LI *et al.*, 2019). Nevertheless, biological methods, including phytoremediation, which uses the natural capacity of some plant species to tolerate and accumulate high amounts of metals, have emerged as one of the most viable options to rectify and re-establish the natural condition of the environment (KHALID *et al.*, 2017). Phytoremediation is often applied as a sole or combined approach to clean up low-to-moderate levels of pollutants as an environmentally friendly and cost-effective technology (SABIR *et al.*, 2015). To achieve successful phytoremediation programs, the appropriate species must be chosen, as well as the appropriate conditions and mechanisms by which plants accumulate and tolerate high concentrations of the elements in the tissues. Therefore, in Chapters 2, 3, and 4, we investigated the phytoremediation potential and also physiological responses and tolerance mechanisms of water lettuce (*Pistia stratiotes* L.) to Fe and Mn, and the combination of these elements with As.

Because of the toxic effects, some plant species have evolved multiple defense mechanisms to control contaminant uptake and detoxification, allowing them to survive under high concentrations of metals in external medium and accumulate them into tissues and cells, which is a desirable trait for phytoremediation purposes (BOECHAT *et al.*, 2021). The toxicity induced by As, particularly, affects several aspects of plant metabolism, even at micromolar concentrations (NABI *et al.*, 2021). As a result, understanding the metabolism of this pollutant in the plant as well as the operation of the adjustments that induce tolerance are of great interest to provide subsidies to increase the efficiency of the phytoremediation process and for the biotechnological generation of more tolerant plants. Thus, in the last chapter of this Thesis, we provide new insights on arsenic toxicity on ATP and glutathione metabolism in plants.

2. Chapter 1 - Evaluation of heavy metals in soil and tissues of economic-interest plants grown in sites affected by the Fundão dam failure in Mariana, Brazil[1]

[1]Paper published on Integrated Environmental Assessment and Management – Volume 16, Issue 5, September 2020, pages 596-607 (https://doi.org/10.1002/ieam.4253https://doi.org/10.1002/ieam.4253)

Resumo

O objetivo deste estudo foi avaliar a concentração de elementos potencialmente tóxicos em plantas de *Brachiaria decumbens*, *Stylosanthes guianensis* e *Saccharum officinarum* e amostras de solos em áreas afetadas e não afetadas pelo rompimento da barragem de Fundão. As amostras foram coletadas em áreas afetadas por resíduos da barragem de Fundão (RAA1, RAA2, RAA3) e em uma área não afetada (controle). O material foi analisado quanto à composição de micronutrientes e elementos-traço no solo e plantas, além de fatores de contaminação (CF), bioacumulação e translocação (TF). No geral, os resultados mostraram que o solo e as plantas apresentaram maiores teores de Fe, Mn, Cu e Cr e menores teores de Zn nas áreas afetadas em comparação ao controle. Folhas e raízes de *B. decumbens* apresentaram aumento no teor de Fe nas áreas afetadas em relação ao controle, atingindo o valor máximo médio de 42.958 μg g^{-1} nas raízes de plantas coletadas em RAA2. Como resultado, CF para Fe de *B. decumbens* foi classificado como muito alto, mas com baixos valores de TF. Além disso, *B. decumbens* coletadas nas áreas afetadas apresentaram aumento de Fe, Mn, Cu e Cr nas folhas, caules e raízes, enquanto que em *S. guianensis* houve aumento da concentração de Fe em todos as partes das plantas e Cr nas folhas. *S. officinarum* também apresentou acúmulo de Mn no caule e Cu nas folhas e caule. Por outro lado, não há contaminação das plantas por elementos perigosos como Pb, Cd e As nas amostras analisadas. Concluindo, foram encontrados aumentos nos teores de Fe, Mn, Cu e Cr no solo e em vários tecidos vegetais, o que pode comprometer o crescimento das plantas e representar riscos potenciais decorrentes do processo de biomagnificação na cadeia alimentar.

Palavras-chave: Desastre de Mariana; Resíduos de Mineração de Ferro; Avaliação ambiental; Plantas forrageiras.

Abstract

The objective of this study was to evaluate the concentration of potentially toxic elements in *Brachiaria decumbens*, *Stylosanthes guianensis*, and *Saccharum officinarum* plants and soil samples in affected and unaffected areas by the rupture of the Fundão dam. Samples were collected in areas affected by residues from the Fundão dam (RAA1, RAA2, RAA3) and in an unaffected area (control). The material was analyzed for the composition of micronutrients and trace elements in soil and plants, as well as contamination (CF), accumulation and translocation factors (TF). Overall, the results showed that soil and plant tissues had increased Fe, Mn, Cu, and Cr content and decreased Zn content in the affected areas compared to the control. Leaves and roots of *B. decumbens* showed an increase in Fe content in affected areas compared to the control, reaching a mean maximum value of 42,958 μg g^{-1} of roots of RAA2 collected plants. As a result, CF for Fe of *B. decumbens* was classified as very high and they presented low TF values. Furthermore, *B. decumbens* collected in affected areas showed an increase of Fe, Mn, Cu and Cr in leaves, stems, and roots, while in *S. guianensis*, there was an increase of Fe concentration in all tissues and Cr in leaves. Also, *S. officinarum* showed the accumulation of Mn in the stem and Cu in the leaves and stems. On the other hand, there was no contamination of plants by hazardous elements such as Pb, Cd, and As in the samples analyzed. In conclusion, increases in the content of Fe, Mn, Cu, and Cr were found in soil and several plant tissues of residue-affected areas, which could compromise plant growth and represent potential hazards arising from the biomagnification process in the food chain.

Keywords: Mariana Disaster; Iron Ore Mining Waste; Environmental Assessment; Forage Plants.

2.1. Introduction

Mining activities can impact different ecosystems, leading to serious environmental damage (Pandey et al. 2016). Disruption of tailings dams, in particular, poses a threat to human health and constitutes a potential environmental hazard as the discharge reaches watercourses and areas hundreds of kilometres away from the mining area (Kossoff et al. 2014). Among the main impacts are the contamination of water, soil, animals, and plants by heavy metal(loid)s such as iron (Fe), cadmium (Cd), lead (Pb), arsenic (As), zinc (Zn), and manganese (Mn) (Sun et al. 2018).

The failure of the Fundão dam, from the mining complex operated by Samarco Mineração SA (the company in charge of the iron exploration in the area, formed by Vale and BHP Billiton), located in Minas Gerais State, represents the worst environmental disaster recorded in the history of Brazil up to that date. The catastrophe added 50 million cubic meters of mining tailings along 679,000 m of the Doce River and some of its tributaries (Omachi et al. 2018). Several studies have been conducted in order to identify the extent and magnitude of the collapse's effect on the quality of affected soils (Guerra et al. 2017) and water bodies (Hatje et al. 2017; Carvalho et al. 2018), on marine biodiversity (Magris et al. 2019), and benthic assemblages and estuarine sediments (Gomes et al. 2017). On the other hand, the impacts on plant species with potential economic interest and/or which are useful in recovery processes are not yet well documented.

The accumulation of potentially toxic elements in plants can be a limiting factor for the growth and development of the species and, therefore, the revegetation processes and reforestation programs ongoing in the affected sites (Prado et al. 2019). Furthermore, there is a risk of biomagnification after the entry of heavy metals into the food chain, leading to excessive consumption by humans and animals, which can cause significant clinical problems (Andrew et al. 2003; Blanc 2018). Analysis of the metal content of plant tissues used for animal and human consumption is therefore critical for the health of populations living in environments with some level of contamination (Peralta-Videa et al. 2009).

In general, the sites affected by the tailings, due to their topological and chemical characteristics, were used intensively as croplands and grazing lands. After the disaster, many areas were degraded, and it is recommended to suspend the use of affected soils for agropastoral purposes, due to the hazards for plants and, consequently, for animals (Aires et al. 2018). Some reports indicate that the mining residue of the Fundão dam is classified as non-hazardous and that the metal content in affected soils, called technosols, is below the threshold levels reported in Brazilian environmental legislation (Segura et al. 2016; Prado et al. 2019). However, trace

metals associated with Fe-oxyhydroxides and other potentially toxic elements present in the river sediments that were exposed to the surface have shown a potential risk for contamination and bioaccumulation over time (Queiroz et al. 2018; Silva et al. 2018). Our working hypothesis is that in the areas affected by the disaster there is some contamination of the soil by potentially toxic elements arising from the tailings and revolving of river sediments, which leads to an increase in the accumulation of these chemicals in plants cultivated in the impacted sites.

We believe the evaluation of heavy metal(loid) accumulation in soil and plants could provide important findings for the monitoring of contamination and land use recommendations of affected sites. The objective of this study was to evaluate the concentration of potentially toxic elements in *Brachiaria decumbens* Stapf and *Stylosanthes guianensis* (Aublet) Sw. which are widely used as forage plants, and *Saccharum officinarum* L., used for various purposes such as animal feed and alcohol and sugar production, on areas affected and unaffected by mining tailings from the Fundão dam.

2.2. Material and methods

Study area

The Fundão dam is located in Mariana, Minas Gerais, Brazil and has been exploited for Fe mining since the 1970s. The dam disruption (on November 5th, 2015, at 20°23.138'S, 43°44.306'W) took place in the Gualaxo do Norte River, a tributary of the Carmo River, which in turn debouches into the Doce River. The regional climate corresponds to type Cwa, according to the Köppen classification system, with an average annual temperature of 19.7 °C. The total annual rainfall is 1375 mm; the dry season is from April to September and the rainy season is from October to March (https://pt.climate-data.org/location/316464/https://pt.climate-data.org/location/316464/).

Soil and plant samples were collected in August 2018 (dry winter) in Paracatu de Baixo, near the Gualaxo do Norte River (Figure 1A).

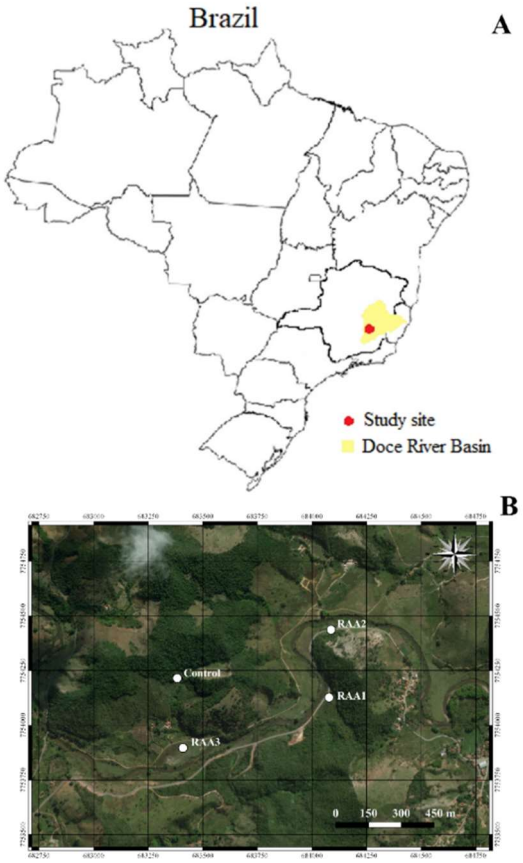

Figure 1. Map of Doce River Basin (A) and the residue affected-areas sampled (B); UTM Zone 23 K. RAA = residue-affected area; UTM = Universal Transverse Mercator.

The samples were collected in a site free of dam residue in the vicinity of the affected area (20°18.070'S, 43°14.625'W), named as the control. This site is used for the cultivation of pastures, fruit, and sugar cane. Also, sampling was made in three residue-affected areas (RAAs) under recovery, as described by Prado et al. (2019): RAA1 (20°18.114'S, 43°14.225'W), RAA2 (20°17.946'S, 43°14.222'W), and RAA3 (20°18.243'S, 43°14.608'W). RAA1 and RAA2 were areas used for crops and pastures, which were abandoned after the disaster and are in the process of reforestation, and RAA3 is still used for agropastoral purposes.

Sampling

Four composite soil samples (each composed of four sub-samples) were collected at a depth of 0–20 cm in a grid-like pattern across each area using an auger. Then, the material was packed into hermetically sealed plastic bags (at approximately 4 °C) and sent to the Viçosa Soil Analysis Laboratory (Viçosa, MG, Brazil), where the total and exchangeable fractions of

micronutrients (Fe, Mn, Cu, and Zn) and trace elements (Cr, As, Cd, and Pb) were determined. Also, routine chemical and some physical analyses (bulk density and particle density) were performed. For physical analyses, four samples were collected with a 100 cm^3 metallic cylinder in each area and transported to the Viçosa Soil Analysis Laboratory, where the soil was oven-dried at 105 °C to constant weight for further analyses.

The plant species sampled were *Brachiaria decumbens*, *Stylosanthes guianensis*, and *Saccharum officinarum*. *S. officinarum* was collected only in RAA1 and RAA3 because in RAA2 there was no cultivation (Figure 1B). The areas were divided into four quadrants (n = 4), and in each one four plants were collected per species, which constituted a composite replicate. Samples were collected from healthy plants with a height of approximately 0.3, 0.5, and 2.0 m for *B. decumbens*, *S. guianensis*, and *S. officinarum*, respectively. Sampling was performed on the third fully expanded leaf and the medial portion of stems and roots. After that, samples were acid-treated in plastic bags and transported to the laboratory, where samples were acid-washed in 0.01% HCl and thoroughly rinsed with deionized water. Following sterilization, the roots were treated with DBC (dithionite-citrate-carbonate) to remove adsorbed iron oxides (Taylor and Crowder 1983). Botanical identification of species was confirmed through specialized literature and by comparison in the VIC Herbarium (registration no. 11,762).

Determination of soil characteristics and element concentrations

The routine chemical analyses of soil were performed according to Defilipo and Ribeiro (1997) and the results are presented in Table 1. Total metal(loid)s were extracted from the soils after microwave-assisted triacid digestion (HCl + HNO_3 + HF; USEPA 1996), while exchangeable and soluble elements were extracted using the Mehlich-1 procedure (Defilipo and Ribeiro 1997). Element concentrations were determined by measuring absorbance in an atomic absorption spectrophotometer (model Spectra AA 220 FS, Varian Inc., Palo Alto, California, United States), which was coupled to a hydride vapor generator (model VGA 77, Agilent Technologies, Santa Clara, California, United States) for arsenic (As) determination. The bulk density (Db) was determined by the volumetric ring method, whereas the particle density (Dp) was assessed by the volumetric flask method (Reeve et al. 1973).

Plant analysis

Plant material was air-dried at room temperature for 48 h and placed into a conventional oven at 80 °C until reaching constant weight. The dried material was macerated and about 100 mg of the dry mass was mineralized in 1.5 mL of nitroperchloric mixture (2:1).

The extract was used in the determination of Fe, Mn, Cu, Cr, Zn, As, Cd, and Pb by atomic absorption spectrophotometry (model AA-6701F, Shimadzu Corporation, Tokyo, Japan). For arsenic determination, a hydride vapor generator (model HVG-1, Shimadzu Corporation, Tokyo, Japan) was used. The accuracy of the chemical analysis technique was assessed using certified reference materials *Lemna minor* (BCR-670), *Spinacia oleracea* (SRM 1570a) and Montana II Soil (SRM 2711a). Blanks and quality control standards were measured every tenth samples to detect contamination and drift. The results are within ± 5% of the certified values. The limits of detection (μg L^{-1}) are 6.0 (Fe); 2.0 (Mn); 1.0 (Zn); 2.0 (Cu); 5.0 (Cr); 2.0 (As); 0.7 (Cd); 2.0 (Pb).

Table 1. Physical-chemical characterization (n=4) of the residue-affected areas (RAA1, RAA2, RAA3) and non-affected site (control) by mining residues from Fundão dam. Means ± se followed by the same lowercase or uppercase letters do not differ by the Tukey's test ($p \leq 0.05$) or Kruskal-Wallis test ($p \leq 0.05$), respectively

Areas	Characteristics													
	pH		P		K		Ca^{2+}		Mg^{2+}		Al^{3+}		H +Al	
			mg dm^{-3}				$cmol_c\ dm^{-3}$							
Control	5.17 ± 0.02	c	0.90 ± 0.15	B	43.00 ± 3.05	A	1.43 ± 0.02	a	0.27 ± 0.01	A	0.36 ± 0.03	A	3.76 ± 0.06	a
RAA1	6.74 ± 0.03	ab	7.00 ± 0.15	a	32.00 ± 0.57	AB	1.51 ± 0.04	a	0.02 ± 0	C	0.00 ± 0	B	0.13 ± 0.06	b
RAA2	6.76 ± 0.02	a	6.40 ± 0.41	a	25.23 ± 0.51	BC	1.18 ± 0.03	b	0.01 ± 0.01	C	0.00 ± 0	B	0.06 ± 0.06	b
RAA3	6.64 ± 0.01	b	6.13 ± 0.37	a	24.30 ± 0.32	C	1.32 ± 0.08	ab	0.05 ± 0	B	0.00 ± 0	B	0.23 ± 0.03	b
	SB		CEC(t)		CEC(T)		V%		Db		Dp			
	$cmol_c\ dm^{-3}$								g cm^{-3}					
Control	1.81 ± 0.01	a	2.17 ± 0.03	A	5.58 ± 0.07	a	32.50 ± 0.33	b	1.65 ± 0.02	c	2.64 ± 0.01	B		
RAA1	1.54 ± 0.04	b	1.54 ± 0.04	b	1.67 ± 0.11	bc	92.52 ± 3.73	a	2.25 ± 0.02	ab	3.13 ± 0.02	A		
RAA2	1.21 ± 0.02	c	1.21 ± 0.02	c	1.28 ± 0.09	c	95.46 ± 4.53	a	2.11 ± 0.03	b	3.03 ± 0.03	AB		
RAA3	1.58 ± 0.09	ab	1.58 ± 0.09	b	1.82 ± 0.07	b	87.06 ± 0.07	a	2.34 ± 0.07	a	3.18 ± 0.10	A		

Extractors used: P, K = Mehlich1; Ca^{2+}, Mg^{2+} and Al^{3+} = KCl 1 mol L^{-1}; H+Al = Calcium acetate 0.5 mol L^{-1}; SB = Sum of exchangeable bases; CEC (t) = Effective cation exchange capacity; CEC (T) = Cation exchange capacity at pH 7.0; V = base saturation index; Db = bulk density; Dp = particle density. Means ± se followed by the same lowercase or uppercase letters do not differ by the Tukey's test ($p \leq 0.05$) or Kruskal-Wallis test ($p \leq 0.05$), respectively

Contamination, Bioconcentration, and Translocation Factors and Metal Accumulation Index (MAI)

The contamination factor (CF) was applied for soil and plant samples in order to evaluate the contamination of affected areas as follows: $c_f^i = \frac{c_{0\text{-}1}^i}{c_n^i}$, where c_f^i is CF, $c_{0\text{-}1}^i$ is the mean concentration of an element in the affected area, and c_n^i is the concentration of the element in the control area (Hakanson 1980).

The bioconcentration factor (BCF) was calculated by dividing the concentration of an element in the entire plant by the total concentration of the element in the soil ($[Element]_{plant}/[Element]_{soil}$; Zayed et al. 1998). The translocation factor (TF) was calculated by dividing the shoot (leaves + stems) concentration of an element by that in the roots ($[Element]_{shoot}/[Element]_{root}$; Bose and Bhattacharyya 2008).

The MAI was calculated according to Liu et al. (2007), defined as follows: $MAI = (1/N) \sum_{j=1}^{N} I_j$, where N = the total number of elements analyzed and $Ij = x/\delta x$ is the sub-index for variable j, obtained by dividing the mean value (x) of each element by its standard deviation (δx).

Statistical analysis

All statistical analyses were performed with R software, version 3.6.2 (R Development Core Team 2016). Data were examined using the Shapiro–Wilk test ($p > 0.05$) to check for normal distribution of the data and Bartlett's test ($p > 0.05$) to check for equal variances across samples. Where data failed on the Shapiro–Wilk test, a Box–Cox transformation [$T(Y) = (Y^{\lambda} - 1)/\lambda$] was performed to obtain the standard normal distribution data. The Box–Cox transformed data which passed the normality test ($p > 0.05$) together with non-transformed data were submitted to ANOVA, and means were compared using Tukey's test ($p \leq 0.05$). Nonparametric data (non-normal and/or non-homogeneous) were compared by the Kruskal–Wallis test ($p \leq 0.05$). The p-values for the normality, homogeneity, ANOVA, and mean tests, as well as the lambda values, are available in Supplementary Tables S1, S2, S3.

2.3. Results and discussion

Samples of soil and three plant species were collected in affected areas and one area free of tailings to assess the impacts of mining tailings from the Fundão collapse on potential plant contamination and phytotoxicity. The characterization of soil samples demonstrated that the affected areas present, among other characteristics, increased pH, P content, base saturation

and bulk and particle density, while the K, Mg, and exchangeable Al content were depleted (Table 1). From the point of view of soil quality for plant development, the major concern is the physical aspect, because the high soil density denotes compaction of these areas, compromising the growth of the roots to uptake water and nutrients. This factor has been considered the main limiting factor in reforestation programs in the impacted areas, coordinated by the company in charge of ore exploration and disaster mitigation actions (Prado et al., 2019).

The material was also analyzed for the composition of some micronutrients and trace elements in soil and plants, as well as contamination, bioaccumulation, and translocation factors.

RAAs presented increased potentially toxic elements in soils

The analysis of micronutrients and trace elements in soil samples showed increases in contents of exchangeable Fe in RAA1 and RAA2, as well as higher Mn, Cr and As contents in all of them, compared to control area (Table 2). Moreover, the concentrations of Fe in total fractions was increased by about 5- to 6-fold in the affected sites, reaching 44,726 mg kg^{-1} in RAA2 (Table 2). The increments of Fe and Mn concentrations found in RAAs are closely related to the composition of mining residue spilled by dam collapse since Fe and Mn (oxy)hydroxides rich ores, such as hematite are the major base of large-scale mining operations in the region (Hatje et al., 2017).

The increasing Fe and Mn contents in the affected areas is reflected in the calculation of the contamination factor, which was classified as considerable and moderate, respectively, in all RAAs (Supplementary Table S4). Despite this, only approximately 0.05% of the Fe present in the residue is found in the exchangeable fraction (Table 2), indicating a low potential to cause short term hazards. Consistently, Queiroz et al. (2018) has been reported high levels of total Fe, of which only a small fraction was available, in the Doce River estuary (Espírito Santo, Brazil). Nonetheless, continuous chemical and biological associated oxireduction processes can, over time, increase the bioavailability and bioaccumulation of the element, possibly leading to chronic contamination in a future scenario.

The results also showed higher accumulation of Cd in RAA2, As in RAA2 and RAA3, whereas Cu and Cr were increased in the total fraction of all analyzed RAAs, although the values of these elements were below the limits established by Brazilian legislation (Table 2; CONAMA 2009).

Table 2. Heavy metals contents (mg kg^{-1}) in soil samples of control (non-affected site) and three residue-affected areas (RAA1, RAA2, RAA3) by mining residues from Fundão dam

Area	Elements							
	Fe		Mn		Zn		Cu	
	EXC	TOT	EXC	TOT	EXC	TOT	EXC	TOT
Control	43.83 ± 3.30 b	7505.83 ± 107.40 D	34.02 ± 1.93 c	144.63 ± 16.45 b	1.40 ± 0.15 a	54.51 ± 4.34 a	1.27 ± 0.09 a	7.25 ± 0.24 b
RAA1	68.90 ± 3.48 a	37446.54 ± 188.71 B	51.55 ± 2.06 ab	264.31 ± 20.34 a	0.54 ± 0.12 b	17.68 ± 1.37 b	0.37 ± 0.01 b	15.96 ± 0.68 a
RAA2	66.55 ± 7.85 a	44726.91 ± 813.76 A	55.25 ± 2.34 a	287.60 ± 20.75 a	0.54 ± 0.02 b	18.99 ± 1.46 b	0.38 ± 0.03 b	17.97 ± 1.37 a
RAA3	62.65 ± 2.05 ab	34510.41 ± 1800.30 C	43.32 ± 1.34 b	214.50 ± 21.60 a	0.56 ± 0.03 b	23.49 ± 1.10 b	0.44 ± 0.00 b	17.08 ± 0.44 a
Thresholds[a]	-		-		300		60	
	Cr		Pb		Cd		As	
	EXC	TOT	EXC	TOT	EXC	TOT	EXC	TOT
Control	0.02 ± 0.01 b	3.21 ± 2.01 B	2.12 ± 0.24 A	12.42 ± 0.25 a	0.11 ± 0.03 a	0.98 ± 0.05 B	0.01 ± 0.00 b	0.25 ± 0.01 b
RAA1	0.24 ± 0.03 a	39.20 ± 10.94 A	0.54 ± 0.05 B	6.10 ± 0.20 b	0.14 ± 0.01 a	1.16 ± 0.06 AB	0.03 ± 0.01 a	0.34 ± 0.07 ab
RAA2	0.28 ± 0.03 a	41.10 ± 4.13 A	0.58 ± 0.04 B	5.12 ± 0.10 c	0.17 ± 0.01 a	1.28 ± 0.07 A	0.05 ± 0.01 a	0.49 ± 0.04 a
RAA3	0.22 ± 0.01 a	41.03 ± 1.59 A	0.67 ± 0.02 AB	5.26 ± 0.51 bc	0.19 ± 0.04 a	1.28 ± 0.09 A	0.05 ± 0.02 a	0.36 ± 0.03 ab
Thresholds[a]	75		72		1.3		15	

EXC = Exchangeable and soluble fraction extracted by Mehlich-1; TOT = Total concentration extracted by triacid digestion (HCl + HNO_3 + HF). Means ± se followed by the same lowercase or uppercase letters do not differ by the Tukey's test ($p \leq 0.05$) or Kruskal-Wallis test ($p \leq 0.05$), respectively; [a]Threshold values according to Brazilian legislation (CONAMA 2009

Table 3. Contents of Fe, Mn, Zn, Cu, Cr, Pb, Cd and As (µg g^{-1} DW) in leaves, stems, and roots and Contamination Factor (CF) of *Brachiaria decumbens* grown in control (non-affected site) and three residue-affected areas (RAA1, RAA2, RAA3) by mining residues from Fundão dam

		Elements									
	Areas	**Fe**		**Mn**		**Zn**		**Cu**		**Cr**	
Leaves	Control	369.89 ± 17.27	C	191.73 ± 26.40	b	32.00 ± 3.31	a	28.95 ± 1.83	b	2.37 ± 0.69	a
	RAA1	982.53 ± 97.95	B	188.40 ± 29.75	b	19.77 ± 1.41	b	21.11 ± 2.73	b	1.25 ± 0.36	a
	RAA2	1029.79 ± 64.74	B	373.69 ± 15.39	a	21.06 ± 1.10	b	32.15 ± 3.03	b	1.18 ± 0.46	a
	RAA3	1351.95 ± 25.63	A	101.80 ± 10.84	b	23.92 ± 2.02	ab	45.83 ± 2.82	a	0.57 ± 0.15	a
Stems	Control	343.97 ± 33.20	b	106.48 ± 7.72	c	105.66 ± 7.85	a	23.94 ± 1.79	b	11.44 ± 1.73	b
	RAA1	364.06 ± 36.05	b	141.89 ± 7.78	ab	22.53 ± 2.91	b	30.98 ± 2.41	b	35.39 ± 8.57	ab
	RAA2	768.08 ± 36.05	a	167.66 ± 7.04	a	27.01 ± 1.75	b	48.27 ± 4.32	a	43.46 ± 6.99	a
	RAA3	680.11 ± 77.33	a	122.43 ± 8.23	bc	41.23 ± 5.27	b	29.47 ± 2.51	b	50.82 ± 9.43	a
Roots	Control	2531.94 ± 267.30	C	59.55 ± 5.47	c	68.88 ± 4.52	a	22.39 ± 2.46	b	46.84 ± 3.10	b
	RAA1	23731.85 ± 3313.77	B	116.41 ± 10.58	b	53.07 ± 5.24	a	20.73 ± 2.26	b	42.61 ± 6.26	b
	RAA2	42958.97 ± 5436.32	A	151.07 ± 7.27	a	50.55 ± 3.67	a	57.91 ± 6.55	a	127.80 ± 16.25	a
	RAA3	37530.60 ± 1945.00	AB	112.67 ± 8.47	b	53.80 ± 4.66	a	66.25± 3.64	a	117.59 ± 7.73	a
CF	RAA1	7.73 (very high)		1.25 (moderate)		0.46 (low)		0.97 (low)		1.31 (moderate)	
	RAA2	13.79 (very high)		1.94 (moderate)		0.48 (low)		1.84 (moderate)		2.84 (moderate)	
	RAA3	12.19 (very high)		0.94 (low)		0.58 (low)		1.88 (moderate)		2.79 (moderate)	

Cd, Pb, and As were not detectable in the samples. Means ± se followed by the same lowercase or uppercase letters in each element and part of the plant do not differ by the Tukey's test ($p \leq 0.05$) or Kruskal-Wallis test ($p \leq 0.05$), respectively. CF Categories: $c_f^i < 1$ = low contamination factor; $1 \leq c_f^i < 3$ = moderate contamination factor; $3 \leq c_f^i < 6$ = considerable contamination factor; $6 \leq c_f^i$ = very high contamination factor

The study region belongs to the so-called Quadrilátero Ferrífero, a well-known mineral deposit exploited for Au, Fe and Al mining since the 17th century. Both the lithology, naturally enriched in metals, and mineral assemblages of Au and Fe ores are rich in potentially toxic elements, which have been deposited in river sediments over the years (Silva et al. 2018). Thus, the source of the increased concentration of Cu, Cr, Cd, and As may be the sediment revolving at the bottom of the river upon the arrival of the tailings, as reported by Gomes et al (2017). The CF evaluation demonstrated moderate ranges for Cu, Cd and As contamination, while Cr contamination was categorized as very high in both analyzed RAAs (Supplementary Table S4). Although the total Cr values found in the control area were low (Table 2), which contributed to the high CF in affected sites (Supplementary Table S4), this assessment raises some concern about the chemical quality of the soil, which may affect the establishment and development of plant species used in reforestation or for economic purposes.

On the other hand, exchangeable Zn, Cu, and Pb and total fraction of Zn and Pb contents were decreased in affected areas (Table 2). These data point to a dilution effect on the content of these elements caused by increments of other major elements of the tailings, such as Fe. Accordingly, the CF values for Zn and Pb were below 1.0 and were classified as low contamination factor (Supplementary Table S4). It is also noteworthy that the Pb content in control area was about 6-fold below those which there is a higher probability of adverse effects to biota (Table 2; CONAMA 2009).

Plants from impacted areas had higher concentrations of Fe, Mn, Cu and Cr

The impact of the mining tailings of the Fundão dam in plants is poorly studied. Some studies make floristic inventory post-catastrophe (Santos et al. 2019) or changes in land cover and use (Aires et al. 2018), indicating quantitative and/or qualitative losses in vegetation. However, analysis of the accumulation of potentially toxic elements in tailings-grown plants is incipient. Our data reveals that the elements accumulation of *Brachiaria decumbens* tissues (whole plant), follows the trend Fe > Mn > Zn > Cu > Cr, while in *Stylosanthes guianensis* and *Saccharum officinarum*, a similar pattern was found, except for the Zn and Cu positions, which were reversed (Tables 3, 4, 5). These results indicate that there are no major changes in the common pattern of accumulation of these micronutrients (Wang et al. 2018). On the other hand, regarding the background site (control), the plants collected in affected areas showed, in most cases, quantitative changes in the concentration of the elements, with greater accumulation of Fe, Mn, Cu, and Cr (Tables 3, 4, 5).

Table 4. Contents of Fe, Mn, Zn, Cu, Cr, Pb, Cd and As (μg g^{-1} DW) in leaves, stems, and roots and Contamination Factor (CF) of *Stylosanthes guianensis* grown in control (non-affected site) and three residue-affected areas (RAA1, RAA2, RAA3) by mining residues from Fundão dam

		Elements									
	Areas	**Fe**		**Mn**		**Zn**		**Cu**		**Cr**	
Leaves	Control	1124.94 ± 26.83	C	291.18 ± 20.49	a	151.64 ± 3.78	a	131.59 ± 5.16	B	1.72 ± 0.23	B
	RAA1	5014.07 ± 173.99	A	304.16 ± 17.09	a	126.97 ± 4.39	b	166.22 ± 4.46	AB	3.04 ± 0.62	AB
	RAA2	3634.46 ± 259.41	B	239.06 ± 14.85	a	112.97 ± 6.33	b	111.48 ± 5.26	AB	3.60 ± 0.79	A
	RAA3	4092.10 ± 334.00	AB	254.42 ± 20.85	a	124.45 ± 5.98	b	169.30 ± 7.88	A	3.43 ± 0.09	AB
Stems	Control	1282.12 ± 62.27	b	131.41 ± 7.38	b	143.55 ± 13.09	a	183.17 ± 6.57	a	7.79 ± 1.26	b
	RAA1	1241.51 ± 89.60	b	55.23 ± 2.73	c	77.26 ± 5.15	b	143.03 ± 7.53	b	15.81 ± 1.43	ab
	RAA2	1160.38 ± 47.37	b	202.53 ± 13.74	a	68.94 ± 3.31	b	161.92 ± 3.38	ab	18.56 ± 2.13	a
	RAA3	2042.50 ± 114.75	a	116.95 ± 10.77	b	96.43 ± 6.57	b	102.50 ± 5.88	c	14.10 ± 2.59	ab
Roots	Control	1412.64 ± 118.13	b	78.04 ± 6.73	a	62.10 ± 1.50	a	154.19 ± 7.09	ab	6.72 ± 1.17	b
	RAA1	3220.45 ± 373.27	a	31.49 ± 5.09	b	46.32 ± 2.91	b	135.27 ± 8.84	b	25.08 ± 2.97	a
	RAA2	2657.45 ± 221.82	a	29.74 ± 4.73	b	39.78 ± 2.67	b	143.35 ± 4.81	ab	19.76 ± 1.99	a
	RAA3	2968.91 ± 252.53	a	17.41 ± 1.83	b	45.25 ± 3.76	b	164.38 ± 1.75	a	35.80 ± 12.62	a
CF	RAA1	2.48 (moderate)		0.78 (low)		0.70 (low)		0.95 (low)		2.71 (moderate)	
	RAA2	1.95 (moderate)		0.94 (low)		0.62 (low)		0.89 (low)		2.58 (moderate)	
	RAA3	2.38 (moderate)		0.78 (low)		0.74 (low)		0.93 (low)		3.28 (considerable)	

Cd, Pb, and As were not detectable in the samples. Means ± se followed by the same lowercase or uppercase letters in each element and part of the plant do not differ by the Tukey's test ($p \leq 0.05$) or Kruskal-Wallis test ($p \leq 0.05$), respectively. CF Categories: $c_f^i < 1$ = low contamination factor; $1 \leq c_f^i < 3$ = moderate contamination factor; $3 \leq c_f^i < 6$ = considerable contamination factor; $6 \leq c_f^i$ = very high contamination factor

The majority of the plant samples collected at the affected sites showed high levels of Fe and Mn (Tables 3, 4, 5), as a result of increased concentration of these elements in the mining tailings of the Fundão dam (Table 2). Also, although RAA1, RAA2, and RAA3 have been affected by the same residue, the accumulation of elements in the plants varied among the sites. Leaves and roots of *B. decumbens* showed an increase in Fe content in affected areas compared to the control, reaching a mean maximum value of 42,958 μg g^{-1} of roots of plants collected from RAA2 (Table 3). Similarly, leaves and roots of *S. guianensis* also showed an increase in Fe content in affected areas, while the stems of plants collected from RAA3 showed increased Fe levels (Table 4). *B. decumbens* and *S. guianensis* leaves of plants collected in all RAAs reached the phytotoxicity range (Supplementary Table S5). Also, CF of *B. decumbens* was the only classified as very high (Table 3). Nevertheless, this value is classified using the sum of the entire plant and visual symptoms of phytotoxicity were not evidenced.

Also, there was a greater Mn accumulation in the stems of both *B. decumbens* and *S. guianensis* and in leaves of *B. decumbens* in RAA2-grown plants (Tables 3, 4). The thresholds for Mn toxicity in animals and plants are not well defined, but some reports show that plants can accumulate more than 300 μg g^{-1} without showing phytotoxic symptoms (Nazari et al. 2018). Moreover, the CF values for Mn are classified as moderate or even low (Table 3, 4, 5), and so, we consider that the values found in this study are not of concern.

Regarding Cu accumulation, *B. decumbens* leaves of plants collected in RAA3, stems and roots of RAA2 and roots of RAA3 showed a higher content than the control (Table 3), exceeding the normal concentration range (5–30 μg g^{-1}) of this element in the shoots of forage plants (Nouri and Haddioui 2016; Supplementary Table S5). Furthermore, the leaves of RAA1 and RAA3-grown *S. guianensis* also presented elevated contents of Cu (Table 4). It is noteworthy that the Cu values in all samples from shoots of *S. guianensis* and *S. officinarum* exceeded the normal range (Tables 4, 5 and Supplementary Table S5). Finally, the Fe content of *S. officinarum* leaves from RAA3 was 1.5 times higher than the control area. Also, Mn contents in stems of RAA1 and RAA3-grown plants was higher compared to the control (Table 5).

Fe, Mn, and Cu are involved in key metabolic processes in plants, such as enzyme cofactor of the electron transport chains, nitrogen fixation, and reversible redox reactions (Broadley et al. 2012).

Table 5. Contents of Fe, Mn, Zn, Cu, Cr, Pb, Cd and As (µg g^{-1} DW) in leaves, stems, and roots and Contamination Factor (CF) of *Saccharum officinarum* grown in control (non-affected site) and three residue-affected areas (RAA1, RAA2, RAA3) by mining residues from Fundão dam

		Elements									
	Areas	**Fe**		**Mn**		**Zn**		**Cu**		**Cr**	
Leaves	Control	343.75 ± 16.41	b	101.64 ± 14.57	a	31.54 ± 2.80	a	78.22 ± 1.28	b	0.20 ± 0.07	a
	RAA1	190.70 ± 16.18	c	136.16 ± 19.61	a	17.91 ± 1.74	b	84.16 ± 4.25	b	0.28 ± 0.10	a
	RAA3	479.06 ± 44.91	a	95.39 ± 17.16	a	10.36 ± 1.23	b	96.78 ± 2.17	a	0.22 ± 0.05	a
Stems	Control	122.54 ± 4.44	a	28.37 ± 4.04	B	30.10 ± 2.76	a	34.73 ± 3.91	b	1.04 ± 0.23	A
	RAA1	81.57 ± 9.29	b	136,13 ± 34.95	A	23.29 ± 2.84	a	36.42 ± 3.88	b	1.69 ± 0.37	A
	RAA3	95.38 ± 7.47	ab	112.79 ± 24.00	A	32.17 ± 0.80	a	65.65 ± 2.67	a	1.97 ± 1.14	A
Roots	Control	1372.28 ± 485.65	a	42.07 ± 12.19	a	56.55 ± 12.46	a	13.48 ± 2.30	a	2.72 ± 0.44	b
	RAA1	1694.96 ± 613.31	a	64.72 ± 18.76	a	45.80 ± 5.42	a	17.98 ± 3.07	a	7.06 ± 0.73	a
	RAA3	2111.20 ± 747.15	a	47.53± 6.57	a	45.24 ± 9.97	a	31.39 ± 7.69	a	3.58 ± 0.58	b
CF	RAA1	1.07 (moderate)		1.96 (moderate)		0.74 (low)		1.10 (moderate)		2.28 (moderate)	
	RAA3	1.46 (moderate)		1.49 (moderate)		0.74 (low)		1.53 (moderate)		1.46 (moderate)	

Cd, Pb, and As were not detectable in the samples. Means ± se followed by the same lowercase or uppercase letters in each element and part of the plant do not differ by the Tukey's test ($p \leq 0.05$) or Kruskal-Wallis test ($p \leq 0.05$), respectively. CF Categories: $c_f^i < 1$ = low contamination factor; $1 \leq c_f^i < 3$ = moderate contamination factor; $3 \leq c_f^i < 6$ = considerable contamination factor; $6 \leq c_f^i$ = very high contamination factor

However, high amounts of these elements cause phytotoxicity by nutritional imbalance, inactivation of enzymes, and consequent inhibition of the metabolic pathways and oxidative damage to proteins, lipids, and nucleic acids triggered by overproduction of reactive oxygen species (Singh et al. 2016). Moreover, accumulation of these elements in forage plants, as *B. decumbens* and *S. guianensis* promotes a potential biomagnification hazard through meat consumption for humans, in which excessive dietary intake of Fe and Mn may be related to neurobehavioral disorders (Hernández et al. 2011; Hare et al. 2017).

B. decumbens stems and roots collected in the RAA2 and RAA3, as well as *S. guianensis* leaves and stems of RAA2-grown plants and roots of all RAAs presented greater accumulation of Cr compared to the control (Tables 3, 4). The CF value for *S. guianensis* in RAA3 are classified as considerable (Table 4). For *S. officinarum*, only roots collected in RAA2 showed increased Cr accumulation (Table 5). Chromium (Cr) is a potentially toxic heavy metal which does not have any essential metabolic function in plants (Shahid et al. 2017). The bioavailability of Cr in soil can be affected by the presence of manganese oxides, which can act as Cr^{III} oxidants, promoting the formation of Cr^{VI}, a highly mobile form in soil and extremely toxic for mammals (Pan et al. 2017). Hence, the elevated concentration of manganese oxides in the areas affected by tailings (Table 2) may be changed the speciation and availability of naturally occurring chromium in the soil.

Unlike other, essential elements like Zn presented decreased in plants grown in affected sites (Tables 3, 4, 5), probably due to competition for uptake by transporters located on root cells (Zhao et al. 2011), in addition to lower Zn contents in soil samples from RAAs (Table 2), demonstrating that plants growing in tailings affected environments may be under some nutrients deficiency. For most species, the Zn content of leaves below 20 $\mu g\ g^{-1}$ of dry weight is considered insufficient (Hafeez et al. 2013), which was found for RAA2-grown B. *decumbens* (Table 3) and RAAs-grown *S. officinarum* (Table 5).

By analyzing the BCF of plants for Fe, Mn, and Cu, we observed that the highest values, in general, were found in the control areas (Table 6). This behavior is explained by the high concentration of these elements in the affected areas, which are not proportionally uptake and accumulated by the plants, in relation to the control area. For example, the concentration of Fe in *S. guianensis* was 2- to 3-fold higher in RAAs (Table 4), while the soil Fe content in these sites was about 6-fold higher compared to control (Table 2).

The overall accumulation of metals by plants, assessed by metal accumulation index (MAI), followed the trend *S. guianensis* > *B. decumbens* > *S. officinarum* (Table 6). This result

suggests that *S. guianensis* and *B. decumbens* has higher potential to accumulate the evaluated elements, which may be interesting for phytoremediation of contaminating sites. This prerogative is corroborated by a study with *B. decumbens*, in which it has been shown that these species can act efficiently in the phytoextraction of metals (Santos et al. 2006). Nonetheless, *B. decumbens* and *S. officinarum* showed increased MAI in RAAs, whereas it was decreased in *S. guianensis* (Table 6), indicating that the general increase of the accumulation of the elements in this last species was not as pronounced as in the others, in areas affected by the tailings.

Table 6. Translocation Factor (TF), Bioconcentration Factor (BCF), and Metal Index Accumulation (MAI) of *Brachiaria decumbens*, *Stylosanthes guianensis* and *Saccharum officinarum* grown in residue-affected areas (RAA1, RAA2, RAA3) and non-affected site (control) by mining residues from Fundão dam

		Fe		Mn		Zn		Cu		Cr	
Index	**Area**	***Brachiaria decumbens***									
TF	Control	0.29 ± 0.02	a	5.10 ± 0.46	A	2.01 ± 0.08	A	2.42 ± 0.17	a	0.29 ± 0.02	A
	RAA1	0.06 ± 0.01	b	2.84 ± 0.04	C	0.82 ± 0.12	C	2.59 ± 0.31	a	0.99 ± 0.33	A
	RAA2	0.04 ± 0.01	b	3.60 ± 0.14	B	0.96 ± 0.05	BC	1.43 ± 0.17	b	0.38 ± 0.08	A
	RAA3	0.05 ± 0.01	b	2.00 ± 0.07	B	1.22 ± 0.04	B	1.14 ± 0.04	b	0.44 ± 0.08	A
BCF	Control	0.43 ± 0.04	c	2.51 ± 0.19	a	3.80 ± 0.06	a	10.39 ± 0.67	a	36.21 ± 15.63	a
	RAA1	0.67 ± 0.09	bc	1.70 ± 0.16	b	5.49 ± 0.63	a	4.56 ± 0.21	c	2.40 ± 0.68	b
	RAA2	1.00 ± 0.12	ab	2.42 ± 0.09	a	5.28 ± 0.57	a	7.69 ± 0.44	b	4.24 ± 0.39	b
	RAA3	1.15 ± 0.07	a	1.60 ± 0.17	b	5.06 ± 0.29	a	8.30 ± 0.38	b	3.90 ± 0.46	b
MAI	Control	RAA1		RAA2		RAA3					
	26.74	28.46		30.08		28.04					
	Stylosanthes guianensis										
Index	**Area**	**Fe**		**Mn**		**Zn**		**Cu**		**Cr**	
TF	Control	1.75 ± 0.18	a	5.61 ± 0.79	b	4.75 ± 0.07	A	2.05 ± 0.10	a	1.61 ± 0.41	A
	RAA1	2.03 ± 0.27	a	12.34 ± 1.92	ab	4.49 ± 0.45	A	2.33 ± 0.23	a	0.76 ± 0.06	A
	RAA2	1.86 ± 0.24	a	16.43 ± 3.39	a	4.62 ± 0.26	A	1.91 ± 0.03	ab	1.15 ± 0.12	A
	RAA3	2.12 ± 0.21	a	22.04 ± 2.52	a	5.07 ± 0.78	A	1.65 ± 0.06	b	0.81 ± 0.34	A
BCF	Control	0.51 ± 0.01	a	3.56 ± 0.40	a	6.64 ± 0.52	b	64.84 ± 3.10	a	10.98 ± 5.61	a
	RAA1	0.25 ± 0.01	b	1.49 ± 0.11	b	14.31 ± 0.96	a	27.96 ± 1.33	b	1.22 ± 0.18	b
	RAA2	0.17 ± 0.01	c	1.66 ± 0.14	b	11.84 ± 1.07	a	23.47 ± 1.81	b	1.04 ± 0.12	b
	RAA3	0.27 ± 0.02	b	1.84 ± 0.16	b	11.40 ± 0.71	a	25.57 ± 0.87	b	1.19 ± 0.17	b
MAI	Control	RAA1		RAA2		RAA3					
	53.58	49.06		47.28		46.29					
	Saccharum officinarum										
Index	**Area**	**Fe**		**Mn**		**Zn**		**Cu**		**Cr**	
TF	Control	0.51 ± 0.17	a	3.91 ± 0.95	a	1.25 ± 0.25	a	9.00 ± 1.29	a	0.50 ± 0.10	a
	RAA1	0.24 ± 0.08	a	6.41 ± 2.83	a	0.95 ± 0.16	a	7.36 ± 1.42	a	0.31 ± 0.10	a
	RAA3	0.43 ± 0.17	a	4.66 ± 0.86	a	1.11 ± 0.26	a	6.23 ± 1.56	a	0.52 ± 0.23	a
BCF	Control	0.25 ± 0.07	A	1.22 ± 0.20	a	2.14 ± 0.17	b	17.44 ± 0.57	a	2.16 ± 0.79	a
	RAA1	0.05 ± 0.02	B	1.27 ± 0.04	a	5.00 ± 0.48	a	8.72 ± 0.54	c	0.27 ± 0.07	b
	RAA3	0.06 ± 0.02	B	0.88 ± 0.09	a	4.59 ± 0.34	a	10.82 ± 0.27	b	0.15 ± 0.06	b
MAI	Control	RAA1		RAA3							
	13.44	24.50		15.49							

Means ± se followed by the same lowercase or uppercase letters in each element and part of the plant do not differ by the Tukey's test ($p \leq 0.05$) or Kruskal-Wallis test ($p \leq 0.05$), respectively

Accumulation of elements in plant tissues differs by species

In addition to the fact that tailings-grown plants accumulated Fe, Mn, Cu, and Cr in their tissues, there was a tendency for greater metal accumulation in specific tissues, depending on the species. In general, *B. decumbens* accumulated mostly in the roots, as evidenced for lower TF values in RAAs, mainly Fe (Table 6), indicating a strategy of avoiding element translocation to the shoot or a poorly capacity to translocate it. Another factor that may have contributed in the case of Fe is the excessive accumulation in the roots, probably adsorbed to the cell wall. Grasses use a chelation-based strategy (also known as Strategy II) for Fe uptake, which complexes trivalent iron (Fe^{3+}) with phytosiderophores (PS) of mugineic acid family and the PS-Fe^{3+} complexes are subsequently transported into the root cells (Nozoye et al. 2011). As Fe in the tailing is predominantly in its trivalent state (Hatje et al. 2017), *B. decumbens* plants may have excessively adsorbed Fe and then excluded it out of the cell.

S. guianensis tended to accumulate greater amounts of metals in the leaves and therefore, showed elevated TF values (Tables 4, 6). Also, TF values for Cr were generally below 0.5 (Table 6), as expected limited translocation to the shoot is expected, irrespective of its available form (Usman et al. 2019). From the hazard perspective, the compartmentalization of potentially toxic elements in the roots minimizes biomagnification in the food chain, since leaves are the major tissues consumed. Regarding *Stylosanthes* sp., although the leaves accumulated higher concentrations of Fe in the three contaminated areas, this species has a lower rate of biomass production compared to grass plants (Zhang et al. 2010). Thus, lower exposure of herbivores is expected from the consumption of their leaves.

Cd, Pb and As were not detected in plant samples

Overall, mining activities have a major environmental impact and dam disruption is a huge aggravating factor. The presence of hazardous metal(loid)s is common in areas exposed to iron, tungsten, and other mining residues (Pistelli et al. 2017; Abad-Valle et al. 2018). The research by Cagnin et al. (2017) demonstrated that the Doce River Continental Shelf exhibited severe As enrichment and contamination before the dam collapse, attributed to long-term iron and gold exploitation in the Doce River watershed. However, no As, Pb, or Cd was detected in plants collected in the areas evaluated in the present study. Although this research refers to a specific region of the Doce River basin, this result indicates a low hazard from toxic elements for animals and humans using these plants cultivated in regions contaminated by residues from the rupture of the Fundão dam.

2.4. Conclusions

Soil and plants of economic interest collected in the areas affected by the Fundão dam rupture accumulated high levels of Fe, Mn, Cu and Cr, which may compromise the growth of plants through processes related to chemical availability of these elements, besides the elevated compaction of the technosol. Furthermore, overconsumption of these elements should be avoided as it is considered a risk factor for the development of neurodegenerative diseases, although they play important physiological roles in most organisms. Thus, the potential environmental hazards and human health risks due to the biomagnification process in the food chain cannot be disregarded, and continuous monitoring of heavy metal ecotoxicity, as well as the proposition of mitigation procedures, is still needed.

On the other hand, plant samples did not present extremely hazardous elements like As, Cd, and Pb in any of the sampled areas, demonstrating that agropastoral activities in the studied areas are not critical for the health of local populations and animals.

References

Abad-Valle P, Álvarez-Ayuso E, Murciego A, Muñoz-Centeno LM, Alonso-Rojo P, Villar-Alonso P. 2018. Arsenic distribution in a pasture area impacted by past mining activities. *Ecotoxicol Environ Saf* 147:228-237.

Aires URV, Santos BSM, Coelho CD, da Silva DD, Calijuri ML. 2018. Changes in land use and land cover as a result of the failure of a mining tailings dam in Mariana, MG, Brazil. *Land Use Policy* 70:63-70.

Andrew AS, Warren AJ, Barchowsky A, Temple KA, Klei L, Soucy NV, O'Hara KA, Hamilton JW. 2003. Genomic and proteomic profiling of responses to toxic metals in human lung cells. *Environ Health Perspect* 111:825-835.

Blanc PD. 2018. The early history of manganese and the recognition of its neurotoxicity, 1837–1936. *Neurotoxicology* 64:5-11.

Bose S, Bhattacharyya A. 2008. Heavy metal accumulation in wheat plant grown in soil amended with industrial sludge. *Chemosphere* 70:1264–1272.

Broadley M, Brown PIC, Rengel Z, Zhao F. 2012. Function of nutrients: micronutrients. In: Marschner P, editor. Marschner's mineral nutrition of higher plants. Amsterdam (NL): Elsevier. p 191–248.

Cagnin RC, Quaresma VS, Chaillou G, Franco T, Bastos AC. 2017. Arsenic enrichment in sediment on the eastern continental shelf of Brazil. *Sci Total Environ* 607:304-316.

Carvalho GO, Pinheiro AA, Sousa DM, Padilha JA, Souza JS, Galvão PM, Paiva TC, Freire AS, Santelli RE, Malm O, Torres JPM. 2018. Metals and arsenic in water supply for riverine communities affected by the largest environmental disaster in Brazil: the dam collapse on Doce River. *Orbital* 10:299-307.

CONAMA. 2009. Resolução No 420, de 28 de Dezembro de 2009. In: Brazilian National Environment Council (Ed.), Diário Oficial da União. Ministério do Meio Ambiente, Brasília, pp. 81–84.

Defilipo BV, Ribeiro AC. 1997. Análise química do solo - metodologia. SciELO Bras. 2 (26p).

FAO/WHO. 2001. Food additives and contaminants. Codex Alimentarius Commission. Joint FAO/WHO Food Standards Program, ALI-NORM 01/12A. p 1–289.

Gomes LEO, Correa LB, Sá F, Rodrigues-Neto R, Bernardino AF. 2017. The impacts of the Samarco mine tailing spill on the Rio Doce estuary, Eastern Brazil. *Mar Pollut Bull* 120:28-36.

Guerra MBB, Teaney BT, Mount BJ, Asunskis DJ, Jordan BT, Barker RJ, Santos EE, Schaefer CEGR. 2017. Post-catastrophe analysis of the Fundão tailings dam failure in the Doce River system, Southeast Brazil: Potentially toxic elements in affected soils. *Water Air Soil Pollut* 228:252.

Hakanson L. 1980. An ecological risk index for aquatic pollution control A sedimentological approach. *Water Res* 14:975– 1001.

Hare DJ, Cardoso BR, Raven EP, Double KL, Finkelstein DI, Szymlek-Gay EA, Biggs BA. 2017. Excessive early-life dietary exposure: a potential source of elevated brain iron and a risk factor for Parkinson's disease. *NPJ Parkinsons Dis* 3:1-5.

Hatje V, Pedreira RM, Rezende CE, Schettini CAF, Souza GC, Marin DC, Hackspacher PC. 2017. The environmental impacts of one of the largest tailing dam failures worldwide. *Sci Rep* 7:10706.

Hernández RB, Farina M, Espósito BP, Souza-Pinto NC, Barbosa Jr F, Suñol C. 2011. Mechanisms of manganese-induced neurotoxicity in primary neuronal cultures: the role of manganese speciation and cell type. *Toxicol Sci* 124:414-423.

Kossoff D, Dubbin WE, Alfredsson M, Edwards SJ, Macklin MG, Hudson-Edwards KA. 2014. Mine tailings dams: Characteristics, failure, environmental impacts, and remediation. *Appl Geochem* 51:229-245.

Liu YJ, Zhu YG, Ding H. 2007. Lead and cadmium in leaves of deciduous trees in Beijing, China: development of a metal accumulation index (MAI). *Environ Pollut* 145:387-390.

Magris RA, Marta-Almeida M, Monteiro JA, Ban NC. 2019. A modelling approach to assess the impact of land mining on marine biodiversity: Assessment in coastal catchments experiencing catastrophic events (SW Brazil). *Sci Total Environ* 659:828-840.

Nazari M, Zarinkamar F, Niknam V. 2018. Changes in primary and secondary metabolites of Mentha aquatica L. exposed to different concentrations of manganese. *Environ Sci Pollut Res Int* 25:7575-7588.

Nouri M, Haddioui A. 2016. Human and animal health risk assessment of metal contamination in soil and plants from Ait Ammar abandoned iron mine, Morocco. *Environ Monit Assess* 188:6.

Nozoye T, Nagasaka S, Kobayashi T, Takahashi M, Sato Y, Sato Y, Uozumi N, Nakanishi H, Nishizawa NK. 2011. Phytosiderophore efflux transporters are crucial for iron acquisition in graminaceous plants. *J Biol Chem* 286:5446-5454.

Omachi CY, Siani SM, Chagas FM, Mascagni ML, Cordeiro M, Garcia G, Thompson CC, Siegle E, Thompson FL. 2018. Atlantic Forest loss caused by the world´ s largest tailing dam collapse (Fundão Dam, Mariana, Brazil). *Remote Sens Appl Soc Environ* 12:30-34.

Pan C, Liu H, Catalano JG, Qian A, Wang Z, Giammar DE. 2017. Rates of Cr(VI) generation from $Cr_xFe_{1-x}(OH)_3$ solids upon reaction with manganese oxide. *Environ Sci Technol* 51:12416-12423.

Pandey B, Agrawal M, Singh S. 2016. Ecological risk assessment of soil contamination by trace elements around coal mining area. *J Soils Sediments* 16:159–168.

Peralta-Videa JR, Lopez ML, Narayan M, Saupe G, Gardea-Torresdey J. 2009. The biochemistry of environmental heavy metal uptake by plants: implications for the food chain. *Int J Biochem Cell Biol* 41:1665-1677.

Pistelli L, D'Angiolillo F, Morelli E, Basso B, Rosellini I, Posarelli M, Barbafieri M. 2017. Response of spontaneous plants from an ex-mining site of Elba island (Tuscany, Italy) to metal(loid) contamination. *Environ Sci Pollut Res*, 24:7809-7820.

Prado IGO, Silva, MCS, Prado DGO, Kemmelmeier K, Pedrosa BG, Silva CC, Kasuya MCM. 2019. Revegetation process increases the diversity of total and arbuscular mycorrhizal fungi in areas affected by the Fundão dam failure in Mariana, Brazil. *Appl Soil Ecol* 141:84-95.

Queiroz HM, Nóbrega GN, Ferreira TO, Almeida LS, Romero TB, Santaella ST, Bernardino AF, Otero XL. 2018. The Samarco mine tailing disaster: A possible time-bomb for heavy metals contamination?. *Sci Total Environ* 637:498-506.

R Core Team. 2016. R: A language and environment for statistical computing. R Foundation for Statistical Computing, Vienna, Austria. URL https://www.R-project.org/.

Reeve MJ, Smith PD, Thomasson J. 1973. The effect of density on water retention properties of field soils. *J Soil Sci* 24:355-367.

Santos FS, Hernández-Allica J, Becerril JM, Amaral-Sobrinho N, Mazur N, Garbisu C. 2006. Chelate-induced phytoextraction of metal polluted soils with *Brachiaria decumbens*. *Chemosphere* 65:43-50.

Santos OSH, Avellar FC, Alves M, Trindade RC, Menezes MB, Ferreira MC, Scotti MR. 2019. Understanding the environmental impact of a mine dam rupture in brazil: Prospects for remediation. *J Environ Qual* 48:439-449.

Segura FR, Nunes EA, Paniz FP, Paulelli ACC, Rodrigues GB, Braga GUL, Pedreira-Filho WR, Barbosa-Júnior F, Cerchiaro G, Ferreira-Silva F, Batista BL. 2016. Potential risks of the residue from Samarco's mine dam burst (Bento Rodrigues, Brazil). *Environ Pollut* 218:813-825.

Shahid M, Shamshad S, Rafiq M, Khalid S, Bibi I, Niazi NK, Dumat C, Rashid MI. 2017. Chromium speciation, bioavailability, uptake, toxicity and detoxification in soil-plant system: A review. *Chemosphere* 178:513-533.

Singh S, Parihar P, Singh R, Singh VP, Prasad SM. 2016. Heavy metal tolerance in plants: role of transcriptomics, proteomics, metabolomics, and ionomics. *Front Plant Sci* 6:1143.

Silva DC, Bellato CR, Marques Neto JDO, Fontes MP. 2018. Trace elements in river waters and sediments before and after a mining dam breach (Bento Rodrigues, Brazil). *Química Nova* 41:857-866.

Sun W, Ji B, Khoso SA, Tang H, Liu R, Wang L, Hu Y. 2018. An extensive review on restoration technologies for mining tailings. *Environ Sci Pollut Res Int* 25:33911–33925.

Taylor GJ, Crowder AA. 1983. Use of the DCB technique for extraction of hydrous iron oxides from roots of wetland plants. *Am J Bot* 70:1254–1257.

[USEPA] U.S. Environmental Protection Agency. 1996. EPA Method3050B (SW-846): Acid digestion of sediments, sludges, and soils: 1996. Cincinnati (OH).

Usman K, Al-Ghouti MA, Abu-Dieyeh MH. 2019. The assessment of cadmium, chromium, copper, and nickel tolerance and bioaccumulation by shrub plant Tetraena qataranse. *Sci Rep* 9:5658.

Wang R, Wang X, Jiang Y, Cerdà A, Yin J, Liu H, Feng X, Shi Z, Dijkstra FA, Li MH. 2018. Soil properties determine the elevational patterns of base cations and micronutrients in the plant–soil system up to the upper limits of trees and shrubs, *Biogeosciences* 15:1763–1774

Zayed A, Gowthaman S, Terry N. 1998. Phytoaccumulation of trace elements by wetland plants: I. Duckweed. *J Environ Qual* 27:715-721.

Zhang X, Xia H, Li Z, Zhuang P, Gao B. 2010. Potential of four forage grasses in remediation of Cd and Zn contaminated soils. *Bioresour Technol* 101:2063-2066.

Zhao AQ, Bao Q, Tian XH, Lu X, William JG. 2011. Combined effect of iron and zinc on micronutrient levels in wheat (*Triticum aestivum* L.). *J Environ Biol* 32:235-239.

3. Chapter 2 - Bioaccumulation and physiological traits qualify *Pistia stratiotes* as a suitable species for phytoremediation and bioindication of iron-contaminated water[1]

[1]Edited in accordance with *Ecological Indicators* guidelines

Abstract: Iron (Fe) is an essential element for almost all organisms. However, serious concerns have recently been raised regarding the association of Fe excess not only with neurodegenerative diseases in mammals but also with nutritional and oxidative disorders in plants. Therefore, the current study aimed to understand the physiological changes induced by Fe excess in *Pistia stratiotes*, a species often employed in phytoremediation studies. *P. stratiotes* were grown under controlled conditions and subjected to five concentrations of Fe: 0.038 (control), 1.0, 3.0, 5.0 and 7.0 mM. Neither alterations in net CO_2 assimilation rate and chlorophyll *a* fluorescence parameters, nor in the concentrations of the photosynthetic pigments were observed in Fe-treated plants. Yet, visual symptoms of Fe-toxicity such as bronzing of leaf edges in 5.0 and 7.0 mM-grown plants were observed after 5 days, which were related to lipid peroxidation, inducing protoplast retraction and breakdown of epidermal cells. In contrast, plants growing for 10 days in high Fe concentrations showed decreased chlorophyll concentrations and lower net CO_2 assimilation rate, as well as decreased apparent electron transport rate and effective quantum yield. Notwithstanding, *P. stratiotes* accumulated high amounts of Fe, especially in roots (about 10,000 μg g^{-1} in the highest concentration) and displayed a robust induction of the enzymatic antioxidant system. In conclusion, we demonstrated that *P. stratiotes* can be applied to clean up Fe-contaminated water, as the species displays high Fe bioaccumulation, mostly in root apoplasts, and can maintain physiological processes under Fe stress by activating compartmentalisation and antioxidant mechanisms. Our results further revealed that by monitoring visual symptoms, *P. stratiotes* could be applied for bioindication purposes.

Keywords: Iron toxicity, aquatic macrophyte, oxidative stress, water lettuce

3.1. Introduction

Iron (Fe) is an essential micronutrient that impacts several physiological and cellular processes in all plants. As a redox metal, Fe plays a major role as an electron acceptor/donor, being a cofactor for several metalloenzymes, including components of photosystem I, photosystem II and the cytochrome complex (Lindsay and Schwab, 1982; Varotto et al., 2002). It is also important in the biosynthetic pathways of DNA, hormones and chlorophyll, as well as in nitrogen fixation (Kryvoruchko et al., 2018; reviewed by Rout and Sahoo, 2015).

Typically, Fe is founded in two oxidation states, ferric (Fe^{+3}), which is most abundant in the environment, or ferrous (Fe^{+2}). Fe uptake in non-graminaceous plants is mediated by a reduction-based mechanism, in which Fe^{3+} is chelated in the apoplast by phenolic compounds, allowing the reduction of Fe^{3+}-chelate to Fe^{2+}, followed by the uptake into root epidermal cells through high-affinity transporter Iron-Regulated Transporter1 (IRT1) (Eide et al., 1996; Rai et al., 2021).

Despite its essentiality, excessive Fe availability in the rhizosphere is potentially harmful to plants, as its overload into the cell leads to reactive oxygen species (ROS) overproduction and nutritional imbalance, ultimately triggering metabolic impairments and cell death (Onaga et al., 2016). The physiological effects of excess Fe have been investigated in several crop plants, especially in rice growing in submerged soils, as reducing environments lead to the prevalence of soluble Fe^{2+} (Kirk et al., 2022; Pawar et al., 2021). Fe toxicity is responsible for the decrease in the productivity of many cereals and vegetables growing in submerged soils around the world, especially in Asia (Mahender et al., 2019). Similar reasoning for Fe toxicity in plants can be applied to mammal organisms, in which Fe plays an essential role, whereas its excess consumption has been pointed out as a risk factor for the development of ageing-related diseases, such as atherosclerosis and Alzheimer's disease (Brewer, 2010). Increased Fe concentration in soil and water bodies is observed because of anthropogenic activities, including agriculture and mining, and is therefore becoming a concerning situation in ecological, agricultural and public health aspects.

In Brazil, there is a particularly concerning situation of Fe environmental contamination due to the disasters involving the disruption of iron ore tailing dams in Brumadinho (2019) and Mariana (2015), both in Minas Gerais State. This disaster spilt out tonnes of oxides and hydroxides of Fe and Mn along the course of water bodies and soils (Quaresma et al., 2021; Vergilio et al., 2020). Therefore, it is imperative to deploy strategies

that could be used to mitigate the risks of Fe contamination, especially in water environments, considering the potential for magnification and the spread of contamination.

Among the approaches to remediate the contamination of water environments, phytoremediation using wetland species is considered an environmentally friendly, non-invasive and cost-effective technology to clean up or refine the decontamination process (Ansari et al., 2020; Khalid et al., 2017). In this scenario, studies with the macrophyte *Pistia stratiotes* suggest it as a promising species for phytoremediation, due to its fast growth dominating other aquatic plants (e.g. *Eichorrnia crassipes* and *Lemna gibba*), displaying high biomass accumulation, rapid reproduction and tolerance to pollutants (Farnese et al., 2014b; Skinner et al., 2007). Furthermore, *P. stratiotes* has been applied for phytoremediation purposes of several metallic elements, such as arsenic (Campos et al., 2019; Farnese et al., 2017), cadmium (Li et al., 2022), lead (S. Das et al., 2021), and chromium (M. Das et al., 2021), as well as organic pollutants (Ntakiyiruta et al., 2022).

Here, we investigated the potential for bioaccumulation and bioindication of Fe coupled with physiological and anatomical responses of *P. stratiotes*, aiming for its application in phytoremediation programmes. Our results demonstrate that Fe was mainly trapped in the apoplastic fraction of the roots, resulting in higher accumulation in the organs, besides preventing further damage to the shoots of *P. stratiotes*. We further observed that *P. stratiotes* can survive and maintain net photosynthetic rates even at high concentrations of Fe. Taken together, our results suggests that *P. stratiotes* can be successfully applied for phytoremediation purposes, as well as for bioindication of Fe-contaminated environments by monitoring visual and physiological responses.

3.2. Material and methods

Plant material and treatments

Specimens of *Pistia stratiotes* L. (Araceae), with approximately 10 g were collected in non-polluted dams at Universidade Federal de Viçosa, Viçosa, Brazil (20°45′25.0″ S 42°52′25.5″ W). Plants were washed and transferred to Clark's nutrient solution (Clark, 1975), pH 6.5, in a growth chamber for acclimatization with controlled temperature and light (25 ± 2 °C, 200 μmol m^{-2} s^{-1}, 12h/12h dark/light photoperiod). The nutrient solution was modified to contain (mM): 2.6 Ca,1.8 K, 0.6 Mg, 0.9 NH^4-N, 6.9 NO^3-N, 0.6 S, 0.069 P, 0.007 Mn, 0.019 B, 0.002 Zn, 0.0006 Mo, 0.0005 Cu and 0.038 Fe as sodium iron (Fe^{3+}) ethylenediaminetetraacetic acid (EDTA). After three days and under the same conditions,

uniform plants were transferred to individual pots in a completely randomized design, containing one of the following five treatments: control (only nutrient solution ½ ionic strength) or nutrient solution added of 1.0, 3.0, 5.0, and 7.0 mM of Fe-EDTA, with five repetitions per treatment. The concentrations used in the present study, from 0.038 to 7 mM, which are equivalent to concentrations up to 400 mg L^{-1}, were based on the Fe-toxic threshold reported for plants (Das et al., 2020; Pinto et al., 2016) and also in the concentrations found in Fe contaminated environments (Coelho et al., 2020).

The plants remained under treatments for five or ten days for further evaluation. At these time points, the biomass and photographic records were taken, in addition to the analysis of gas exchange and fluorescence of chlorophyll *a* and the sample harvesting for further analyses.

Symptomatology characterization

Before harvesting the plants, digital full HD photographs were obtained to perform a visual characterization of the toxicity symptoms. Additionally, the images were transferred to ImageJ software (v 1.52) to quantify the necrotic area of the leaves. The images were firstly converted to black and white particles using the binary function followed by the automatic calibration of the threshold values.

Growth and Fe bioaccumulation

The fresh weight of the plants was calculated prior to the experiment as well as five and ten days later. Plant shoots and roots were dried in an oven set at 60 ºC. The percentage of dry mass and the initial dry mass were calculated for the plant harvested at the 5^{th} and 10^{th} days. Following that, the relative growth rate was computed using the following Hoffmann and Poorter (2002).

$$\text{i) } RGR = \frac{(\ln W2 - \ln W1)}{(t2 - t1)}$$

where ln W1 and ln W2 are the means of the natural logarithm-transformed plant dry weights and t2 and t1 are the final and initial times (days).

The roots were previously washed with dithionite-citrate-carbonate solution (3 g of sodium dithionite, 40 mL of 0.3 M sodium citrate and 5 mL of 1 M sodium bicarbonate) to remove adsorbed Fe oxides (Taylor and Crowder, 1983). The resulting solution had its final volume adjusted to 100 mL with deionized water and the Fe concentration was quantified by

atomic absorption spectrometry (model AA-6701F, Shimadzu Corporation, Tokyo, Japan), using an iron standard for AAS (1000 mg L^{-1} Fe in nitric acid).

The dried plant material was homogenized and about 100 mg of the dry mass was mineralized in 1.5 mL of nitroperchloric mixture (2:1). The extract was used in the determination of Fe content by atomic absorption spectrophotometry.

The bioconcentration factor (BCF) was calculated considering the Fe concentration in plants (shoot + roots) and in the nutrient solution, whereas the translocation factor (TF) was calculated using the ratio between the concentration in shoots and roots, according to the following equations (Bao et al., 2009).

$$\text{i) BCF} = \frac{\text{Fe concentration in the plant } (\mu g\ g^{-1}\ DW)}{\text{Fe concentration in the nutrient solution } (mg\ L^{-1})}$$

$$\text{ii) TF} = \frac{\text{Fe concentration in shoots } (\mu g\ g^{-1} DW)}{\text{Fe concentration in shoots } (\mu g\ g^{-1} DW)}$$

The rhizofiltration potential (RP) for Fe were calculated according to the following equation (Veselý et al., 2011):

$$\text{iii) RP} = \left(\frac{C_{shoot} * M_{shoot}}{M_{total}} + \frac{C_{roots} * M_{roots}}{M_{total}}\right) * M_{plant}$$

Where: M_{shoot} and M_{roots} is the shoot and root dry biomass, (g), respectively; M_{total} is the total (shoot and roots) dry biomass (g); C_{shoot} and C_{roots} is the concentration of Mn in shoot and root ($\mu g\ g^{-1}$ DW), respectively; and M_{plant} is equal to 2919.75, the annual mean of *P. stratiotes* yield (g DW m^{-2} $year^{-1}$).

Anatomical characterization in light microscopy

To avoid the selection of necrosed tissues from 7 mM Fe-EDTA treatment, the effects of Fe in the plant anatomy were evaluated only in plants of control or 5 mM Fe-EDTA treatments, according to O'Brien and McCully (1981). Samples of the middle of the leaves (without necrotic spots) and from 2 cm of root tips were fixed in 2.5% glutaraldehyde and 4% paraformaldehyde in a sodium phosphate buffer 0.1 M (pH 7.0) for 48 h, and stored in 70% alcohol (Karnovsky, 1985). The samples were dehydrated in ethylic series and included in methacrylate (Historesin, Leica). The leaves were cross-sectioned (5 µm thick) in an automatic advance microtome (RM 2155, Leica Microsystems Inc, Deerfield, USA). The sections were stained with 0.05% Toluidine Blue, pH 6.5, for 30 s and assembled with Permount synthetic resin (Permount, Fisher). The images were obtained in a light microscope (model AX-70 TRF,

Olympus Optical, Tokyo, Japan) coupled with a digital camera (model AxioCam HRc, Zeiss, Göttinger, Germany) and a microcomputer equipped with the software Axio Vision.

Histochemical detection of Fe

To detect the presence of Fe in tissues, after sample fixation in Karnovsky, cross sections were obtained using a table microtome (model LPC, Rolemberg and Bhering). After washing with demineralized water, the sections were incubated for 48 h in a solution containing 4% potassium ferricyanide and 4% hydrochloric acid (Silva et al., 2006). Then, the sections were washed and mounted in 50% glycerinated water and observed under a microscope Olympus (model AX-70 TRF, Olympus Optical, Tokyo, Japan) equipped with the software Axio Vision. The reaction was considered positive in the regions of the sections that presented blue staining.

Gas exchange, and fluorescence of chlorophyll *a* and photosynthetic pigments

Gas exchange and fluorescence of chlorophyll *a* measurements were performed using an open-flow infrared gas exchange analyzer system (LI-6400XT; LI-COR) equipped with an integrated fluorescence chamber (LI-6400-40; LI-COR). The light-saturated net CO_2 assimilation rate (A), internal CO_2 concentration (Ci), stomatal conductance (g_s), and transpiration rate (E) were measured on attached, fully expanded leaves between 8:00 and 11:00 a.m. using a 2 cm^2 leaf chamber at 25 °C, a flow rate of 300 mol s^{-1}, a 0.5 stomatal ratio (amphistomatic leaves), under saturating light at leaf level (1000 µmol photons m^{-2} s^{-1}; 10% blue light) and 400 µmol CO_2 mol^{-1} air.

Simultaneously, the transient fluorescence (F_s) was obtained in actinic light (1000 µmol photon m^{-2} s^{-1}) acclimated leaves, followed by a saturating light pulse to estimate the maximal fluorescence (Fm'). Finally, the actinic light was switched off, and far-red illumination was applied (around 2 µmol photons m^{-2} s^{-1}) to measure the light-adapted initial fluorescence (F_0'). These parameters were used to estimate the actual PSII photochemical efficiency (Φ_{PSII}), the linear electron transport rate (ETR) and the non-photochemical quenching (NPQ), according to Genty et al. (1989). The ratio F_0/F_m was also determined, as suggested by Banks (2018).

The minimal fluorescence (F_0) was obtained in dark-acclimated leaves via the excitation with a modulated red light of low intensity (0.03 µmol photon m^{-2} s^{-1}), followed by application of saturation pulses (8000 µmol photons m^{-2} s^{-1}) to obtain maximum fluorescence (F_m). The potential quantum yield of the photosystem II was calculated (Fv/Fm) using the

variable fluorescence (F_v), determined by the difference between F_0 and F_m (Genty et al., 1989). Dark respiration (R_N) was measured before dawn using the infrared-gas analyzer mentioned above. The photorespiratory rate (P_R) and the electron flow to RuPB carboxylation (ETR_C) and oxygenation (ETR_O) were estimated using the following equations (Bai et al., 2008; Guan et al., 2004):

i) $P_R = 1/12\ [ETR - 4 \times (A + R_D)]$;

ii) $R_D = R_N \times Q_{10}^{(Td-Tn)/10}$ (with $Q_{10} = 2.2$, Td: leaf temperature; Tn: leaf temperature at dawn, R_N: dark respiration).

iii) $ETR_C = 1/3\ [ETR + 8 \times (A + R_D)]$;

iv) $ETR_O = 2/3\ [ETR - 4 \times (A + R_D)]$.

Photosynthetic pigments were extracted from three leaf discs (1 cm diameter). The discs were incubated in 2 mL of dimethylsulfoxide (DMSO) solution, in test tubes properly capped and covered with aluminium foil. After 24 hours, the tubes were incubated in a water bath at 65 °C for 45 minutes and the absorbances were taken at wavelengths 665, 649, and 480 nm. The readings obtained were used to estimate the contents of chlorophyll *a* and *b* and carotenoids, as proposed by Wellburn (1994).

Antioxidant enzyme activities

The sampling for the measurement of antioxidant enzymes, H_2O_2 and TBARS contents was performed in a pool of shoots or roots from control and 5 mM Fe-treated plants to better understand contrasting effects induced by Fe in the plants. The extract for determination of the activity of ROS scavenging enzymes was obtained by the homogenization of 20 mg freeze-dried tissues in a ball mill for 4 min at 27 Hz. To the samples, were added 0.02 g polyvinylpyrrolidone (PVPP) and 1.8 mL of the extraction buffer containing 0.1 M potassium phosphate buffer pH = 6.8, 0.1 mM EDTA disodium salt, and 1 mM phenylmethylsulfonyl fluoride (PMSF) (Peixoto et al., 1999). The homogenate was centrifuged for 15 min at 15,000 x*g* at 4 ºC and the supernatant was collected for further analysis.

The activity of superoxide dismutase (SOD; EC. 1.15.1.1) was assessed following the procedures described by Giannopolitis and Ries (1977), with the addition of 50 µL of enzymatic extract into 5-mL tubes containing 1 mL of 50 mM potassium phosphate buffer, pH 7.8, 0.1 mM EDTA and 19.5 mM methionine. The solution was mixed and 300 µL of 10 µM riboflavin and 150 µL of 0.75 mM nitro-blue tetrazolium chloride were added. After 5 minutes of illumination exposure, the absorbance of the samples at 560 nm was recorded. Negative and

positive controls were also included using extraction buffer instead of enzymatic extract and placed in the dark and under illumination, respectively. SOD activity was determined based on the inhibition of NBT reduction, defining an activity unit (1 U) as the amount of enzyme needed to inhibit 50% of photoreduction.

The catalase (CAT, EC. 1.11.1.6) assay was performed according to Havir and Mchale (1987). Briefly, 10 µL of enzymatic extract in 96-Microtiter plate wells was added to 290 µL of 50 mM potassium phosphate buffer, pH 7.0, containing 20 mM H_2O_2. The absorbance was read in kinetic mode at 240 nm in a microplate reader (VersaMax, Molecular Devices, San Jose, USA) every 15 s during 5 min at 30 ºC. Catalase activity was calculated based on the consumption of H_2O_2 ($\varepsilon = 36\ M^{-1}\ cm^{-1}$), and expressed in µmol H_2O_2 min^{-1} mg^{-1} protein.

For the determination of peroxidase (POX, EC. 1.11.1.7) activity, 185 µL of 25 mM potassium phosphate buffer, pH 6.8, containing 20 mM H_2O_2 were added to10 µL of enzymatic extract in 96-Microtiter plate wells. After 3 min, 5 µL of 800 mM pyrogallol was added and the absorbance at 470 nm was read in a microplate reader (VersaMax, Molecular Devices, San Jose, USA), during 5 minutes at 25 ºC. Peroxidase activity was calculated based on the molar extinction coefficient of 2.47 mM^{-1} cm^{-1} and expressed in µmol purpurogallin min^{-1} mg^{-1} protein (Kwak et al., 1996).

Ascorbate peroxidase (APX, EC. 1.11.1.11) assay was performed according to Nakano and Asada (1981), modified by Murshed et al. (2008). In a 96-Microtiter plate was added 185 µL of 50 mM potassium phosphate buffer pH 7.0 containing 0.54 mM ascorbate to 10 µL of enzymatic extract. After that, 5 µL of 200 mM H_2O_2 was added and the absorbance at 290 nm was recorded using a microplate reader (VersaMax, Molecular Devices, San Jose, USA), during 5 minutes at 25 ºC. Ascorbate peroxidase activity was calculated based on the molar extinction coefficient of 2.8 mM^{-1} cm^{-1} and expressed in µmol AsA min^{-1} mg^{-1} protein.

The protein content in the samples was quantified using the Coomassie blue assay (Bradford, 1976).

Lipid peroxidation and H_2O_2 content

For the determination of net peroxidation, through the quantification of Thiobarbituric Acid Reactive Substances (TBARS) content, 100 mg of plant material were macerated in liquid nitrogen with 2 mL of ethanol 80%. Then, the homogenate was centrifuged at 3000 x*g* for 10 min, 4˚C. Aliquots of 0.5 mL of the supernatant was taken and added to 0.5 ml of 20% TCA. Another 0.5 mL aliquot of the supernatant was added to 0.5 mL of the 20% TCA and 0.5%

TBA mixture. The samples were heated at 90°C for 1 hour and then cooled in an ice bath. The samples were again centrifuged at 3000 x*g* for 10 min at 4˚C and the supernatant was used for the absorbance readings at 440, 532 and 600 nm. The results were estimated according to Hodges et al. (1999).

The H_2O_2 content was determined according to the protocol proposed by Gay and Gebicki (2000). The extract was obtained homogenizing 200 mg of fresh plant material together with 2 mL of 50 mM potassium phosphate buffer, pH 6.5. The homogenate was centrifuged at 10,000 x*g* for 15 min at 4˚C and the supernatant was used for the assay. Aliquots of 10 µL of the extract were added to 50 µL of 400 mM sorbitol, 80 µL of $FeNH_4SO_4$ prepared in 62.5 mM sulfuric acid, 50 µL of 0.5 mM xylenol orange, and 10 µL H_2O into 96-microplate wells. After 30 minutes in the dark, the absorbance was detected at 560 nm (VersaMax, Molecular Devices, San Jose, USA). The H_2O_2 was quantified based on a standard curve and the results were expressed as nmol g^{-1} FW.

Data analysis

Statistical tests were performed using R software, version 3.6.2. Data were examined using the Shapiro–Wilk test ($p > 0.05$) to check for normal distribution of the data and Bartlett's test ($p > 0.05$) to check for equal variances across samples. Where data failed on the Shapiro–Wilk test, a Box–Cox transformation [$T(Y) = (Y^{\lambda} - 1)/\lambda$] was performed to obtain the standard normal distribution. Parametrical data were submitted to ANOVA and regression models were adjusted. For nonparametrical or non-fitting model data, dispersion data is presented as box-plots.

3.3. Results

Effects of Fe excess on appearance, bioaccumulation and anatomical structure of *P. stratiotes*

To assess the potential of water lettuce (*Pistia stratiotes*) for phytoremediation and bioindication of Fe contaminated water environments, representative images of the plants were registered after 5 and 10 days of treatment along with Fe quantification in shoots and roots. Plants treated with 1 mM Fe-EDTA maintained a similar visual appearance to that of the control plants after 5 days (Figure 1a). By contrast, plants growing under 3 mM Fe-EDTA after 5 days, along with those ones under 1 and 3 mM Fe-EDTA after 10 days of treatments, presented browning of leaf edges, an initial symptom of toxicity (Figure 1a). In higher concentrations (5

and 7 mM), the visual symptoms of toxicity were observed after 5 days and intensified after 10 days. Plants growing for 10 days under 5 mM Fe-EDTA showed necrosis on the leaf edges, radiating to the centre of the leaf. More intense effects were observed in plants treated with 7 mM Fe-EDTA, as revealed by yellowing followed by necrosis on the leaf margins, coupled with necrosis in young leaves at the shoot apex (Figure 1a). Accordingly, the quantitative measurement of the necrotic area showed an increase in toxic effects following an increase in the concentration of Fe-EDTA in nutrient solution at both 5 and 10 days (Figure 1b, c). Furthermore, the total necrotic area was about 5% of the total leaf area at 5 days and close to 20% at 10 days (Figure 1b, c).

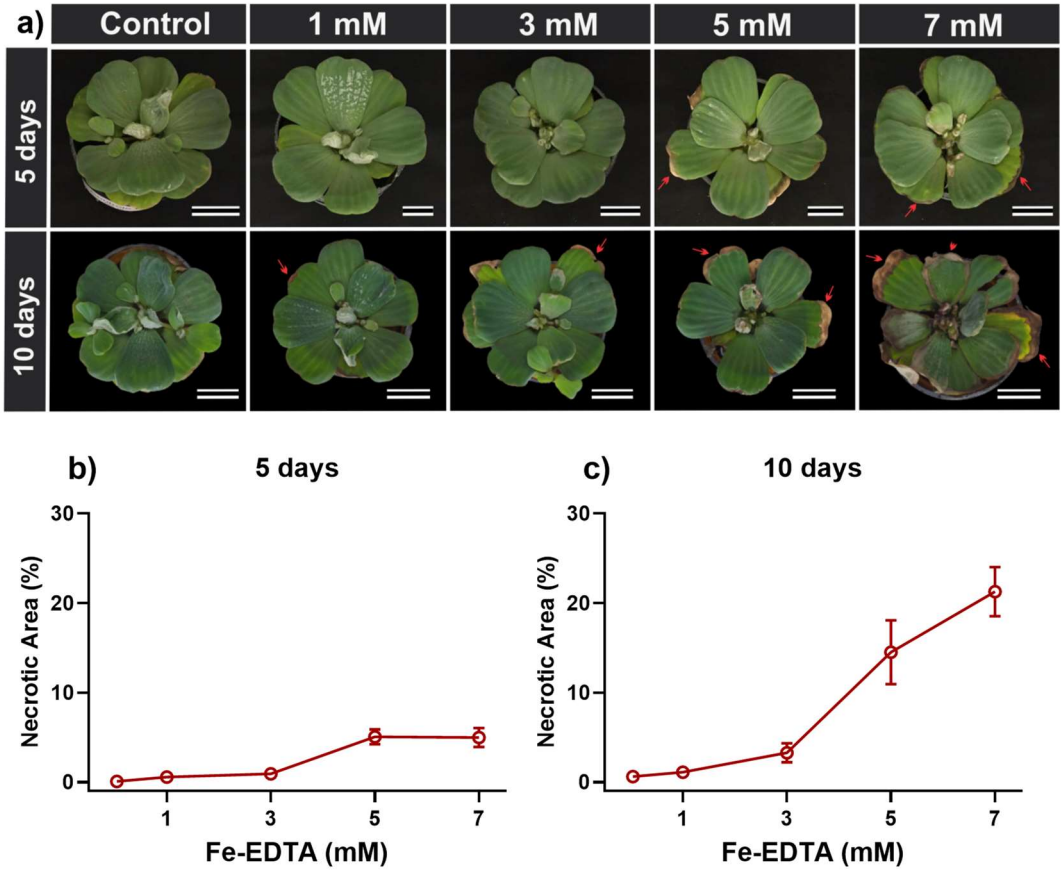

Figure 1. General appearance and necrotic area in *Pistia stratiotes* growing in medium containing different concentrations of Fe. Representative images of *P. stratiotes* plants growing for five and ten days in a nutrient solution containing 0.038 – control; 1; 3; 5 or 7 mM of Fe-EDTA (a). Red arrows indicate Fe toxicity symptoms such as yellowing and necrosis. Bars = 4 cm. Necrotic area (mean ± standard error) of leaves at 5 (b) and 10 (c) days in *Pistia stratiotes* plants growing for five or ten days in a nutrient solution containing 0.038, 1, 3, 5 or 7 mM of Fe-EDTA.

Overall, there were no effects of Fe stress on the shoot and roots of the plants at either time point (Figure 2a–d). Although the relative growth rate (RGR) was similar between the treatments after 5 days (Figure 2e), there was a linear decrease in the variable after 10 days (Figure 2f).

A greater accumulation of Fe was observed in the leaves and roots with increasing cultivation time in the nutrient solution (Figure 3a–d). At the first time point (5 days), the shoot concentration of Fe was similar to plants grown in 1, 3 and 5 mM Fe-EDTA. Higher values of shoot Fe after 5 days were observed in plants subjected to 7 mM Fe-EDTA (Figure 3a). In the roots, the concentration of Fe at 5 days was estimated by a cubic regression model, in which

the values increased in the intermediate concentrations, with a new increase in the highest concentration (Figure 3c).

After 10 days, the data for shoot Fe passed parametric tests, and a regression model was plotted. In the shoots, the Fe accumulation increased according to the concentration of the element in the solution, reaching about 6000 μg g^{-1} dry weight (Figure 3b). After 10 days, the nonparametric data showed higher root Fe values for concentrations of 5 and 7 mM (Figure 3d). Interestingly, the lower remaining Fe in the nutrient solution and the higher removal capacity at 5 days were observed at the 3 mM Fe-EDTA concentration (Figure S1a, b). Furthermore, plants growing at 1 and 5 mM of Fe-EDTA showed higher removal capacities than control (0.038 mM) and 7 mM plants (Figure S1b).

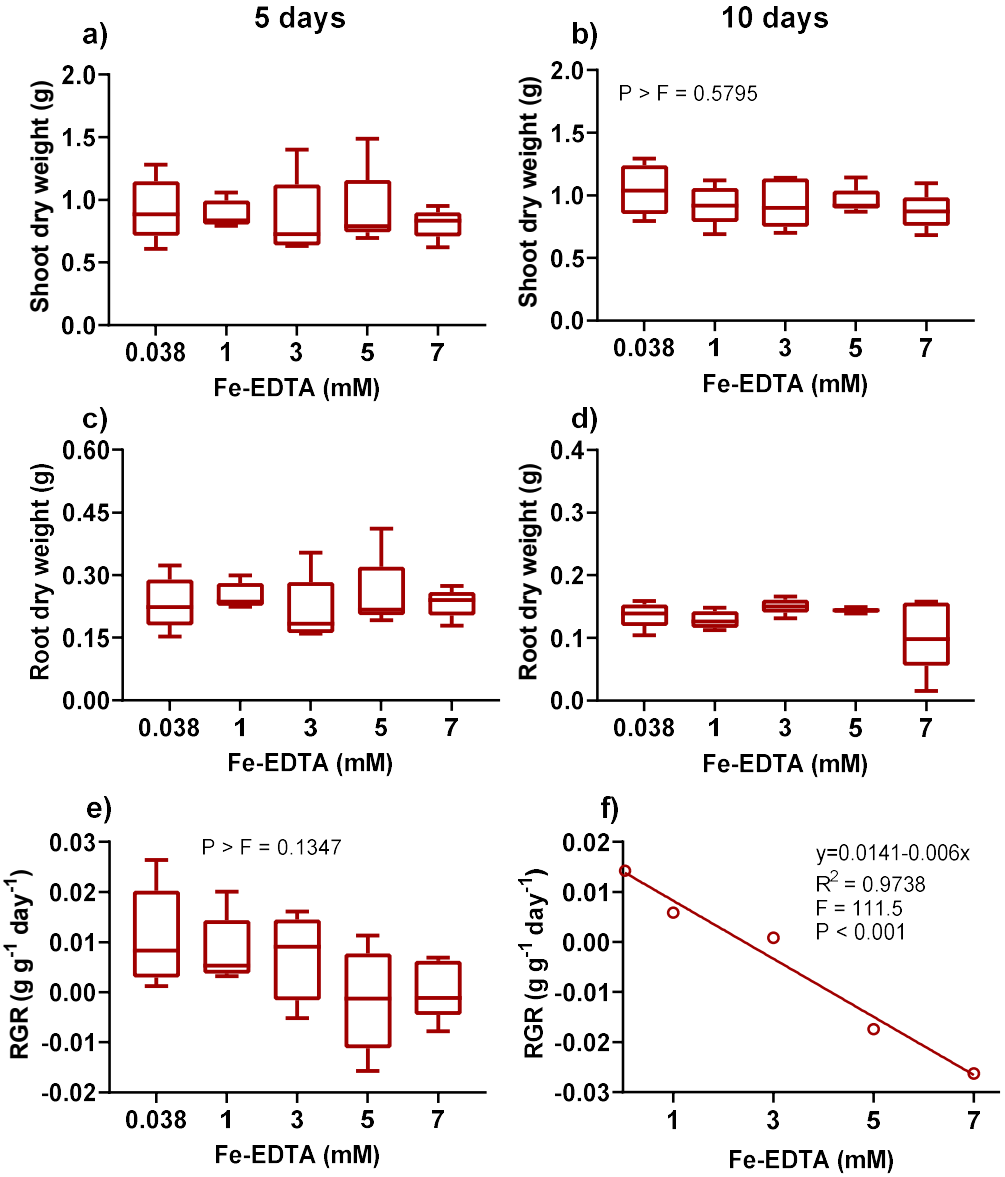

Figure 2. Growth of *Pistia stratiotes* growing in medium containing different concentrations of Fe. Shoot (a, b), and root (c, d) dry weight, and relative growth rate (e, f) in *P. stratiotes* plants growing for 5 or 10 days in a nutrient solution containing 0.038, 1, 3, 5 or 7 mM of Fe-EDTA. Regression models were estimated for the parametric data ($p \leq 0.05$), whereas nonparametric or non-significant differences between Fe concentrations ($p > 0.05$) data are presented as box-plot charts.

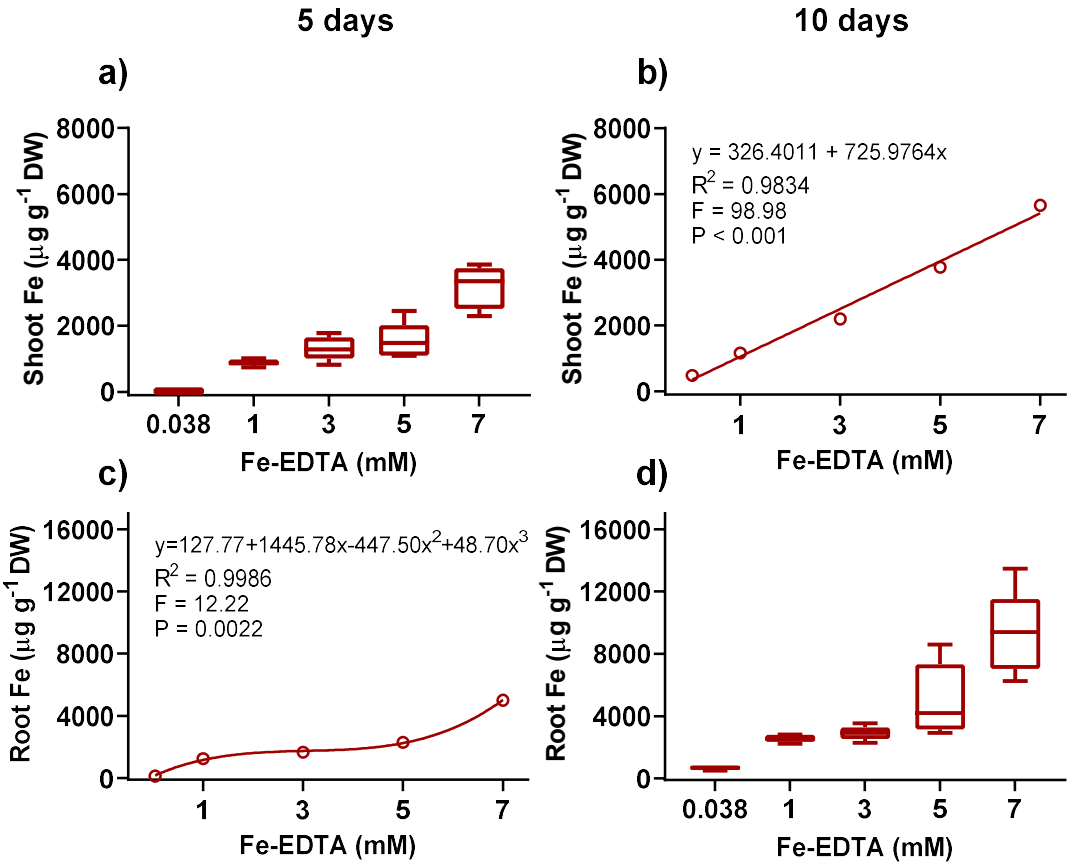

Figure 3. Fe accumulation in *Pistia stratiotes* growing in medium containing different concentrations of Fe. Concentrations of Fe in shoots (a, b), and roots (c, d) in *P. stratiotes* plants growing for 5 or 10 days in a nutrient solution containing 0.038, 1, 3, 5 or 7 mM of Fe-EDTA. Regression models were estimated for the parametric data ($p \leq 0.05$), whereas nonparametric or non-significant regarding differences between Fe concentrations ($p > 0.05$) data are presented as box-plot charts.

The bioconcentration factor (BCF) of Fe into *P. stratiotes* decreases following a quadratic model at 5 days (Figure 4a). At the second time-point, the control plants had the highest mean value, while Fe-treated plants had a decrease in BCF, varying from 64 to 31 for plants grown at 1 and 3 mM, respectively (Figure 4b). The translocation factor (TF) of plants showed no significant changes regardless of the Fe concentration in the nutrient solution, either at 5 or 10 days (Figure 4c, d). As expected, the rhizofiltration potential (RP) was similar to the accumulation of root and shoot Fe, with a tendency to increase up to close to 20,000 mg Fe m^{-2} $year^{-1}$ in plants growing at 7 mM Fe-EDTA (Figure 4c, f).

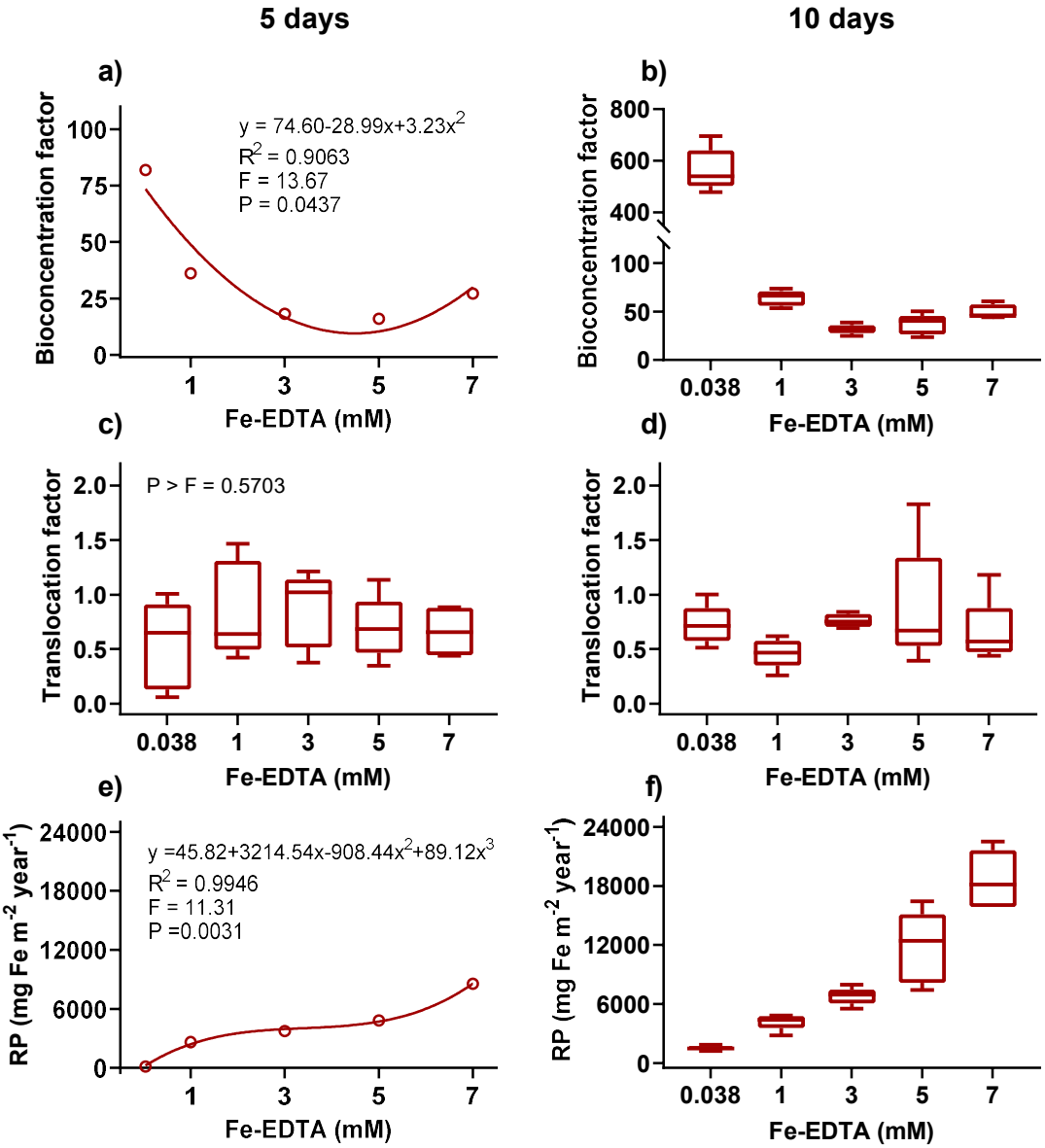

Figure 4. Bioaccumulation indexes of *Pistia stratiotes* growing in medium containing different concentrations of Fe. Bioconcentration factor (a, b), Translocation factor (c, d), and Rhizofiltration potential (e, f) of *P. stratiotes* plants growing for 5 or 10 days in a nutrient solution containing 0.038, 1, 3, 5, or 7 mM of Fe-EDTA. Regression models were estimated for the parametric data ($p \leq 0.05$), whereas nonparametric or non-significant regarding differences between Fe concentrations ($p > 0.05$) data are presented as box-plot charts.

In addition to visual appearance and Fe quantification in plant tissues, the anatomical characterisation, evaluation of Fe-induced structural damage and histochemical detection of Fe were performed in leaves and roots of plants growing in control or 5 mM Fe-EDTA treatments (Figures 5 and 6). The anatomical traits of *P. stratiotes* included amphistomatic leaves displaying tector trichomes and dorsiventral mesophyll. Indeed, the cell layer pattern of leaves was composed of a single epidermis, palisade parenchyma with 1 to 2 layers and spongy

parenchyma with 8 to 9 layers cells, interspersed with large aerenchyma (Figure 5a–h). The roots displayed a cortex with large aerenchyma and endoderm that internally delimited the vascular cylinder constituted by xylem, phloem and parenchymatic pith (Figure 5i–p). Phenolic compounds were also present in the epidermis, and oxalate crystals were present in the aerenchyma (Figure 5m, n).

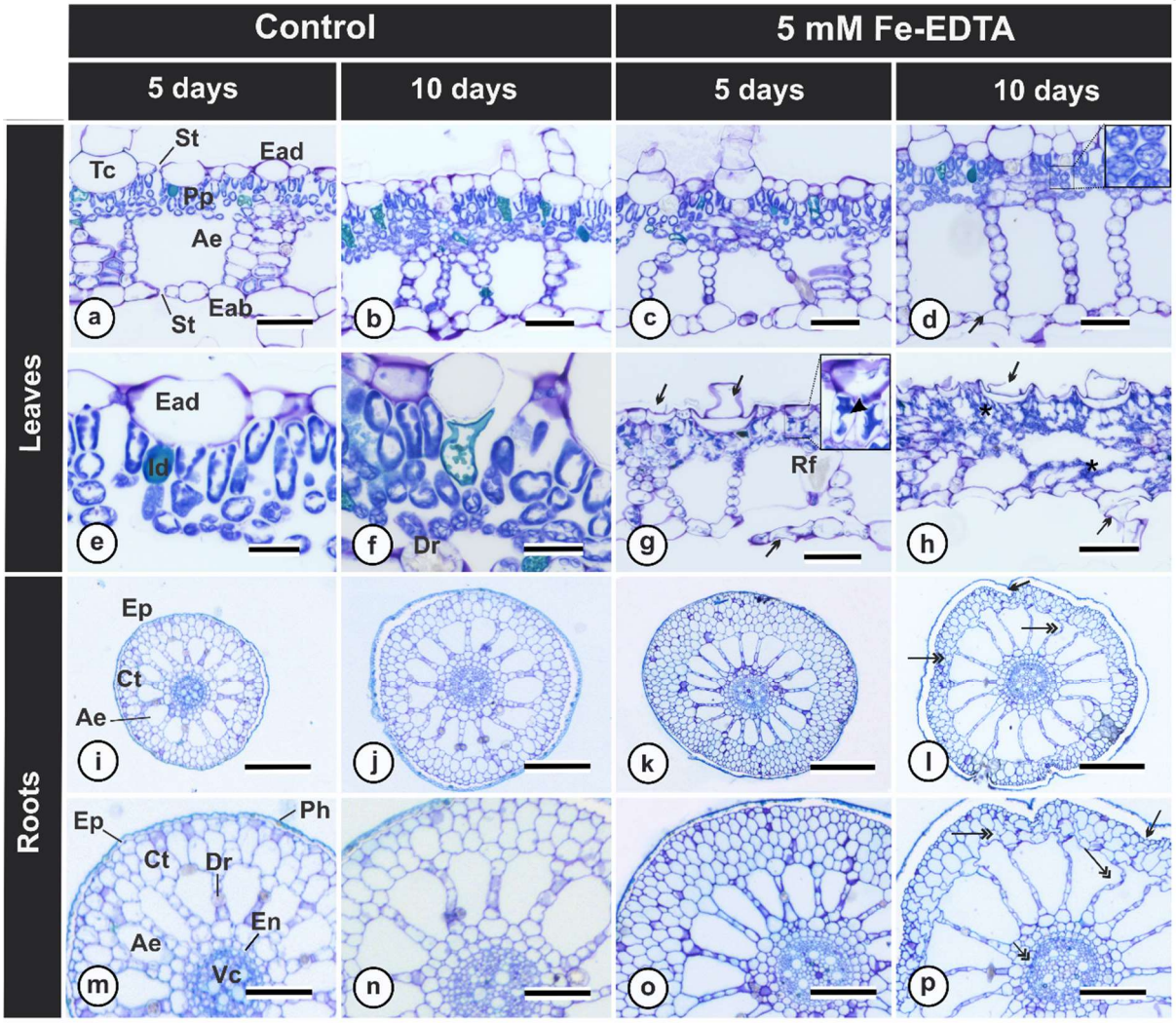

Figure 5. Anatomical characterization of leaves and roots of *Pistia stratiotes* growing in control condition or with 5 mM Fe-EDTA. Leaves (a-h) and roots (i-p) cross-section of *P. stratiotes* subjected to control – 0.038 mM (a, b, e, f, i, j, m, and n) or 5 mM Fe-EDTA (c, g, k, o, d, h, l, and p) for 5 and 10 days. Ae (aerenchyma); Ct (cortex); Vc (vascular cylinder); Dr (druse crystals); Ep (epidermis); Eab (abaxial epidermis); Ead (adaxial epidermis); En (endodermis); St (stoma); Id (idioblast); Pp (palisade parenchyma); Ph (phenolic compounds); Rf (raphides); Tc (tector trichome); Asterisk * (collapse of chlorenchyma cells); Arrowhead ► (protoplast retraction); Arrow → (collapse of epidermal cells). Double headed arrow ↠ (change in the shape of cells from cortex and endodermis). Bars: (a-d, g-h, m-p) =100 µm; (e and f) = 30 µm; (i-l) = 200 µm.

Fe-treated plants displayed more structural damage in the leaves and roots after 10 days (Figure 5). In cells near the leaf margin, there was protoplast retraction, collapse and thinning visual of the leaf blade (Figure 5c, d, g, h), as well as an apparent increase in chloroplast size (Figure 5d). Nevertheless, no apparent changes in the tissues furthest from the margins or cells of the vascular bundle were observed (Figure 5c, d, g, h). For root tissues, major changes included a slight collapse in the cortical cells close to the epidermis after 10 days, with sinuous walls, changing the general shape of the cell to elliptical shapes (Figure 5l, p), whereas in the control plants it has an isodiametric shape (Figure 5i, j, m, n). Interestingly, no major damage was detected in the vascular cylinder of roots exposed to 5 mM Fe-EDTA compared to the control (Figure 5i–p).

For the qualitative assessment of Fe distribution in the tissues of the leaves and roots, a Prussian blue staining assay was performed (Figure 6). In agreement with Fe quantification by AAS, positive reactions for Fe presence were more intense (blue colour) in the tissues of Fe-treated plants, especially in roots after 10 days of treatment (Figure 4). In the leaves, Fe was detected in epidermal cells of both abaxial and adaxial surfaces, trichomes and vascular tissues (Figure 6c, d, g, h). In addition, intense reactions were detected in idioblasts, structures associated with phenolic compound accumulation (Figure 6h). For roots, intense reactions for Fe detection were observed in the cells of the epidermis, and in the portion of the apoplast, especially in the cell walls and middle lamella of cells of the cortical portion and around the endoderm (Figure 6k, l, o, p).

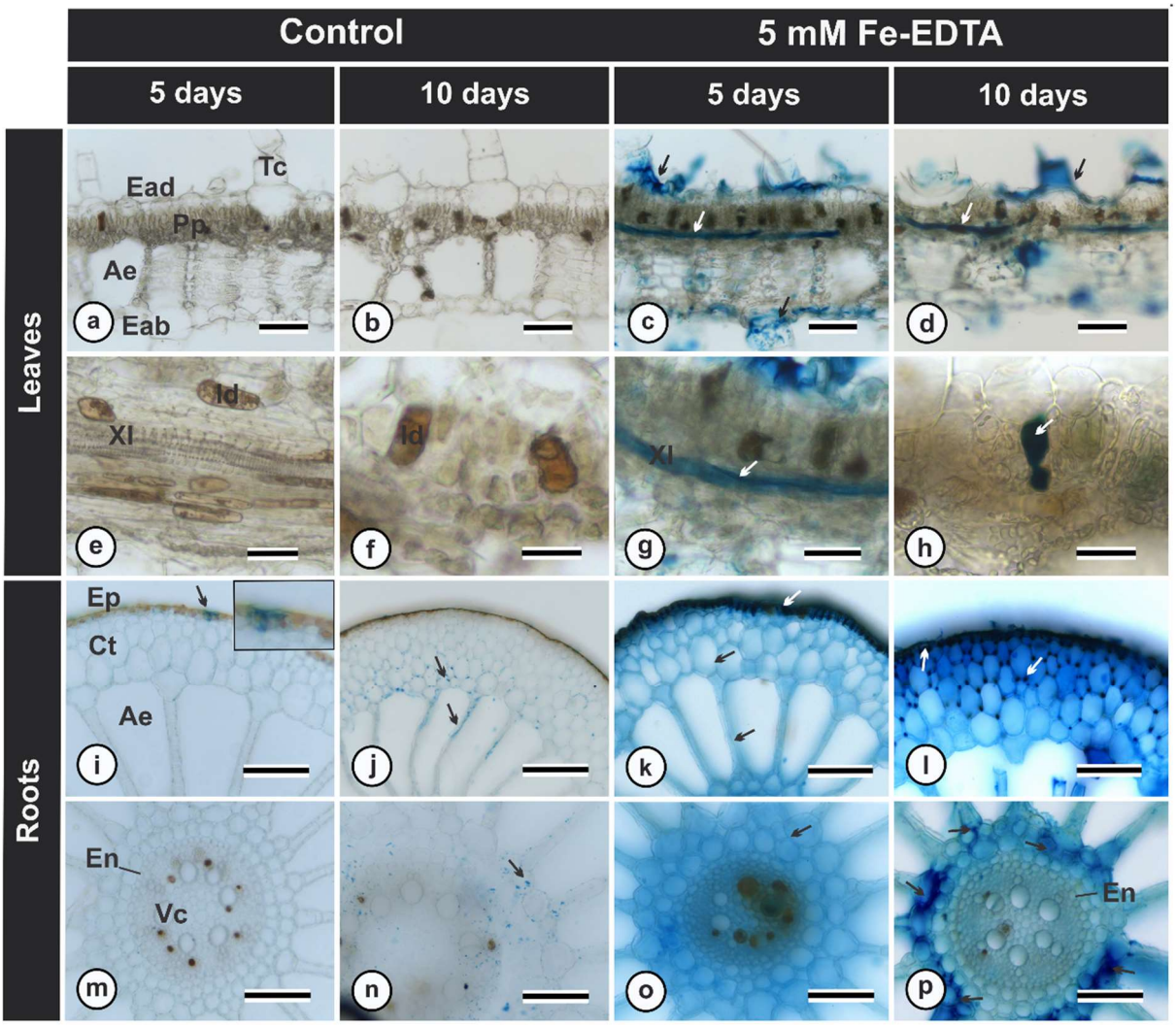

Figure 6. Histochemical detection of Fe in leaves and roots of *Pistia stratiotes* growing in control condition or with 5 mM Fe-EDTA. Leaves (A-H) and roots of *P. stratiotes* subjected to control – 0.038 mM (a, b, e, f, i, j, m, and n) or 5 mM Fe-EDTA (c, g, k, o, d, h, l, and p) for five and ten days. Blue color indicates typical positive reaction after 48h of exposition to Prussian blue staining solution. Ae (aerenchyma); Ct (cortex); Dr (druse crystals); Ep (epidermis); Eab (abaxial epidermis); Ead (adaxial epidermis); En (endodermis); Id (idioblast); Tc (tector trichome); Vc (Vascular cylinder); Xl (xylem). White or black arrows (Positive reaction for Fe). Bars: (a-d, i-j, m-p) =100 µm; (e, g-h) = 50 µm; (f) = 30 µm.

Photosynthetic performance of *P. stratiotes* challenged with Fe excess

P. stratiotes plants showed no impact on photosynthetic performance growing in all concentrations of Fe in the nutrient solution after 5 days, with carbon assimilation (*A*) values around 15 µmol CO_2 m^{-2} s^{-1} and stomatal conductance close to 0.7 mol H_2O m^{-2} s^{-1} (Figures 7a, b and S2). The internal concentration of CO_2 (C_i) also remained unaltered in plants growing under Fe excess, compared with the control, after 5 and 10 days (Figure 7c, d). However, the net CO_2 assimilation rate decreased in Fe-excess cultivated plants after 10 days (Figure 7b). Nevertheless, plants treated with 7 mM maintained around 60% of the net CO_2 assimilation

rate, even after 10 days of treatment (Figure 7b). Similarly, the single-point RuBisCO carboxylation efficiency remained unaltered at 5 days (Figure 7e) and decreased following a quadratic model at 10 days (Figure 7f).

Respiration rate (R_N) was not affected by Fe exposure after 5 days (Figure 7g). After 10 days, there was a decrease in the mean and median values of R_N in the higher concentrations of Fe, indicating an increase in the respiratory rate (Figure 7h). In contrast, plants grown with additional Fe did not show a change in the photorespiration rate (P_R) after 5 and 10 days (Figure S2e, f). Finally, the water status-dependent parameters (transpiration and stomatal conductance) of the plants did not show changes regardless of the Fe concentration (Figure S3a–d).

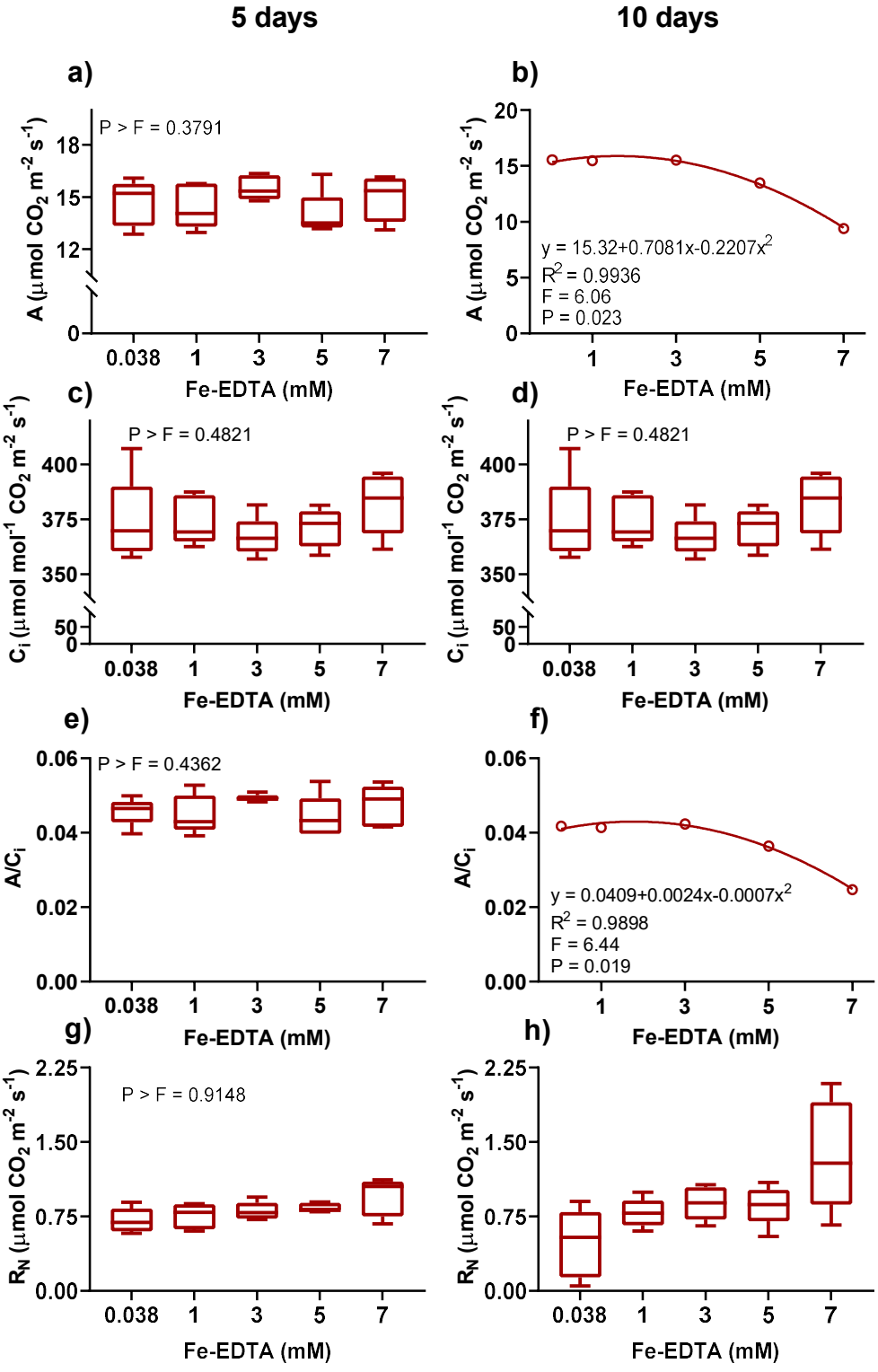

Figure 7. Gas exchange parameters of *Pistia stratiotes* plants growing in medium containing different concentrations of Fe. Net CO_2 assimilation rate (a, b), internal CO_2 concentration in the (c, d), carboxylation efficiency (A/C_i; e, f), and respiration in the dark (e, f), of *P. stratiotes* plants growing for 5 or 10 days in a nutrient solution containing 0.038, 1, 3, 5 or 7 mM of Fe-EDTA. Regression models were estimated for the parametric data ($p \leq 0.05$), whereas nonparametric or non-significant differences between Fe concentrations ($p > 0.05$) data are presented as box-plot charts.

Increasing Fe concentration in nutrient solution did not affect the fluorescence parameters of chlorophyll *a* after 5 days of exposure (Figure 8a, c, e, g). At the second time point (10 days), the potential quantum yield (F_v/F_m) and the ratio F_0/F_m were not altered by the increase in the concentration of Fe (Figure 8b, d). In contrast, the effective quantum yield ($\phi PSII$) decreased linearly according to the increasing Fe concentration (Figure 8f), whereas non-photochemical quenching (*NPQ*) had no changes, regardless of the Fe concentration at both time points (Figure 8g, h).

The increase in the concentration of Fe-EDTA in the nutrient solution did not alter the electron transport rate derivations in the carboxylation and oxygenation components (ETR_C, ETR_O and ETR_c/ETR; Figure S3) of the plants after 5 days. However, Fe excess imposed for 10 days culminated with a 34% reduction in ETR_C in plants grown at 7 mM Fe-EDTA compared to the control (Figure S3b). Interestingly, both ETR_O and ETR_C/ETR ratio were not affected by increasing Fe after 10 days (Figure S3c, f).

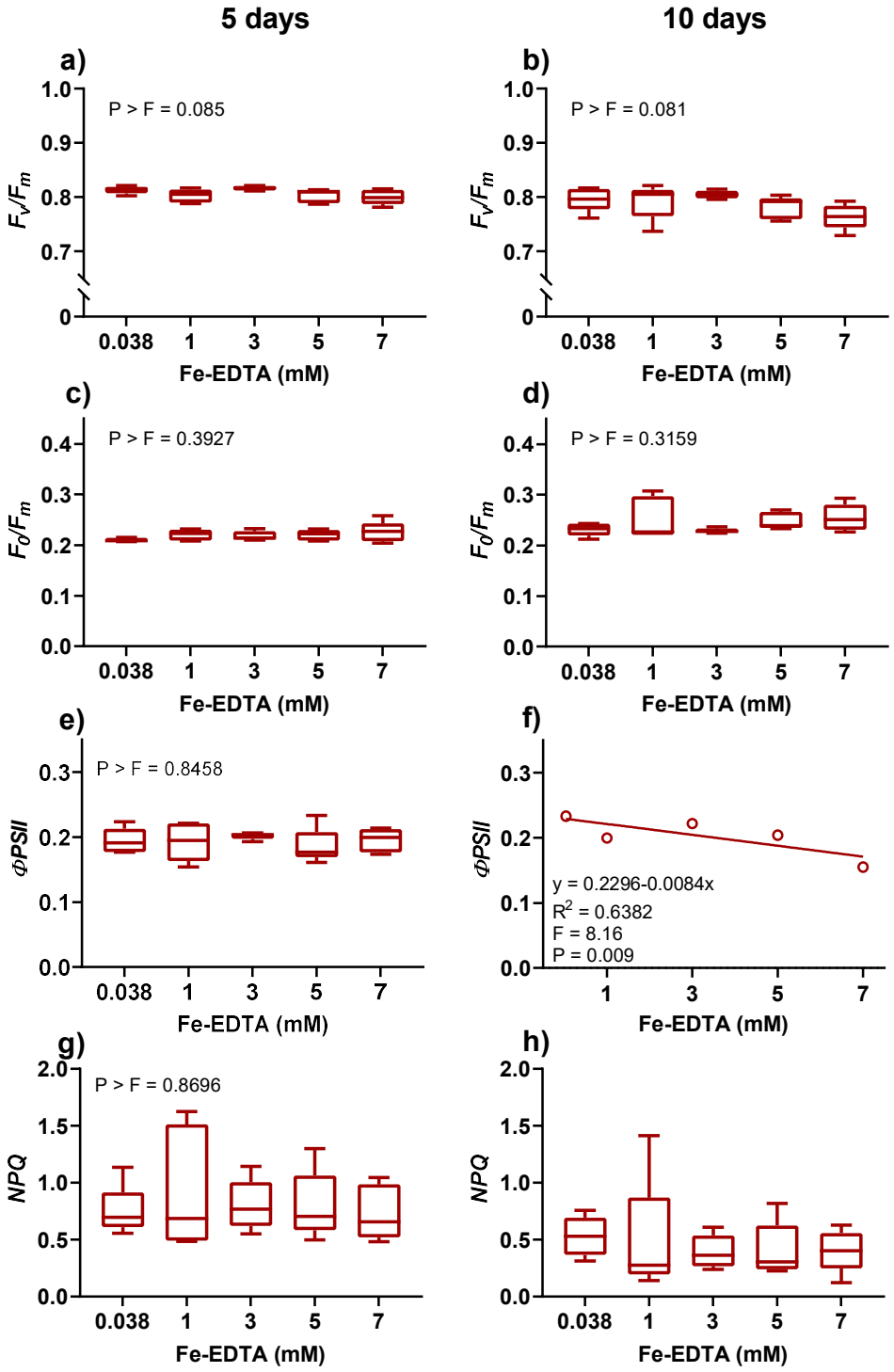

Figure 8. Fluorescence of chlorophyll *a* parameters of *Pistia stratiotes* plants growing in medium containing different concentrations of Fe. Potential quantum yield of the photosystem II (a, b), ratio between minimal and maximum fluorescence (F_0/F_m) (c, d), actual PSII photochemical efficiency (e, f), and non-photochemical quenching (g, h) of *P. stratiotes* plants growing for 5 or 10 days in a nutrient solution containing 0.038, 1, 3, 5 or 7 mM of Fe-EDTA. Regression models were estimated for the parametric data ($p \leq 0.05$), whereas nonparametric or non-significant differences between Fe concentrations ($p > 0.05$) data are presented as box-plot charts.

Regarding the pigments, the plants exposed to Fe excess (1–7 mM) maintained chlorophyll and carotenoid contents similar to the control plants after 5 days (Figure 9a, c, e). Otherwise, at the second time point, the chlorophyll *a* and *b* concentrations decreased linearly according to the concentration of Fe-EDTA in the solution (Figure 9b, d, f). Compared to the control, chlorophyll *a* and *b* content decreased by 16% and 49%, respectively, in plants grown at 7 mM Fe-EDTA after 10 days (Figure 9b, d). A cubic model adjustment described the concentration of carotenoids at 10 days. Our results indicated an increase in the concentration of these accessory pigments up to concentrations of Fe of around 5 mM, followed by a decrease in higher concentrations (Figure 9f).

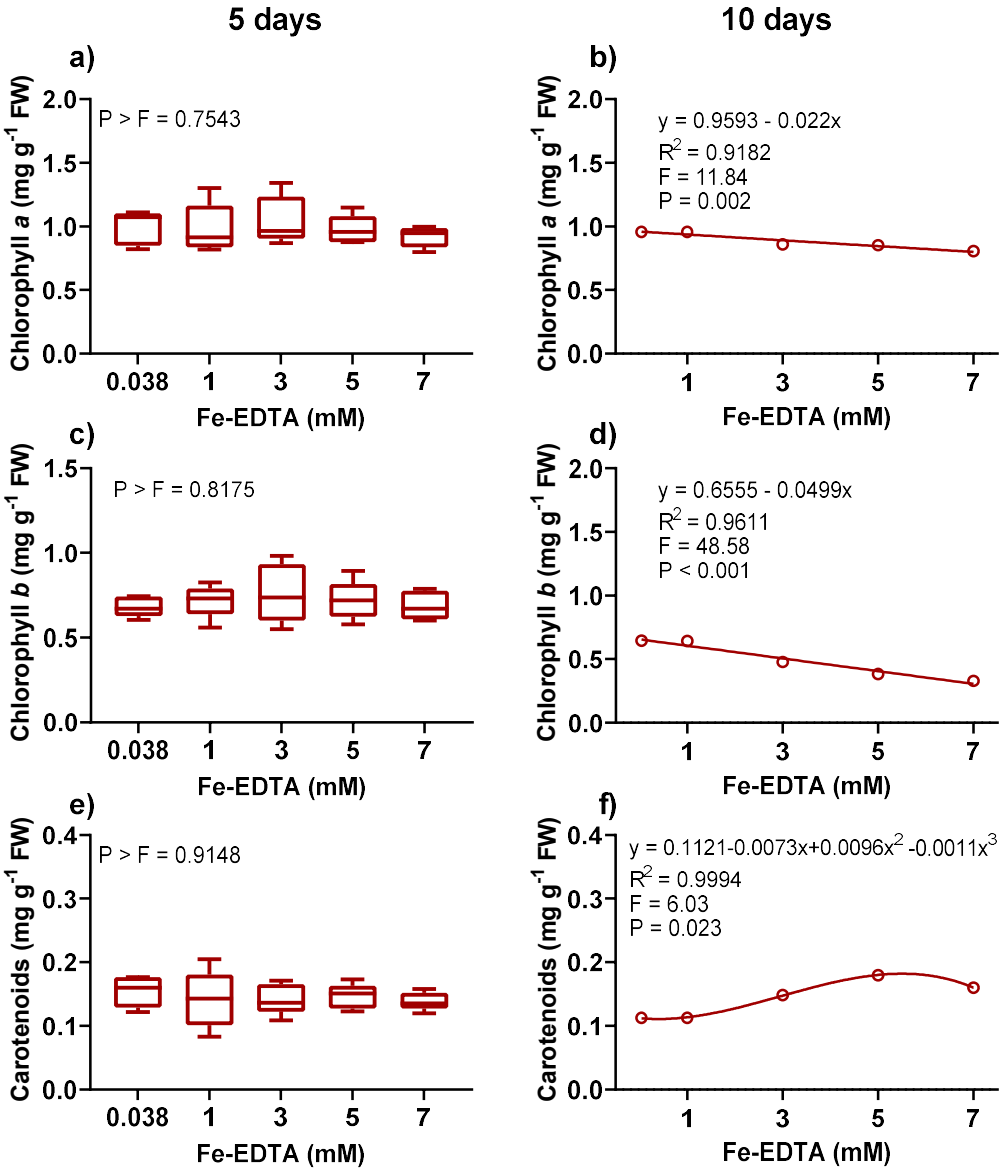

Figure 9. Photosynthetic pigments of *Pistia stratiotes* plants growing in medium containing different concentrations of Fe. Contents of chlorophyll *a* (a, b), chlorophyll *b* (c, d), and carotenoids (e, f) in *P. stratiotes* plants growing for 5 or 10 days in a nutrient solution containing 0.038, 1, 3, 5 or 7 mM of Fe-EDTA. Regression models were estimated for the parametric data ($p \leq 0.05$), whereas nonparametric or non-significant differences between Fe concentrations ($p > 0.05$) data are presented as box-plot charts.

Effects of Fe excess on oxidative damage and antioxidant enzyme activity

Following the application of 5 mM Fe-EDTA, significant changes in biomarkers of oxidative metabolism compared to the control were observed, especially lipid peroxidation and the activity of major enzymatic players in ROS scavenging (Table 1). The activities of superoxide dismutase (SOD) and peroxidase (POX) were strongly increased (6 and 5-fold),

respectively, in shoots after 5 days of treatment. Similarly, the enzyme activity in shoots were characterized by an increase after 10 days compared to the control (Table 1). In roots, the activity of these enzymes was higher than in shoots, although in the comparison between control and Fe-treated plants, the values only increased after 10 days (Table 1).

For ascorbate peroxidase (APX) activity, there was an increase in Fe-treated plants between 3 and 4-times compared to control plants in both shoots and roots at either time point (Table 1). Similarly, lipid peroxidation, measured through thiobarbituric acid reactive substances (TBARS) content, was induced by 5 mM Fe-EDTA after 5 and 10 days of treatment in both plant organs (Table 1). Interestingly, the TBARS content in leaves was 3.35 times higher in Fe-stressed plants compared to the control at 5 days and 1.7 times higher at 10 days (Table 1). Otherwise, catalase (CAT) activity and H_2O_2 content in shoots and roots remained unaltered regardless of Fe concentration and time of treatment (Table 1).

Table 1. Activity of superoxide dismutase (SOD - U min^{-1} mg^{-1} protein), catalase (CAT - µmol H_2O_2 min^{-1} mg^{-1} protein), peroxidase (POX - µmol purpurogallin min^{-1} mg^{-1} protein), ascorbate peroxidase (APX - µmol AsA min^{-1} mg^{-1} protein), and thiobarbituric acid-reactive substances (nmol g^{-1} FW) and peroxide (H_2O_2 - nmol g^{-1} FW) contents in shoots and roots of *Pistia stratiotes* plants growing for five or ten days under control or Fe-stress (5 mM Fe-EDTA) conditions. Asterisks represent statistical differences between control and Fe-stressed plants in the same time-point, determined by the Welch Two Sample t-test at 5 (*) or 1% (**) of significance.

	SOD	CAT	POX	APX	TBARS	H_2O_2
	Shoot					
	5 days					
Control	6.16 ± 3.50	32.59 ± 9.37	3.76 ± 1.05	1.98 ± 0.74	13.60 ± 1.29	98.11 ± 8.04
5 mM Fe	36.65 ± 10.83*	31.44 ± 7.05^{ns}	17.65 ± 3.79*	8.47 ± 1.76*	45.69 ± 8.95*	72.10 ± 18.28^{ns}
	10 days					
Control	7.31 ± 2.04	29.63 ± 6.92	5.95 ± 1.21	4.30 ± 1.52	15.95 ± 1.42	74.65 ± 4.46
5 mM Fe	31.47 ± 3.78**	24.02 ± 2.42^{ns}	13.33 ± 0.70**	13.50 ± 3.16*	27.26 ± 4.81*	74.48 ± 30.60^{ns}
	Root					
	5 days					
Control	47.08 ± 14.51	27.97 ± 5.21	27.24 ± 6.53	3.67 ± 0.49	5.06 ± 1.19	70.03 ± 5.41
5 mM Fe	98.00 ± 32.77^{ns}	48.06 ± 15.32^{ns}	64.29 ± 15.73^{ns}	11.13 ± 1.37**	10.19 ± 1.67*	76.02 ± 9.35^{ns}
	10 days					
Control	30.16 ± 3.48	20.84 ± 6.13	19.19 ± 6.53	3.79 ± 0.38	5.75 ± 0.89	77.65 ± 4.46
5 mM Fe	123.91 ± 25.87*	25.18 ± 3.96^{ns}	75.02 ± 6.22**	15.17 ± 2.43**	19.88 ± 3.36*	74.66 10.99^{ns}

3.4. Discussion

Characteristic and progressive symptoms of Fe toxicity along with notorious Fe accumulation in root apoplast ensure *P. stratiotes* bioindication and phytoremediation potential

Iron (Fe) is a well-known essential nutrient and non-hazardous element for all living organisms, except for specific bacteria (Weinberg, 1997). Nevertheless, recent studies have pointed out neurodegenerative-related risks for excessive consumption and accumulation of Fe in mammals (Martins et al., 2022; Salami et al., 2021; Viktorinova and Durfinova, 2021). Not surprisingly, toxic effects in plants have been demonstrated in association with disturbances in nutritional and redox homeostasis, inducing environmental disorders and agricultural losses (Aung and Masuda, 2020). Given that *Pistia stratiotes* plants have been successfully applied for cleaning up water environments contaminated with metallic elements (Ali et al., 2020; Li et al., 2022), we investigated the performance of this species for the bioindication and phytoremediation of Fe.

Initial symptoms of Fe toxicity in leaves include chlorosis and "bronzing," a brown colouration caused by the accumulation of phenols in the vacuole that progresses to necrosis, which is related to nutritional imbalance and oxidative stress (Das et al., 2020; Kabir et al., 2016). Visual symptoms and structural damage, such as protoplast retraction and cell collapse, upon Fe exposure in *P. stratiotes* plants were observed in the leaf margins progressing to the centre, increasing according to the concentration and time of exposure (Figure 1a). These results indicate an intensification of Fe accumulation in the peripheral region of the leaf, which can be related to the hydraulic architecture of the leaf, which is composed of parallel veins that facilitate Fe transport to the apical regions. Further quantification of Fe in specific fraction of leaf segments are still required to test this hypothesis. Notwithstanding, the progression of leaf necrosis at the highest Fe concentrations reached a maximum of 20% of the leaf area (Figure 1b, c), indicating that the species has longevity and tolerance in stress conditions caused by pollutants, which are fundamental aspects for application in phytoremediation programmes (Rezania et al., 2016).

Furthermore, the biomass of leaves and roots alone was not affected by excess Fe (Figure 2a–d), although the RGR decreased at 10 days (Figure 2f), probably because of the integrated effects on the whole plant. The negative RGR observed may be due to the loss of roots by the plants, a strategy observed by other authors in studies on species subjected to arsenic and other metallic elements (Campos et al., 2019; Farnese et al., 2014b).

The bioaccumulation of Fe in *P. stratiotes* is notorious when compared to other plant species. In rice (*Oryza sativa*), a typical model for Fe toxicity studies due to its availability in waterlogged soils, the Fe content in plant shoots growing in a medium containing 7 mM Fe-EDTA for 7 to 10 days is in the range between 400 and 1200 μg g^{-1} (Pinto et al., 2016) against 6000 μg g^{-1} observed for *P. stratiotes* in similar conditions (Figure 3b). Compared to other aquatic plants, *Eichhornia crassipes* takes about six weeks to accumulate the same Fe concentrations found here (Jayaweera et al., 2008), while *Lemna minor* has a bioaccumulation efficiency similar to that found herein for *P. stratiotes* (Teixeira et al., 2014). Nevertheless, the biomass production per area, and consequently, the rhizofiltration potential of *Pistia* (Figure 4e, f) is significantly higher than that of *Lemna* (Galal et al., 2018). It is important to mention, however, that other factors such as adaptation to the environment must be considered when selecting species for the phytoremediation programme (Ali et al., 2020).

We further investigated the partitioning of Fe between roots and shoots, in which there was higher accumulation in the roots (Figure 3a - d). A similar response—low translocation of Fe into shoots—was observed for most plant species subjected to high concentrations of Fe (Ahammed et al., 2020; Das et al., 2020; Kabir et al., 2016). It is important to highlight that there was no significant Fe exclusion or plaque formation outside of the roots since the quantification of the adsorbed form was not different between treatments (Figure S1c, d), indicating that Fe retention in the roots occurs in the apoplastic and symplastic fractions. Fe retention in roots generated a low translocation factor (TF < 1), regardless of the concentration and time of exposure (Figure 4c, d). For most plant species, TF > 1 is an essential criterion used to evaluate the potential for phytoremediation (Garbisu and Alkorta, 2001), as the belowground organs are usually maintained in the environment. Notwithstanding, in the case of floating macrophytes, including *P. stratiotes*, the entire plant can easily be collected and removed from the medium, so the element accumulated in the roots may also be removed from the environment.

The observed Fe retention in roots may occur through the oxidation of Fe^{2+} to Fe^{3+}, consequent precipitation in the apoplast and through the use of a vacuolar compartmentalisation mechanism in the symplast (Aung and Masuda, 2020; Stein et al., 2014). The histochemical detection of Fe showed intense reactions for Fe in the apoplast of the roots (Figure 6), supporting the hypothesis of Fe^{3+} precipitation. Additionally, the cell wall is the main structural element in roots, which is made of primarily pectin, cellulose and hemicellulose (Zhang et al., 2020). These polysaccharides contain strongly negatively charged sites that have a high affinity

to metal ions, thus showing a strong ability to bind Fe (Ye et al., 2015). Furthermore, a gradient for the Fe reaction is evident in the endoderm region of the roots (Figure 6), evidencing the role of Casparian strips in preventing Fe translocation (Araújo et al., 2020b; Lapaz et al., 2022), together with the maintenance of the structural integrity of the vascular cylinder (Figure 5).

Root retention of Fe also suggests a likely control for the transport across the membranes into the xylem, which may be related to downregulation of Fe transporters through Fe homeostasis regulators, such as the Hemerythrin motif-containing Interesting New Gene- and Zinc-finger protein (HRZ) (Aung et al., 2018). In shoots, Prussian blue reactions were detected in the vascular bundle and within the idioblast structures (Figure 6), indicating the action of chelating agents, such as phenolic compounds and nicotinamide, a major chelator of metal cations in higher plants (Aung et al., 2019).

4.2. Longer exposure to Fe excess induced photosynthesis impairments associated with chlorophyll degradation and lowered carboxylation efficiency

Spatial restriction of visual and structural damage to leaf margins (Figure 1a, 5), accumulation of Fe in non-photosynthetic leaf cells, such as trichomes (Figure 6) and Fe retention mainly in roots (Figure 3, 4) may have been crucial factors to ensure the photosynthetic performance of the plants after 5 days of treatment (Figure 7, 8), despite an increased membrane damage (Table 1). After 10 days, however, higher concentrations of Fe-EDTA (5 and 7 mM) triggered a series of physiological and biochemical damages, such as a decrease in chlorophyll contents (Figure 9) and photochemical efficiency, ultimately leading to lower CO_2 assimilation rate (Figure 7b). The inhibition of photosynthesis following excess Fe is reported in several plant species (Ahammed et al., 2020; Araújo et al., 2020a; Pereira et al., 2013; Pinto et al., 2016), which is usually associated to stomatal and non-stomatal limitations. For *P. stratiotes*, photosynthetic impairments are most likely originated from non-stomatal limitations, since no major changes in water status and CO_2 diffusion (Figure S2; Farnese et al., 2014a) were observed. This hypothesis is reinforced by the evaluation of the carboxylation efficiency of RuBisCO, decreased in high concentrations of Fe (Figure 7f). Moreover, it has already been reported that the content of Rubisco polypeptide was reduced by 60% in Fe-stressed leaves, which was directly correlated with decreases in chlorophyll content (Winder and Nishio, 1995).

In the present study, even under higher concentrations of Fe-EDTA after 10 days of exposure, the potential quantum yield of PSII (F_v/F_m) remained unchanged, whereas the *ΦPSII*

decreased (Figure 8f), indicating a short-term reversible photoinhibition (Werner et al., 2002). Fe excess can also elevate the cytochrome b_6/f content of thylakoids, lowering the photosynthetic rate by inducing a spatial disorder between the proteins of the electron transport chain (ETC) in the chloroplast (Suh et al., 2002). Ultimately, Fe overload in chloroplasts can have impacted carbon assimilation through an effect on the electron transport rate and, consequently, on the availability of ATP and NADPH for CO_2 fixation. On the contrary, the respiratory rate after 10 days was increased in Fe-treated plants with 7 mM Fe-EDTA (Figure 7h), indicating that a metabolic reprogramming likely occurred enhancing carbon and energy fluxes to repair damaged cell structures and trigger defense mechanisms (Campos et al., 2016; Menezes-Silva et al., 2017). Nevertheless, it should be noted that in the long-term, an increased respiration without photosynthetic compensation results in a negative carbon balance, which tends to deplete the plant's reserves.

4.3. Oxidative stress likely triggered by Fe-mediated Fenton reaction was opposed by the induction of antioxidant machinery

Photosynthesis impairment, degradation of chlorophyll, and structural damage observed in Fe^{2+}-stressed plants (Figures 4, 7 and 9) can be attributed to the generation of reactive oxygen species (ROS), especially due to the Fenton reaction, which involves the oxidation of Fe^{2+} by H_2O_2 producing a highly reactive hydroxyl radical ($^{\bullet}OH$) (Gutteridge et al., 1981). Oxidized Fe^{3+} produced by this reaction can be reduced again to Fe^{2+} by the superoxide anion radical ($O_2^{\bullet-}$) via the Haber–Weiss reaction, generating an oxidative burst (Richardson and Ponka, 1995). This reaction is likely to occur in chloroplasts, where more than 90% of free Fe^{2+} in leaf cells is located and the chloroplasts are especially prone to oxidative stress because of light-driven photosynthetic processes (Pereira et al., 2013; Terry and Abadia, 1986). Accordingly, we observed an increase in the size of chloroplasts in plants subjected to Fe (Figure 5).

The hydroxyl radical is extremely unstable and harmful to cell membranes, indicating that its production is likely responsible for an increased level of lipid peroxidation, measured by TBARS content (Table 1; El-Beltagi et al., 2020). Plasma membrane deterioration, in turn, was probably the main cause of the anatomical changes observed in the leaves and roots of *P. stratiotes*, such as protoplast retraction and cell collapse (Araújo et al., 2015; Freitas-Silva et al., 2020; Santana et al., 2014). Similarly, ROS generation may have affected cell wall components, as hydroxyl radicals are capable of non-specifically cleaving cell wall

polysaccharides in a site-specific reaction, which would explain the changes in the shape of root cells (Schopfer, 2002). Araújo et al. (2015), studying grass species exposed to excess Fe, argued that nutritional disorders triggered by this metal are also capable of influencing the structure of cell walls. Therefore, the changes observed in *P. stratiotes* exposed to Fe excess, including necrosis in the margins of the leaves, changes in plant anatomy, and changes in the concentration of biochemical markers (e.g., TBARS and chlorophyll content), have the potential to be used as general bioindicators of contaminated aquatic environments with Fe.

Even though lipid peroxidation has increased in leaves and roots since the first time point of Fe-stressed plants (Table 1), the activity of antioxidant enzymes was remarkably increased, which must have contributed to the maintenance of H_2O_2 levels similar to control plants (Table 1). A robust antioxidant system is an essential tolerance mechanism for stress in general, especially when dealing with transition metallic elements, such as Fe (Aung and Masuda, 2020). Furthermore, high Fe availability in cells induces the expression of heme-containing enzymes, such as peroxidases and catalases (Tewari et al., 2005).

Our results revealed an induction of SOD activity (Table 1), which is responsible for the dismutation of the superoxide anion ($O_2^{\bullet-}$) in different subcellular compartments, in which the Fe-dependent SOD isoform is mainly active in the chloroplast, a critical site for ROS generation in Fe-stressed plants (Pereira et al., 2013; Stein et al., 2014). Another highly active heme-enzyme in plastids (Tewari et al., 2005), APX, was also strongly induced in Fe-treated plants, and together with increased POX activity, it seemingly maintained H_2O_2 homeostasis in the cell (Table 1). However, CAT activity was not induced (Table 1), probably due to the maintenance of photorespiration levels (Figure S2), in which the enzyme is primarily involved (Mhamdi et al., 2012). Interestingly, there was a less pronounced increase in Fe-induced membrane damage in the leaves at 10 days than at 5 days (Table 1). This outcome demonstrates the effectiveness of the leaves' increased antioxidant system activity. This was not observed in the roots, most likely due to higher Fe concentrations in the tissues (Figure 3), which made it more challenging to contain the damage. Nevertheless, by maintaining the photosynthetic system through the protection of the leaves, the plant increases its chances of surviving, even in a challenging environment (Foyer and Shigeoka, 2011).

In addition to the activation of the antioxidant system, it is possible that non-enzymatic defence mechanisms were also activated in *P. stratiotes* plants exposed to Fe. An example of a nonenzymatic mechanism is the increased production of phenolic compounds. These antioxidants tend to chelate Fe, thus preventing the formation of free radicals (Michalak, 2006).

Interestingly, in this study, we observed the accumulation of phenolic compounds in the leaf epidermis (Figure 5), precisely the cells in which Fe accumulation was detected (Figure 6). Taken together, these findings indicate that oxidative protection induced by *P. stratiotes* under Fe excess was likely of crucial significance for plants at the highest Fe concentrations to maintain distinct physiological processes.

3.5. Conclusions

Water lettuce (*Pistia stratiotes*) display a robust set of valuable characteristics for application in the phytoremediation of Fe-contaminated sites that include: i) high Fe bioaccumulation, especially in the roots; ii) Fe capture mechanism, mainly in the apoplast of the root system; iii) apparent absence of a mechanism for element exclusion and formation of a barrier (iron plate) that would prevent further accumulation of the element; iv) robust activation of enzymatic antioxidant protection; and, v) maintenance of vital physiological processes, such as photosynthesis. Together, those aforementioned characteristics combined with its intrinsic characteristics of rapid growth and reproduction, *P. stratiotes* presents itself as a highly viable alternative for application in phytoremediation and biomonitoring programmes for Fe-contaminated sites, using visual symptoms and TBARS content as biomarkers. Further studies employing more sophisticated multi-disciplinary omic analyses, will likely be of fundamental importance in offering a holistic understanding of the mechanisms responsible for the high Fe-tolerance observed in *P. stratiotes*.

Supporting information

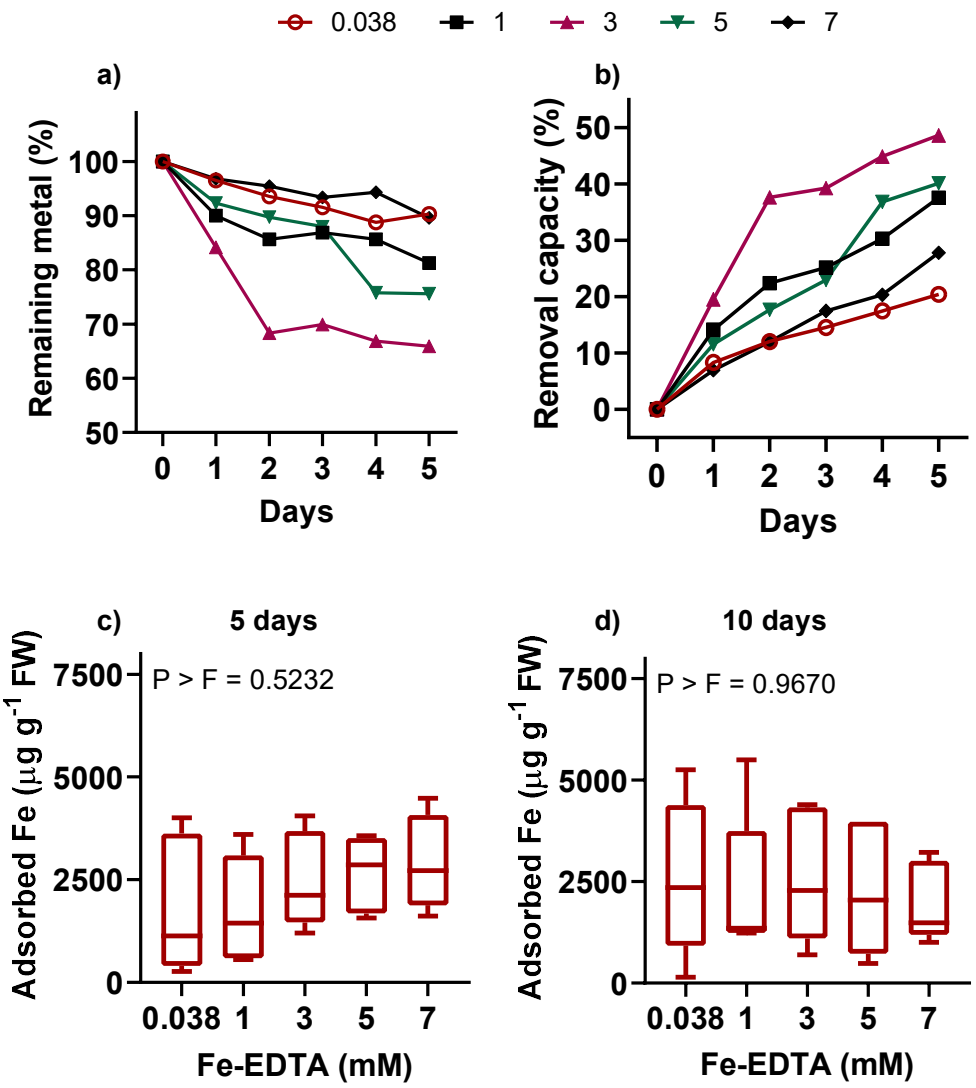

Figure S1. a) Remaining metal (%), b) removal capacity (%) and adsorbed Fe (c, d) of *Pistia stratiotes* plants growing for five days in a nutrient solution containing 0.038, 1, 3, 5, or 7 mM of Fe-EDTA. Values are presented as means of five repetitions. Adsorbed Fe in *Pistia stratiotes* plants growing for five or ten days in a nutrient solution containing 0.038, 1, 3, 5 or 7 mM of Fe-EDTA.

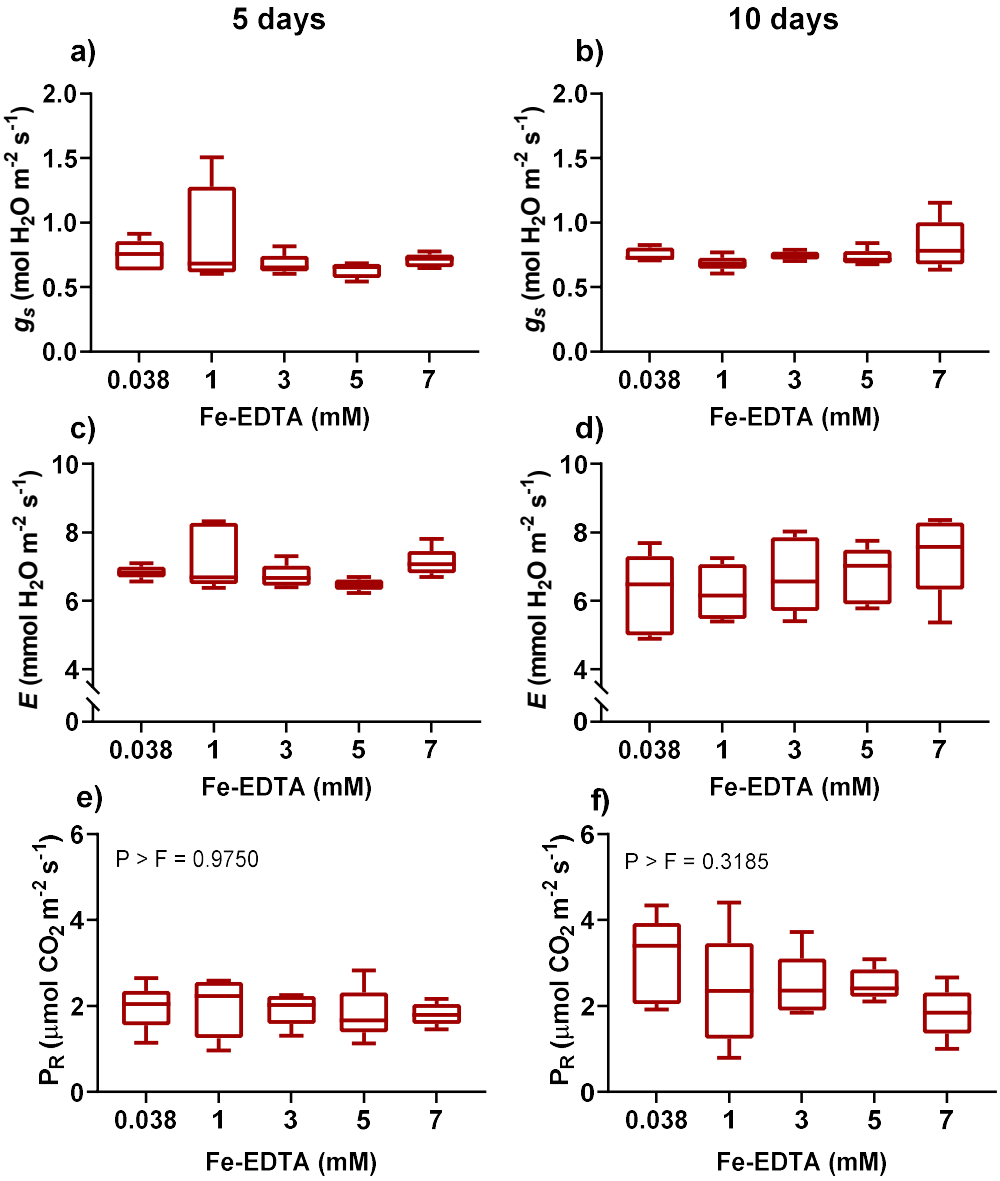

Figure S2. Stomatal conductance (a, b) transpiration rate (c, d), and photorespiration estimative (e, f) of *Pistia stratiotes* plants growing for five or ten days in a nutrient solution containing 0.038, 1, 3, 5 or 7 mM of Fe-EDTA. Regression models were estimated for the parametric data ($p \leq 0.05$), whereas nonparametric or non-significant differences between Fe concentrations ($p > 0.05$) data are presented as box-plot charts.

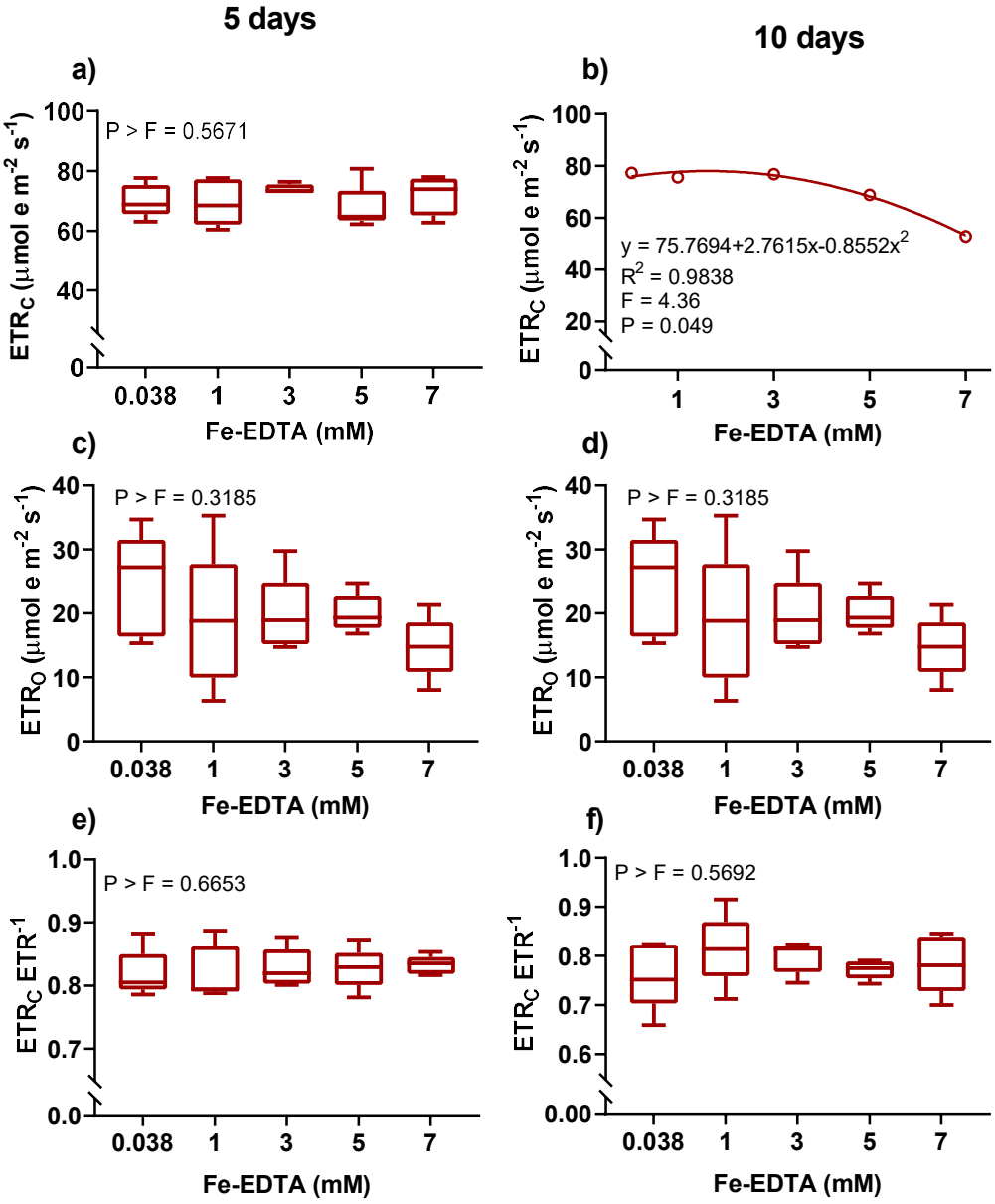

Figure S3. Apparent electron flow to RuBP carboxylation (a, b), electron flow to RuBP oxygenation (c, d), and the ratio between electron flow to RuBP carboxylation and electron transportation rate (e, f) of *Pistia stratiotes* plants growing for five or ten days in a nutrient solution containing 0.038, 1, 3, 5, or 7 mM of Fe-EDTA. Regression models were estimated for the parametric data ($p \leq 0.05$), whereas nonparametric or non-significant differences between Fe concentrations ($p > 0.05$) data are presented as box-plot charts.

References

Ahammed, G.J., Wu, M., Wang, Y., Yan, Y., Mao, Q., Ren, J., Ma, R., Liu, A., Chen, S., 2020. Melatonin alleviates iron stress by improving iron homeostasis, antioxidant defense and secondary metabolism in cucumber. Sci. Hortic. (Amsterdam). 265, 109205. https://doi.org/10.1016/j.scienta.2020.109205

Ali, S., Abbas, Z., Rizwan, M., Zaheer, I.E., Yavas, I., Ünay, A., Abdel-Daim, M.M., Bin-Jumah, M., Hasanuzzaman, M., Kalderis, D., 2020. Application of floating aquatic plants in phytoremediation of heavy metals polluted water: A review. Sustain. 12, 1–33. https://doi.org/10.3390/su12051927

Ansari, A.A., Naeem, M., Gill, S.S., AlZuaibr, F.M., 2020. Phytoremediation of contaminated waters: An eco-friendly technology based on aquatic macrophytes application. Egypt. J. Aquat. Res. 46, 371–376. https://doi.org/10.1016/j.ejar.2020.03.002

Araújo, T.O., Freitas-Silva, L., Franklin, F.M., Ribeiro, C., Kuki, K.N., Pereira, E.G., Nunes-Nesi, A., Silva, L.C., 2020a. Understanding photosynthetic and metabolic adjustments in iron hyperaccumulators grass. Theor. Exp. Plant Physiol. 32, 147–162. https://doi.org/10.1007/s40626-020-00176-9

Araújo, T.O., Freitas-Silva, L., Santana, B.V.N., Kuki, K.N., Pereira, E.G., Azevedo, A.A., da Silva, L.C., 2015. Morphoanatomical responses induced by excess iron in roots of two tolerant grass species. Environ. Sci. Pollut. Res. 22, 2187–2195. https://doi.org/10.1007/s11356-014-3488-1

Araújo, T.O., Isaure, M.P., Alchoubassi, G., Bierla, K., Szpunar, J., Trcera, N., Chay, S., Alcon, C., Campos da Silva, L., Curie, C., Mari, S., 2020b. *Paspalum urvillei* and *Setaria parviflora,* two grasses naturally adapted to extreme iron-rich environments. Plant Physiol. Biochem. 151, 144–156. https://doi.org/10.1016/j.plaphy.2020.03.014

Aung, M.S., Kobayashi, T., Masuda, H., Nishizawa, N.K., 2018. Rice HRZ ubiquitin ligases are crucial for the response to excess iron. Physiol. Plant. 163, 282–296. https://doi.org/10.1111/ppl.12698

Aung, M.S., Masuda, H., 2020. How does rice defend against excess iron?: physiological and molecular mechanisms. Front. Plant Sci. 11, 1–8. https://doi.org/10.3389/fpls.2020.01102

Aung, M.S., Masuda, H., Nozoye, T., Kobayashi, T., Jeon, J.S., An, G., Nishizawa, N.K., 2019. Nicotianamine synthesis by OsNAS3 is important for mitigating iron excess stress in rice. Front. Plant Sci. 10, 1–16. https://doi.org/10.3389/fpls.2019.00660

Bai, J., Xu, D.H., Kang, H.M., Chen, K., Wang, G., 2008. Photoprotective function of

photorespiration in *Reaumuria soongorica* during different levels of drought stress in natural high irradiance. Photosynthetica 46, 232–237. https://doi.org/10.1007/s11099-008-0037-5

Banks, J.M., 2018. Chlorophyll fluorescence as a tool to identify drought stress in Acer genotypes. Environ. Exp. Bot. 155, 118–127. https://doi.org/10.1016/j.envexpbot.2018.06.022

Bao, T., Sun, L., Sun, T., Zhang, P., Niu, Z., 2009. Iron-deficiency induces cadmium uptake and accumulation in *Solanum nigrum* L. Bull. Environ. Contam. Toxicol. 82, 338–342. https://doi.org/10.1007/s00128-008-9573-8

Bradford, M.M., 1976. A Rapid and sensitive method for the quantitation microgram quantities of protein utilizing the principle of protein-dye binding. Anal. Biochem. 72, 248–254.

Brewer, G.J., 2010. Risks of copper and iron toxicity during aging in humans. Chem. Res. Toxicol. 23, 319–326. https://doi.org/10.1021/tx900338d

Campos, F.V., Oliveira, J.A., Silva, A.A., Ribeiro, C., Farnese, F.S., 2019. Phytoremediation of arsenite-contaminated environments: is *Pistia stratiotes* L. a useful tool? Ecol. Indic. 104, 794–801. https://doi.org/10.1016/j.ecolind.2019.04.048

Campos, N. V., Araújo, T.O., Arcanjo-Silva, S., Freitas-Silva, L., Azevedo, A.A., Nunes-Nesi, A., 2016. Arsenic hyperaccumulation induces metabolic reprogramming in *Pityrogramma calomelanos* to reduce oxidative stress. Physiol. Plant. 157, 135–146. https://doi.org/10.1111/ppl.12426

Clark, R.B., 1975. Characterization of phosphatase of intact maize roots. J. Agric. Food Chem. 23, 458–460. https://doi.org/10.1021/jf60199a002

Coelho, D.G., Marinato, C.S., Matos, L.P., Andrade, H.M., da Silva, V.M., Neves, P.H.S., Oliveira, J.A., 2020. Evaluation of heavy metals in soil and tissues of economic-interest plants grown in sites affected by the Fundão dam failure in Mariana, Brazil. Integr. Environ. Assess. Manag. 0–3. https://doi.org/10.1002/ieam.4253

Das, M., Bramhanand, P.S., Laxminarayana, K., 2021. Performance and efficiency services for the removal of hexavalent chromium from water by common macrophytes. Int. J. Phytoremediation 23, 1095–1103. https://doi.org/10.1080/15226514.2021.1878104

Das, S., Das, A., Mazumder, P.E.T., Paul, R., Das, Swagata, 2021. Lead phytoremediation potentials of four aquatic macrophytes under hydroponic cultivation. Int. J. Phytoremediation 23, 1279–1288. https://doi.org/10.1080/15226514.2021.1895714

Das, U., Rahman, Md Motiur, Roy, Z.R., Rahman, Md Mominur, Kabir, A.H., 2020. Morpho-

physiological retardations due to iron toxicity involve redox imbalance rather than photosynthetic damages in tomato. Plant Physiol. Biochem. 156, 55–63. https://doi.org/10.1016/j.plaphy.2020.08.034

Eide, D., Broderius, M., Fett, J., Guerinot, M. Lou, 1996. A novel iron-regulated metal transporter from plants identified by functional expression in yeast. Proc. Natl. Acad. Sci. U. S. A. 93, 5624–5628. https://doi.org/10.1073/pnas.93.11.5624

El-Beltagi, H.S., Sofy, M.R., Aldaej, M.I., Mohamed, H.I., 2020. Silicon alleviates copper toxicity in flax plants by up-regulating antioxidant defense and secondary metabolites and decreasing oxidative damage. Sustain. 12. https://doi.org/10.3390/su12114732

Farnese, F.S., Oliveira, J.A., Gusman, G.S., Leão, G.A., Silveira, N.M., Silva, P.M., Ribeiro, C., Cambraia, J., 2014a. Effects of adding nitroprusside on arsenic stressed response of *Pistia stratiotes* L. under hydroponic conditions. Int. J. Phytoremediation 16, 123–137. https://doi.org/10.1080/15226514.2012.759532

Farnese, F.S., Oliveira, J.A., Lima, F.S., Leão, G.A., Gusman, G.S., Silva, L.C., 2014b. Evaluation of the potential of *Pistia stratiotes* L. (water lettuce) for bioindication and phytoremediation of aquatic environments contaminated with arsenic. Brazilian J. Biol. 74, 103–112. https://doi.org/10.1590/1519-6984.01113

Farnese, F.S., Oliveira, J.A., Paiva, E.A.S., Menezes-Silva, P.E., Silva, A.A., Campos, F.V., Ribeiro, C., 2017. The involvement of nitric oxide in integration of plant physiological and ultrastructural adjustments in response to arsenic. Front. Plant Sci. 8, 1–14. https://doi.org/10.3389/fpls.2017.00979

Foyer, C.H., Shigeoka, S., 2011. Understanding oxidative stress and antioxidant functions to enhance photosynthesis. Plant Physiol. 155, 93–100. https://doi.org/10.1104/pp.110.166181

Freitas-Silva, L., de Araújo, T.O., Nunes-Nesi, A., Ribeiro, C., Costa, A.C., da Silva, L.C., 2020. Evaluation of morphological and metabolic responses to glyphosate exposure in two neotropical plant species. Ecol. Indic. 113, 106246. https://doi.org/10.1016/j.ecolind.2020.106246

Galal, T.M., Eid, E.M., Dakhil, M.A., Hassan, L.M., 2018. Bioaccumulation and rhizofiltration potential of *Pistia stratiotes* L. for mitigating water pollution in the Egyptian wetlands. Int. J. Phytoremediation 20, 440–447. https://doi.org/10.1080/15226514.2017.1365343

Garbisu, C., Alkorta, I., 2001. Phytoextraction: A cost-effective plant-based technology for the removal of metals from the environment. Bioresour. Technol. 77, 229–236.

https://doi.org/10.1016/S0960-8524(00)00108-5

Gay, C., Gebicki, J.M., 2000. A critical evaluation of the effect of sorbitol on the ferric-xylenol orange hydroperoxide assay. Anal. Biochem. 284, 217–220. https://doi.org/10.1006/abio.2000.4696

Genty, B., Briantais, J.M., Baker, N.R., 1989. The relationship between the quantum yield of photosynthetic electron transport and quenching of chlorophyll fluorescence. Biochim. Biophys. Acta - Gen. Subj. 990, 87–92. https://doi.org/10.1016/S0304-4165(89)80016-9

Giannopolitis, C.N., Ries, S.K., 1977. Superoxide dismutases: I. Occurrence in higher plants. Plant Physiol. 59, 309–314. https://doi.org/10.1104/pp.59.2.309

Guan, X.Q., Zhao, S.J., Li, D.Q., Shu, H.R., 2004. Photoprotective function of photorespiration in several grapevine cultivars under drought stress. Photosynthetica 42, 31–36. https://doi.org/10.1023/B:PHOT.0000040566.55149.52

Gutteridge, J.M.C., Rowley, D.A., Halliwell, B., 1981. Superoxide-dependent formation of hydroxyl radicals in the presence of iron salts. Detection of "free" iron in biological systems by using bleomycin-dependent degradation of DNA. Biochem. J. 199, 263–265. https://doi.org/10.1042/bj1990263

Havir, E.A., Mchale, N.A., 1987. Biochemical and developmental characterization of multiple forms of catalase in tobacco leaves. Plant Physiol. 84, 450–455.

Hodges, D.M., DeLong, J.M., Forney, C.F., Prange, R.K., 1999. Improving the thiobarbituric acid-reactive-substances assay for estimating lipid peroxidation in plant tissues containing anthocyanin and other interfering compounds. Planta 207, 604–611. https://doi.org/10.1007/s004250050524

Hoffmann, W.A., Poorter, H., 2002. Avoiding bias in calculations of relative growth rate. Ann. Bot. 90, 37–42. https://doi.org/10.1093/aob/mcf140

Jayaweera, M.W., Kasturiarachchi, J.C., Kularatne, R.K.A., Wijeyekoon, S.L.J., 2008. Contribution of water hyacinth (*Eichhornia crassipes* (Mart.) Solms) grown under different nutrient conditions to Fe-removal mechanisms in constructed wetlands. J. Environ. Manage. 87, 450–460. https://doi.org/10.1016/j.jenvman.2007.01.013

Kabir, A.H., Begum, M.C., Haque, A., Amin, R., Swaraz, A.M., Haider, S.A., Paul, N.K., Hossain, M.M., 2016. Genetic variation in Fe toxicity tolerance is associated with the regulation of translocation and chelation of iron along with antioxidant defence in shoots of rice. Funct. Plant Biol. 43, 1070–1081. https://doi.org/10.1071/FP16068

Karnovsky, M.J., 1985. A formaldehyde-glutaraldehyde fixative of high osmolality for use in

electron microscopy. J. Cell Biol. 27, 137–138.

Khalid, S., Shahid, M., Niazi, N.K., Murtaza, B., Bibi, I., Dumat, C., 2017. A comparison of technologies for remediation of heavy metal contaminated soils. J. Geochemical Explor. 182, 247–268. https://doi.org/10.1016/j.gexplo.2016.11.021

Kirk, G.J.D., Manwaring, H.R., Ueda, Y., Semwal, V.K., Wissuwa, M., 2022. Below-ground plant–soil interactions affecting adaptations of rice to iron toxicity. Plant Cell Environ. https://doi.org/10.1111/pce.14199

Kryvoruchko, I.S., Routray, P., Sinharoy, S., Torres-Jerez, I., Tejada-Jiménez, M., Finney, L.A., Nakashima, J., Pislariu, C.I., Benedito, V.A., González-Guerrero, M., Roberts, D.M., Udvardi, M.K., 2018. An iron-activated citrate transporter, MtMATE67, is required for symbiotic nitrogen fixation. Plant Physiol. 176, 2315–2329. https://doi.org/10.1104/pp.17.01538

Kwak, S.S., Kim, S.K., Park, I.H., Liu, J.R., 1996. Enhancement of peroxidase activity by stress-related chemicals in sweet potato. Phytochemistry 43, 565–568. https://doi.org/10.1016/0031-9422(96)00315-9

Lapaz, A.D.M., Yoshida, C.H.P., Gorni, P.H., Freitas-Silva, L. de, Araújo, T. de O., Ribeiro, C., 2022. Iron toxicity: effects on the plants and detoxification strategies. Acta Bot. Brasilica 36, 1–9. https://doi.org/10.1590/0102-33062021abb0131

Li, Y., Xin, J., Tian, R., 2022. Physiological defense and metabolic strategy of *Pistia stratiotes* in response to zinc-cadmium co-pollution. Plant Physiol. Biochem. 178, 1–11. https://doi.org/10.1016/j.plaphy.2022.02.020

Lindsay, W.L., Schwab, A.P., 1982. The chemistry of iron in soils and its availability to plants. J. Plant Nutr. 5, 821–840. https://doi.org/10.1080/01904168209363012

Mahender, A., Swamy, B.P.M., Anandan, A., Ali, J., 2019. Tolerance of iron-deficient and -toxic soil conditions in rice. Plants 8. https://doi.org/10.3390/plants8020031

Martins, A.C., Virgolini, M.B., Tinkov, A.A., Skalny, A. V, Tirumala, R.P., Farina, M., Santamaria, A., Lu, R., Aschner, M., 2022. Iron overload and neurodegenerative diseases: What can we learn from *Caenorhabditis elegans*? Toxicol. Res. Appl. 6, 1–9. https://doi.org/10.1177/23978473221091852

Menezes-Silva, P.E., Sanglard, L.M.V.P., Ávila, R.T., Morais, L.E., Martins, S.C.V., Nobres, P., Patreze, C.M., Ferreira, M.A., Araújo, W.L., Fernie, A.R., DaMatta, F.M., 2017. Photosynthetic and metabolic acclimation to repeated drought events play key roles in drought tolerance in coffee. J. Exp. Bot. 68, 4309–4322.

https://doi.org/10.1093/jxb/erx211

Mhamdi, A., Noctor, G., Baker, A., 2012. Plant catalases: Peroxisomal redox guardians. Arch. Biochem. Biophys. https://doi.org/10.1016/j.abb.2012.04.015

Michalak, A., 2006. Phenolic compounds and their antioxidant activity in plants growing under heavy metal stress. Polish J. Environ. Stud. 15, 523–530.

Murshed, R., Lopez-Lauri, F., Sallanon, H., 2008. Microplate quantification of enzymes of the plant ascorbate-glutathione cycle. Anal. Biochem. 383, 320–322. https://doi.org/10.1016/j.ab.2008.07.020

Nakano, Y., Asada, K., 1981. Hydrogen peroxide is scavenged by ascorbate-specific peroxidase in spinach chloroplasts. Plant Cell Physiol. 22, 867–880. https://doi.org/10.1093/oxfordjournals.pcp.a076232

Ntakiyiruta, P., Briton, B.G.H., Nsavyimana, G., Adouby, K., Nahimana, D., Ntakimazi, G., Reinert, L., 2022. Optimization of the phytoremediation conditions of wastewater in post-treatment by *Eichhornia crassipes* and *Pistia stratiotes* : kinetic model for pollutants removal. Environ. Technol. 43, 1805–1818. https://doi.org/10.1080/09593330.2020.1852445

O'Brien, T.P., McCully, M.E., 1981. The study of plant structure: Principles and methods, Blackwell Scientific. Blackwell Scientific, Oxford, UK. https://doi.org/10.1111/1365-3040.ep11572627

Onaga, G., Dramé, K.N., Ismail, A.M., 2016. Understanding the regulation of iron nutrition: Can it contribute to improving iron toxicity tolerance in rice? Funct. Plant Biol. 43, 709–726. https://doi.org/10.1071/FP15305

Pawar, S., Pandit, E., Mohanty, I.C., Saha, D., Pradhan, S.K., 2021. Population genetic structure and association mapping for iron toxicity tolerance in rice. PLoS One 16, 1–19. https://doi.org/10.1371/journal.pone.0246232

Peixoto, P.H.P., Cambraia, J., Sant'Anna, R., Mosquim, P.R., Moreira, M.A., 1999. Aluminum effects on lipid peroxidation and on the activities of enzymes of oxidative metabolism in sorghum. Rev. Bras. Fisiol. Veg. 11, 137–143.

Pereira, E.G., Oliva, M.A., Rosado-Souza, L., Mendes, G.C., Colares, D.S., Stopato, C.H., Almeida, A.M., 2013. Iron excess affects rice photosynthesis through stomatal and non-stomatal limitations. Plant Sci. 201–202, 81–92. https://doi.org/10.1016/j.plantsci.2012.12.003

Pinto, S. de S., de Souza, A.E., Oliva, M.A., Pereira, E.G., 2016. Oxidative damage and

photosynthetic impairment in tropical rice cultivars upon exposure to excess iron. Sci. Agric. 73, 217–226. https://doi.org/10.1590/0103-9016-2015-0288

Quaresma, V.S., Aguiar, V.M.C., Bastos, A.C., Oliveira, K.S., Vieira, F. V., Sá, F., Baptista Neto, J.A., 2021. The impact of trace metals in marine sediments after a tailing dam failure: the Fundão dam case (Brazil). Environ. Earth Sci. 80. https://doi.org/10.1007/s12665-021-09817-x

Rai, S., Singh, P.K., Mankotia, S., Swain, J., Satbhai, S.B., 2021. Iron homeostasis in plants and its crosstalk with copper, zinc, and manganese. Plant Stress 1, 100008. https://doi.org/10.1016/j.stress.2021.100008

Rezania, S., Taib, S.M., Md Din, M.F., Dahalan, F.A., Kamyab, H., 2016. Comprehensive review on phytotechnology: Heavy metals removal by diverse aquatic plants species from wastewater. J. Hazard. Mater. 318, 587–599. https://doi.org/10.1016/j.jhazmat.2016.07.053

Richardson, D.R., Ponka, P., 1995. Identification of a mechanism of iron uptake by cells which is stimulated by hydroxyl radicals generated via the iron-catalysed Haber-Weiss reaction. Biochim. Biophys. Acta - Mol. Cell Res. 1269, 105–114. https://doi.org/10.1016/0167-4889(95)00096-B

Rout, G.R., Sahoo, S., 2015. Role of Iron in Plant Growth and Metabolism. Rev. Agric. Sci. 3, 1–24. https://doi.org/10.7831/ras.3.1

Salami, A., Papenberg, G., Sitnikov, R., Laukka, E.J., Persson, J., Kalpouzos, G., 2021. Elevated neuroinflammation contributes to the deleterious impact of iron overload on brain function in aging. Neuroimage 230, 117792. https://doi.org/10.1016/j.neuroimage.2021.117792

Santana, B.V.N., de Araújo, T.O., Andrade, G.C., de Freitas-Silva, L., Kuki, K.N., Pereira, E.G., Azevedo, A.A., da Silva, L.C., 2014. Leaf morphoanatomy of species tolerant to excess iron and evaluation of their phytoextraction potential. Environ. Sci. Pollut. Res. 21, 2550–2562. https://doi.org/10.1007/s11356-013-2160-5

Schopfer, P., 2002. Hydroxyl radical-induced cell-wall loosening in vitro and in vivo: implications for the control of elongation growth. Plant J. 28, 679–688. https://doi.org/10.1046/j.1365-313x.2001.01187.x

Silva, L.C. Da, Oliva, M.A., Azevedo, A.A., Araújo, J.M. De, 2006. Responses of restinga plant species to pollution from an iron pelletization factory. Water. Air. Soil Pollut. 175, 241–256. https://doi.org/10.1007/s11270-006-9135-9

Skinner, K., Wright, N., Porter-Goff, E., 2007. Mercury uptake and accumulation by four species of aquatic plants. Environ. Pollut. 145, 234–237. https://doi.org/10.1016/j.envpol.2006.03.017

Stein, R.J., Lopes, S.I.G., Fett, J.P., 2014. Iron toxicity in field-cultivated rice: Contrasting tolerance mechanisms in distinct cultivars. Theor. Exp. Plant Physiol. 26, 135–146. https://doi.org/10.1007/s40626-014-0013-3

Suh, H.-J., Sook Kim, C., Lee, J.-Y., Jung, J., 2002. Photodynamic effect of iron excess on Photosystem II function in pea plants. Photochem. Photobiol. 75, 513. https://doi.org/10.1562/0031-8655(2002)075<0513:peoieo>2.0.co;2

Taylor, G.J., Crowder, A.A., 1983. Uptake and accumulation of heavy metals by *Typha latifolia* in wetlands of the Sudbury, Ontario region. Can. J. Bot. 61, 63–73. https://doi.org/10.1139/b83-005

Teixeira, S., Vieira, M.N., Marques, J.E., Pereira, R., 2014. bioremediation of an iron-rich mine effluent by *Lemna minor*. Int. J. Phytoremediation 16, 1228–1240. https://doi.org/10.1080/15226514.2013.821454

Terry, N., Abadia, J., 1986. Function of iron in chloroplasts. J. Plant Nutr. 9, 609–646. https://doi.org/10.1080/01904168609363470

Tewari, R.K., Kumar, P., Neetu, Sharma, P.N., 2005. Signs of oxidative stress in the chlorotic leaves of iron starved plants. Plant Sci. 169, 1037–1045. https://doi.org/10.1016/j.plantsci.2005.06.006

Varotto, C., Maiwald, D., Pesaresi, P., Jahns, P., Salamini, F., Leister, D., 2002. The metal ion transporter IRT1 is necessary for iron homeostasis and efficient photosynthesis in Arabidopsis thaliana. Plant J. 31, 589–599. https://doi.org/10.1046/j.1365-313X.2002.01381.x

Vergilio, C. dos S., Lacerda, D., Oliveira, B.C.V. de, Sartori, E., Campos, G.M., Pereira, A.L. de S., Aguiar, D.B. de, Souza, T. da S., Almeida, M.G. de, Thompson, F., Rezende, C.E. de, 2020. Metal concentrations and biological effects from one of the largest mining disasters in the world (Brumadinho, Minas Gerais, Brazil). Sci. Rep. 10, 1–12. https://doi.org/10.1038/s41598-020-62700-w

Veselý, T., Tlustoš, P., Száková, J., 2011. The use of water lettuce (*Pistia stratiotes* L.) for rhizofiltration of a highly polluted solution by cadmium and lead. Int. J. Phytoremediation 13, 859–872. https://doi.org/10.1080/15226514.2011.560214

Viktorinova, A., Durfinova, M., 2021. Mini-Review: Is iron-mediated cell death (ferroptosis)

an identical factor contributing to the pathogenesis of some neurodegenerative diseases? Neurosci. Lett. 745, 135627. https://doi.org/10.1016/j.neulet.2021.135627

Weinberg, E.D., 1997. The lactobacillus anomaly: Total iron abstinence. Perspect. Biol. Med. 40, 578–583. https://doi.org/10.1353/pbm.1997.0072

Wellburn, A.R., 1994. The spectral determination of chlorophylls a and b, as well as total carotenoids, using various solvents with spectrophotometers of different resolution. J. Plant Physiol. 144, 307–313. https://doi.org/10.1016/S0176-1617(11)81192-2

Werner, C., Correia, O., Beyschlag, W., 2002. Characteristic patterns of chronic and dynamic photoinhibition of different functional groups in a Mediterranean ecosystem. Funct. Plant Biol. 29, 999–1011. https://doi.org/10.1071/PP01143

Winder, T.L., Nishio, J.N., 1995. Early iron deficiency stress response in leaves of sugar beet. Plant Physiol. 108, 1487–1494. https://doi.org/10.1104/pp.108.4.1487

Ye, Y.Q., Jin, C.W., Fan, S.K., Mao, Q.Q., Sun, C.L., Yu, Y., Lin, X.Y., 2015. Elevation of NO production increases Fe immobilization in the Fe-deficiency roots apoplast by decreasing pectin methylation of cell wall. Sci. Rep. 5, 1–13. https://doi.org/10.1038/srep10746

Zhang, J., Qian, Y., Chen, Z., Amee, M., Niu, H., Du, D., Yao, J., Chen, K., Chen, L., Sun, J., 2020. Lead-induced oxidative stress triggers root cell wall remodeling and increases lead absorption through esterification of cell wall polysaccharide. J. Hazard. Mater. 385, 121524. https://doi.org/10.1016/j.jhazmat.2019.121524

4. Chapter 3 - Acknowledging *Pistia stratiotes* as a tolerant and hyperaccumulator species for phytoremediation of manganese-contaminated water[1]

[1]Edited in accordance with *Aquatic Botany* guidelines

Abstract: Effective phytoremediation of manganese (Mn) contaminated water requires the selection of Mn-tolerant species. We herein reported physiological changes and bioaccumulation of Mn in the aquatic macrophyte *Pistia stratiotes* subjected to Mn excess. Plants were grown in nutrient solution at 7 concentrations of Mn (7 - control; 80; 340; 600; 1000; 2000 and 4000 μM $MnCl_2$). Initial visual symptoms of Mn toxicity were noted, such as dark spots on leaf margins after 10 days, especially for plants treated with 2000 and 4000 μM $MnCl_2$. Although biomass accumulation was not significantly affected in shoots and roots by Mn-stress, there was a reduction in RGR at 10 days. The plants also accumulated high amounts of Mn, with maximum values of 23,700 and 24,600 μg g^{-1} DW in shoots and roots of plants subjected to 4000 μM Mn, respectively. Interestingly, about 90% of the Mn in the roots was detected in the apoplast, supporting the translocation of the element. With these results, it was found that there is a high translocation of Mn to shoots, with TF values close to 1. Manganese concentrations from 1000 μM promoted a decrease of chlorophyll *a* after 5 days and also a decrease of chlorophylls and carotenoids after 10 days of treatments. Similarly, Mn-treated plants showed decreased photochemical efficiency, as observed by the lower effective quantum yield (ϕPSII). Nevertheless, *P. stratiotes* plants showed no significant changes in net CO_2 assimilation and respiratory rates at 5 and 10 days growing under Mn treatments. Together, our results demonstrate that *P. stratiotes* is a Mn hyperaccumulator species with a high potential for phytoremediation, showing great bioaccumulation capacity and efficient strategies to maintain the photosynthetic rate.

Keywords: Manganese toxicity; decontamination; water pollution; heavy metals.

4.1. Introduction

Manganese (Mn) occurs ubiquitously in the environment as the third most abundant transition metal in the earth's crust and is largely used in many industrial sectors, applied in steel and metallurgy. Although Mn was in the past not considered a metal that significantly pollutes the environment, the increase in its concentration in water and soils resulting from human activities has become a global concern in recent times (Neculita and Rosa, 2019). Accumulation of Mn has converged in water bodies over the previous several decades as a result of indiscriminate sewage discharge from industry activities, reaching concentrations in the range of 100–400 mg L^{-1} worldwide (Aguiar et al., 2013; Tobiason et al., 2016). In Brazil, long-term mining exploration and recent disasters involving the disruption of mining tailing dams increased the concentration of Mn oxides and soluble Mn^{2+} in the affected areas (Carvalho et al., 2017; Vergilio et al., 2020).

Although the removal of Mn from drinking water is usually motivated by aesthetic and potential distribution system challenges, rather than public health concerns, several studies have been pointing out that exposure to excess Mn in humans leads to serious health problems, including reproductive, immune, and neurological disorders (Budinger et al., 2021; Neculita and Rosa, 2019; Roels et al., 2012). Therefore, some efforts have been made to establish a well-defined regulatory framework on acceptable standards for Mn in drinking water (Tobiason et al., 2016). For instance, the United States Environmental Protection Agency (USEPA) published a secondary maximum contaminant level (SMCL) of 0.05 mg L^{-1} and a lifetime health advisory level of 0.3 mg L^{-1} for Mn (Tobiason et al., 2016). Likewise, Brazilian legislation (CONAMA 357/2005) allows a maximum of 0.1 mg L^{-1} of Mn for class I water (for human supply after simplified treatment) and 1.0 mg L^{-1} for wastewater (Vergilio et al., 2020).

Considering ecological and health risks of Mn pollution in freshwater ecosystems, a wide range of physical, chemical, and biological methods, as well as combined approaches have been applied to provide a successful Mn removal (Neculita and Rosa, 2019). Phytoremediation, which uses the natural abilities of plants to stabilize or extract and accumulate the pollutants in their tissues, is attracting more attention from governments and enterprises due to its cost-effectiveness and environmental friendliness (Wei et al., 2021). Nevertheless, the selection of species is usually a critical step for application in large-scale phytoremediation programs, as the plant should assemble tolerance to the pollutant together with hyperaccumulation, high biomass, fast growth and adaptation to different environmental conditions (Rezania et al., 2016).

Despite being an essential nutrient for plant nutrition and involved in several redox processes, including the role in the oxygen-evolving complex and the activation of around 35 enzymes (Schmidt et al., 2016), excess Mn induces metabolic, nutritional and redox disturbances (Bai et al., 2021; Rajpoot et al., 2021). Mn stress causes energy flow disruption, limitation of stomatal conductance and impaired oxygen-evolving photosynthetic machinery, resulting in oxidative stress as a consequence of reactive oxygen species overproduction (Millaleo et al., 2010). However, several plant species are known to have the capacity to accumulate high quantities of Mn without showing serious toxicity symptoms and physiological impairments, by displaying a robust antioxidant system as well as chelating-based exclusion and compartmentalization mechanisms (Alejandro et al., 2020; Li et al., 2019).

For terrestrial plants, around 24 species are known as hyperaccumulators because they can accumulate Mn in concentrations from 10,000 μg g^{-1} on a dry weight basis (DW) in the tissues (Magri et al., 2020; Reeves et al., 2018). On the other hand, only a few studies discuss the application of aquatic or wetland species for the phytoremediation of water bodies (Haokip and Gupta, 2021; Hua et al., 2012). In a comparative study with water hyacinth (*Eichhornia crassipes* (Mart.) Solms), water lettuce (*Pistia stratiotes* L.) and alligator alternanthera (*Alternanthera philoxeroides*), three macrophyte species often employed in phytoremediation, water lettuce had greater bioaccumulation of Mn, indicating standout potentials for cleaning-up Mn-contaminated environments (Hua et al., 2012). However, the physiological and biochemical mechanisms for the tolerance to the element are poorly understood, and a comprehensive study for bioaccumulation of Mn in this species remains to be performed.

Therefore, we investigated the bioaccumulation, phytoremediation potential and physiological responses of *P. stratiotes* subjected to Mn stress in different concentrations. We found a great Mn accumulation in both leaves and roots of the plant, along with maintenance of photosynthetic rates, which are excellent indicators of tolerance and phytoremediation potential of the species.

4.2. Material and methods

Plant material and treatments

Water lettuce [*Pistia stratiotes* L. (Araceae)] plants collected in non-polluted dams in the Botanical Garden of the Universidade Federal de Viçosa, Brazil (20°45′25.0″ S; 42°52′25.5″ W) were used in this study. The plants with approximately 10 g were washed and transferred to Clark's nutrient solution (Clark, 1975) ½ ionic strength, pH 6.5, in a growth

chamber with controlled temperature and light (25 ± 2 °C, 200 μmol s^{-1} m^{-2}, 12h/12h dark/light photoperiod). After three days of acclimatization, uniform plants were weighed and transferred to individual pots in a completely randomized design containing one of the following concentrations of $MnCl_2$: 7 (control - only nutrient solution ½ strength) 80; 340; 600; 1000; 2000 or 4000 μM, with five repetitions per treatment. These concentrations are equivalent to 0.38 – 220 mg L^{-1} in consonance with several studies investigating Mn stress in plants and also with concentrations of the element in polluted sites (Coelho et al., 2020; Costa et al., 2017; Hua et al., 2012; Liu et al., 2021). The plants remained under treatments for 5 or 10 days for further evaluation.

Growth and bioaccumulation analyses

Before starting the experiments and after five and ten days, the fresh weight of plants was determined. Shoots and roots of the plants were placed in a 60 ºC oven for drying. In possession of the plant dry mass on the evaluated days, the percentage of dry mass and the initial dry mass were estimated. Then, the relative growth rate was calculated, according to the following equation proposed by Hoffmann and Poorter (2002).

$$\text{i) } RGR = \frac{(\ln W2 - \ln W1)}{(t2 - t1)}$$

where ln W1 and ln W2 are the means of the natural logarithm-transformed plant dry weights and t2 and t1 are the final and initial times (days).

The dried plant material was homogenized and about 100 mg of the dry mass was mineralized in 1.5 mL of nitroperchloric mixture (2:1). The extract was used in the determination of Mn content by atomic absorption spectrophotometry (Shimadzu AA-6701F, Shimadzu Corporation, Tokyo, Japan).

The determination of Mn concentration in root symplast and apoplast fractions were determined according to Lavres Junior et al. (2008), modified by Furlan et al. (2020). In summary, two longitudinal sections of fresh roots of equivalent masses were separated: the first one was immersed in 150 mL of the "desorption" solution (0.5 mM $CaCl_2$, 2 mM $CuCl_2$, and 100 mM HCl) at 4 ºC for 30 min for determination of the symplast concentration, and the other one was not immersed for the determination of total Mn. After that, the two root sections were washed in deionized water, dried and mineralized as described previously. The Mn concentration in the apoplast was calculated as the total Mn concentration minus Mn concentration in the symplast (root part immersed in the desorption solution).

The bioconcentration factor (BCF), translocation factor (TF) and rhizofiltration potential (RP) for Mn were calculated according to the following equations (Bao et al., 2009; Veselý et al., 2011).

$$\text{i) BCF} = \frac{\text{Element concentration in the plant } (\mu g\ g^{-1}\ DW)}{\text{Element concentration in the medium } (mg\ L^{-1})}$$

$$\text{ii) TF} = \frac{\text{Element in shoots } (\mu g\ g^{-1} DW)}{\text{Element in roots } (\mu g\ g^{-1}\ DW)}$$

$$\text{iii) RP} = \left(\frac{C_{shoot} * M_{shoot}}{M_{total}} + \frac{C_{roots} * M_{roots}}{M_{total}}\right) * M_{plant}$$

Where: M_{shoot} and M_{roots} is the shoot and root dry biomass, (g), respectively; M_{total} is the total (shoot and roots) dry biomass (g); C_{shoot} and C_{roots} is the concentration of Mn in shoot and root ($\mu g\ g^{-1}$ DW), respectively; and M_{plant} is equal to 2919.75, the annual mean of *P. stratiotes* yield (g DW m^{-2} $year^{-1}$).

Biochemical analyses

The analyzes of oxidative metabolism were performed in the control plants and compared to the highest Mn concentration (4 mM). The extract for determination of the activity of antioxidant enzymes was obtained according to Peixoto et al. (1999). Briefly, 20 mg of freeze-dried and grounded tissues were homogenized in extraction buffer containing 0.1 M potassium phosphate buffer pH 6.8, 0.1 mM EDTA disodium salt, 1 mM phenylmethylsulfonyl fluoride (PMSF) and 1% polyvinylpyrrolidone (PVPP). The homogenate was centrifuged for 15 min at 15,000 x*g* at 4 ºC and the supernatant was collected for the analysis.

The activity of the enzyme superoxide dismutase (SOD, EC. 1.15.1.1) was determined according to Giannopolitis and Ries (1977). One unit of SOD was defined as the amount of enzyme required to inhibit nitroblue tetrazolium reduction by 50%. The catalase (CAT, EC. 1.11.1.6) activity was determined by incubating enzymatic extract in 50 mM phosphate buffer, pH 6.8, containing 20 mM H_2O_2. Enzyme activity was estimated from measurements of H_2O_2 consumption at 240 nm (Havir and McHale, 1987). The determination of peroxidase (POX, EC. 1.11.1.7) activity in the extract was measured through the production of purpurogallin in presence of 20 mM H_2O_2 and 800 mM pyrogallol. Peroxidase activity was calculated based on the molar extinction coefficient of 2.47 mM^{-1} cm^{-1} and expressed in µmol purpurogallin min^{-1} mg^{-1} protein (Kwak et al., 1996). Finally, ascorbate peroxidase (APX, EC. 1.11.1.11) assay was carried out according to Nakano and Asada (1981), modified by Murshed et al. (2008), in a

reaction medium containing 50 mM phosphate buffer (pH 6.0), 0.54 mM ascorbic acid and 200 mM H_2O_2. The ascorbate oxidation rate was monitored at 290 nm and the activity was calculated based on the molar extinction coefficient of 2.8 mM^{-1} cm^{-1}. The total protein content in the leaf and root samples was determined according to the method of Bradford (1976).

Lipid peroxidation was measured by the thiobarbituric acid reactive substances (TBARS) test, according to the protocol described by Hodges et al. (1999), using the molar extinction coefficient ($\varepsilon = 0.155$ M^{-1} cm^{-1}). The H_2O_2 content was determined according to the protocol proposed by Gay and Gebicki (2000), using 250 µM xylenol orange as an indicator, and the concentrations were estimated from a calibration curve prepared with H_2O_2 standards.

Photosynthesis-related parameters

The chlorophyll *a* and *b* and carotenoids contents were determined by incubating three leaf discs (1 cm diameter) in 2 mL of dimethylsulfoxide (DMSO) solution. After 24 hours, the tubes were incubated in a water bath at 65 °C for 45 minutes. The absorbances were taken at wavelengths 665, 649, and 480 nm and used to calculate the contents of the pigments, as proposed by Wellburn (1994).

Gas exchange and fluorescence of chlorophyll *a* measurements were performed using an open-flow infrared gas exchange analyzer system (LI-6400XT; LI-COR) equipped with an integrated fluorescence chamber (LI-6400-40; LI-COR). In dark-acclimated leaves, the minimal fluorescence (F_0) was obtained via the excitation with a modulated red light of low intensity (0.03 µmol photon m^{-2} s^{-1}), followed by application of light saturating pulses of 8000 µmol photon m^{-2} s^{-1} to obtain maximum fluorescence (F_m). The potential quantum yield of the photosystem II was calculated (F_v/F_m) using the variable fluorescence (F_v), determined by the difference between F_0 and F_m (Genty et al., 1989). The ratio F_0/F_m was also calculated, as recommended by Banks (2018). The respiration in the darkness (R_N) was measured before dawn using the infrared-gas analyzer mentioned above. The photorespiratory rate (P_R) and the electron flow to RuPB carboxylation (ETR_C) and oxygenation (ETR_O) were estimated using the following equations (Bai et al., 2008; Guan et al., 2004):

i) $P_R = 1/12\ [ETR - 4 \times (A + R_D)]$;

ii) $R_D = R_N \times Q_{10}^{(Td-Tn)/10}$ (with $Q_{10} = 2.2$, Td: leaf temperature; Tn: leaf temperature at dawn, R_N: respiratory rate)).

iii) $ETR_C = 1/3\ [ETR + 8 \times (A + R_D)]$;

iv) $ETR_O = 2/3\ [ETR - 4 \times (A + R_D)]$

Two hours after the beginning of light period, the light-saturated net CO_2 assimilation rate (A), internal CO_2 concentration (Ci), stomatal conductance (g_s), and transpiration rate (E) were measured on fully expanded leaves. The leaves were placed in a 2 cm^2 leaf chamber at 25 °C, using a flow rate of 300 mol s^{-1}, a 0.5 stomatal ratio (amphistomatic leaves), under saturating light at leaf level (1000 µmol photon m^{-2} s^{-1}; 10% blue light) and 400 µmol CO_2 mol^{-1} air.

Simultaneously, the transient fluorescence (F_s) and maximal fluorescence (Fm') were obtained in actinic light (1000 µmol photon m^{-2} s^{-1}) acclimated leaves, followed by a saturating light pulse. After that, the actinic light was switched off, and far-red illumination was applied to measure the light-adapted initial fluorescence (F_0'). These parameters were used to estimate the actual PSII photochemical efficiency (ΦPSII) and the non-photochemical quenching (NPQ), according to Genty et al. (1989).

Data analysis

The data were submitted to Shapiro–Wilk test ($p > 0.05$) to check for normal distribution of the data and Bartlett's test ($p > 0.05$) to check for equal variances across samples. Where data failed on the Shapiro–Wilk test, a Box–Cox transformation [$T(Y) = (Y\lambda - 1)/\lambda$] was performed to obtain the normal distribution. Parametrical data were submitted to ANOVA and regression models were adjusted. For nonparametrical or non-fitting model data, dispersion data is presented as box-plots. All statistical tests were performed using R software, version 3.6.2.

4.3. Results

General appearance and bioaccumulation

Water lettuce plants growing in low Mn concentrations (from 7 to 340 µM $MnCl_2$) remained visually healthy, without symptoms of toxicity in the leaves, regardless the time-point (Figure 1). The increase of Mn concentration in nutrient solution from 600 µM induced a few chlorotic points of leaf margins at ten days. These symptoms became subtly more intense at concentrations of 2000 and 4000 µM, with chlorosis in the leaf blade (Figure 1). Individually, the biomass of leaves and roots was also not significantly impacted by the increase in Mn concentrations (Figure 2 a–d). Nevertheless, the relative growth rate (RGR) decreased linearly

at ten days of treatment with increasing element concentration in the nutrient solution (Figure 2f), which was not observed at five days (Figure 2e).

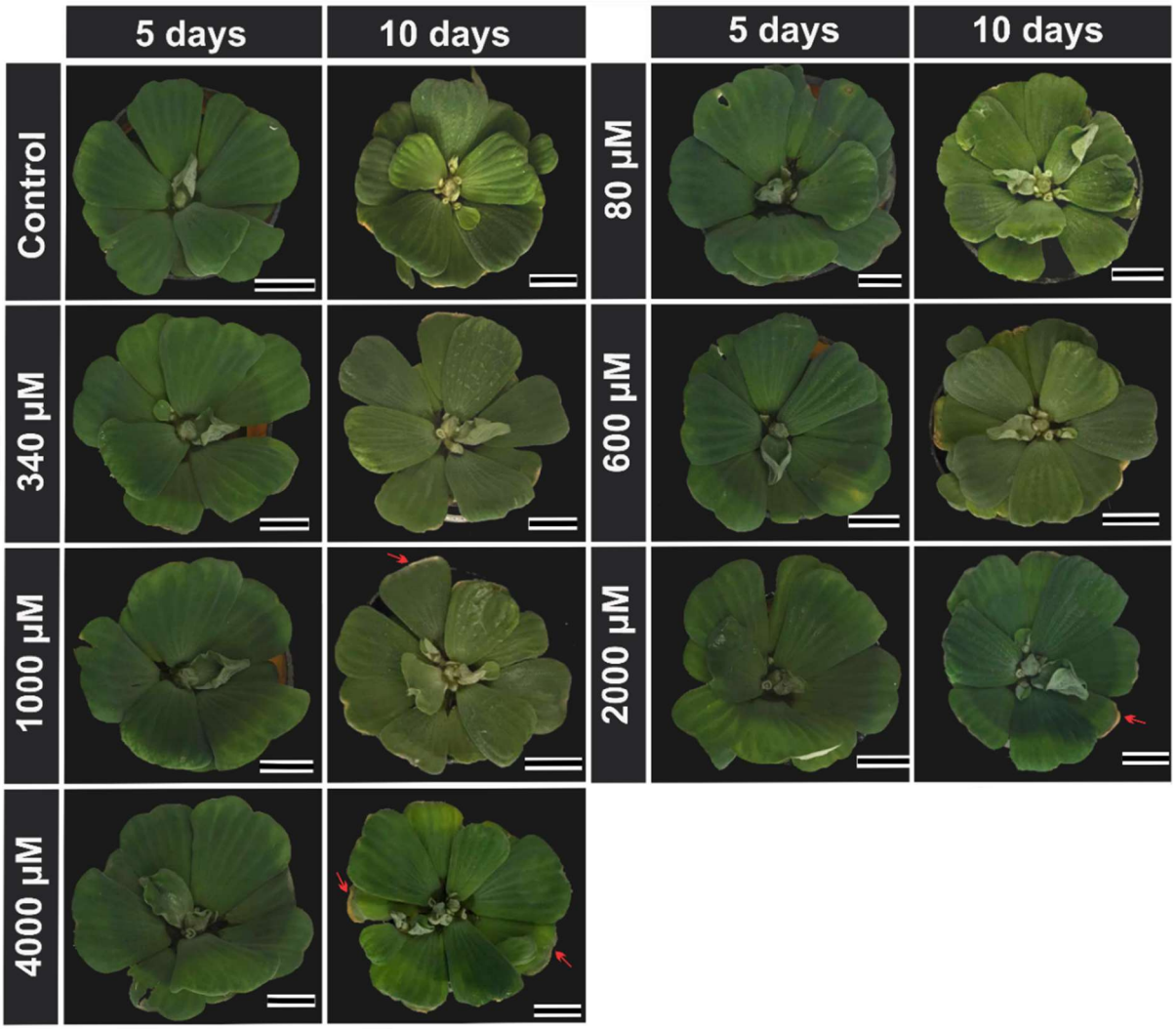

Figure 1. General appearance of *Pistia stratiotes* plants growing under different concentrations of $MnCl_2$. Representative images of *P. stratiotes* plants growing for 5 or 10 days in a nutrient solution containing 7; 80; 340; 600; 1000; 2000; and 4000 µM $MnCl_2$. Red arrows highlight Mn toxicity symptoms such as chlorosis on leaf margins.

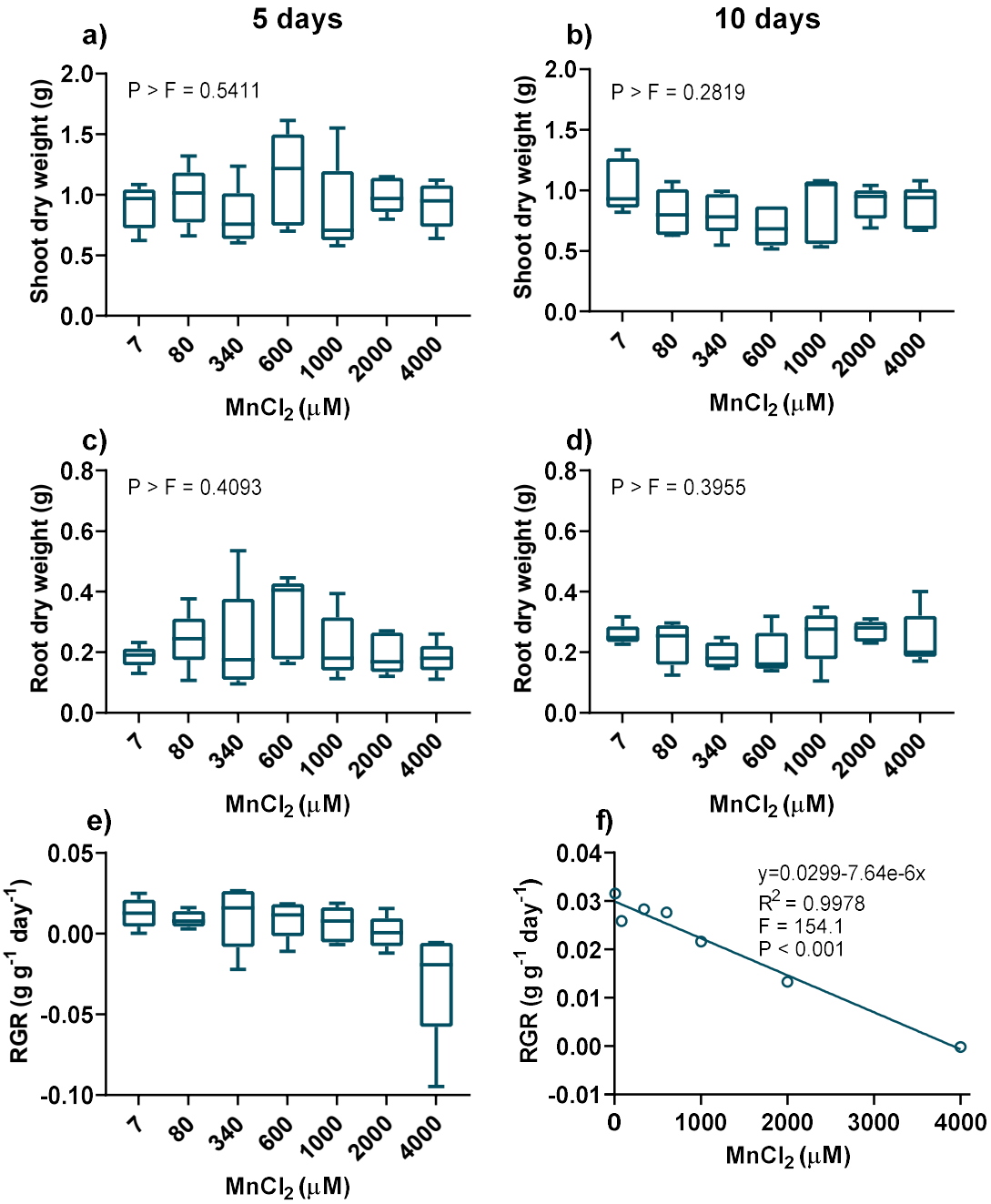

Figure 2. Growth of *Pistia stratiotes* plants growing under different concentrations of $MnCl_2$. Shoot dry weight (a, b), root dry weight (c, d), and relative growth rate (e, f) of *P. stratiotes* plants growing for 5 or 10 days in a nutrient solution containing 7; 80; 340; 600; 1000; 2000; and 4000 µM $MnCl_2$. Regression models were estimated for the parametric data ($p \leq 0.05$), whereas nonparametric or non-significant data are presented as box-plot charts.

The accumulation of Mn was evaluated in shoots, roots, as well as in the symplast and apoplast fractions of roots (Figure 3a-f). The plants were able to accumulate concentrations higher than 10,000 µg g^{-1} DW in both shoots and roots already after 5 days of treatment with

2000 µM $MnCl_2$ (Figure 3a, c). The shoot concentration in plants at five days increases following a cubic model according the Mn concentration in nutrient solution (Figure 3a). At ten days, the mean Mn concentration in shoots also increases in plants growing in higher concentration of $MnCl_2$, reaching around 24,000 µg g^{-1} DW (Figure 3b). Due to the nonparametric data, it was not possible to adjust a regression model for the concentration of Mn in the roots at both time points (Figure 3c, d). There was a tendency to increase the Mn concentration in the roots according to the increase in the concentration of the element in the nutrient solution (Figure 3c, d). After 10 days, the mean value for Mn concentration in roots of 4000 µM-treated plants was close to 25,000 µg g^{-1} DW (Figure 3d). Fractionation in the symplast and apoplast portions of the root showed that the largest proportion of Mn accumulated in the plant is restricted to the apoplast (Figure 3e, f). In the control condition, about 90% of the Mn was found in the apoplast after 5 days, while after 10 days this portion reduced to 68.5%. On the contrary, in plant roots growing at high Mn concentration (4000 µM), the apoplastic fraction corresponds to about 86% at both time-points (Figure 3e, f).

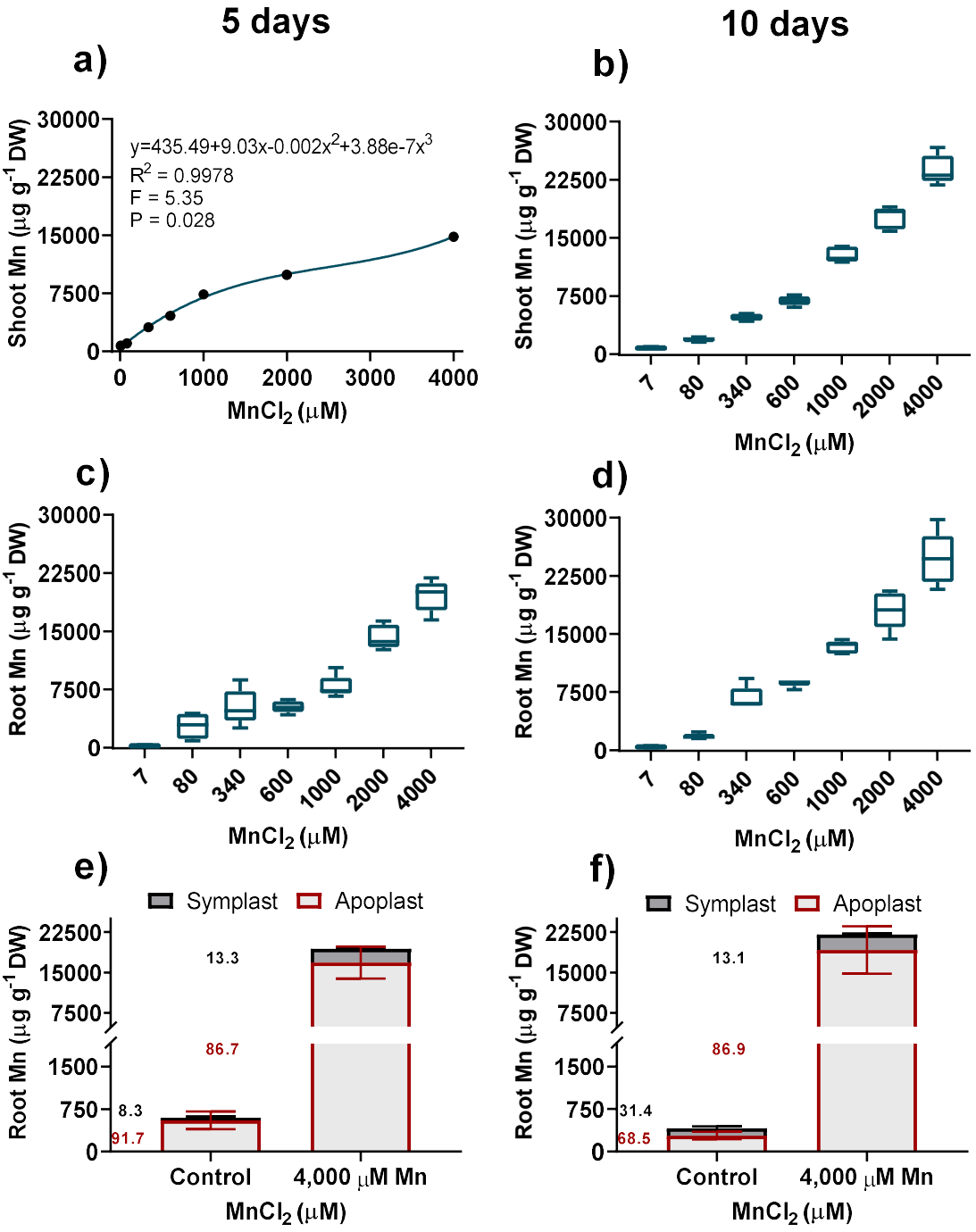

Figure 3. Bioaccumulation of Mn in *Pistia stratiotes* plants growing under different concentrations of $MnCl_2$. Concentration of Mn in shoots (a, b), roots (c, d), and apoplast and symplast fractions of roots (e, f) of *P. stratiotes* plants growing for 5 or 10 days in a nutrient solution containing 7; 80; 340; 600; 1000; 2000; and 4000 µM $MnCl_2$. Red arrows highlight Mn toxicity symptoms such as chlorosis on leaf margins. Regression models were estimated for the parametric data ($p \leq 0.05$), whereas nonparametric or non-significant data are presented as box-plot charts.

The bioconcentration factor (BCF) of Mn in plants reached stable levels from the concentration of 80 µM, with values between 400 to 150 at 5 days and between 550 and 220 at 10 days (Figure 4a, b). The translocation of Mn from roots to shoots was quite high in the control plants, reaching a translocation factor (TF) close to 4 at 5 days and around 2 after 10 days (Figure 4c, d). In plants treated with additional concentrations of Mn, the FT was close to 1 at both time points, also indicating a high translocation of the element, with a similar partition between roots and shoots (Figure 4c, d). Regarding the rhizofiltration potential (RP), there was an increase according to the increase in the concentration of Mn in the solution, reaching values close to 70,000 in the highest concentration, after ten days (Figure 4e, f).

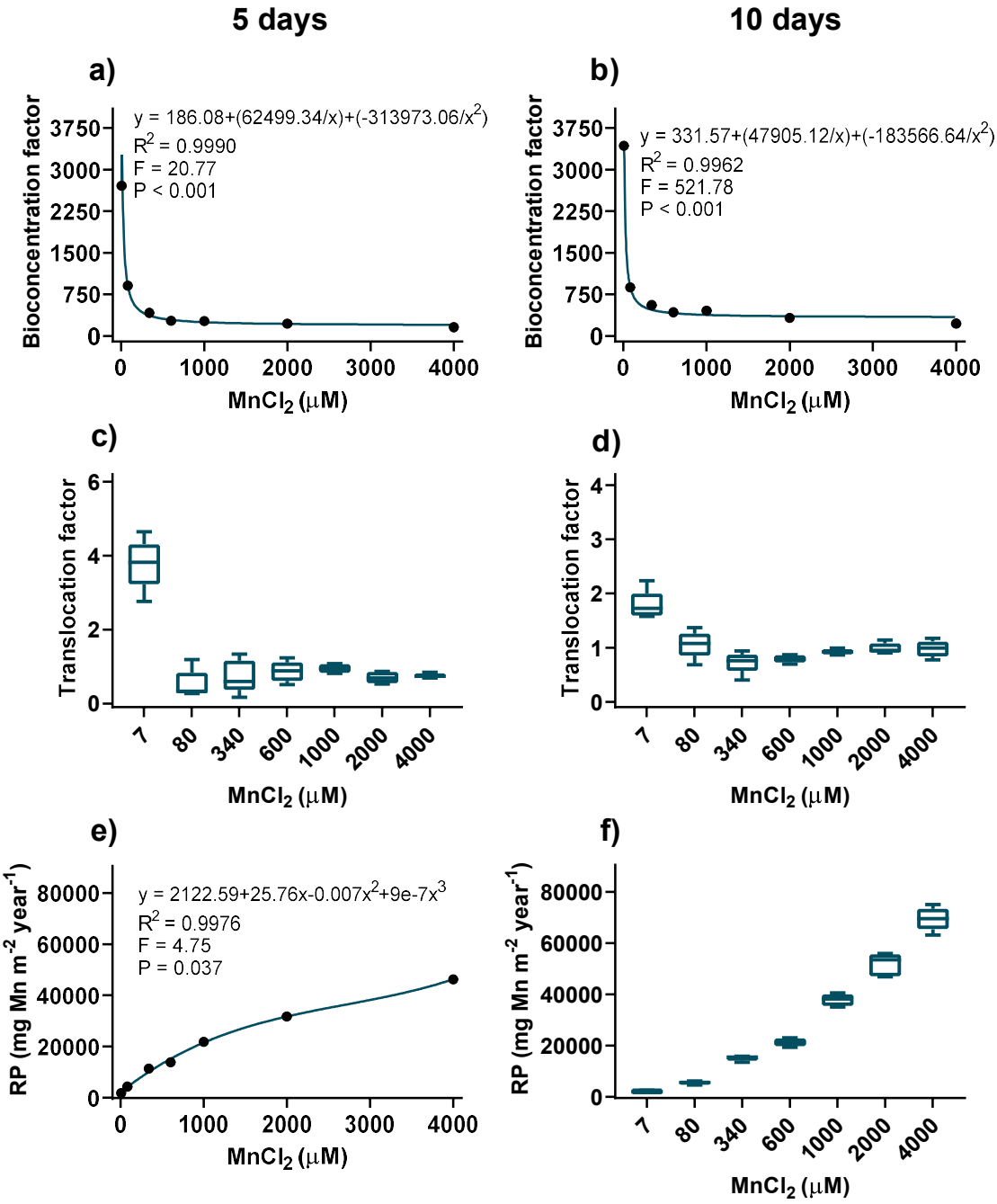

Figure 4. Phytoremediation indexes of *Pistia stratiotes* plants growing under different concentrations of $MnCl_2$. Bioconcentration factor (a, b), translocation factor (c, d), and rhizofiltration potential (e, f) of *P. stratiotes* plants growing for five or ten days in a nutrient solution containing 7; 80; 340; 600; 1000; 2000; and 4000 µM $MnCl_2$. Regression models were estimated for the parametric data ($p \leq 0.05$), whereas nonparametric or non-significant data are presented as box-plot charts.

Oxidative metabolism

The quantification of biomarkers for oxidative stress and the activity of ROS scavenging enzymes were performed in plants subjected to control Mn level and compared to those growing under Mn excess condition of 4000 µM $MnCl_2$ (Table 1). The activity of SOD in shoots was induced in 4000 µM -treated plants in both time-points, whereas CAT activity was not changed by Mn concentration (Table 1). The POX and APX activities were increased by approximately 2.5 times in shoots of plants subjected to Mn stress after 10 days (Table 1). An increase in the lipid peroxidation in shoots, measured by TBARS contents, was also induced in similar conditions, whereas increased H_2O_2 were detected in both time-points for Mn-treated plants (Table 1). Interestingly, no changes were detected in roots, regardless Mn treatment or time of exposure (Table 1).

Table 1. Activity of superoxide dismutase (SOD - U min^{-1} mg^{-1} protein), catalase (CAT - µmol H_2O_2 min^{-1} mg^{-1} protein), peroxidase (POX - µmol purpurogallin min^{-1} mg^{-1} protein), ascorbate peroxidase (APX - µmol AsA min^{-1} mg^{-1} protein), and thiobarbituric acid-reactive substances (nmol g^{-1} FW) and peroxide (H_2O_2 - nmol g^{-1} FW) contents in shoots and roots of *Pistia stratiotes* plants growing for 5 or 10 days under control or Mn-stress (4000 µM $MnCl_2$) conditions. Asterisks represent statistical differences between control and Mn-stressed plants in the same time-point according to Welch Two Sample t-test at 5 (*) or 1% (**) of significance.

	SOD	**CAT**	**POX**	**APX**	**TBARS**	**H_2O_2**
			Shoot			
			5 days			
Control	9.97 ± 2.29	10.24 ± 2.61	1.89 ± 0.69	0.68 ± 0.12	12.85 ± 1.32	55.61 ± 2.76
4000 µM Mn	20.54 ± 2.36*	11.11 ± 3.35^{ns}	1.50 ± 0.49^{ns}	0.55 ± 0.15^{ns}	16.31 ± 2.21^{ns}	69.37 ± 4.07*
			10 days			
Control	10.25 ± 1.66	21.30 ± 5.32	1.66 ± 0.46	0.44 ± 0.15	14.03 ± 1.75	42.12 ± 3.28
4000 µM Mn	16.74 ± 0.95*	13.14 ± 4.36^{ns}	4.25 ± 0.32**	1.20 ± 0.14**	29.52 ± 5.26*	61.26± 2.41**
			Root			
			5 days			
Control	16.11 ± 1.56	4.27 ± 1.08	7.63 ± 1.31	4.12 ± 0.70	8.80 ± 0.56	43.69 ± 3.89
4000 µM Mn	12.87 ± 0.86^{ns}	7.26 ± 2.82^{ns}	6.67 ± 1.36^{ns}	2.20 ± 0.83^{ns}	7.61 ± 0.43^{ns}	42.39 ± 2.33^{ns}
			10 days			
Control	16.49 ± 3.29	8.27± 2.74	7.12 ± 1.31	3.92 ± 0.41	6.81 ± 0.78	37.52 ± 1.95
4000 µM Mn	13.81 ± 0.87^{ns}	8.64 ± 2.35^{ns}	5.80 ± 1.42^{ns}	5.07 ± 1.50^{ns}	6.95 ± 0.29^{ns}	40.85 ± 3.18^{ns}

Photosynthetic performance

The increases in Mn concentration affected the content of photosynthetic pigments, especially after 10 days of exposure (Figure 5). The chlorophyll *a* concentration decreased linearly according to the increased Mn in the nutrient solution in both time-points (Figure 5a, b). Comparatively, the decrease in the concentration of chlorophyll *a* was by 32% at 5 days and 52% at 10 days in 4000 μM $MnCl_2$-grown plants compared to the control (Figure 5a, b). Regarding chlorophyll *b*, the model adjusted at 10 days showed a linear drop with the increase in the concentration of Mn in the solution (Figure 5c, d). Surprisingly, the carotenoid values at 5 days tended to increase in the intermediate Mn concentrations (340 to 1000 μM), with a subsequent decrease in the highest concentrations (Figure 5e). However, the increase in Mn concentration promoted a linear decrease of this accessory pigment after 10 days (Figure 5f).

In general, the gas exchange parameters of *P. stratiotes* plants were not affected, regardless of the Mn concentration (Figure 6). There was a small decrease in the average values of the net photosynthetic rate of Mn-treated plants compared to the control, although there was no significant difference (Figure 6a, b). Furthermore, the internal concentration of CO_2 (C_i) remained unaltered with increasing Mn concentration, at both time points (Figure 6c, d). Measured dark respiration (R_N) also had no changes in both time-points, even increasing Mn in the medium (Figure 6e, f). The photorespiration, however, decreased at 10 days, especially in the highest concentrations of 2000 and 4000 μM $MnCl_2$ (Figure 6g, h).

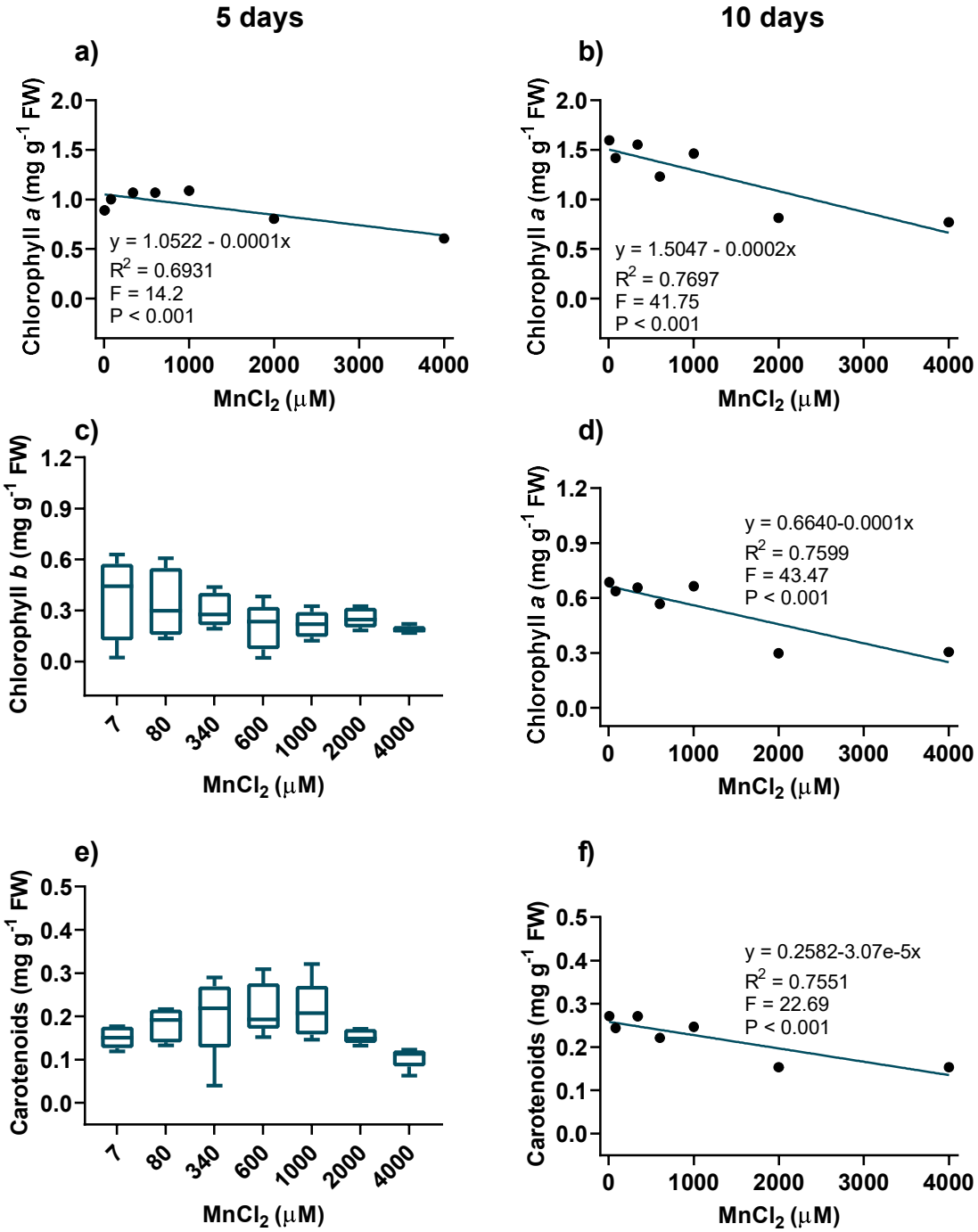

Figure 5. Photosynthesis-related pigments contents in *Pistia stratiotes* plants growing under different concentrations of $MnCl_2$. Contents of chlorophyll *a* (a, b), chlorophyll *b* (c, d), and carotenoids (e, f) in *P. stratiotes* plants growing for 5 or 10 days in a nutrient solution containing 7; 80; 340; 600; 1000; 2000; and 4000 μM $MnCl_2$. Regression models were estimated for the parametric data ($p \leq 0.05$), whereas nonparametric or non-significant data are presented as box-plot charts.

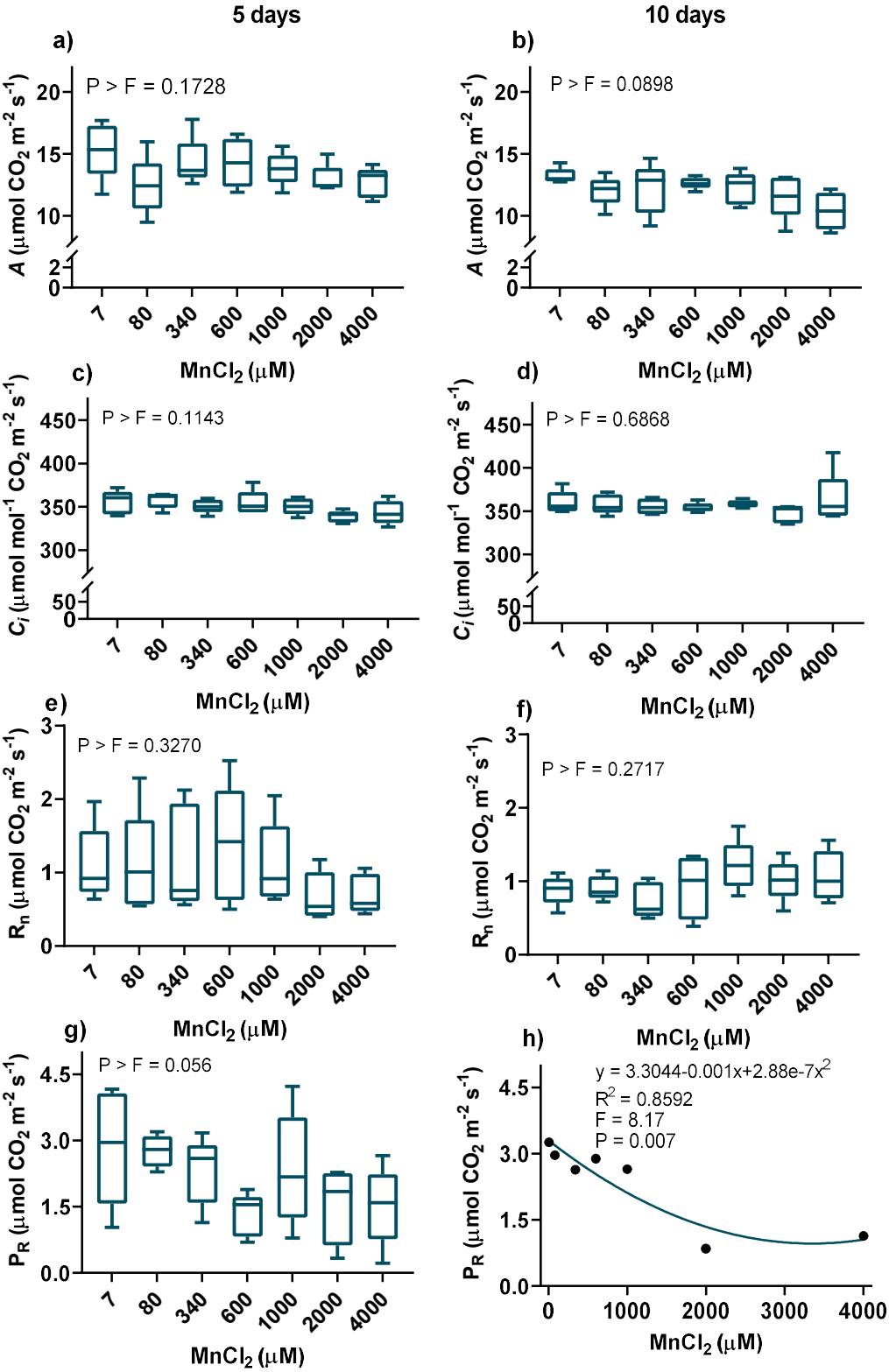

Figure 6. Gas exchange measurements in *Pistia stratiotes* plants growing under different concentrations of $MnCl_2$. Net CO_2 assimilation rate (a, b), internal CO_2 concentration in the leaf (c, d), dark respiration (e, f), and photorespiration estimation (g, h) of *P. stratiotes* plants growing for 5 or 10 days in a nutrient solution containing 7; 80; 340; 600; 1000; 2000; and 4000 µM $MnCl_2$. Regression models were estimated for the parametric data ($p \leq 0.05$), whereas nonparametric or non-significant data are presented as box-plot charts.

Exposing *P. stratiotes* to additional Mn for 5 days does not alter photochemical yield (F_v/F_m) in dark-adapted plants, as well as the photochemical efficiency in light (Figure 7a, c). However, at the second-time point, the plants showed linear drop in the effective quantum yield (*ΦPSII*; Figure 7d). Despite this, the potential quantum yield remained unchanged with the increase in the concentration of the element in the nutrient solution (Figure 7b). Also, no significant changes were observed in non-photochemical quenching values, in both time-points, regardless the concentration of $MnCl_2$ (Figure 7e, f).

Regarding apparent electron transport rate (ETR) and its derivations, no major changes were observed in plants measured after 5 days of treatment (Figure 8a, c, e). Otherwise, increased Mn concentration promoted a linear decrease of the total rate (Figure 8b), as well as the partition of the electron transport destined for RuBP carboxylation (Figure 8d), after 10 days. At the same time-point, estimated electron flow to RuBP oxygenation (ETR_O) also decreased following a quadratic model in higher concentrations of $MnCl_2$-grown plants (Figure 8f).

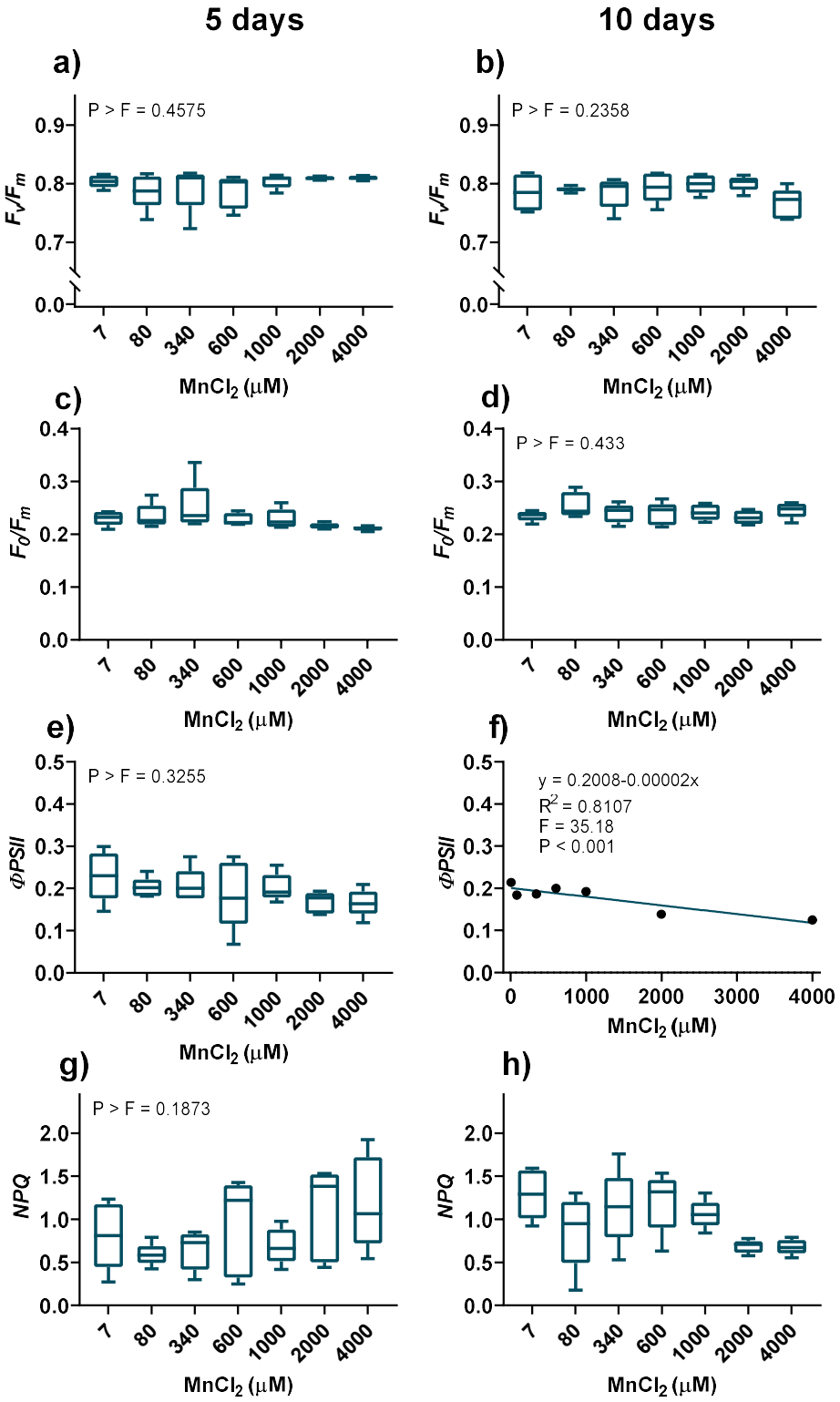

Figure 7. Fluorescence of chlorophyll *a* parameters in *Pistia stratiotes* plants growing under different concentrations of $MnCl_2$. Potential quantum yield of the photosystem II – F_v/F_m (a, b), ratio between the minimal (F_0) and maximal (F_m) fluorescence (c, d), actual PSII photochemical efficiency - ΦPSII (e, f), and non-photochemical quenching - NPQ (g, h) of *P. stratiotes* plants growing for 5 or 10 days in a nutrient solution containing 7; 80; 340; 600; 1000; 2000; and 4000 μM $MnCl_2$. Regression models were estimated for the parametric data ($p \leq 0.05$), whereas nonparametric or non-significant data are presented as box-plot charts.

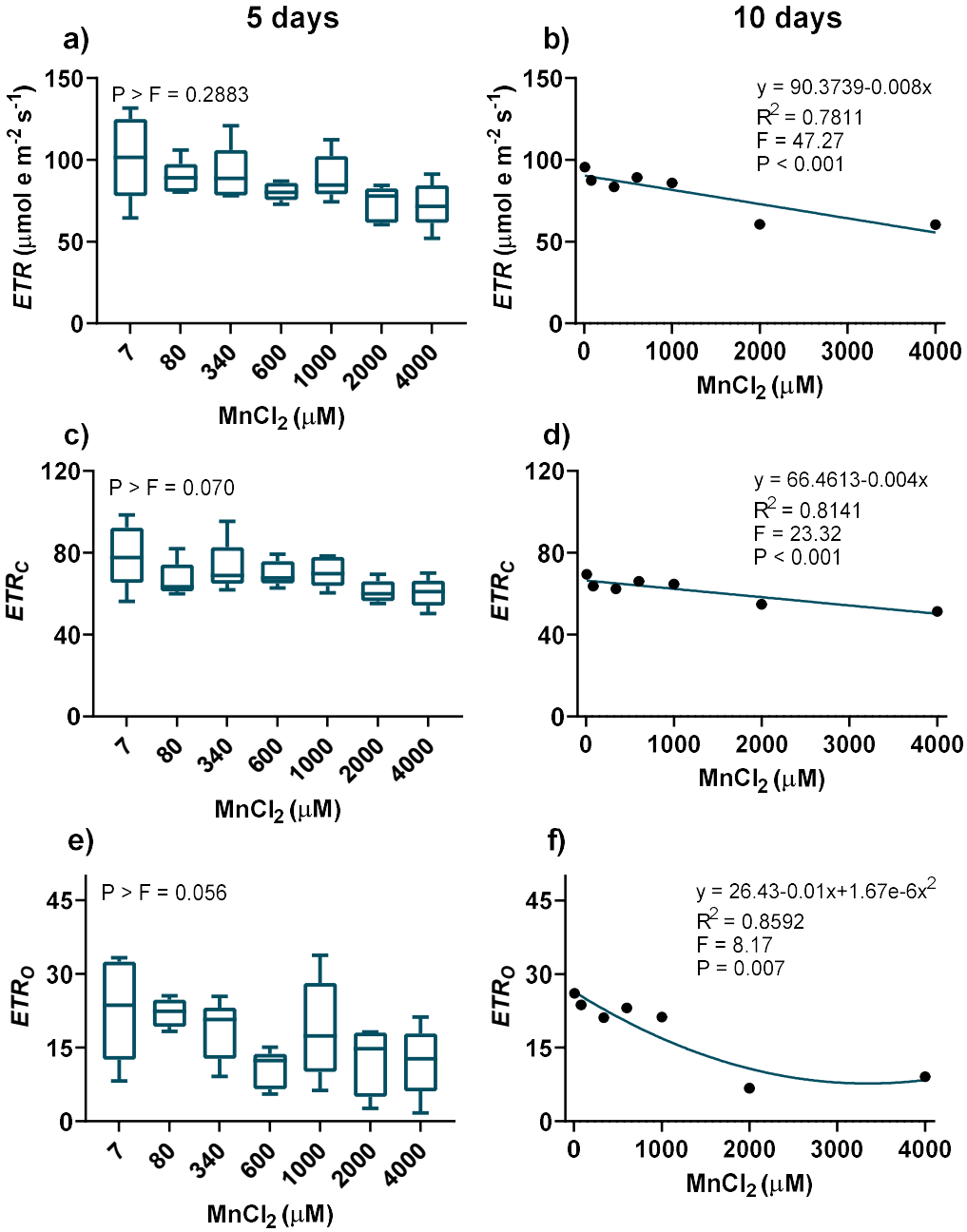

Figure 8. Electron transport rate and derived estimates in *Pistia stratiotes* plants growing under different concentrations of $MnCl_2$. Apparent electron transportation rate (a, b), electron flow to RuBP carboxylation (c, d), and electron flow to RuBP oxygenation (e, f) of *P. stratiotes* plants growing for 5 or 10 days in a nutrient solution containing 7; 80; 340; 600; 1000; 2000; and 4000 µM $MnCl_2$. Regression models were estimated for the parametric data ($p \leq 0.05$), whereas nonparametric or non-significant data are presented as box-plot charts.

4.4. Discussion

High concentrations of Mn in freshwater became of ecological and public health concern worldwide in the last decades due to the recent findings associating Mn excess with disturbances to the central nervous system in mammals and physiological impairments in plants

(Budinger et al., 2021; Li et al., 2019; Park and Berg, 2018). In addition to the already known technical and aesthetic problems in water distribution, these discoveries have made the study and application of solutions for the removal of excess Mn in water bodies of great relevance (Neculita and Rosa, 2019). In a pioneering study by Hua et al. (2012), comparing the potential of aquatic macrophytes to remediate water contaminated with Mn, water lettuce (*Pistia stratiotes*) stood out with the highest element accumulation among the studied species.

In the present study, we performed a detailed evaluation of Mn bioaccumulation along physiological responses of water lettuce challenged with Mn excess. Interestingly, excess Mn did not cause dramatic toxicity symptoms (Figure 1) or significant biomass decreases (Figure 2 a–d) in water lettuce, effects commonly reported in other species under similar conditions (Inostroza-Blancheteau et al., 2017; Pan et al., 2018). Furthermore, plants tend to accumulate a greater amount of Mn than necessary for their vital functions, due to poor regulation of Mn uptake (Shao et al., 2017). However, Mn-hyperaccumulator plants are not common, as the toxicity threshold for some species is around 200 μg g^{-1} DW (Millaleo et al., 2010). Nevertheless, water lettuce plants accumulate large amounts of Mn in roots and also shoots, being classified as hyperaccumulator for the element (van der Ent et al., 2013), with concentrations exceeding 10,000 μg g^{-1} DW (Figure 3a–d). Mn concentrations found in shoots of water lettuce, around 25,000 μg g^{-1} DW, are noticeably higher than for other aquatic species, including *Eichhornia crassipes* (around 16,000 μg g^{-1} DW), *Alligator alternanthera* (around 8000 μg g^{-1} DW) and *Sagittaria montevidensis,* close to 2300 μg g^{-1} DW (Demarco et al., 2019; Hua et al., 2012).

In comparison to terrestrial plants candidates for application in phytoremediation, the difference is even greater, with most records between 200 to 1000 μg g^{-1} DW (Bai et al., 2021; He et al., 2022; Inostroza-Blancheteau et al., 2017) and some examples of plants that accumulate concentrations around 10,000 μg g^{-1} DW (Magri et al., 2020; Rossini-Oliva et al., 2021). Water lettuce plants are also able to remove Mn nanoparticles from mixtures of colloidal solutions with 94% efficiency (Olkhovych et al., 2016), demonstrating the versatility and usefulness of the species.

Interestingly, Mn accumulation in shoots after 5 days was lower than in roots, whereas after 10 days the concentrations were similar between the organs (Figure 3b, d), culminating in a TF close to 1, especially in elevated concentrations of Mn (Figure 4c, d). These results indicate a high root-to-shoot transport capacity of the element, allowing the roots to uptake Mn from the medium and accumulate it in the tissues, even at high concentrations. Although the molecular

basis of xylem loading of Mn remains elusive, the potential candidates are members of Zinc-Regulated Transporter/Iron-Regulated Transporter (ZRT/IRT)-related Protein (ZIP) family, which are normally general carriers of metals with low selectivity, and Yellow Stripe-Like (YSL) family, which are putative Mn-nicotianamine (Mn^{2+}-NA) transporters (Alejandro et al., 2020). Therefore, it is possible to hypothesize that the accumulation of Mn mainly observed in the apoplast (Figure 3e, f) is associated with poor control of xylem loading, allowing water lettuce plants to keep up an elevated Mn uptake and translocation. As a consequence, plants maintained a high BCF (Figure 4a, b) and continue to increase the RP with increasing concentration in the nutrient solution (Figure 4e, f). Unsurprisingly, BCF and TF were elevated in the control conditions (Figure 4a–d), as the plants already has naturally accumulated Mn in the tissues, especially in the shoot, as reported by Bai et al. (2021) and Hua et al. (2012).

The massive accumulation of Mn in apoplast (Figure 3e, f) may also have been determinant for the absence of ROS accumulation and lipid peroxidation in the roots (Table 1). This could prevent the access of the metal to cellular organelles, which are critical points for redox reactions and ROS generation sites (Gill and Tuteja, 2010). Otherwise, the oxidative protection given by antioxidant enzymes in shoots (Table 1) seems to have been fundamental to prevent the proliferation of oxidative stress and consequent cell death and damage to photosynthetic machinery (Figure 6, 7).

In redox active organelles, like chloroplast and mitochondria, disturbances caused by excess of Mn lead to ROS overproduction, including superoxide anion (O_2^-), hydrogen peroxide (H_2O_2), and hydroxyl radical ($^{\cdot}OH$) (Liu et al., 2019). The enhanced SOD activity in shoots at five days is likely to be contributed to mitigate membrane damage and generate H_2O_2 (Table 1), as SOD gives frontline protection against ROS by directly catalyzing the dismutation of O_2^- to H_2O_2 (Reddi et al., 2009). Accordingly, enzymes responsible for H_2O scavenging, such as APX and POX, were induced in shoots at 10 days (Table 1). Thus, although an increase in lipid peroxidation was detected, the antioxidant system of the plant was operative under Mn stress condition.

Ultimately, the antioxidant system may also have been important for the maintenance of photosynthetic rates, even at high concentrations of Mn (Figure 6a, b). Even the decreases in chlorophylls and carotenoids (Figure 3), which are probably related to degradation and recycling pathways (Schumacher et al., 2022), and losses of photochemical efficiency (Figure 7d) were not sufficient to impact plant carbon assimilation.

4.5. Conclusion

Our results demonstrate that *Pistia stratiotes* accumulate great concentrations of Mn in both roots and shoot as a result of maintaining the element in the apoplast, providing an efficient translocation. Furthermore, the plant has a robust enzymatic antioxidant system and is able to hold the photosynthesis even with decreased pigment contents and photochemical efficiency. The maintenance of photosynthetic performance seems to be related to two factors: i) the spatial restriction of pigment degradation in the leaf margins, as observed in the symptoms and, ii) the deviation of electrons from the oxygenating pathway of RuBisCO, resulting in a decrease in photorespiration and maintenance of CO_2 assimilation.

References

Aguiar, A.O., Duarte, R.A., Ladeira, A.C.Q., 2013. The application of MnO_2 in the removal of manganese from acid mine water. Water. Air. Soil Pollut. 224, 1–8. https://doi.org/10.1007/s11270-013-1690-2

Alejandro, S., Höller, S., Meier, B., Peiter, E., 2020. Manganese in plants: From acquisition to subcellular allocation. Front. Plant Sci. 11, 1–23. https://doi.org/10.3389/fpls.2020.00300

Bai, J., Xu, D.H., Kang, H.M., Chen, K., Wang, G., 2008. Photoprotective function of photorespiration in *Reaumuria soongorica* during different levels of drought stress in natural high irradiance. Photosynthetica 46, 232–237. https://doi.org/10.1007/s11099-008-0037-5

Bai, Y., Zhou, Y., Gong, J., 2021. Physiological mechanisms of the tolerance response to manganese stress exhibited by *Pinus massoniana*, a candidate plant for the phytoremediation of Mn-contaminated soil. Environ. Sci. Pollut. Res. 28, 45422–45433. https://doi.org/10.1007/s11356-021-13912-8

Banks, J.M., 2018. Chlorophyll fluorescence as a tool to identify drought stress in Acer genotypes. Environ. Exp. Bot. 155, 118–127. https://doi.org/10.1016/j.envexpbot.2018.06.022

Bao, T., Sun, L., Sun, T., Zhang, P., Niu, Z., 2009. Iron-deficiency induces cadmium uptake and accumulation in *Solanum nigrum* L. Bull. Environ. Contam. Toxicol. 82, 338–342. https://doi.org/10.1007/s00128-008-9573-8

Bradford, M.M., 1976. A Rapid and sensitive method for the quantitation microgram quantities

of protein utilizing the principle of protein-dye binding. Anal. Biochem. 72, 248–254.

Budinger, D., Barral, S., Soo, A.K.S., Kurian, M.A., 2021. The role of manganese dysregulation in neurological disease: emerging evidence. Lancet Neurol. 20, 956–968. https://doi.org/10.1016/S1474-4422(21)00238-6

Carvalho, M.S. de, Ribeiro, K.D., Moreira, R.M., Almeida, A.M. de, 2017. Concentração de metais no rio Doce em Mariana, Minas Gerais, Brasil. Acta Bras. 1, 37. https://doi.org/10.22571/actabra13201758

Clark, R.B., 1975. Characterization of phosphatase of intact maize roots. J. Agric. Food Chem. 23, 458–460. https://doi.org/10.1021/jf60199a002

Coelho, D.G., Marinato, C.S., Matos, L.P., Andrade, H.M., Silva, V.M., Neves, P.H.S., Oliveira, J.A., 2020. Evaluation of metals in soil and tissues of economic-interest plants grown in sites affected by the fundão Dam failure in Mariana, Brazil. Integr. Environ. Assess. Manag. 16, 596–607. https://doi.org/10.1002/ieam.4253

Costa, G.B., Simioni, C., Ramlov, F., Maraschin, M., Chow, F., Bouzon, Z.L., Schmidt, É.C., 2017. Effects of manganese on the physiology and ultrastructure of *Sargassum cymosum*. Environ. Exp. Bot. 133, 24–34. https://doi.org/10.1016/j.envexpbot.2016.09.007

Demarco, C.F., Afonso, T.F., Pieniz, S., Quadro, M.S., Camargo, F.A. de O., Andreazza, R., 2019. Phytoremediation of heavy metals and nutrients by the *Sagittaria montevidensis* into an anthropogenic contaminated site at Southern of Brazil. Int. J. Phytoremediation 21, 1145–1152. https://doi.org/10.1080/15226514.2019.1612843

Furlan, F., Borgo, L., Rabêlo, F.H.S., Rossi, M.L., Linhares, F.S., Martinelli, A.P., Azevedo, R.A., Lavres, J., 2020. Aluminum-induced toxicity in *Urochloa brizantha* genotypes: A first glance into root Al-apoplastic and -symplastic compartmentation, Al-translocation and antioxidant performance. Chemosphere 243. https://doi.org/10.1016/j.chemosphere.2019.125362

Gay, C., Gebicki, J.M., 2000. A critical evaluation of the effect of sorbitol on the ferric-xylenol orange hydroperoxide assay. Anal. Biochem. 284, 217–220. https://doi.org/10.1006/abio.2000.4696

Genty, B., Briantais, J.M., Baker, N.R., 1989. The relationship between the quantum yield of photosynthetic electron transport and quenching of chlorophyll fluorescence. Biochim.

Biophys. Acta - Gen. Subj. 990, 87–92. https://doi.org/10.1016/S0304-4165(89)80016-9

Giannopolitis, C.N., Ries, S.K., 1977. Superoxide dismutases: I. Occurrence in higher plants. Plant Physiol. 59, 309–314. https://doi.org/10.1104/pp.59.2.309

Gill, S.S., Tuteja, N., 2010. Reactive oxygen species and antioxidant machinery in abiotic stress tolerance in crop plants. Plant Physiol. Biochem. 48, 909–930. https://doi.org/10.1016/j.plaphy.2010.08.016

Guan, X.Q., Zhao, S.J., Li, D.Q., Shu, H.R., 2004. Photoprotective function of photorespiration in several grapevine cultivars under drought stress. Photosynthetica 42, 31–36. https://doi.org/10.1023/B:PHOT.0000040566.55149.52

Haokip, N., Gupta, A., 2021. Phytoremediation of chromium and manganese by *Ipomoea aquatica* Forssk. from aqueous medium containing chromium-manganese mixtures in microcosms and mesocosms. Water Environ. J. 35, 884–891. https://doi.org/10.1111/wej.12676

Havir, E.A., McHale, N.A., 1987. Biochemical and developmental characterization of multiple forms of catalase in tobacco leaves. Plant Physiol. 84, 450–455. https://doi.org/10.1104/pp.84.2.450

He, L., Su, R., Chen, Y., Zeng, P., Du, L., Cai, B., Zhang, A., Zhu, H., 2022. Integration of manganese accumulation, subcellular distribution, chemical forms, and physiological responses to understand manganese tolerance in *Macleaya cordata*. Environ. Sci. Pollut. Res. 29, 39017–39026. https://doi.org/10.1007/s11356-022-19562-8

Hodges, D.M., DeLong, J.M., Forney, C.F., Prange, R.K., 1999. Improving the thiobarbituric acid-reactive-substances assay for estimating lipid peroxidation in plant tissues containing anthocyanin and other interfering compounds. Planta 207, 604–611. https://doi.org/10.1007/s004250050524

Hoffmann, W.A., Poorter, H., 2002. Avoiding bias in calculations of relative growth rate. Ann. Bot. 90, 37–42. https://doi.org/10.1093/aob/mcf140

Hua, J., Zhang, C., Yin, Y., Chen, R., Wang, X., 2012. Phytoremediation potential of three aquatic macrophytes in manganese-contaminated water. Water Environ. J. 26, 335–342. https://doi.org/10.1111/j.1747-6593.2011.00293.x

Inostroza-Blancheteau, C., Reyes-Díaz, M., Berríos, G., Rodrigues-Salvador, A., Nunes-Nesi, A., Deppe, M., Demanet, R., Rengel, Z., Alberdi, M., 2017. Physiological and biochemical responses to manganese toxicity in ryegrass (*Lolium perenne* L.) genotypes. Plant Physiol. Biochem. 113, 89–97. https://doi.org/10.1016/j.plaphy.2017.02.003

Kwak, S.S., Kim, S.K., Park, I.H., Liu, J.R., 1996. Enhancement of peroxidase activity by stress-related chemicals in sweet potato. Phytochemistry 43, 565–568. https://doi.org/10.1016/0031-9422(96)00315-9

Lavres Junior, J., Moraes, M.F., Cabral, C.P., Malavolta, E., 2008. Influência genotípica na absorção e na toxidez de manganês em soja. Rev. Bras. Ciência do Solo 32, 173–181. https://doi.org/10.1590/s0100-06832008000100017

Li, J., Jia, Y., Dong, R., Huang, R., Liu, P., Li, X., Wang, Z., Liu, G., Chen, Z., 2019. Advances in the mechanisms of plant tolerance to manganese toxicity. Int. J. Mol. Sci. 20. https://doi.org/10.3390/ijms20205096

Liu, K., Xu, J., Dai, C., Li, C., Li, Y., Ma, J., Yu, F., 2021. Exogenously applied oxalic acid assists in the phytoremediation of Mn by *Polygonum pubescens* Blume cultivated in three Mn-contaminated soils. Front. Environ. Sci. Eng. 15, 1–13. https://doi.org/10.1007/s11783-020-1380-4

Liu, P., Huang, R., Hu, X., Jia, Y., Li, J., Luo, J., Liu, Q., Luo, L., Liu, G., Chen, Z., 2019. Physiological responses and proteomic changes reveal insights into Stylosanthes response to manganese toxicity. BMC Plant Biol. 19, 1–21. https://doi.org/10.1186/s12870-019-1822-y

Magri, E., Gugelmin, E.K., Grabarski, F.A.P., Barbosa, J.Z., Auler, A.C., Wendling, I., Prior, S.A., Valduga, A.T., Motta, A.C.V., 2020. Manganese hyperaccumulation capacity of *Ilex paraguariensis* A. St. Hil. and occurrence of interveinal chlorosis induced by transient toxicity. Ecotoxicol. Environ. Saf. 203. https://doi.org/10.1016/j.ecoenv.2020.111010

Millaleo, R., Reyes-Díaz, M., Ivanov, A.G., Mora, M.L., Alberdi, M., 2010. Manganese as essential and toxic element for plants: Transport, accumulation and resistance mechanisms. J. Soil Sci. Plant Nutr. 10, 476–494. https://doi.org/10.4067/s0718-95162010000200008

Murshed, R., Lopez-Lauri, F., Sallanon, H., 2008. Microplate quantification of enzymes of the

plant ascorbate-glutathione cycle. Anal. Biochem. 383, 320–322. https://doi.org/10.1016/j.ab.2008.07.020

Nakano, Y., Asada, K., 1981. Hydrogen peroxide is scavenged by ascorbate-specific peroxidase in spinach chloroplasts. Plant Cell Physiol. 22, 867–880. https://doi.org/10.1093/oxfordjournals.pcp.a076232

Neculita, C.M., Rosa, E., 2019. A review of the implications and challenges of manganese removal from mine drainage. Chemosphere 214, 491–510. https://doi.org/10.1016/j.chemosphere.2018.09.106

Olkhovych, O., Svietlova, N., Konotop, Y., Karaushu, O., Hrechishkina, S., 2016. Removal of metal nanoparticles colloidal solutions by water plants. Nanoscale Res. Lett. 11. https://doi.org/10.1186/s11671-016-1742-9

Pan, G., Liu, W., Zhang, H., Liu, P., 2018. Morphophysiological responses and tolerance mechanisms of *Xanthium strumarium* to manganese stress. Ecotoxicol. Environ. Saf. 165, 654–661. https://doi.org/10.1016/j.ecoenv.2018.08.107

Park, R.M., Berg, S.L., 2018. Manganese and neurobehavioral impairment. A preliminary risk assessment. Neurotoxicology 64, 159–165. https://doi.org/10.1016/j.neuro.2017.08.003

Peixoto, P.H.P., Cambraia, J., Sant'Anna, R., Mosquim, P.R., Moreira, M.A., 1999. Aluminum effects on lipid peroxidation and on the activities of enzymes of oxidative metabolism in sorghum. Rev. Bras. Fisiol. Veg. 11, 137–143.

Rajpoot, R., Srivastava, R.K., Rani, A., Pandey, P., Dubey, R.S., 2021. Manganese-induced oxidative stress, ultrastructural changes, and proteomics studies in rice plants. Protoplasma 258, 319–335. https://doi.org/10.1007/s00709-020-01575-0

Reddi, A.R., Jensen, L.T., Naranuntarat, A., Rosenfeld, L., Leung, E., Shah, R., Culotta, V.C., 2009. The overlapping roles of manganese and Cu/Zn SOD in oxidative stress protection. Free Radic. Biol. Med. 46, 154–162. https://doi.org/10.1016/j.freeradbiomed.2008.09.032

Reeves, R.D., van der Ent, Antony, Baker, A.J.M., 2018. Global distribution and ecology of hyperaccumulator plants, in: Van der Ent, A., Echevarria, G., Baker, A., Morel, J. (Eds.), Agromining: Farming for Metals. Springer International Publishing, pp. 75–92. https://doi.org/10.1007/978-3-319-61899-9_5

Rezania, S., Taib, S.M., Md Din, M.F., Dahalan, F.A., Kamyab, H., 2016. Comprehensive review on phytotechnology: Heavy metals removal by diverse aquatic plants species from wastewater. J. Hazard. Mater. 318, 587–599. https://doi.org/10.1016/j.jhazmat.2016.07.053

Roels, H.A., Bowler, R.M., Kim, Y., Claus Henn, B., Mergler, D., Hoet, P., Gocheva, V. V., Bellinger, D.C., Wright, R.O., Harris, M.G., Chang, Y., Bouchard, M.F., Riojas-Rodriguez, H., Menezes-Filho, J.A., Téllez-Rojo, M.M., 2012. Manganese exposure and cognitive deficits: A growing concern for manganese neurotoxicity. Neurotoxicology 33, 872–880. https://doi.org/10.1016/j.neuro.2012.03.009

Rossini-Oliva, S., Abreu, M.M., Leidi, E.O., 2021. Strategies in a metallophyte species to cope with manganese excess. Environ. Geochem. Health 43, 1523–1535. https://doi.org/10.1007/s10653-020-00625-z

Schmidt, S.B., Jensen, P.E., Husted, S., 2016. Manganese deficiency in plants: The impact on Photosystem II. Trends Plant Sci. 21, 622–632. https://doi.org/10.1016/j.tplants.2016.03.001

Schumacher, I., Menghini, D., Ovinnikov, S., Hauenstein, M., Fankhauser, N., Zipfel, C., Hörtensteiner, S., Aubry, S., 2022. Evolution of chlorophyll degradation is associated with plant transition to land. Plant J. 109, 1473–1488. https://doi.org/10.1111/tpj.15645

Shao, J.F., Yamaji, N., Shen, R.F., Ma, J.F., 2017. The key to Mn homeostasis in plants: regulation of Mn transporters. Trends Plant Sci. 22, 215–224. https://doi.org/10.1016/j.tplants.2016.12.005

Tobiason, J.E., Bazilio, A., Goodwill, J., Mai, X., Nguyen, C., 2016. Manganese removal from drinking water sources. Curr. Pollut. Reports 2, 168–177. https://doi.org/10.1007/s40726-016-0036-2

van der Ent, A., Baker, A.J.M., Reeves, R.D., Pollard, A.J., Schat, H., 2013. Hyperaccumulators of metal and metalloid trace elements: Facts and fiction. Plant Soil 362, 319–334. https://doi.org/10.1007/s11104-012-1287-3

Vergilio, C. dos S., Lacerda, D., Oliveira, B.C.V. de, Sartori, E., Campos, G.M., Pereira, A.L. de S., Aguiar, D.B. de, Souza, T. da S., Almeida, M.G. de, Thompson, F., Rezende, C.E. de, 2020. Metal concentrations and biological effects from one of the largest mining

disasters in the world (Brumadinho, Minas Gerais, Brazil). Sci. Rep. 10, 1–12. https://doi.org/10.1038/s41598-020-62700-w

Veselý, T., Tlustoš, P., Száková, J., 2011. The use of water lettuce (*Pistia stratiotes* L.) for rhizofiltration of a highly polluted solution by cadmium and lead. Int. J. Phytoremediation 13, 859–872. https://doi.org/10.1080/15226514.2011.560214

Wei, Z., Van Le, Q., Peng, W., Yang, Y., Yang, H., Gu, H., Lam, S.S., Sonne, C., 2021. A review on phytoremediation of contaminants in air, water and soil. J. Hazard. Mater. 403, 123658. https://doi.org/10.1016/j.jhazmat.2020.123658

Wellburn, A.R., 1994. The spectral determination of chlorophylls *a* and *b*, as well as total carotenoids, using various solvents with spectrophotometers of different resolution. J. Plant Physiol. 144, 307–313. https://doi.org/10.1016/S0176-1617(11)81192-2

5. Chapter 4 - Individual and associated effects of iron, manganese and arsenic on physiology and metal bioaccumulation of *Pistia stratiotes* L. plants[1]

[1]Edited in accordance with *Environmental Pollution* guidelines

Abstract: In the environment, the occurrence of contamination by more than one metallic element is frequent, as observed in several studies carried out in areas affected by the rupture of ore tailings dams. In these places, in addition to the elevation of iron (Fe) and manganese (Mn) levels caused by the mud, the occurrence of arsenic (As) from gold mining is common. Thus, it is mandatory to understand how this multi-element interaction of pollutants specifically modulates several aspects of plant physiology and, therefore, interferes with the dynamics of the phytoremediation processes. We, therefore, investigated the physiological responses and bioaccumulation of these elements on water lettuce (*Pistia stratiotes*) plants. The specimens were subjected to eight treatments: control (nutrient solution only); Fe (5 mM Fe-EDTA); Mn (4 mM $MnCl_2$); As (10 μM $Na_2HAsO_4.7H_2O$); FeMn, FeAs, MnAs, FeMnAs and assessed at the 10th day of exposition to treatments. The plants showed necrosis, chlorosis and root loss as the main toxicity symptoms of Fe, Mn, and As, respectively. Also, the exposure to associated and isolated elements led to decreased root nutrients contents and structural changes. However, the accumulation of the pollutants in the tissues was not altered by the association of the elements. Furthermore, despite the absence of alterations in photochemical measurements, plants displayed decreased CO_2 assimilation, apart from Mn-treated plants. The treatments also induced accumulation of sugars and starch in shoots and a decrease of the contents in roots, indicating impairments in the sucrose transport. Overall, a remarkable induction of antioxidant enzyme activities was observed, especially in Fe and Fe-associated treatments, as well as the maintenance of the redox state culminating in the mitigation of oxidative stress. Altogether, our results demonstrate that the association of metallic elements, usual in contaminated environments, does not constitute an additional challenge for the phytoremediation of aquatic environments using water lettuce plants.

Keywords: Water lettuce, phytoremediation, carbon metabolism, oxidative stress

5.1. Introduction

Several chemical elements, including Fe (iron), Mn (manganese), Zn (zinc), Co (cobalt), Cu (copper), Mo (molybdenum), Ni (nickel), Si (silicon), and Se (selenium) are essential or beneficial for plant growth and development. Nonetheless, when the concentrations in plant tissues exceed threshold levels, they might cause toxicity (Arif et al., 2016; Muszyńska and Labudda, 2019). Other elements, such as As (arsenic), Cd (cadmium), Cr (chromium), Pb (lead), and Hg (mercury), on the other hand, are not physiologically necessary and can cause toxicity at considerably lower concentrations than the aforementioned (Angulo-Bejarano et al., 2021).

These elements have different toxic effects on plants, which depend on their concentration, bioavailability, chemical form and biological processes with which it interferes (Muszyńska and Labudda, 2019). One of the main metal-induced disorders in plants is a nutritional imbalance, due to the need to re-orchestrate the charge balance in cellular compartments, in addition to competition for the protein transporters in the uptake and redistribution of the elements (Palmer and Guerinot, 2009; Tian et al., 2021). Moreover, metal overload has severe effects on metabolic pathways, among which the enzymatic inhibition, energy depletion, impairment of normal electron flow, degradation of macromolecules and cell death (Georgiadou et al., 2018; Pita-Barbosa et al., 2019; Yang et al., 2020).

In nature, the pollution by metallic elements can occur individually, with a predominant pollutant, or more commonly as a mixture of two or more elements, constituting an additional challenge for the survival and growth of plants and other organisms and also threatening human health (Li et al., 2019; Sankhla et al., 2016). In the last decade, two disasters involving the disruption of mining tailing dams spread millions of tons of iron and manganese oxide along two watersheds in the Southeast region of Brazil. These events triggered massive socio-environmental impacts, including increased concentrations and accumulation of metallic elements in organisms (Quaresma et al., 2021; Vergilio et al., 2020). In addition to Fe and Mn, present in the tailings mud, there were records of an increase in the concentration of other elements, including As, due to sediment disturbance along the rivers (Coelho et al., 2020; Silva et al., 2018). The presence of As contamination in these regions is widely reported, as a result of the historical exploration of gold from arsenopyrite (Teixeira et al., 2020). The concentrations of these elements in water samples collected after the Fundão dam collapse were 2 to 250 times higher than reference samples collected before the disaster, exceeding the limits established by legislation (Quadra et al., 2019).

Several efforts have been made to study alternatives that will minimize contamination in sites affected by metallic elements. Among them, the plant-based decontaminating approach, the so-called phytoremediation, arises as an interesting alternative from an environmental and economic perspective to be used as a main or complementary technique in decreasing the concentration of metals. For cleaning-up water bodies, *Eicchornia crassipes*, *Lemna* spp., and *Pistia stratiotes* are examples of aquatic macrophytes commonly employed in phytoremediation programs (Ntakiyiruta et al., 2022; Prasertsup and Ariyakanon, 2011). The latter has been highlighted by the potential for bioaccumulation and tolerance to different pollutants (Campos et al., 2019; Hua et al., 2012; Yasar et al., 2017). Nevertheless, most studies have been performed using a single element, neglecting the fact that they occur associated in nature, which can have synergistic effects on plant toxicity, reducing the phytoremediation efficiency (Török et al., 2015).

Therefore, our study was addressed to investigate the bioaccumulation along with biochemical and physiological responses of water lettuce (*Pistia stratiotes*) plants for the phytoremediation of environments contaminated with Fe, Mn, and As, as single contaminants or in associations.

5.2. Material and methods

Plant material and treatments

Water lettuce (*Pistia stratiotes* L.) plants (Araceae) with approximately 10 g of fresh weight were collected in nonpolluted dams at the Universidade Federal de Viçosa, Viçosa, Minas Gerais State, Brazil. After the sampling, plants were washed and transferred to Clark's (1975) nutrient solution (1/2 of ionic strength, pH 6.0) in a growth chamber for acclimatization with controlled conditions (25 ± 2 °C temperature, 200 μmol s^{-1} m^{-2} light intensity, 12h light photoperiod). After three days, healthy and uniform plants were selected and transferred to pots containing 0.5 L of nutrient solution 1/2 of ionic strength, pH 6.0, added of the following treatments: control (nutrient solution only); Fe, Mn, As, Fe + Mn, Fe + As, Mn + As, or Fe + Mn + As, with five repetitions. Iron was supplied as 5 mM ethylenediaminetetraacetic acid iron (III) sodium salt hydrate (Fe-EDTA), manganese as 4 mM manganese (II) chloride ($MnCl_2$) and arsenic as 10 μM sodium arsenate dibasic heptahydrate ($Na_2HAsO_4.7H_2O$). The concentrations of Fe and Mn were determined based on preliminary experiments, while the As concentration was based on studies by Farnese et al. (2014, 2017). The pH was adjusted to 6.0 daily, following previous optimization studies for As uptake (de Souza et al., 2019; Farnese et

al., 2013) and considering that changing the pH from 5.0, the optimum range for Fe and Mn uptake, from 6.0 in the nutrient solution did not impact the accumulation of these elements in water lettuce plants (Table S1). The solution was renewed after five days and the plants remained for ten days in the treatments for further evaluations.

Growth and mineral contents

The visual aspects of the plants were registered by capturing high resolution images to identify toxicity symptoms. After that, shoots and roots of the plants were placed in a 60 ºC oven for drying and the dry weight was determined after reaching the constant weight. To remove adsorbed Fe oxides, the roots were washed with a dithionite–citrate–bicarbonate solution (3 g sodium dithionite, 40 mL 0.3 M sodium citrate, and 5 mL 1 M sodium bicarbonate) (Taylor and Crowder, 1983). The dried plant material was homogenized and 100 mg of the dry mass was mineralized in 1.5 mL of nitroperchloric mixture (2:1) at 150 ºC. The extract was used in the determination of mineral contents by atomic absorption spectrophotometry (Shimadzu AA-6701F, Shimadzu Corporation, Tokyo, Japan), using authentic standards for curve calibrations. For As quantification, 0.4 mL of mineral extract were added to 1.8 mL of 6 N HCl, 0.2 mL of 50% potassium iodide (KI) and 7.6 mL of deionized H_2O (Nieniewska and Curtius, 1986). The tubes were shaken vigorously and kept at room temperature for 50 min in the dark. After that, the samples were analysed using a hydride vapour generator (HVG-1, Shimadzu Corporation) coupled to the atomic absorption spectrophotometry. Blanks and quality control standards were measured every tenth sample to detect contamination and drift.

According to Liu et al. (2007), the metal accumulation index (MAI) was determined as follows: $MAI = (1/N) \sum_{j=1}^{N} I_j$, in which N = the total number of elements analysed and $Ij = x/\delta x$ is the sub-index for variable j, calculated by dividing the mean value (x) of each element by its standard deviation (δx).

Structural changes

The effects of the treatments on plant anatomy and structural changes were evaluated according to O'Brien and McCully (1981). Samples of the middle of the fully expanded leaves and from 2 cm of root tips were fixed in 2.5 % glutaraldehyde and 4% paraformaldehyde in a sodium phosphate buffer 0.1 M (pH 7.0) for 48 h, then stored in 70% alcohol (Karnovsky, 1985). The samples were dehydrated in ethylic series before being included in methacrylate solution (Historesin, Leica). Then, the material was cross sectioned (5 μm thick) using an

automatic advance microtome (RM 2155, Leica Microsystems Inc, Deerfield, USA). The sections were stained with 0.05% Toluidine Blue pH 6.5 for 30 seconds and assembled with Permount synthetic resin (Permount, Fisher). Finally, the images were captured using a light microscope (model AX-70 TRF, Olympus Optical, Tokyo, Japan) coupled with a digital camera (model AxioCam HRc, Zeiss, Göttinger, Germany) and a computer running Axio Vision software.

Pigments contents, gas exchange and fluorescence of chlorophyll a

Three leaf discs (1 cm diameter) were incubated in 2 mL of dimethylsulfoxide (DMSO) solution for 24 hours to assess the concentrations of chlorophyll *a* and *b*, as well as carotenoids. The tubes were incubated in a water bath at 65 °C for 45 minutes. The absorbances at wavelengths of 665, 649, and 480 nm were measured and used to calculate the chlorophyll *a* and *b*, as well as carotenoids concentration, respectively, as described by Wellburn (1994).

An open-flow infrared gas exchange analyser system (LI-6400XT; LI-COR) with an integrated fluorescence chamber (LI-6400-40; LI-COR) was used to monitor gas exchange and chlorophyll a fluorescence. On completely expanded leaves, the light-saturated net CO_2 assimilation rate (*A*), and internal CO2 concentration (C_i), were measured two hours after the start of the light period. The leaves were placed in a 2 cm^2 leaf chamber at 25 °C, with a flow rate of 300 mol s^{-1}, a 0.5 stomatal ratio (amphistomatic leaves), under saturating light at leaf level (1000 µmol photon m^{-2} s^{-1}; 10% blue light) and 400 µmol CO_2 mol^{-1} air.

Simultaneously, the transient fluorescence (F_s) and maximal fluorescence (Fm') were recorded in actinic light (1,000 µmol photon m^{-2} s^{-1}) acclimated leaves, followed by a saturating light pulse. The actinic light was then turned off, and the light-adapted initial fluorescence (F_0') was measured using far-red illumination. These parameters were utilized to estimate the actual PSII photochemical efficiency ($\Phi PSII$) and the non-photochemical quenching (NPQ), according to Genty et al. (1989).

In dark-acclimated leaves, the minimal fluorescence (F_0) was obtained via the excitation with a modulated red light of low intensity (0.03 µmol photon m^{-2} s^{-1}), followed by application of light saturating pulses of 8000 µmol photon m^{-2} s^{-1} to obtain maximal fluorescence (F_m). The potential quantum yield of the photosystem II was calculated (F_v/F_m) using the variable fluorescence (F_v), which is determined by the difference between F_0 and F_m (Genty et al., 1989). The ratio F_0/F_m was also calculated, as suggested by Banks (2018). The

above-mentioned infrared-gas analyzer was used to monitor respiration in the dark (R_N) before dawn.

Metabolite contents

The extract for the determination of sugars, starch, organic acids, and total phenols was obtained by methanolic extraction, according to Fernie et al. (2001). Briefly, 700 µL of methanol were added to approximately 10 mg of freeze-dried tissues of shoots and roots and heated for 20 minutes at 80 ºC. After cooling down and centrifugation, 375 µL of chloroform and 750 µL deionized H_2O were added to the samples followed by another centrifugation. The resultant pellet was washed with 70% ethanol to be used for the determination of starch. In turn, the upper phase (polar fraction) was collected for the determination of other metabolites.

The contents of sucrose, fructose, and glucose were assessed by adding the methanolic extract (40 µL) to 150 µL 0.1 M Hepes/KOH buffer pH 7.0 containing 0.3 mM $MgCl_2$, 4.65 µL 109 mM ATP, 4.65 µL 48.4 mM $NADP^+$ and 0.77 µL glucose-6P dehydrogenase (G6PDH) 700 U mL^{-1}. The quantification was based on NADPH production using sugar standards as references, detected at 340 nm after addition of hexokinase (0.3 U μL^{-1}), phosphoglucose isomerase (0.14 U μL^{-1}) and invertase (1 U μL^{-1}), for glucose, fructose and sucrose contents, respectively.

The resulting starch in the insoluble fraction of the extract was degraded to glucose by the addition of 59 µL 50 mM sodium acetate buffer, pH 4.9, 1 µL amyloglucosidase (170 U mL^{-1}) + 0.012 µL α-amylase (325 U mL^{-1}). Subsequently, the glucose concentration in the samples was determined as described and expressed as glucose equivalent.

For malate and fumarate determination, the production of NADH was monitored at 560 nm after applying malate dehydrogenase (1 U) and fumarase (0.1 U) in a medium containing 2.5 µL of methanolic extract, 25 µL 0.4 M Tricine/KOH buffer, pH 9, containing 20 mM $MgCl_2$, 10 µL MTT (methylthiazolyldiphenyl-tetrazolium bromide) 10 mM, 5 µL 60 mM NAD^+, 2 µL of 20 mM PES (phenazine ethosulfate), 5 µL 10% Triton and 3 µL deionized H_2O.

Finally, the total phenols contents were determined by the Folin–Ciocalteu (FC) method. Briefly, 10 µL of the methanolic extract was added to the Folin reagent and the absorbance was detected at 725 nm. The results were calculated based on a tannic acid standard curve.

Oxidative metabolism

For the determination of the activity of SOD, CAT, and POX, the extract was obtained according to Peixoto et al. (1999). To summarize, 20 mg of freeze-dried tissues were homogenized in extraction buffer comprising 0.1 M potassium phosphate buffer pH 6.8, 0.1 mM EDTA disodium salt, 1 mM phenylmethylsulfonyl fluoride (PMSF) and 1% polyvinylpyrrolidone (PVPP). The homogenate was centrifuged for 15 min at 15,000 x*g* at 4 ºC with the supernatant collected for the analysis.

The activity of the enzyme superoxide dismutase (SOD, EC. 1.15.1.1) was determined according to Giannopolitis and Ries (1977). The amount of enzyme required to prevent nitroblue tetrazolium reduction by 50% was defined as one unit of SOD. The catalase (CAT, EC. 1.11.1.6) activity was determined by incubating enzymatic extract in 50 mM phosphate buffer, pH 6.8, containing 20 mM H_2O_2. Enzyme activity was estimated from measurements of H_2O_2 consumption at 240 nm (Havir and McHale, 1987). In turn, the formation of purpurogallin in the presence of 20 mM H2O2 and 800 mM pyrogallol was used to determine peroxidase (POX, EC. 1.11.1.7) activity in the extract (Kwak et al., 1996).

The extraction and determination of ascorbate peroxidase (APX, EC. 1.11.1.11), glutathione reductase (GR, EC. 1.8.1.7), monodehydroascorbate reductase (MDHAR, EC. 1.6.5.4) and dehydroascorbate reductase (DHAR, EC 1.8.5.1) activities were performed according to Murshed et al. (2008). The APX assay was carried out in a reaction medium containing 50 mM phosphate buffer (pH 6.0), 0.54 mM ascorbic acid and 200 mM H_2O_2. The ascorbate oxidation rate was monitored at 290 nm and the activity was calculated based on the molar extinction coefficient of 2.8 mM^{-1} cm^{-1}. For GR activity measurement, the degradation of NADPH (ε = 6.22 mM^{-1} cm^{-1}) for reducing disulfide glutathione (GSSG) was monitored at 340 nm. The activity of MDHAR was determined through the decrease in the NADH-dependent reaction rate at 340 nm (ε = 6.22 mM^{-1} cm^{-1}). Finally, the activity of DHAR was determined by monitoring the glutathione-dependent reduction of dehydroascorbate, using the molar extinction coefficient of 14 mM^{-1} cm^{-1} for ascorbate. The total protein content in the leaf and root samples was determined according to the method of Bradford (1976) and used for the normalization of all the enzymatic activities.

The concentration of total glutathione and its reduced (GSH) and disulfide (GSSG) forms were determined by modifying the protocol described by Rahman et al. (2007). Approximately 20 mg of freeze-dried plant tissues were homogenized in 1.3% (w/v) sulfosalicylic acid diluted in 8 mM HCl. The homogenate was centrifuged at 13000 x*g* for 5

min at 4 °C. Then, 20 µL of the supernatant was added to 60 µL 1.66 mM Ellman's reagent (DTNB), 60 µL glutathione reductase (3.3 U mL^{-1}) and 60 µL 0.8 mM β-NADPH for the determination of total glutathione. For GSSG assay, 100 µL of the extract was previously incubated for 1 hour with 2 µL 2-vinylpyridine and mixed well to derivatize GSH. After that, 12 µL of triethanolamine was added to the tubes. The absorbances were immediately read at 412 nm for 5 min every 30s and rate of 2-nitro-5-thiobenzoic acid formation rate was calculated. The results were estimated based on authentic GSH and GSSG standards curves.

The assay for extraction and determination of ascorbate (AsA) and dehydroascorbate (DHA) was performed according to Kampfenkel et al. (1995). Samples of around 20 mg (freeze-dried) tissues were homogenized with 1.8 mL 5% (w/v) trichloroacetic acid (TCA). The homogenate was centrifuged at 12000 x*g* for 15 min at 4 °C and the supernatant was collected for the analysis. The measurement of AsA was performed by adding 10 µL of the extract into a medium containing 30 µL 0.2 M phosphate buffer, pH 7.4, 10 µL deionized H_2O, 50 µL 10% TCA(w/v), 40 µL 42% (w/v) H_3PO_4, 40 µL 4% (w/v) 2,2'-bipyridyl and 20 µL 3% (w/v) $FeCl_3$ in a 96-well microplate. The samples were incubated for 40 min at 42 ºC and the absorbances were registered at 525 nm. For the measurement of total ascorbate, the samples were incubated with 10 mM DTT before the reaction. The contents were calculated based on an ascorbate standard curve and the content of DHA was estimated based on the difference between total ascorbate and AsA.

The thiobarbituric acid reactive substances (TBARS) test was used to determine lipid peroxidation using the molar extinction coefficient ($\varepsilon = 0.155\ M^{-1}\ cm^{-1}$) as stated by Hodges et al. (1999). The contents of H_2O_2 were estimated according to the Gay and Gebicki (2000) methodology, using 250 µM xylenol orange as an indicator. The results were calculated based on a calibration curve prepared with H_2O_2 standards.

Data analysis

The data were subjected to the Shapiro–Wilk test ($p > 0.05$) to determine whether the data had a normal distribution and the Bartlett's test ($p > 0.05$) to determine whether the samples had equal variances. When data failed on the Shapiro–Wilk test, a Box–Cox transformation [$T(Y) = (Y\lambda - 1)/\lambda$] was performed to obtain the normal distribution. Parametrical data were submitted to ANOVA followed by Scott-Knott post hoc test. For nonparametrical data, the Kruskal-Wallis' test with the Bonferroni method for P value correction was employed. All statistical tests were performed using R software, version 3.6.2.

5.3. Results

Effects of individual and associated Fe, Mn, and As on appearance, growth, and mineral bioaccumulation in the water lettuce plants

The toxic effects of Fe, Mn, and As were manifested in the leaves of the plants, including necrotic points progressing to leaf margin browning in Fe-treated plants (Figure 1c), whereas for plants treated with Mn and As, it was observed leaf yellowing and chlorosis (Figure 1e, g). In the combined treatments, it was possible to observe the presence of the characteristic symptoms of each element, such as browning of the margins and chlorosis of the leaf blade in plants grown with Fe + Mn and/or Fe + As and in the mixture of the three elements (Figure 1i, k, m, o). However, the effects were not intensified in the combinations of the elements in comparison with the single metals (Figure 1). In roots, the main effect was the detachment of the plant organs and consequent reduction of root volume, especially in the treatments with As, alone or in mixture (Figure 1h, l, n, p). However, the re-emission of new roots was observed at the end of the treatment period (data not shown). There was also the browning of the roots, especially in the combinations (Figure 1).

Interestingly, there was no changes in the shoot dry weight of the treated plants compared to the control (Table 1), considering uniformity at the installation of the experiment. Otherwise, root dry weight decreased in all treatments, apart from Mn-treated plants (Table 1). The As exposure, alone or in combinations, led to the decrease of about 50% of the root dry weight (Table 1).

As expected, there was an increase in the accumulation of metallic elements in the shoots and roots of plants subjected to pollutants (Table 1). In the shoots, the accumulation of Fe increased in plants that contained the association of Fe and Mn in the nutrient solution, compared to metal supplied alone (Table 1). On the other hand, the Mn concentration, which reached more than 18 mg g^{-1} DW, was higher in the single treatment, compared to mixtures with the other elements (Table 1). Similarly, As concentration was higher in As and FeAs-treated plants than in other combinations. The accumulation of Fe and Mn in roots was similar in single treatments plants Fe compared to associated ones (Table 1). For As accumulation, on the other hand, the concentration in the mixtures was higher than in As-treated plants (Table 1). The metal accumulation index (MAI) in both shoots and roots was increased as the elements were associated, especially in plants subjected to Fe and Mn (Table 1).

Surprisingly, the contents of macro-and micro nutrients remained unchanged in shoots of water lettuce plants, regardless of the metallic element applied, isolated or in combinations

(Table 2). Otherwise, the root contents of mineral nutrients were widely affected by the exposure to the treatments. The K^+ content decreased in the plants grown in the element mixtures (Table 2), whereas P_i decreased in all treatments by between 35 and 54%, compared to control plants (Table 2). Mn-stressed led to the decrease in Ca^{2+} root content, whereas the mixture of elements and also the exposure to As alone induced the decrease of Mg content in roots (Table 2). The Cu content was decreased in the presence of excess Fe, As, and also the mixture Fe + As and Fe + Mn + As in roots, compared to control plants (Table 2). Finally, the content of Zn was not significantly changed only in Mn and MnAs-treated plants (Table 2).

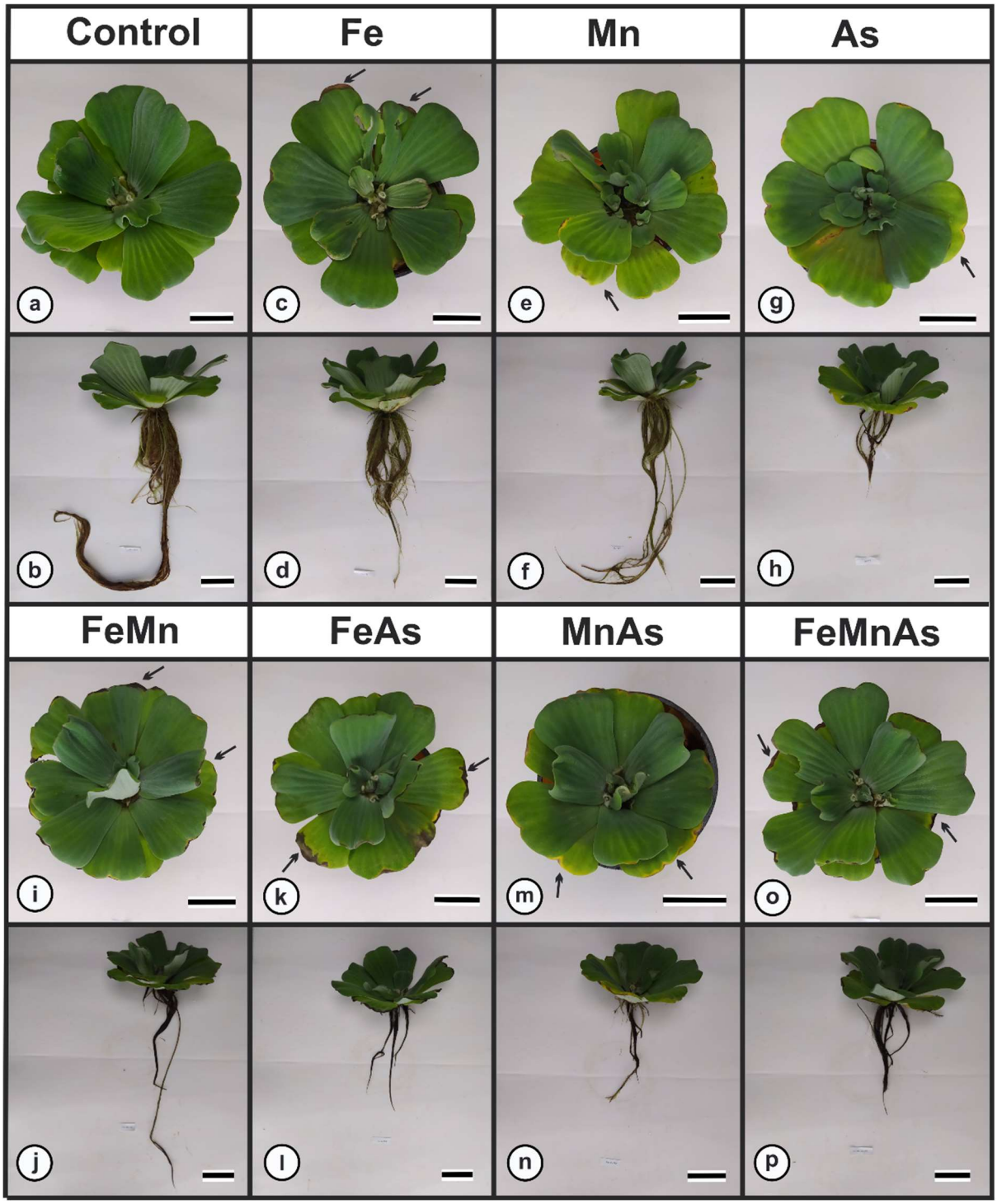

Figure 1. General appearance of *Pistia stratiotes* plants subjected to stress by Fe, Mn, As, and combination of these elements. Appearance of *P. stratiotes* plants growing for ten days in nutrient solution or in a medium containing 5 mM of Fe-EDTA or 4 mM $MnCl_2$ or 10 µM $Na_2HAsO_4.7H_2O$ isolated or in combinations. Control (a, b), Fe (c, d), Mn (e, f), As (g, h), FeMn (i, j), FeAs (k, l), MnAs (m, n), FeMnAs (o, p). Black arrows indicate toxicity symptoms such as chlorosis, dark spots, and necrosis. Bars = 5 cm.

Table 1. Effects of 5 mM of Fe-EDTA, 4 mM $MnCl_2$, and 10 µM $Na_2HAsO_4.7H_2O$, isolated or in combination in the dry weight, bioaccumulation of Fe, Mn, and As, and metal accumulation index (MAI) in water lettuce *(Pistia stratiotes)* plants after 10 days of treatment. Means ± standard errors (n = 5) followed by different letters are statistically different ($P \leq 0.05$) according to one-way analysis of variance (ANOVA) with post hoc Scott-Knott test

	Dry weight (g)	Fe (mg g^{-1} DW)	Mn (mg g^{-1} DW)	As (µg g^{-1} DW)	MAI
			Shoots		
Control	1.27 ± 0.20 a	0.59 ± 0.08 d	0.62 ± 0.08 d	nd	405.61
Fe	1.05 ± 0.10 a	4.76 ± 1.04 b	0.71 ± 0.05 d	nd	1825.31
Mn	1.24 ± 0.21 a	0.82 ± 0.07 c	18.31 ± 0.79 a	nd	6380.91
As	1.14 ± 0.22 a	1.11 ± 0.15 c	0.73 ± 0.04 d	95.31 ± 14.53 a	645.59
FeMn	1.11 ± 0.15 a	5.88 ± 0.28 a	11.47 ± 0.73 c	nd	5783.69
FeAs	1.03 ± 0.19 a	4.50 ± 0.51 b	0.74 ± 0.04 d	83.38 ± 5.96 a	1776.39
MnAs	1.14 ± 0.24 a	0.55 ± 0.02 d	14.53 ± 0.75 b	63.00 ± 2.96 b	5047.72
FeMnAs	1.01 ± 0.09 a	7.50 ± 0.93 a	13.74 ± 0.39 b	61.68 ± 2.28 b	7099.41
			Roots		
Control	0.36 ± 0.07 a	0.45 ± 0.17 b	0.84 ± 0.10 b	nd	429.44
Fe	0.29 ± 0.05 b	9.64 ± 0.92 a	0.69 ± 0.04 b	nd	3444.24
Mn	0.35 ± 0.07 a	0.78 ± 0.18 b	13.66 ± 1.00 a	nd	4815.09
As	0.16 ± 0.02 c	0.64 ± 0.16 b	0.61 ± 0.12 b	207.71 ± 18.64 b	486.74
FeMn	0.29 ± 0.04 b	11.41 ± 0.36 a	11.85 ± 1.06 a	nd	7755.65
FeAs	0.16 ± 0.04 c	11.41 ± 1.23 a	0.73 ± 0.13 b	374.91 ± 80.45 a	4172.30
MnAs	0.18 ± 0.04 c	0.79 ± 0.17 b	20.35 ± 4.83 a	325.11 ± 70.50 a	7157.12
FeMnAs	0.16 ± 0.02 c	11.37 ± 0.96 a	13.31 ± 0.16 a	330.14 ± 53.95 a	8339.12

nd = non detected

Table 2. Effects of 5 mM of Fe-EDTA, 4 mM $MnCl_2$, and 10 µM $Na_2HAsO_4.7H_2O$, isolated or in combination in the contents of K, Pi, Ca, Mg, Cu, and Zn in water lettuce *(Pistia stratiotes)* plants after 10 days of treatment. Means ± standard errors (n = 5) followed by different letters are statistically different ($P \leq 0.05$) according to one-way analysis of variance (ANOVA) with post hoc Scott-Knott test (regular letters) or nonparametric Kruskal-Wallis's test using Bonferroni method for P value adjustment (italicized letters).

	Control	**Fe**	**Mn**	**As**	**FeMn**	**FeAs**	**MnAs**	**FeMnAs**
				Shoot				
	----------mg g^{-1}----------							
K	36.18 a	36.84 a	37.26 a	37.90 a	35.14 a	34.90 a	34.82 a	31.93 a
P_i	1.29 a	1.44 a	1.28 a	1.40 a	1.16 a	1.54 a	1.29 a	1.37 a
Ca	25.24 a	27.50 a	25.56 a	31.47 a	25.74 a	28.72 a	28.39 a	29.73 a
Mg	5.33 a	4.82 a	4.63 a	5.14 a	4.37 a	4.76 a	4.68 a	4.82 a
	----------µg g^{-1}----------							
Cu	10.15 a	11.61 a	9.83 a	11.55 a	8.85 a	10.13 a	11.39 a	12.56 a
Zn	28.29 a	23.95 a	12.69 a	15.43 a	11.67 a	13.53 a	16.32 a	16.15 a
				Root				
	----------mg g^{-1}----------							
K	30.64 *a*	24.19 *abc*	28.62 *ab*	20.91 *abc*	20.22 *c*	21.98 *abc*	20.51 *bc*	19.55 *c*
P_i	0.95 a	0.47 b	0.58 b	0.61 b	0.61 b	0.55 b	0.52 b	0.44 b
Ca	19.04 *a*	18.28 *a*	14.68 *b*	20.04 *a*	16.64 *ab*	19.05 *a*	15.70 *ab*	16.40 *ab*
Mg	5.02 a	4.78 a	4.04 a	3.14 b	2.96 b	3.26 b	2.66 b	3.49 b
	----------µg g^{-1}----------							
Cu	35.42 a	27.51 b	43.10 a	28.47 b	33.76 a	22.77 b	36.89 a	29.06 b
Zn	85.34 a	36.95 b	51.02 a	23.43 b	31.68 b	25.18 b	63.06 a	32.44 b

Structural changes induced by single and mixture of Fe, Mn, and As

Despite the plants showed no severe toxicity symptoms upon exposure to the metallic elements (Figure 1), important structural changes were induced by the treatments, in both leaves and roots (Figure 2, 3). The leaves of Fe-treated plants displayed protoplast retraction, besides collapse and reduction of leaf blade thickness in cells closer to the leaf edge, both in the epidermis and in the mesophyll (Figure 2c, d). On the other hand, in cells furthest from the leaf margin and in the vascular bundle there were no detected changes. In plants subjected to single Mn and As, there was a more generalized collapse and retraction of the protoplast along the leaf blade, but with less intensity in relation to Fe-treated leaves (Figure 2e-h).

There were also apparent additive effects of the mixture of elements on the leaf structure of plants (Figure 2i-p). The plants treated with the combination of the elements displayed intense retraction of the cell protoplast, along with the collapse of the epidermis and trichomes cells in the margins of the leaf blade. There was also the formation of intercellular spaces due to the collapse of the parenchyma cells, especially in the combinations Fe + Mn, Fe + As, and in the mixture of the three elements (2i-l, o, p). Despite this, the vascular tissues remained without noticeable changes (Figure 2i-p).

In roots, Fe and Mn-stressed plants showed cortex cells close to the epidermis slightly collapsed, with sinuous walls. However, the overall cell integrity was maintained (Figure 3c-f). These alterations were intensified in the combination of these two elements, with the occurrence of collapse in the parenchyma cells (Figure 3 i, j). However, extensive changes were observed in the roots of plants treated with As, either alone or in combinations (Figure 3g, h, k–p). The roots showed changes in the shape of the cortex and vascular cylinder cells, in addition to retraction of the cortex and parenchyma protoplast cells.

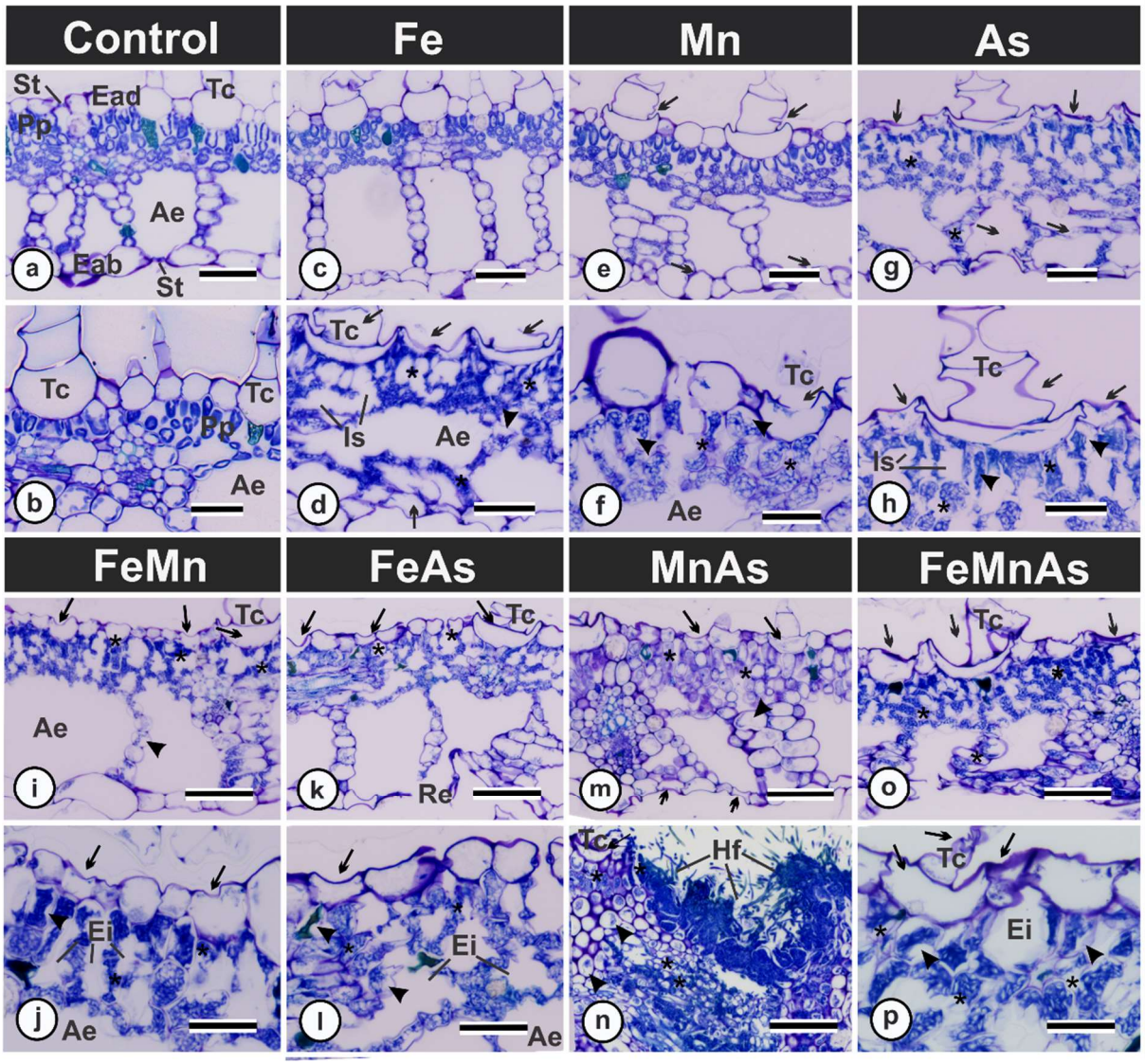

Figure 2. Structural effects on leaves of *Pistia stratiotes* plants caused by Fe, Mn, and As, isolated and in combination. Cross section of *P. stratiotes* leaves growing for ten days in the control nutrient solution or in a medium containing 5 mM of Fe-EDTA or 4 mM $MnCl_2$ or 10 µM $Na_2HAsO_4.7H_2O$ isolated or in combinations. Control (a, b), Fe (c, d), Mn (e, f), As (g, h), FeMn (i, j), FeAs (k, l), MnAs (m, n), FeMnAs (o, p). Ae (aerenchyma); Eab (abaxial epidermis); Ead (adaxial epidermis); Is (intercellular spaces); St (stomata); Hf (fungal hyphae); Pp (palisade parenchyma); Re (rupture of the epidermis); Tc (tector trichome); Asterisk (collapse of chlorophyll parenchyma cells); Arrowhead (protoplast retraction); Arrow (collapse of epidermal cells and tector trichomes). Bars: (a, c, d, e, g, i, k, m, n, o) = 100 µm; (b, f, h, j, l, p) = 50 µm.

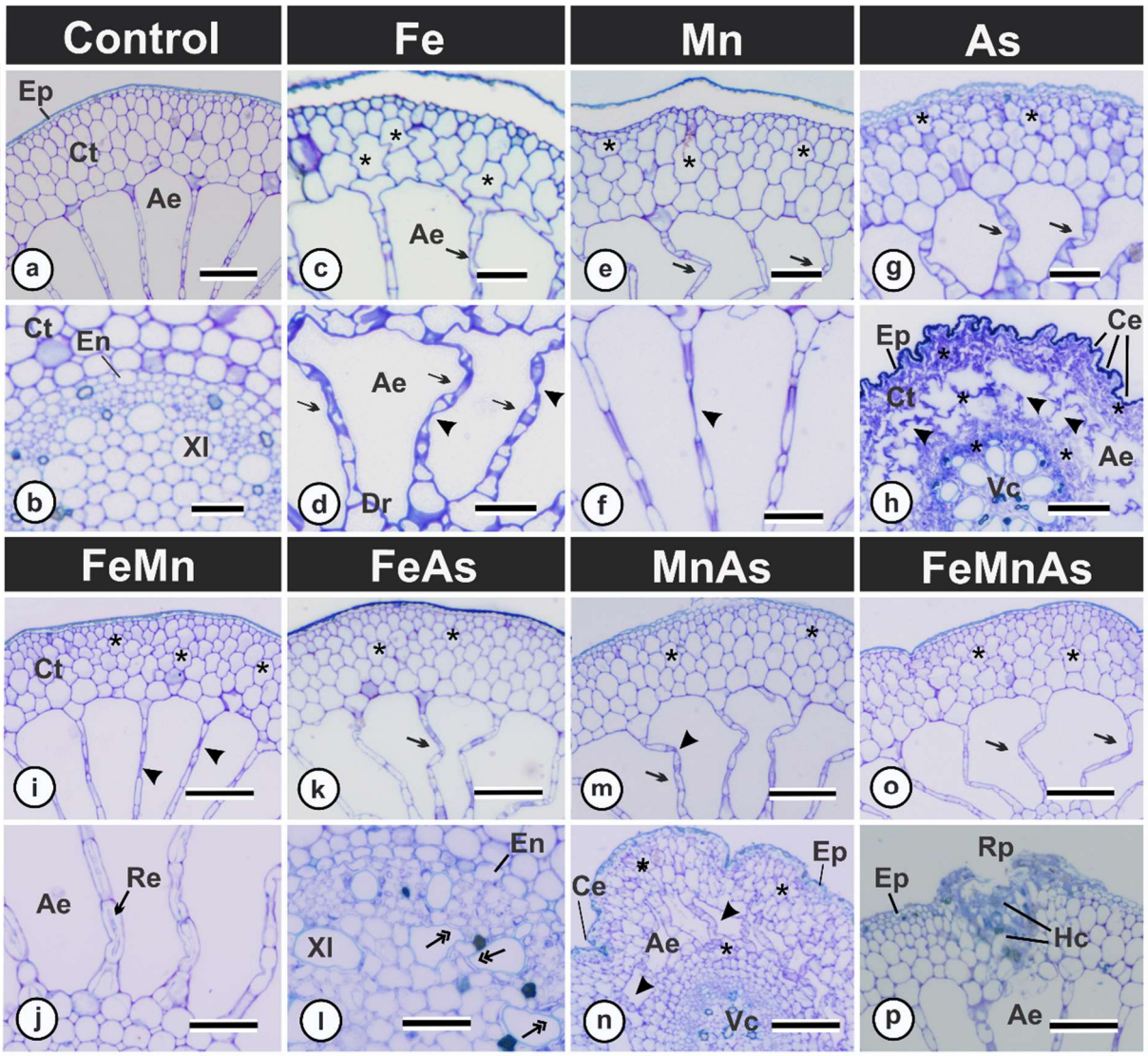

Figure 3. Effects of the stress induced by Fe, Mn, and As, isolated and in combination on root structure of *Pistia stratiotes* plants. Cross section of *P. stratiotes* roots growing for ten days in a control or modified nutrient solution containing 5 mM of Fe-EDTA or 4 mM $MnCl_2$ or 10 µM $Na_2HAsO_4.7H_2O$, isolated or in combinations. Control (a, b), Fe (c, d), Mn (e, f), As (g, h), FeMn (i, j), FeAs (k, l), MnAs (m, n), FeMnAs (o, p). Ae (aerenchyma); Ce (collapse of the epidermis); Ct (cortex); Vc (vascular cylinder); En (endoderm); Ep (epidermis); Hc (cortical cell hypertrophy); Re (protoplast retraction); Rp (rupture of the epidermis); X1 (xylem); Asterisk (change in the shape of cortex cells); Arrowhead (aerenchyma cell collapse); Arrow (change in the shape of aerenchyma cells). Double-headed arrow (change in xylem shape). Bars: (a, c, e, g, i, k, m, o, p) =150 µm; (b, d, f, j, l) = 40 µm; (h, n) = 100 µm

Effects of the Fe, Mn and As on the photosynthetic performance

The contents of chlorophyll *a* and *b* as well as the gas exchange were also altered by the metallic elements in water lettuce plants (Figure 4a - f). There was a decrease in chlorophyll *a* content in Mn and As-stressed plants, as well as in the combination Mn + As (Figure 4a). A similar response was observed for chlorophyll *b*, although the content of the pigment was higher for plants subjected to Fe and Fe + Mn + As (Figure 4b). Interestingly, carotenoid contents, the dark respiration and also the fluorescence of chlorophyll *a* parameters were not significantly changed by the treatments (Figure 4c, g - j). Otherwise, the net CO_2 assimilation was decreased by around 45% in plants grown in all singles and combinations of the metallic elements, apart from Mn (Figure 4d). As a result, internal CO_2 concentration was also similar between control and Mn-treated plants and higher for the other (Figure 4e). Also, only MnAs-treated plants displayed a decreased Rubisco carboxylation efficiency, compared to control plants (Figure 4f).

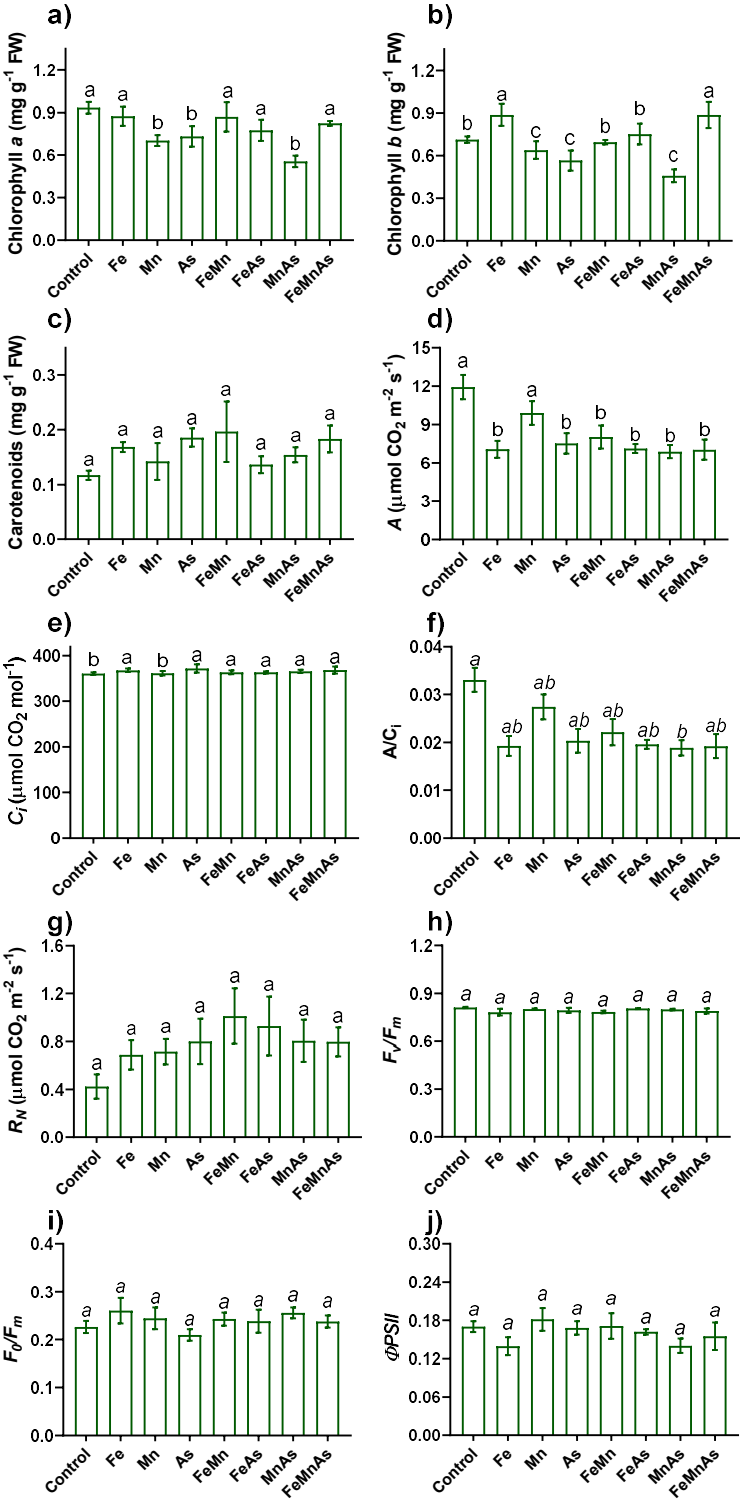

Figure 4. Effects of the stress induced by Fe, Mn, and As, isolated and in combination on photosynthetic performance of *Pistia stratiotes* plants. Contents of chlorophyll *a* (a), chlorophyll *b* (b) and carotenoids (c), along with net CO_2 assimilation (d), internal CO_2 concentration (e), carboxylation efficiency – A/C_i (f), respiration in the dark g), potential quantum yield of the photosystem II – F_v/F_m (h), ratio between the minimal (F_0) and maximal (F_m) fluorescence (i), and actual PSII photochemical efficiency – ΦPSII (j) in water lettuce *(P. stratiotes)* plants growing for ten days in a control or modified nutrient solution containing 5 mM of Fe-EDTA or 4 mM $MnCl_2$ or 10 µM $Na_2HAsO_4.7H_2O$, isolated or in combinations.

Different letters above the bars showing mean ± standard errors (n = 5) indicate significant differences ($P < 0.05$) between treatments according to one-way analysis of variance (ANOVA) with post hoc Scott-Knott test (regular letters) or nonparametric Kruskal-Wallis's test using Bonferroni method for P value adjustment (italicized letters).

Single and combined Fe, Mn, and As-induced changes in plant metabolites

In general, the exposure to the metallic elements triggered an increased accumulation of sugars and starch in shoots and decreased contents of these metabolites in roots (Figure 5 a - d). The sucrose contents in shoots were higher in all the treatments, especially in Mn, MnAs and FeMnAs-treated plants, whereas in roots of plants subjected to Fe, As, and the combination of Fe, Mn, and As had the lower contents (Figure 5a). A similar response was observed for fructose and glucose measurements, in which the combination of FeMn, followed by MnAs and FeMnAs-treated plants displayed increased shoot contents (Figure 5b, c). In roots, the contents of fructose were lower in the plants treated with Fe, As, and the combination of MnAs and FeMnAs, compared to control plants (Figure 5b). On the other hand, the root glucose of Mn and FeMnAs was similar to control, whereas the other elements and mixtures induced decreases in the metabolite (Figure 5c). Interestingly, the starch content was decreased in FeMn-treated plants in shoots and in the mixtures involving Fe + Mn and Mn + As in roots (Figure 5d).

The content of the organic acids malate and fumarate had a general decreasing trend in both shoots and roots in most treatments with the pollutants (Figure 5e, f). For malate, there was a decrease in shoots of plants subjected to Mn, as well as in the combinations of FeMn and MnAs, whereas the root contents were lower in all treatments, apart from Fe, compared to control (Figure 5e). Furthermore, the exposure to Mn, FeMn, and MnAs induced a decrease in shoot fumarate content (Figure 5f). Similarly, the plants subjected to MnAs and FeMnAs combinations displayed lowered fumarate in roots (Figure 5f). Interestingly, the total phenol contents remained unchanged, regardless of the treatment or the plant tissue (Figure 5g).

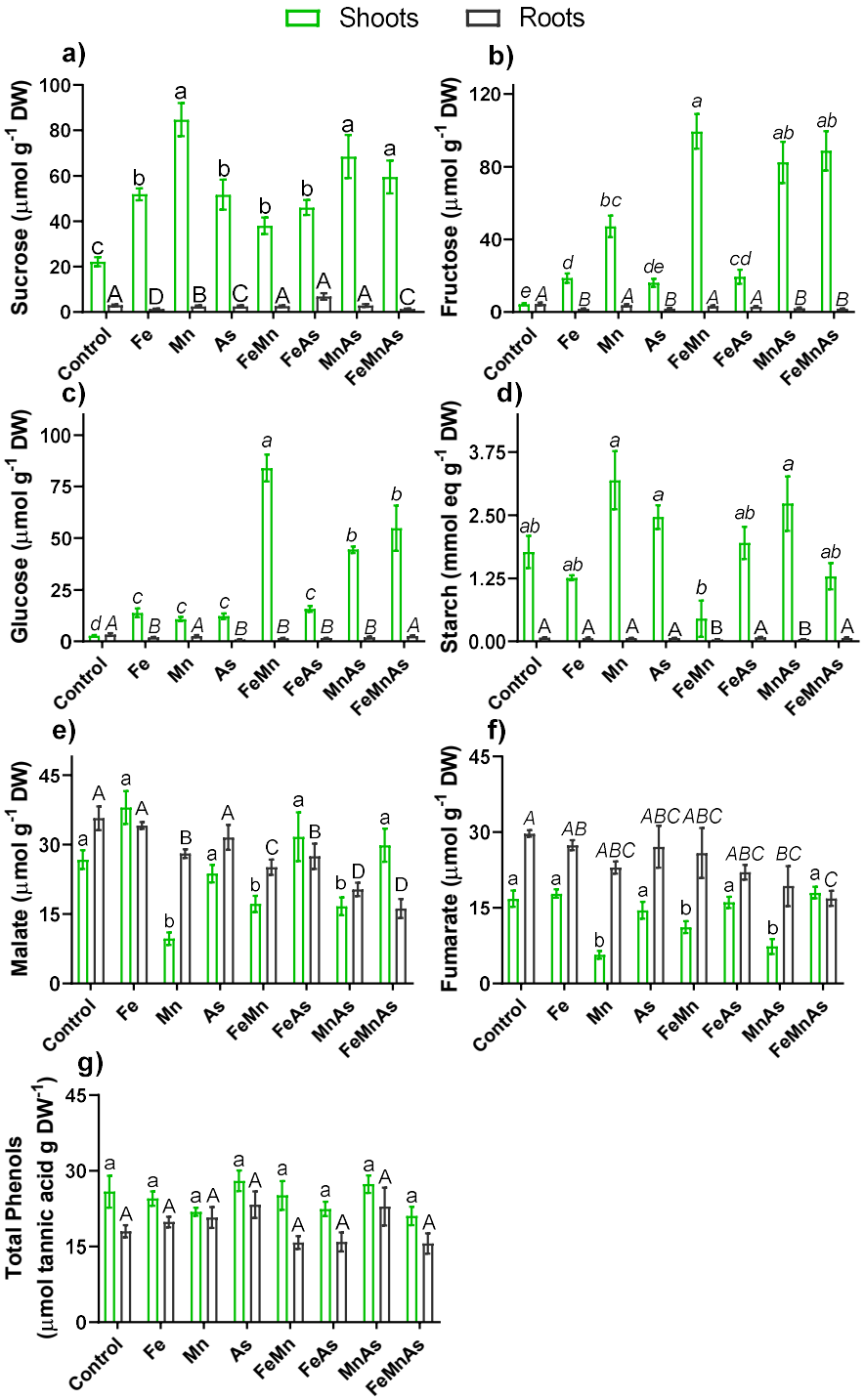

Figure 5. Effects of the stress induced by Fe, Mn, and As, isolated and in combination on metabolites contents of *Pistia stratiotes* plants. Contents of sucrose (a), fructose (b), glucose (c), starch (d), malate (e), fumarate (f), and total phenols (g), in water lettuce *(P. stratiotes)* shoots (green bars) and roots (gray bars) growing for ten days in a control or modified nutrient solution containing 5 mM of Fe-EDTA or 4 mM $MnCl_2$ or 10 µM $Na_2HAsO_4.7H_2O$, isolated or in combinations. Different letters above the bars showing mean ± standard errors (n = 5) indicate significant differences ($P < 0.05$) between treatments according to one-way analysis of variance (ANOVA) with post hoc Scott-Knott test (regular letters) or nonparametric Kruskal-Wallis's test using Bonferroni method for P value adjustment (italicized letters).

Antioxidant responses, oxidative biomarkers and redox status changes

The exposure to single or associated Fe, Mn, and As in the nutrient solution led to an induction of enzymatic antioxidant protection (Figure 6a - d). According to the statistical analysis, the SOD and POX activities in shoots were increased in plants subjected to isolated excess Fe, or in combination with Mn and Mn + As (Figure 6a, c). The same treatments and also the combination of FeAs induced an increase in SOD activity in roots (Figure 6a). The CAT activity, on the other hand, was only induced in roots, in all treatments, apart from Mn, compared to control plants (Figure 6b). Furthermore, the root activity of POX was only increased in Fe-treated plants (Figure 6c). Otherwise, the shoot APX activity was improved in all treated-plants, regardless of the element, whereas in the roots, the presence of Fe, isolated or in combination with the other elements induced an increase in the enzyme activity (Figure 6d).

It was observed an increase in shoot H_2O_2 contents in MnAs combination and also in the same single elements, whereas no significant changes were detected in the root contents among treatments (Figure 6e). Likewise, shoot TBARS contents was not modulated by the addition of the elements in the nutrient solution (Figure 6f). In roots, the exposure to Fe, as well as the combinations of FeMn and FeMnAs triggered an increase in TBARS contents (Figure 6f).

Interestingly, the contents of total glutathione and its disulfide form (GSSG) remained unaltered in both shoot and roots upon the exposure to the pollutants (Figure 7a, b). However, the ratio GSH/GSSG was higher in the roots of treated-plants, except for those ones grown with Fe and the combination FeMnAs, and lower in the As-treated plants (Figure 7c). Regarding the ascorbate measurements, there were no significant changes the treated plants for the contents of total ascorbate in both shoots and roots, compared to the control ones (Figure 7d). Nevertheless, the contents of DHA in shoots were increased in Fe and As-treated plants and also in the combination of the elements (Figure 7e). In the roots, on the other hand, only the combination FeAs was able to increase the concentration of DHA in the plants (Figure 7e). Interestingly, the ratio AsA/DHA in shoots was only decreased in Fe-treated plants, whereas no significant changes were detected in the roots of treated plants compared to the control (Figure 7f).

There was no significant modulation of GR and MDHAR activity in shoots and roots of the plants and also for DHAR activity in roots, regardless the treatment (Figure 8a, b). On

the other hand, a higher DHAR activity was observed in the roots of plants subjected to the elements, except Mn and the combination MnAs (Figure 8c).

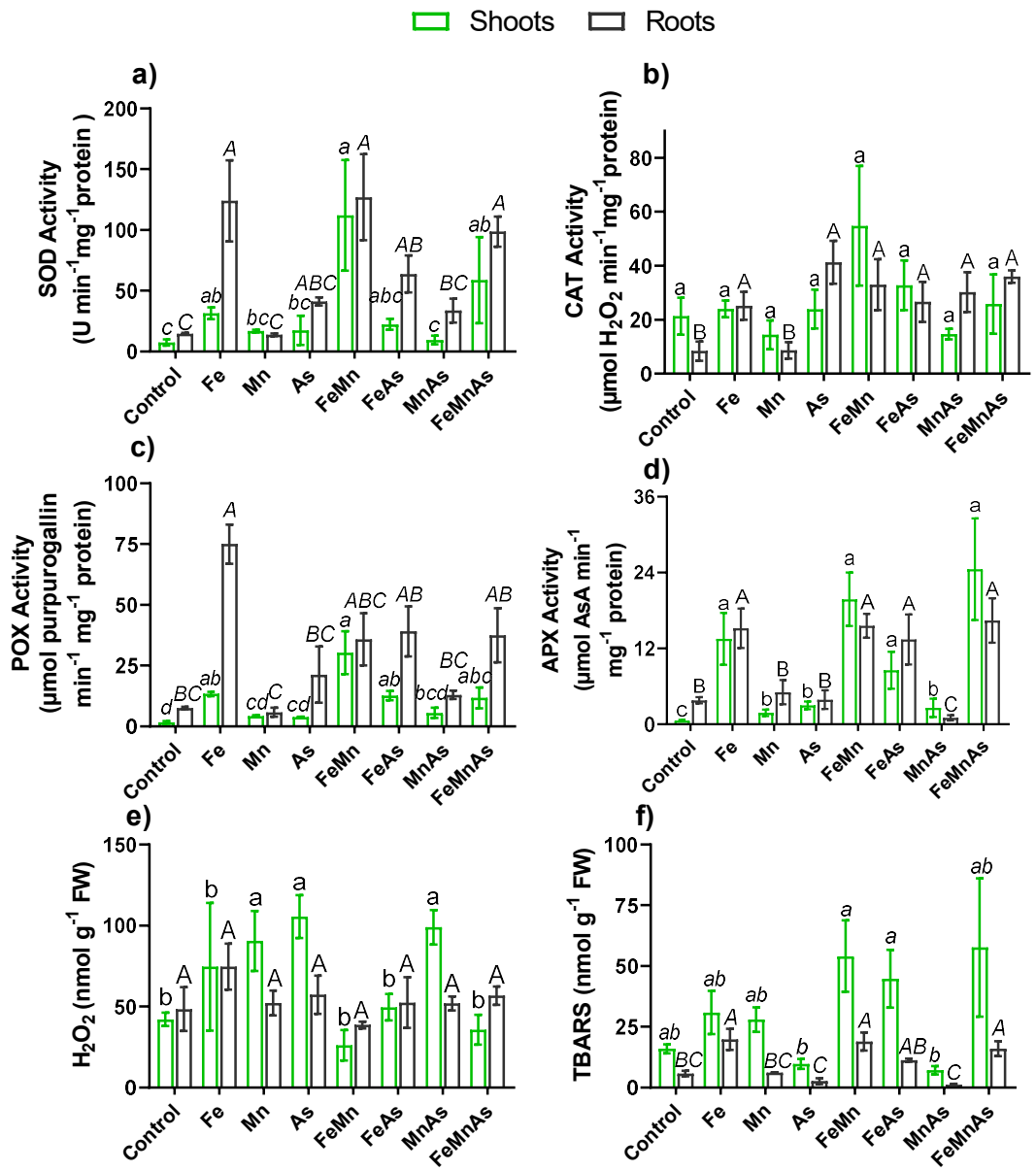

Figure 6. Effects of the stress induced by Fe, Mn, and As, isolated and in combination on antioxidant enzymes and oxidative biomarkers of *Pistia stratiotes* plants. Activity of superoxide dismutase - SOD (a), catalase - CAT (b), peroxidase - POX (c), ascorbate peroxidase - APX (d), along with the contents of H_2O_2 (e), and TBARS (f) in water lettuce *(P. stratiotes)* shoots (green bars) and roots (gray bars) growing for ten days in a control or modified nutrient solution containing 5 mM of Fe-EDTA or 4 mM $MnCl_2$ or 10 µM $Na_2HAsO_4.7H_2O$, isolated or in combinations. Different letters above the bars showing mean ± standard errors (n = 5) indicate significant differences ($P < 0.05$) between treatments according to one-way analysis of variance (ANOVA) with post hoc Scott-Knott test (regular letters) or nonparametric Kruskal-Wallis's test using Bonferroni method for P value adjustment (italicized letters).

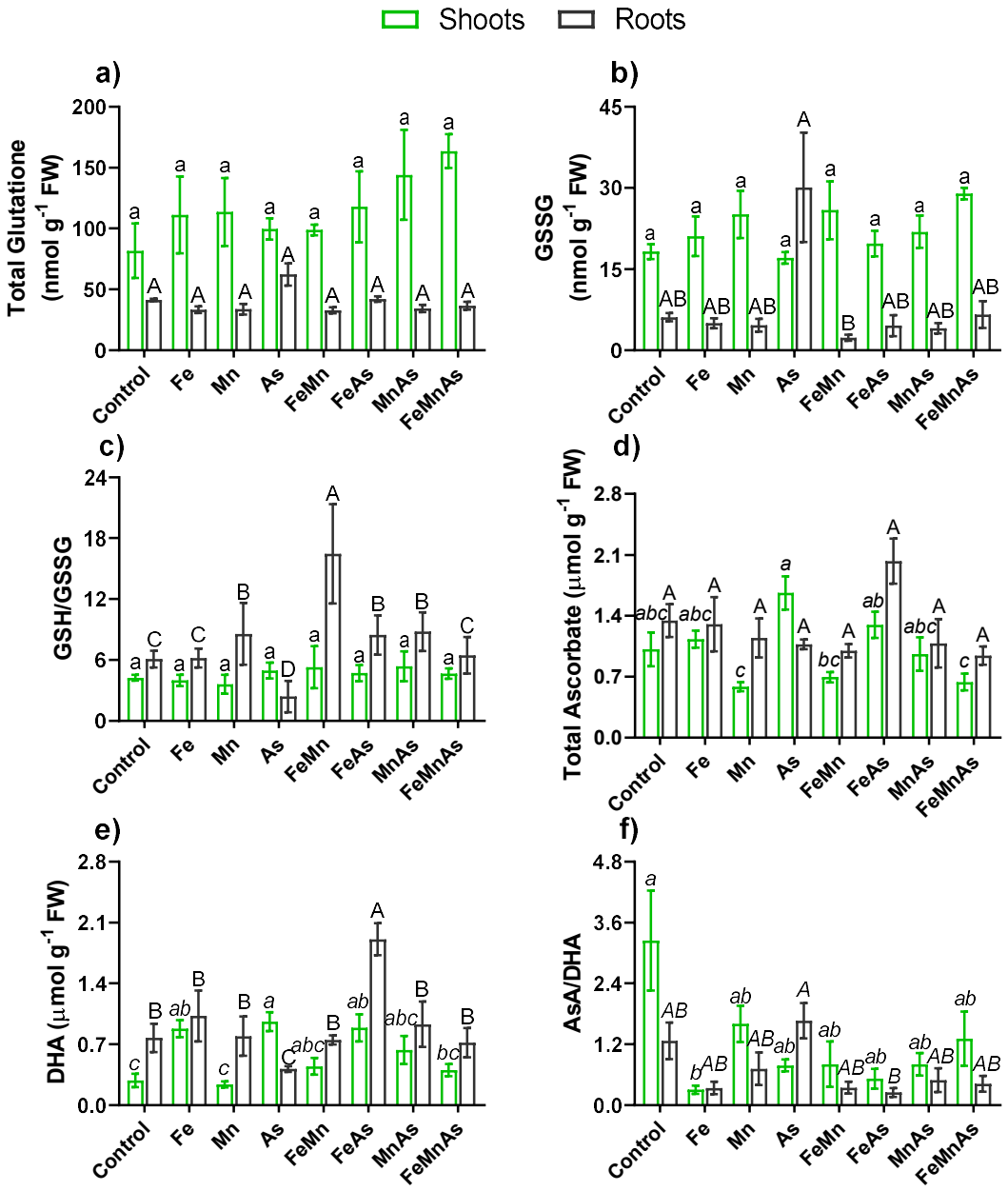

Figure 7. Effects of the stress induced by Fe, Mn, and As, isolated and in combination on non-enzymatic antioxidants of *Pistia stratiotes* plants. Contents of total glutathione (a), disulfide glutathione (b), reduced/disulfide glutathione ratio (c), total ascorbate (d), dehydroascorbate (e), and reduced/oxidized ascorbate ratio (f) in water lettuce *(P. stratiotes)* shoots (green bars) and roots (gray bars) growing for ten days in a control or modified nutrient solution containing 5 mM of Fe-EDTA or 4 mM $MnCl_2$ or 10 µM $Na_2HAsO_4.7H_2O$, isolated or in combinations. Different letters above the bars showing mean ± standard errors (n = 5) indicate significant differences ($P < 0.05$) between treatments according to one-way analysis of variance (ANOVA) with post hoc Scott-Knott test (regular letters) or nonparametric Kruskal-Wallis's test using Bonferroni method for P value adjustment (italicized letters).

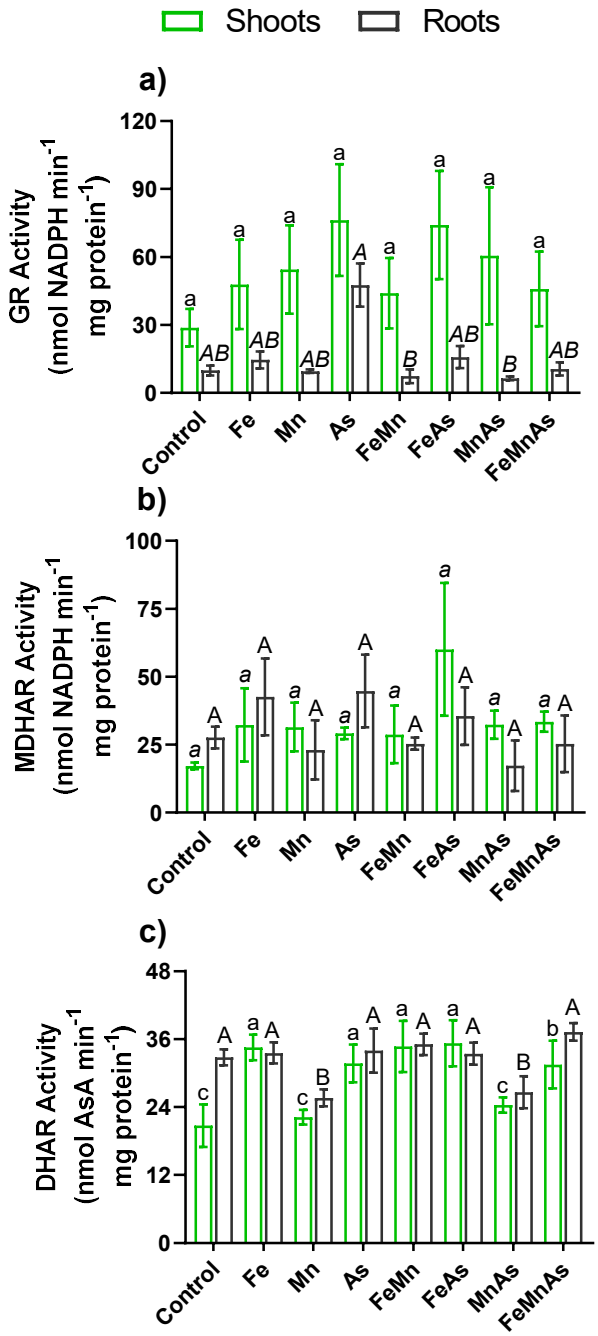

Figure 8. Effects of the stress induced by Fe, Mn, and As, isolated and in combination on glutathione-ascorbate cycle enzymes of *Pistia stratiotes* plants. Activity of glutathione reductase - GR (a), monodehydroascorbate reductase - MDHAR (b), and dehydroascorbate reductase - DHAR (c) in water lettuce *(P. stratiotes)* shoots (green bars) and roots (gray bars) growing for ten days in a control or modified nutrient solution containing 5 mM of Fe-EDTA or 4 mM $MnCl_2$ or 10 µM $Na_2HAsO_4.7H_2O$, isolated or in combinations. Different letters above the bars showing mean ± standard errors (n = 5) indicate significant differences ($P < 0.05$) between treatments according to one-way analysis of variance (ANOVA) with post hoc Scott-Knott test (regular letters) or nonparametric Kruskal-Wallis's test using Bonferroni method for P value adjustment (italicized letters).

5.4. Discussion

The combination of Fe, Mn, and As had additive but not synergic effects on appearance, growth as well as on nutritional homeostasis of water lettuce plants

In the environment, almost all the pollutants are composed of mixtures that contain more than one chemical element or substance. Pollutant mixtures vary in their effects on living organisms, being additive, synergistic, or inhibitory (Ramakrishnan et al., 2011). Nevertheless, virtually all studies are done with single elements or heterogeneous and complex mixtures in the field, making it difficult to understand plant responses, tolerance mechanisms and accumulation efficiency for phytoremediation purposes (Khalid et al., 2017; Rezania et al., 2016). In the present study, water lettuce (*Pistia stratiotes*) plants were subjected to Fe, Mn, and As concentrations, isolated or in associations, for ten days to better understand specific as well as combined effects of the elements on the plants.

Overall, the plants subjected to the elements, either single or in mixtures, were able to sustain their growth and the removal of the pollutants (Table 1), despite the notorious symptoms of toxicity, which followed a characteristic pattern depending on the element in the nutrient solution (Figure 1). Fe-treated plants display dark spots progressing to browning of leaf margins and also in roots, a common coloration caused by phenols accumulation (Wu et al., 2014). Despite this, the total content of phenol was not changed by the treatments (Figure 5g), indicating that there was a metabolic reprogramming towards complexation and vacuolar compartmentalization rather than changes in the biosynthesis. Furthermore, the chlorosis and yellowing in plants subjected to Mn, As, or the combination, are likely related to the decrease observed in chlorophyll *a* and *b* contents (Figure 4a, b).

Another remarkable effect in plants treated with As, including the mixtures, was the root abscission, as also previously related by Farnese et al. (2014). These authors hypothesized the formation of an abscission meristem as part of a plant acclimatization strategy, also observed with other pollutants (Arif et al., 2016), to avoid an initial overload and enable the activation of defense mechanisms. Root loss may be related to cell death events, which are attributed to the increase in ethylene synthesis in the process of aerenchyma formation in roots under hypoxic conditions (Yamauchi et al., 2020). Other related aspects may include the attack of free radicals, such as the process of rapid root abscission that occurs in species of the genus Azolla (Cohen et al., 2014), as well as the mechanisms of cell cycle inhibition (Alvarenga et al., 2020).

Curiously, the association of two or three elements did not enhance the effects seen individually but rather resulted in an additive effect of these symptoms (Figure 1), which may be connected to how the materials are partitioned into shoots and roots (Table 1). While As and Fe were predominantly confined to the roots, as previously reported by Campos et al. (2019) and Das et al. (2020), Mn was translocated in large amounts to the shoots (Table 1). Furthermore, although Fe and Mn share some of the influx transporters (Alejandro et al., 2020; Tripathi et al., 2018), the association of the elements did not decrease bioaccumulation. On the other hand, Mn translocation was impacted by the association with As and Fe (Table 1). These effects are probably due to the Mn/Fe competitive inhibition for the xylem loading (Green and Rogers, 2004) or As-induced down-regulation of root-to-shoot transporters (Chauhan et al., 2020).

Despite the observation of some symptoms of toxicity in the leaves, such as yellowing (Figure 1), there were no significant changes in the concentration of macro and micronutrients in the organs with exposure to the elements excess (Table 2). On the other hand, the concentration of mineral nutrients in plants was affected in different extensions depending on the element and treatments (Table 2). The impairments observed in mineral accumulation as a result of increasing Fe, Mn, As or combinations can be related to the inhibitory competition by the uptake of elements that share the same transporters due to similar coordination geometry and/or ionic radii. For instance, the diminished Ca^{2+} triggered by excess Mn observed in our study was discovered in the 1970s (reviewed by He et al., 2021) and further confirmed in Arabidopsis and other species (Blamey et al., 2015; Lešková et al., 2017).

The decreased P_i concentration in all treatments (Table 2) perhaps originated also from uptake competition, in As-treated plants, due to the similarity in the physical properties of arsenate and phosphate. Also, this response can arise from the pollutants-induced changes in the energy charge of the cell (Srivastava et al., 2013), through the ratio of adenylates concentration, considering that the absorption of P_i is energy-costly (Wang et al., 2018). Furthermore, solutes uptake by plant cells is strictly regulated to maintain the membrane potential (Pantoja, 2021), relying on the P-type H^+ ATPases-dependent pumping of H^+ from the cytosol into the apoplast at the expense of ATP hydrolysis, and therefore the overload of Fe and Mn can induce may limit the uptake of other cations, as observed for Cu and Zn, especially in Fe excess conditions (Table 2).

Taken together, the distribution of nutrients to the shoot was not affected, whereas the overaccumulation of elements in the root caused a decrease in the concentration of certain

nutrients. Furthermore, the combination of elements had an additional effect, not decreasing the concentration of an element itself, compared to the single treatments, but causing a deficit in the concentration of a greater number of nutrients.

Single or mixture of metallic elements triggered specific structural disorders but maintained vascular tissues arrangement

The main structural alterations, such as the protoplast retraction and collapse of epidermal and mesophilic leaf cells are likely to be related to the ROS-induced plasma membrane damage, especially in plants subject to Fe treatments (Figure 2), as observed by Araújo et al. (2015) in two Fe-tolerant grass species. Interestingly, even in combination of the metallic elements, the structural damage was not observed throughout the leaf tissue (Figure 2), remaining restricted to peripheral regions, which may have contributed in part to the maintenance of metabolic processes and mineral transport (Table 2).

Even in treatments where leaf damage was not visibly clear, as in plants subjected to Mn and As, structural changes occurred, such as changes in the shape of the cell. Therefore, anatomical assessment can provide prognostic information on the effect of stressors agents in plants, as pointed out by Cruz et al. (2021) and Freitas-Silva et al. (2020). The alterations in the shape of cells were also pronounced in roots, where the generation of hydroxyl radicals may have caused the cleavage of cell wall polysaccharides, as observed by Liszkay et al. (2004). Similarly, these compounds are likely to induce membrane damage, contributing to structural changes and also impairments in nutrient uptake (Shabala and Pottosin, 2014).

The excess of metallic elements, especially in combinations, altered the appearance of intercellular spaces, which may have contributed to decreases in photosynthetic performance due to impediments in the gas diffusion in mesophilic cells (Freitas-Silva et al., 2020). On the other hand, vascular tissues had their structure preserved both in leaves and roots, which must have contributed to the translocation of nutrients (Table 2), as well as to the maintenance of the accumulation of pollutants, especially in mixtures (Table 3).

Metallic elements induced changes in sugar translocation and decreased photosynthetic parameters despite unaltered photochemical traits

Photosynthetic impairments observed through the decreased net CO_2 assimilation in the treatments, except Mn-grown plants (Figure 4d), were associated with lower pigments contents (Figure 4a, b) and biochemical disorders, as the chlorophyll *a* parameters were not affected (Figure 4g - j), indicating preservation of thylakoid reactions for NADPH and ATP generation in chloroplasts.

A key step for photosynthetic carbon metabolism in plants is the carboxylation of RUBP catalyzed by RuBisCO, which is also a critical target of toxic metals (Chauhan et al., 2020; Rajpoot et al., 2021). Several investigations have shown that metals like copper and cadmium, cobalt, manganese, and zinc cause the degradation and/or fragmentation of RuBisCO in tolerant and non-tolerant plants (Führs et al., 2008; Kieffer et al., 2009; Tuomainen et al., 2006). Moreover, recent observation of the downregulation of RuBisCO in response to As stress was made at both transcriptome and proteome levels in rice plants (Chauhan et al., 2020), suggesting that this step was decisive for the reduction of photosynthesis observed in our data (Figure 4d).

It is fundamental to point out that the mixture of elements did not cause additive or synergistic effects in the reduction of photosynthesis, which may be related to the accumulation of these elements in trichomes (non-photosynthetic cells) or in the epidermis, which has a diminished abundance of chloroplasts in water lettuce. Interestingly, in these tissues, a greater occurrence of damage and structural alterations were detected, especially when combinations of the elements were made (Figure 2).

Moreover, decreases in CO_2 accompanied by local accumulation of assimilates, as observed by the higher contents of sucrose, fructose, glucose, and starch in shoots of most single and associated metal-grown plants (Figure 5 a - d), indicate the presence of feedback inhibition of photosynthesis under sink limitation (Fabre et al., 2019). This hypothesis seems even stronger in plants treated with single and combinations of As, in which there was loss and re-emission of roots (Figure 1).

Furthermore, in the roots, the content of these metabolites was decreased (Figure 4 a - d), which may be related to disturbances in the process of loading assimilates into the phloem, as phloem loading in most herbaceous species is dependent upon metabolic energy for active transport into phloem companion cell/sieve element complexes (CC–SE) (Ainsworth and Lemonnier, 2018). Alterations in assimilates phloem loading and associated feedback

regulation on carbon metabolism also rely on short peptides and transcription factors signaling and amino acid cycling between shoot and root, which could inhibit sucrose transport (Tegeder and Hammes, 2018).

Malate and fumarate depletion upon metals accumulation, on other hand, can be associated with two main aspects: i) H^+ scavenging to maintain membrane polarization for nutrient uptake associated with malate decarboxylation catalyzed by the malic enzyme (Wegner and Shabala, 2020) and, ii) anaplerotic pathways from 2-oxoglutarate for the biosynthesis of amino acids involved in defense mechanisms and N metabolism, or from fumarate for polyamine biosynthesis (Campos et al., 2016).

The content of phenolic compounds, which has antioxidant function and plays a role in the complexation of metals (Onaga et al., 2016), was not altered by the treatments (Figure 5g). Even so, it is likely that these compounds have been redirected to structures of complexation and compartmentalization of the elements, considering the color changes in the roots (Figure 1).

Plants subjected to excess metals were able to induce antioxidant protection and maintain redox balance

Most abiotic stressors, including metallic elements, have ROS overproduction as a common outcome as a result of overwhelm on electron transfer processes as well as disturbances in redox reactions (García-Caparrós et al., 2021). The plant cells capacity to respond defensively to prevent ROS-induced oxidative damage by using antioxidant mechanisms to operate in ROS removal and signaling plays a major role to provide metal tolerance (Ali et al., 2019; Branco-Neves et al., 2017; Foyer and Noctor, 2005).

Water lettuce plants subjected to excess Fe, Mn, As and the combinations of these elements display an overall outstanding induction of ROS-scavenging enzyme activity, especially played by SOD, CAT, and APX (Figure 6). Interestingly, excess Fe treatment, isolated and in combination with the other elements, seems to be more effective in triggering the induction of the enzymes (Figure 6 a–d, 8c), which can be associated with the Fenton reaction (Gutteridge et al., 1981). In this mechanism, Fe^{2+} is first oxidized to Fe^{3+} by H_2O_2, resulting in the highly reactive hydroxyl radical ($^{\bullet}OH$), which is then reduced back to Fe^{2+} by the superoxide anion radical ($O_2^{\bullet-}$) via the Haber-Weiss reaction, causing oxidative damage in the cells (Aung and Masuda, 2020). Furthermore, it is well documented that antioxidant enzymes use Fe and Mn as cofactors and have their expression and activity induced in the

presence of these metallic elements (Ahammed et al., 2020; Hasanuzzaman et al., 2019; Stein et al., 2014).

The oxidative protection provided by the enzymes and also by the maintenance of the plant redox status (Figure 7) seems to have been fundamental to avoiding the increase in membrane damage, measured by the TBARS content, in the shoot (Figure 6e). In roots, the additional TBARS content must have been generated by the higher concentration of pollutants, especially Fe and As, in these organs (Table 2, Figure 6e). This same reasoning may explain the increase in CAT activity (Figure 6b), which possibly played an important role in ROS homeostasis in roots.

The presence of Mn and As also induced ROS overproduction and consequent oxidative protection, as observed by increased H_2O_2 contents in shoots (Figure 6e) and DHAR activity in roots (Figure 8c). Nevertheless, the association of Mn and/or As with Fe did not promote any additional effects in both oxidative stress biomarkers and antioxidant system, which may be associated with efficient maintenance of ionic homeostasis and distribution of these elements both in plant organs (Table 2) and in subcellular fractions.

Interestingly, APX activity was induced in shoots of all treated plants compared to control ones and also in roots of Fe-treated plants, isolated or in association (Figure 6d), highlighting the importance of the connection of the ascorbate-glutathione pathway in the oxidative protection of this species. APX activity is supported by the recycling of AsA, in a GSH-dependent manner, catalyzed by DHAR, and independently, through the action of MDHAR, both pathways using NAD(P)H reducing power, which is used in DHAR pathway to regenerate GSH through GR activity (Hasanuzzaman et al., 2019).

In general, the activities of the enzymes of the ascorbate-glutathione cycle were not induced by the treatments (Figure 8), which may have occurred in the short term after exposure to the treatments. This hypothesis is plausible in view of the maintenance of the redox status of both glutathione (GSH/GSSG ratio, Figure 7c) and ascorbate (AsA/DHA ratio; Figure 7f). Apart from that, GR activity (Figure 8a) was induced in the roots of the As-treated plants, probably associated with the higher contents of GSSG in the same plants (Figure 7b). The ascorbate and glutathione pools are well-known redox buffers and also are supposed to operate in zeaxanthin biosynthesis dissipating excess light energy in the thylakoid membranes of chloroplast (Plumb et al., 2018). Therefore, the conservation of the redox state and of the glutathione and ascorbate pools must have contributed both to the removal of ROS and to the preservation of the photochemical performance of the plants submitted to the treatments (Figure

4). Similar results were observed by Li et al. (2022) in *P. stratiotes* plants in response to zinc-cadmium co-pollution, in which plants displayed an enhanced APX activity and DHA content in the shoots to improve the antioxidant capacity of the AsA-GSH cycle, and preserved the stability of the GSH/GSSG ratio.

It is also important to note that several studies report the induction of ROS-scavenging enzymes and the ascorbate-glutathione cycle in the short term, approximately 24 to 48 hours after exposure to pollutants (Campos et al., 2020; Farnese et al., 2017). Here, we observed that water lettuce plants sustain these mechanisms active even for a longer period, within ten days, a valuable characteristic for the use of these plants in the field, in phytoremediation programs.

5.5. Conclusion

Excess of the elements Fe, Mn, and As, imposed individually or associated triggered root nutritional imbalance, photosynthetic impairments, structural changes, and metabolic disturbances. Nevertheless, the plants were able to maintain the photochemical performance, the production of photoassimilates and demonstrated to have a robust antioxidant system, minimizing oxidative damage and maintaining the redox state. More importantly, the specimen was able to uptake and accumulate high concentrations of the elements in the tissues, even when the pollutants were associated, demonstrating that the mixing of metallic elements does not constitute an additional challenge for the phytoremediation of aquatic environments.

Supporting information

Table S1. Effects of the pH on Fe and Mn bioaccumulation in *Pistia stratiotes* plants growing in control and 5 mM Fe-EDTA or 4 mM $MnCl_2$ for ten days. Means ± standard errors followed by different lowercase letters for pH condition and uppercase letters for treatment indicate significant differences ($P < 0.05$) according to two-way analysis of variance (ANOVA) with post hoc Tukey test. For Mn concentration in shoots, there was a significant interaction, whereas for the other variables the isolated effects were tested, in which mean values of a same treatment in different pH as well as in a same pH in different treatments were compared

Fe concentration (µg g^{-1})			
	pH = 5.0	***pH = 6.0***	
	Shoots		
Control	234.05 ± 27.27	156.00 ± 17.95	$\bar{x}$=195.03 B
Fe 5 mM	1537.60 ± 178.93	1602.73 ± 291.25	$\bar{x}$=1570.16 A
	$\bar{x}$=885.83 a	$\bar{x}$=879.37 a	
	Roots		
Control	1089.88 ± 238.41	804.46 ± 349.53	$\bar{x}$=947.17 B
Fe 5 mM	7960.99 ± 521.65	8801.93 ± 874.77	$\bar{x}$=8381.46 A
	$\bar{x}$=4525.44 a	$\bar{x}$=4803.20 a	
Mn concentration (µg g^{-1})			
	pH = 5.0	***pH = 6.0***	
	Shoots		
Control	879.48 ± 77.43 Ba	825.02 ± 126.89 Ba	
Mn 4 mM	11271.98 ± 692.58 Ab	13504.25 ± 537.82 Aa	
	Roots		
Control	2175.02 ± 558.03	1587.53 ± 280.54	$\bar{x}$=1881.27 B
Mn 4 mM	13501.84 ± 2593.94	19357.75 ± 4171.17	$\bar{x}$=16429.8 A
	$\bar{x}$=7838.43 a	$\bar{x}$=10472.64 a	

References

Ahammed, G.J., Wu, M., Wang, Y., Yan, Y., Mao, Q., Ren, J., Ma, R., Liu, A., Chen, S., 2020. Melatonin alleviates iron stress by improving iron homeostasis, antioxidant defense and secondary metabolism in cucumber. Sci. Hortic. (Amsterdam). 265, 109205. https://doi.org/10.1016/j.scienta.2020.109205

Ainsworth, E.A., Lemonnier, P., 2018. Phloem function: a key to understanding and manipulating plant responses to rising atmospheric [CO2]? Curr. Opin. Plant Biol. 43, 50–56. https://doi.org/10.1016/j.pbi.2017.12.003

Alejandro, S., Höller, S., Meier, B., Peiter, E., 2020. Manganese in plants: From acquisition to subcellular allocation. Front. Plant Sci. 11, 1–23. https://doi.org/10.3389/fpls.2020.00300

Ali, M.A., Fahad, S., Haider, I., Ahmed, N., Ahmad, S., Hussain, S., Arshad, M., 2019. Oxidative stress and antioxidant defense in plants exposed to metal/metalloid toxicity, in: Reactive oxygen, nitrogen and sulfur species in plants. Wiley, pp. 353–370. https://doi.org/10.1002/9781119468677.ch15

Alvarenga, I.F.S., dos Santos, F.E., Silveira, G.L., Andrade-Vieira, L.F., Martins, G.C., Guilherme, L.R.G., 2020. Investigating arsenic toxicity in tropical soils: A cell cycle and DNA fragmentation approach. Sci. Total Environ. 698, 134272. https://doi.org/10.1016/j.scitotenv.2019.134272

Angulo-Bejarano, P.I., Puente-Rivera, J., Cruz-Ortega, R., 2021. Metal and metalloid toxicity in plants: An overview on molecular aspects. Plants 10, 1–28. https://doi.org/10.3390/plants10040635

Araújo, T.O., Isaure, M.P., Alchoubassi, G., Bierla, K., Szpunar, J., Trcera, N., Chay, S., Alcon, C., Campos da Silva, L., Curie, C., Mari, S., 2020. *Paspalum urvillei* and *Setaria parviflora*, two grasses naturally adapted to extreme iron-rich environments. Plant Physiol. Biochem. 151, 144–156. https://doi.org/10.1016/j.plaphy.2020.03.014

Arif, N., Yadav, V., Singh, Shweta, Singh, Swati, Ahmad, P., Mishra, R.K., Sharma, S., Tripathi, D.K., Dubey, N.K., Chauhan, D.K., 2016. Influence of high and low levels of plant-beneficial heavy metal ions on plant growth and development. Front. Environ. Sci. 4. https://doi.org/10.3389/fenvs.2016.00069

Aung, M.S., Masuda, H., 2020. How Does rice defend against excess iron?: physiological and molecular mechanisms. Front. Plant Sci. 11, 1–8. https://doi.org/10.3389/fpls.2020.01102

Banks, J.M., 2018. Chlorophyll fluorescence as a tool to identify drought stress in Acer genotypes. Environ. Exp. Bot. 155, 118–127.

https://doi.org/10.1016/j.envexpbot.2018.06.022

Blamey, F.P.C., Hernandez-Soriano, M.C., Cheng, M., Tang, C., Paterson, D.J., Lombi, E., Wang, W.H., Scheckel, K.G., Kopittke, P.M., 2015. Synchrotron-based techniques shed light on mechanisms of plant sensitivity and tolerance to high manganese in the root environment. Plant Physiol. 169, 2006–2020. https://doi.org/10.1104/pp.15.00726

Bradford, M.M., 1976. A Rapid and sensitive method for the quantitation microgram quantities of protein utilizing the principle of protein-dye binding. Anal. Biochem. 72, 248–254.

Branco-Neves, S., Soares, C., de Sousa, A., Martins, V., Azenha, M., Gerós, H., Fidalgo, F., 2017. An efficient antioxidant system and heavy metal exclusion from leaves make *Solanum cheesmaniae* more tolerant to Cu than its cultivated counterpart. Food Energy Secur. 6, 123–133. https://doi.org/10.1002/fes3.114

Campos, F.V. de, Oliveira, J.A. de, Silva, A.A. da, Ribeiro, C., Montoya, S.G., Farnese, F. dos S., 2020. Involvement of glutathione and glutathione metabolizing enzymes in *Pistia stratiotes* tolerance to arsenite. Int. J. Phytoremediation 22, 404–411. https://doi.org/10.1080/15226514.2019.1667951

Campos, F.V., Oliveira, J.A., Silva, A.A., Ribeiro, C., Farnese, F.S., 2019. Phytoremediation of arsenite-contaminated environments: is *Pistia stratiotes* L. a useful tool? Ecol. Indic. 104, 794–801. https://doi.org/10.1016/j.ecolind.2019.04.048

Campos, N. V., Araújo, T.O., Arcanjo-Silva, S., Freitas-Silva, L., Azevedo, A.A., Nunes-Nesi, A., 2016. Arsenic hyperaccumulation induces metabolic reprogramming in *Pityrogramma calomelanos* to reduce oxidative stress. Physiol. Plant. 157, 135–146. https://doi.org/10.1111/ppl.12426

Chauhan, R., Awasthi, S., Indoliya, Y., Chauhan, A.S., Mishra, S., Agrawal, L., Srivastava, S., Dwivedi, S., Singh, P.C., Mallick, S., Chauhan, P.S., Pande, V., Chakrabarty, D., Tripathi, R.D., 2020. Transcriptome and proteome analyses reveal selenium mediated amelioration of arsenic toxicity in rice (*Oryza sativa* L.). J. Hazard. Mater. 390, 122122. https://doi.org/10.1016/j.jhazmat.2020.122122

Clark, R.B., 1975. Characterization of phosphatase of intact maize roots. J. Agric. Food Chem. 23, 458–460. https://doi.org/10.1021/jf60199a002

Coelho, D.G., Marinato, C.S., Matos, L.P., Andrade, H.M., da Silva, V.M., Neves, P.H.S., Oliveira, J.A., 2020. Evaluation of heavy metals in soil and tissues of economic-interest plants grown in sites affected by the Fundão dam failure in Mariana, Brazil. Integr. Environ. Assess. Manag. 0–3. https://doi.org/10.1002/ieam.4253

Cohen, M.F., Gurung, S., Fukuto, J.M., Yamasaki, H., 2014. Controlled free radical attack in the apoplast: A hypothesis for roles of O, N and S species in regulatory and polysaccharide cleavage events during rapid abscission by Azolla. Plant Sci. 217–218, 120–126. https://doi.org/10.1016/j.plantsci.2013.12.008

Cruz, C.E.S., de Freitas-Silva, L., Ribeiro, C., da Silva, L.C., 2021. Physiological and morphoanatomical effects of glyphosate in *Eugenia uniflora*, a Brazilian plant species native to the Atlantic Forest biome. Environ. Sci. Pollut. Res. 28, 21334–21346. https://doi.org/10.1007/s11356-020-12003-4

Das, U., Rahman, Md Motiur, Roy, Z.R., Rahman, Md Mominur, Kabir, A.H., 2020. Morpho-physiological retardations due to iron toxicity involve redox imbalance rather than photosynthetic damages in tomato. Plant Physiol. Biochem. 156, 55–63. https://doi.org/10.1016/j.plaphy.2020.08.034

de Araújo, T.O., de Freitas-Silva, L., Santana, B.V.N., Kuki, K.N., Pereira, E.G., Azevedo, A.A., da Silva, L.C., 2015. Morphoanatomical responses induced by excess iron in roots of two tolerant grass species. Environ. Sci. Pollut. Res. 22, 2187–2195. https://doi.org/10.1007/s11356-014-3488-1

de Souza, T.D., Borges, A.C., Braga, A.F., Veloso, R.W., Teixeira de Matos, A., 2019. Phytoremediation of arsenic-contaminated water by *Lemna valdiviana*: An optimization study. Chemosphere 234, 402–408. https://doi.org/10.1016/j.chemosphere.2019.06.004

Fabre, D., Yin, X., Dingkuhn, M., Clément-Vidal, A., Roques, S., Rouan, L., Soutiras, A., Luquet, D., 2019. Is triose phosphate utilization involved in the feedback inhibition of photosynthesis in rice under conditions of sink limitation. J. Exp. Bot. 70, 5773–5785. https://doi.org/10.1093/jxb/erz318

Farnese, F.S., De Oliveira, J.A., Gusman, G.S., Leão, G.A., Ribeiro, C., Siman, L.I., Cambraia, J., 2013. Plant responses to arsenic: The role of nitric oxide. Water. Air. Soil Pollut. 224. https://doi.org/10.1007/s11270-013-1660-8

Farnese, F.S., Oliveira, J.A., Lima, F.S., Leão, G.A., Gusman, G.S., Silva, L.C., 2014. Evaluation of the potential of *Pistia stratiotes* L. (water lettuce) for bioindication and phytoremediation of aquatic environments contaminated with arsenic. Brazilian J. Biol. 74, 103–112. https://doi.org/10.1590/1519-6984.01113

Farnese, F.S., Oliveira, J.A., Paiva, E.A.S., Menezes-Silva, P.E., Silva, A.A., Campos, F.V., Ribeiro, C., 2017. The Involvement of nitric oxide in integration of plant physiological and ultrastructural adjustments in response to arsenic. Front. Plant Sci. 8, 1–14.

https://doi.org/10.3389/fpls.2017.00979

Fernie, A.R., Roscher, A., Ratcliffe, R.G., Kruger, N.J., 2001. Fructose 2,6-bisphosphate activates pyrophosphate: fructose-6-phosphate 1-phosphotransferase and increases triose phosphate to hexose phosphate cycling in heterotrophic cells. Planta 212, 250–263. https://doi.org/10.1007/s004250000386

Foyer, C.H., Noctor, G., 2005. Oxidant and antioxidant signalling in plants: A re-evaluation of the concept of oxidative stress in a physiological context. Plant, Cell Environ. 28, 1056–1071. https://doi.org/10.1111/j.1365-3040.2005.01327.x

Freitas-Silva, L., de Araújo, T.O., Nunes-Nesi, A., Ribeiro, C., Costa, A.C., da Silva, L.C., 2020. Evaluation of morphological and metabolic responses to glyphosate exposure in two neotropical plant species. Ecol. Indic. 113, 106246. https://doi.org/10.1016/j.ecolind.2020.106246

Führs, H., Hartwig, M., Molina, L.E.B., Heintz, D., Van Dorsselaer, A., Braun, H.P., Horst, W.J., 2008. Early manganese-toxicity response in *Vigna unguiculata* L. - A proteomic and transcriptomic study. Proteomics 8, 149–159. https://doi.org/10.1002/pmic.200700478

García-Caparrós, P., De Filippis, L., Gul, A., Hasanuzzaman, M., Ozturk, M., Altay, V., Lao, M.T., 2021. Oxidative stress and antioxidant metabolism under adverse environmental conditions: a review. Bot. Rev. 87, 421–466. https://doi.org/10.1007/s12229-020-09231-1

Gay, C., Gebicki, J.M., 2000. A critical evaluation of the effect of sorbitol on the ferric-xylenol orange hydroperoxide assay. Anal. Biochem. 284, 217–220. https://doi.org/10.1006/abio.2000.4696

Genty, B., Briantais, J.M., Baker, N.R., 1989. The relationship between the quantum yield of photosynthetic electron transport and quenching of chlorophyll fluorescence. Biochim. Biophys. Acta - Gen. Subj. 990, 87–92. https://doi.org/10.1016/S0304-4165(89)80016-9

Georgiadou, E.C., Kowalska, E., Patla, K., Kulbat, K., Smolińska, B., Leszczyńska, J., Fotopoulos, V., 2018. Influence of heavy metals (Ni, Cu, and Zn) on nitro-oxidative stress responses, proteome regulation and allergen production in basil (*Ocimum basilicum* L.) plants. Front. Plant Sci. 9, 1–16. https://doi.org/10.3389/fpls.2018.00862

Giannopolitis, C.N., Ries, S.K., 1977. Superoxide dismutases: I. Occurrence in higher plants. Plant Physiol. 59, 309–314. https://doi.org/10.1104/pp.59.2.309

Green, L.S., Rogers, E.E., 2004. FRD3 controls iron localization in Arabidopsis. Plant Physiol. 136, 2523–2531. https://doi.org/10.1104/pp.104.045633

Gutteridge, J.M.C., Rowley, D.A., Halliwell, B., 1981. Superoxide-dependent formation of hydroxyl radicals in the presence of iron salts. Detection of “free” iron in biological systems by using bleomycin-dependent degradation of DNA. Biochem. J. 199, 263–265. https://doi.org/10.1042/bj1990263

Hasanuzzaman, M., Borhannuddin Bhuyan, M.H.M., Anee, T.I., Parvin, K., Nahar, K., Al Mahmud, J., Fujita, M., 2019. Regulation of ascorbate-glutathione pathway in mitigating oxidative damage in plants under abiotic stress. Antioxidants. https://doi.org/10.3390/antiox8090384

Havir, E.A., McHale, N.A., 1987. Biochemical and developmental characterization of multiple forms of catalase in tobacco leaves. Plant Physiol. 84, 450–455. https://doi.org/10.1104/pp.84.2.450

He, J., Rössner, N., Hoang, M.T.T., Alejandro, S., Peiter, E., 2021. Transport, functions, and interaction of calcium and manganese in plant organellar compartments. Plant Physiol. 187, 1940–1972. https://doi.org/10.1093/plphys/kiab122

Hodges, D.M., DeLong, J.M., Forney, C.F., Prange, R.K., 1999. Improving the thiobarbituric acid-reactive-substances assay for estimating lipid peroxidation in plant tissues containing anthocyanin and other interfering compounds. Planta 207, 604–611. https://doi.org/10.1007/s004250050524

Hua, J., Zhang, C., Yin, Y., Chen, R., Wang, X., 2012. Phytoremediation potential of three aquatic macrophytes in manganese-contaminated water. Water Environ. J. 26, 335–342. https://doi.org/10.1111/j.1747-6593.2011.00293.x

Kampfenkel, K., Van Montagu, M., Inzé, D., 1995. Extraction and determination of ascorbate and dehydroascorbate from plant tissue. Anal. Biochem. 225, 165–167. https://doi.org/10.1006/abio.1995.1127

Karnovsky, M.J., 1985. A formaldehyde-glutaraldehyde fixative of high osmolality for use in electron microscopy. J. Cell Biol. 27, 137–138.

Khalid, S., Shahid, M., Niazi, N.K., Murtaza, B., Bibi, I., Dumat, C., 2017. A comparison of technologies for remediation of heavy metal contaminated soils. J. Geochemical Explor. 182, 247–268. https://doi.org/10.1016/j.gexplo.2016.11.021

Kieffer, P., Planchon, S., Oufir, M., Ziebel, J., Dommes, J., Hoffmann, L., Hausman, J.F., Renaut, J., 2009. Combining proteomics and metabolite analyses to unravel cadmium stress-response in poplar leaves. J. Proteome Res. 8, 400–417. https://doi.org/10.1021/pr800561r

Kwak, S.S., Kim, S.K., Park, I.H., Liu, J.R., 1996. Enhancement of peroxidase activity by stress-related chemicals in sweet potato. Phytochemistry 43, 565–568. https://doi.org/10.1016/0031-9422(96)00315-9

Lešková, A., Giehl, R.F.H., Hartmann, A., Fargašová, A., von Wirén, N., 2017. Heavy metals induce iron deficiency responses at different hierarchic and regulatory levels. Plant Physiol. 174, 1648–1668. https://doi.org/10.1104/pp.16.01916

Li, C., Zhou, K., Qin, W., Tian, C., Qi, M., Yan, X., Han, W., 2019. A Review on heavy metals contamination in soil: effects, sources, and remediation techniques. Soil Sediment Contam. 28, 380–394. https://doi.org/10.1080/15320383.2019.1592108

Li, Y., Xin, J., Tian, R., 2022. Physiological defense and metabolic strategy of *Pistia stratiotes* in response to zinc-cadmium co-pollution. Plant Physiol. Biochem. 178, 1–11. https://doi.org/10.1016/j.plaphy.2022.02.020

Liszkay, A., Van Der Zalm, E., Schopfer, P., 2004. Production of reactive oxygen intermediates ($O_2^{\cdot -}$, H_2O_2, and $^{\cdot}OH$) by maize roots and their role in wall loosening and elongation growth. Plant Physiol. 136, 3114–3123. https://doi.org/10.1104/pp.104.044784

Liu, Y.J., Zhu, Y.G., Ding, H., 2007. Lead and cadmium in leaves of deciduous trees in Beijing, China: Development of a metal accumulation index (MAI). Environ. Pollut. 145, 387–390. https://doi.org/10.1016/j.envpol.2006.05.010

Murshed, R., Lopez-Lauri, F., Sallanon, H., 2008. Microplate quantification of enzymes of the plant ascorbate-glutathione cycle. Anal. Biochem. 383, 320–322. https://doi.org/10.1016/j.ab.2008.07.020

Muszyńska, E., Labudda, M., 2019. Dual role of metallic trace elements in stress biology—from negative to beneficial impact on plants. Int. J. Mol. Sci. 20. https://doi.org/10.3390/ijms20133117

Nieniewska, J., Curtius, A.J., 1986. Determinação de arsênio em plantas por geração de hidreto e absorção atômica. Quim. Nova 9, 194–197.

Ntakiyiruta, P., Briton, B.G.H., Nsavyimana, G., Adouby, K., Nahimana, D., Ntakimazi, G., Reinert, L., 2022. Optimization of the phytoremediation conditions of wastewater in post-treatment by *Eichhornia crassipes* and *Pistia stratiotes* : kinetic model for pollutants removal. Environ. Technol. 43, 1805–1818. https://doi.org/10.1080/09593330.2020.1852445

O'Brien, T.P., McCully, M.E., 1981. The study of plant structure: Principles and methods, Blackwell Scientific. Blackwell Scientific, Oxford, UK. https://doi.org/10.1111/1365-

3040.ep11572627

Onaga, G., Dramé, K.N., Ismail, A.M., 2016. Understanding the regulation of iron nutrition: Can it contribute to improving iron toxicity tolerance in rice? Funct. Plant Biol. 43, 709–726. https://doi.org/10.1071/FP15305

Palmer, C.M., Guerinot, M. Lou, 2009. Facing the challenges of Cu, Fe and Zn homeostasis in plants. Nat. Chem. Biol. https://doi.org/10.1038/nchembio.166

Pantoja, O., 2021. Recent advances in the physiology of ion channels in plants. Annu. Rev. Plant Biol. 72, 463–495. https://doi.org/10.1146/annurev-arplant-081519-035925

Peixoto, P.H.P., Cambraia, J., Sant'Anna, R., Mosquim, P.R., Moreira, M.A., 1999. Aluminum effects on lipid peroxidation and on the activities of enzymes of oxidative metabolism in sorghum. Rev. Bras. Fisiol. Veg. 11, 137–143.

Pita-Barbosa, A., Williams, T.C.R., Loureiro, M.E., 2019. Effects of short-term arsenic exposure in *Arabidopsis thaliana*: Tolerance versus toxicity responses. Biol. Plant. 63, 43–53. https://doi.org/10.32615/bp.2019.006

Plumb, W., Townsend, A.J., Rasool, B., Alomrani, S., Razak, N., Karpinska, B., Ruban, A. V., Foyer, C.H., 2018. Ascorbate-mediated regulation of growth, photoprotection, and photoinhibition in *Arabidopsis thaliana*. J. Exp. Bot. 69, 2823–2835. https://doi.org/10.1093/jxb/ery170

Prasertsup, P., Ariyakanon, N., 2011. Removal of chlorpyrifos by water lettuce (*Pistia stratiotes* L.) And duckweed (*Lemna minor* L.). Int. J. Phytoremediation 13, 383–395. https://doi.org/10.1080/15226514.2010.495145

Quadra, G.R., Roland, F., Barros, N., Malm, O., Lino, A.S., Azevedo, G.M., Thomaz, J.R., Andrade-Vieira, L.F., Praça-Fontes, M.M., Almeida, R.M., Mendonça, R.F., Cardoso, S.J., Guida, Y.S., Campos, J.M.S., 2019. Far-reaching cytogenotoxic effects of mine waste from the Fundão dam disaster in Brazil. Chemosphere 215, 753–757. https://doi.org/10.1016/j.chemosphere.2018.10.104

Quaresma, V.S., Aguiar, V.M.C., Bastos, A.C., Oliveira, K.S., Vieira, F. V., Sá, F., Baptista Neto, J.A., 2021. The impact of trace metals in marine sediments after a tailing dam failure: the Fundão dam case (Brazil). Environ. Earth Sci. 80. https://doi.org/10.1007/s12665-021-09817-x

Rahman, I., Kode, A., Biswas, S.K., 2007. Assay for quantitative determination of glutathione and glutathione disulfide levels using enzymatic recycling method. Nat. Protoc. 1, 3159–3165. https://doi.org/10.1038/nprot.2006.378

Rajpoot, R., Srivastava, R.K., Rani, A., Pandey, P., Dubey, R.S., 2021. Manganese-induced oxidative stress, ultrastructural changes, and proteomics studies in rice plants. Protoplasma 258, 319–335. https://doi.org/10.1007/s00709-020-01575-0

Ramakrishnan, B., Megharaj, M., Venkateswarlu, K., Sethunathan, N., Naidu, R., 2011. Mixtures of environmental pollutants: effects on microorganisms and their activities in soils, in: Reviews of Environmental Contamination and Toxicology. pp. 63–120. https://doi.org/10.1007/978-1-4419-8011-3_3

Rezania, S., Taib, S.M., Md Din, M.F., Dahalan, F.A., Kamyab, H., 2016. Comprehensive review on phytotechnology: Heavy metals removal by diverse aquatic plants species from wastewater. J. Hazard. Mater. 318, 587–599. https://doi.org/10.1016/j.jhazmat.2016.07.053

Sankhla, M.S., Kumari, M., Nandan, M., Kumar, R., Agrawal, P., 2016. Heavy Metals Contamination in water and their hazardous effect on human health- a review. Int. J. Curr. Microbiol. Appl. Sci. 5, 759–766. https://doi.org/10.20546/ijcmas.2016.510.082

Shabala, S., Pottosin, I., 2014. Regulation of potassium transport in plants under hostile conditions: Implications for abiotic and biotic stress tolerance. Physiol. Plant. 151, 257–279. https://doi.org/10.1111/ppl.12165

Silva, D., Bellato, C., Marques Neto, J., Fontes, M., 2018. Trace elements in river waters and sediments before and after a mining dam breach (Bento Rodrigues, Brazil). Quim. Nova 41, 857–866. https://doi.org/10.21577/0100-4042.20170252

Srivastava, S., Akkarakaran, J.J., Suprasanna, P., D'Souza, S.F., 2013. Response of adenine and pyridine metabolism during germination and early seedling growth under arsenic stress in *Brassica juncea*. Acta Physiol. Plant. 35, 1081–1091. https://doi.org/10.1007/s11738-012-1146-0

Stein, R.J., Lopes, S.I.G., Fett, J.P., 2014. Iron toxicity in field-cultivated rice: Contrasting tolerance mechanisms in distinct cultivars. Theor. Exp. Plant Physiol. 26, 135–146. https://doi.org/10.1007/s40626-014-0013-3

Taylor, G.J., Crowder, A.A., 1983. Uptake and accumulation of heavy metals by *Typha latifolia* in wetlands of the Sudbury, Ontario region. Can. J. Bot. 61, 63–73. https://doi.org/10.1139/b83-005

Tegeder, M., Hammes, U.Z., 2018. The way out and in: phloem loading and unloading of amino acids. Curr. Opin. Plant Biol. 43, 16–21. https://doi.org/10.1016/j.pbi.2017.12.002

Teixeira, M.C., Santos, A.C., Fernandes, C.S., Ng, J.C., 2020. Arsenic contamination

assessment in Brazil – Past, present and future concerns: A historical and critical review. Sci. Total Environ. 730, 138217. https://doi.org/10.1016/j.scitotenv.2020.138217

Tian, W., He, G., Qin, L., Li, D., Meng, L., Huang, Y., He, T., 2021. Genome-wide analysis of the NRAMP gene family in potato (*Solanum tuberosum*): Identification, expression analysis and response to five heavy metals stress. Ecotoxicol. Environ. Saf. 208, 111661. https://doi.org/10.1016/j.ecoenv.2020.111661

Török, A., Gulyás, Z., Szalai, G., Kocsy, G., Majdik, C., 2015. Phytoremediation capacity of aquatic plants is associated with the degree of phytochelatin polymerization. J. Hazard. Mater. 299, 371–378. https://doi.org/10.1016/j.jhazmat.2015.06.042

Tripathi, D.K., Singh, Shweta, Gaur, S., Singh, Swati, Yadav, V., Liu, S., Singh, V.P., Sharma, S., Srivastava, P., Prasad, S.M., Dubey, N.K., Chauhan, D.K., Sahi, S., 2018. Acquisition and homeostasis of Iron in higher plants and their probable role in abiotic stress tolerance. Front. Environ. Sci. 5, 1–15. https://doi.org/10.3389/fenvs.2017.00086

Tuomainen, M.H., Nunan, N., Lehesranta, S.J., Tervahauta, A.I., Hassinen, V.H., Schat, H., Koistinen, K.M., Auriola, S., McNicol, J., Kärenlampi, S.O., 2006. Multivariate analysis of protein profiles of metal hyperaccumulator *Thlaspi caerulescens* accessions. Proteomics 6, 3696–3706. https://doi.org/10.1002/pmic.200501357

Vergilio, C. dos S., Lacerda, D., Oliveira, B.C.V. de, Sartori, E., Campos, G.M., Pereira, A.L. de S., Aguiar, D.B. de, Souza, T. da S., Almeida, M.G. de, Thompson, F., Rezende, C.E. de, 2020. Metal concentrations and biological effects from one of the largest mining disasters in the world (Brumadinho, Minas Gerais, Brazil). Sci. Rep. 10, 1–12. https://doi.org/10.1038/s41598-020-62700-w

Wang, F., Deng, M., Xu, J., Zhu, X., Mao, C., 2018. Molecular mechanisms of phosphate transport and signaling in higher plants. Semin. Cell Dev. Biol. 74, 114–122. https://doi.org/10.1016/j.semcdb.2017.06.013

Wegner, L.H., Shabala, S., 2020. Biochemical pH clamp: the forgotten resource in membrane bioenergetics. New Phytol. 225, 37–47. https://doi.org/10.1111/nph.16094

Wellburn, A.R., 1994. The spectral determination of chlorophylls a and b, as well as total carotenoids, using various solvents with spectrophotometers of different resolution. J. Plant Physiol. 144, 307–313. https://doi.org/10.1016/S0176-1617(11)81192-2

Wu, L.B., Shhadi, M.Y., Gregorio, G., Matthus, E., Becker, M., Frei, M., 2014. Genetic and physiological analysis of tolerance to acute iron toxicity in rice. Rice 7, 1–12. https://doi.org/10.1186/s12284-014-0008-3

Yamauchi, T., Tanaka, A., Tsutsumi, N., Inukai, Y., Nakazono, M., 2020. A role for auxin in ethylene-dependent inducible aerenchyma formation in rice roots. Plants 9, 1–11. https://doi.org/10.3390/plants9050610

Yang, Y., Zhang, L., Huang, X., Zhou, Y., Quan, Q., Li, Y., Zhu, X., 2020. Response of photosynthesis to different concentrations of heavy metals in *Davidia involucrata*. PLoS One 15, 1–16. https://doi.org/10.1371/journal.pone.0228563

Yasar, A., Zaheer, A., Tabinda, A.B., Khan, M., Mahfooz, Y., Rani, S., Siddiqua, A., 2017. Comparison of reed and water lettuce in constructed wetlands for wastewater treatment. Water Environ. Res. 90, 129–135. https://doi.org/10.2175/106143017x14902968254728

6. Chapter 5 - Cytosolic dynamics of arsenic-induced changes in energy and redox metabolism in *Arabidopsis thaliana*[1,2]

[1]Developed during the Interuniversity exchange (CAPES Internationalization Program, November 2021 – April 2022), at the University of Münster (Germany), under the supervision of Prof. Markus Schwarzländer

[2]Edited in accordance with *Journal of Hazardous Materials* guidelines

Abstract: Arsenic (As) is considered highly toxic to all living organisms. In view of a lack of knowledge about the *in vivo* plant responses triggered by As, this study aimed to elucidate cellular responses to As stress in *Arabidopsis thaliana* plants using a fluorescent protein sensor-based system for multiparametric monitoring of cytosolic dynamic changes. Plants expressing the 35S:cyt-ATeam1.03-nD/nA for Mg-ATP^{2-} detection showed unexpected stable ATP levels upon arsenate (AsV) exposure, even in high concentrations using different plant organs. To test whether an efficient AsV reduction prevents ATP depletion, we use *hac1-1* lines, mutant for arsenate reductase, expressing ATeam sensor. There were no changes in cytosolic ATP status in leaf discs exposed to AsV compared to control, indicating the absence of a direct AsV effect on phosphate metabolism. Furthermore, AsV-treated plants showed a fast oxidation of cytosolic glutathione redox potential (E_{GSH}). We investigated the oxidation of E_{GSH} using mutant lines for glutathione metabolism expressing the sensor, which displayed full oxidation of the sensor in the steady-state. In the assay using Buthionine-sulfoximine (BSO), a chemical inhibitor of glutathione biosynthesis, there was no further oxidation of E_{GSH} upon AsV treatment, indicating that the depletion of GSH pool as the most likely cause of E_{GSH} oxidation. We also confirm that depletion of the GSH pool eliminates arsenic tolerance in plants, and arsenite (AsIII) in lower concentrations inhibits plant growth more than AsV, which appears to be related to the strict regulation of AsV transport. Taken together, our findings show that ATP content in the cytosol does not appear to be depleted as a direct result of short-term arsenate exposure, and that depletion of the GSH pool is the most likely cause of E_{GSH} oxidation, though more research is needed to understand the redox control of phytochelatin synthesis and glutathione pool maintenance.

Keywords: Arsenic toxicity, fluorescent redox sensors, *in vivo* sensing, mitochondrial metabolism

6.1. Introduction

Arsenic (As) is a metallic element with potent carcinogenic potential, which is released in the environment as a result of natural (volcanic) or anthropogenic (industrial, mining and agricultural) activities [1]. The widespread As contamination represents a significant environmental and health concern due to its prevalence in nature and toxicity across life [2]. Arsenate [As(V)] is the predominant inorganic form of As under oxygenated conditions. Because of its chemical analogy with phosphate, As impairs several processes in plant metabolism, including protein phosphorylation, ATP synthesis, as well as other aspects of cellular phosphate homeostasis [3].

A remarkable effect of As(V) widely reported in mammals and also described in plants is the uncoupling of ATP synthesis from electron transport due to the synthesis of the highly unstable molecule ADP-As(V) which generates a futile cycle that compromises the energy status of the cell [4,5]. The chemical characteristics of this reaction and its implication for plant metabolism are well known, but the understanding of the dynamics of the occurrence of the futile cycles and its implication during early stages of As(V)-induced stress remains to be elucidated. The decrease in ATP synthesis is also indirectly caused by the decrease in acidification of mitochondrial intermembrane space that provides the proton-motive force to ATP synthase [6].

Furthermore, once inside the cells As(V) is readily reduced to arsenite [As(III)] by arsenate reductase using glutathione (GSH) as reductant. The main class of As(V) reductases in plants, named HAC1 or ATQ1, play an important role in controlling As accumulation in the shoots through the phytochelatin-dependent compartmentalization of As(III) [7,8]. Free As(III) reacts with protein sulfhydryl groups (-SH), interfering with protein structure and function [4,9]. As part of its impact on cellular redox metabolism, As(III) promotes the production of reactive oxygen species (ROS) and oxidative stress in plants through lipid peroxidation [10]. Under oxidative stress, plants use their antioxidant machinery by overexpressing ROS scavenging enzymes such as superoxide dismutase (SOD), catalase (CAT), ascorbate peroxidase (APX), glutathione reductase (GR), dehydroascorbate reductase (DHAR), glutathione-S- transferase (GST) and glutathione peroxidase (GPX). Non-enzymatic compounds like ascorbic acid, glutathione, phenolic compounds, amino acids and α-tocopherols also play key roles in ROS detoxification [11]. Among these molecules, glutathione besides acting in the redox metabolism, plays a role in the metallic element compartmentalization mechanism, as a constituent of phytochelatins [12]. Therefore, the

evaluation of glutathione redox potential and the glutathione contents in plants during As exposure have been used as a marker for As stress [13]. Nevertheless, it is still unclear whether the increased E_{GSH} caused by As comes from the depletion of GSH used to compartmentalize the element in the vacuole or from the alterations in the GSH/GSSG ratio. Deckers et al. (2022) [14] studying acclimation responses of *Arabidopsis* plants to cadmium (Cd) stress suggested that chelating capacity of GSH is prioritized over its antioxidative function, indicating an outstanding role of GSH depletion on the redox potential oxidation.

Several other responses and mechanisms of plants to cope with As stress have been studied over the last years, especially in bioaccumulator plants, including *Pistia stratiotes*, *Lemna valdiviana,* and *Pteris vittata*, which have elevated potential to clean-up As-contaminated environments [15-18]. Furthermore, new insights on As-induced oxidative stress, antioxidant responses and metabolic adjustments were obtained by using comparative approaches with the model plant *Arabidopsis thaliana* [19,20]. However, the technical and practical limitations to understanding the overall responses during all stages of As stress in living plant tissues are a barrier to fully understand the mechanisms of tolerance and the physiological changes that underpin tolerance. These limitations include the need for cell tissue homogenization, not reflecting differential effects in different cells and/or cell compartments as they occur in vivo, as well as possible alterations in the redox status of these molecules during their extraction and the long duration of protocols to isolate the organelles and quantify the molecules in different cell compartments. Moreover, the oxidation-reduction state of the redox pairs (NAD^+/NADH, $NADP^+$/NADPH, GSSG/GSH) found in the redox machinery of intact cells can be perturbed by extraction [21].

In recent years, several fluorescent protein sensors have become available with favorable technical properties for *in vivo* real-time detection of a set of biological indicators, such as ATP, pH, NADH/NAD^+, H_2O_2 and glutathione redox potential (E_{GSH}), providing new insights into the dynamics of subcellular physiology *in vivo* (Schwarzländer et al., 2016; Walia et al., 2018; Nietzel et al., 2019; Steinbeck et al., 2020). More recently, parallelized measurements of different lines of plant sensors have proven to be an efficient approach for understanding dynamic changes in a high set of physiological parameters in plants under hypoxia [24].

Given that genetically encoded biosensors represent a helpful tool to understand *in vivo* subcellular physiology, our main goal is to investigate the cytosolic physiological responses induced by As stress, including the monitoring of Mg-ATP^{2-}, H_2O_2 and NADH/NAD^+ and the

E_{GSH}. For this aim, plants expressing biosensors in Columbia-0 ecotype as well as in mutants impaired in glutathione biosynthesis and GSSG reduction were used and treated with As. Comprehending how plants cope with As at the molecular and metabolic levels could provide tools for understanding tolerance mechanisms in the metalloid hyperaccumulating plants. Furthermore, it makes it possible to generate more efficient plants in removing pollutants from the environment through phytoremediation.

6.2. Material and methods

Plant materials and growth conditions

The plant materials used included Arabidopsis thaliana L. Heynh. wild-type (WT) Columbia-0 (Col-0), and the GSH-deficient mutants *cad-2* [25], *pad2* [26], *rml1* [27], *nrc1* [28], *rax1* [29], and *zir1* [30]. Also, the T-DNA insertion knockout mutants of high arsenic content 1 (HAC1) (*hac1-1*; [8]) and glutathione reductase 1 (GR1) (*gr1-1*; [31]) were used. For monitoring in vivo cytosolic responses, the lines expressing 35S:cyt-ATeam1.03-nD/nA [32], Ubq10:cyt-Peredox-mCherry [24], 35S:cyt-Grx1-roGFP2 [31], and 35S:cyt-roGFP2-Orp1 [33] were used. Furthermore, GSH-deficient and *gr1-1* mutant lines expressing the Grx1-roGFP2 sensor were provided by Professor Andreas Meyer (University of Bonn). Homozygous mutants were identified by PCR genotyping or sequencing of the F3 progeny (Supporting Information Figure S1). Because the line rml1 was identified as heterozygous (Supporting Information Figure S1), it was not used in further experiments. All mutants are in the Col-0 background.

To generate the *hac1-1* lines expressing the sensor 35S:cyt-ATeam1.03-nD/nA, the binary vector pH2GW7:cyt-ATeam1.03-nD/nA [32] was electroporated into *Agrobacterium tumefaciens* strain GV3101. The Agrobacterium culture was used to transform *A. thaliana hac1-1* by Agrobacterium-mediated floral dip transformation [34]. Seeds were plated on agar plates containing 15 μg mL^{-1} hygromycin to select for transformants and screened by fluorescence microscopy.

For the plate reader assays using leaf discs, the seeds were sowed in Jiffy pots, stratified at 4ºC for 48 hours in the dark and then transferred to growth chambers running under long-day conditions (16 h at 22 ˚C and 80–100 μmol m^{-2} s^{-1}, 8 h at 18 ˚C and darkness, 65% RH). For the root, seedling and arsenic tolerance assays, the seeds were surface-sterilized for 2 min in 80% Ethanol, 20 min in 5% sodium hypochlorite + 0.1% Tween 20 and washed three times with deionized sterile H_2O. Then, the seeds were plated on 0.7% agar plates supplemented with 1/2-strength MS medium [35] containing 0.1% sucrose and 10 mM MES followed by

stratification for 48 hours at 4 ºC. The plates were transferred to the growth chamber under the same conditions aforementioned.

Plate reader assays

The real-time detection of fluorescent sensors was performed according to Wagner et al. (2019) [24], using transparent 96-well plates filled with 180 µL assay medium containing 10 mM MES, pH 5.8 (potassium hydroxide), 10 mM $MgCl_2$, 10 mM $CaCl_2$, 5 mM KCl. Eight leaf discs of 5-week-old plants and 10-day-old seedlings (three per well) and roots (ten per well) of each genotype or treatment grown in agar plates were submerged in the wells before inserting the plate into a CLARIOstar plate reader (BMG Labtech, Ortenberg, Germany) pre-equilibrated to 25°C for recording the fluorescence in the steady-state. The treatments were imposed accordingly in each assay: for arsenic assays, the treatments were imposed by adding sodium arsenate dibasic heptahydrate (AsV) or sodium (meta)arsenite (AsIII). The concentration of 250 As(V) for the preliminary assays was chosen based on the results by Kumar et al. (2019) [13]. Fluorescence was read sequentially for each well using the 'well multichromatics' mode. The appropriate excitation (Ex) and emission (Em) wavelengths chosen for each sensor were: ATeam: Ex = 430 ± 10 nm/Em = 480 ± 10 and 530 ± 10 nm; Peredox-mCherry: Ex = 400 ± 5 and 540 ± 20 nm/Em = 520 ± 10 and 615 ± 18 nm; reduction–oxidation-sensitive green fluorescent protein2 (roGFP2): Ex = 400 ± 5 and 482 ± 16 nm/Em = 520 ± 10 nm. Before analysis, the fluorescence of Col-0 plants without sensor was recorded and subtracted from all data. In the experiments, the internal plate reader temperature was kept at 25°C.

Arsenic tolerance assay

Surface-sterilized and stratified seeds were vertically grown on 0.7 agar plates (50 mL per plate) containing half-strength MS medium (Murashige and Skoog, 1962) + 1% (w/v) sucrose under long-day conditions. For pH stabilization at 5.8 (KOH), culture plate medium was supplemented with 10 mM MES. After 5 days, seedlings were carefully transferred onto new agar plates supplemented with sterile-filtered 50; 100; 250; and 500 µM sodium arsenate dibasic heptahydrate (AsV) or 5; 10; 25; and 50 µM sodium arsenite (AsIII). Three seedlings of *cad-2* and *zir1* mutant lines, which contain approximately 30 and 15% GSH levels of WT plants [25,30], respectively, along with the corresponding WT were placed side-by-side on the freshly prepared plates, being five plates per treatment. Plates were sealed with Micropore surgical tape (3M) and returned to long-day conditions. After ten days, seedlings were subjected

to photographic documentation. The increase of primary root length was quantified from images with ImageJ software v 1.52.

Data analysis

Time series of plate reader assays were presented as mean ± standard deviation. Fluorescence-derived calculations, as well as growth measurements, were subjected to ANOVA followed by Tukey's post hoc test ($P \leq 0.05$) for qualitative data or regression analysis for qualitative ones. All statistical tests were performed using R Studio version 4.1.2 software.

Accession numbers

The following accession numbers can be used to obtain the sequence data from this article in the GenBank data libraries: GSH1, AT4G23100; GR1, AT3G24170; HAC1, AT2G21045.

6.3. Results

Cytosolic responses to arsenate

To establish an overview of arsenic-induced cytosolic responses on redox and metabolic status, leaf discs, seedlings and roots of plants expressing biosensors for monitoring Mg-ATP^{2-} level, $NADH/NAD^+$ ratio, glutathione redox potential, and H_2O_2 level to As(V) were analyzed in plate reader assays (Figure 1). Overall, the responses observed by the application of As(V) were similar in the different tissues (Figure 1). An unexpected maintenance of cytosolic ATP levels upon 250 µM As(V) exposure in leaf discs, seedlings, and roots (Figure 1a, b, c) were also observed, contradicting the established dogma of As(V) interference in ATP depletion due to phosphate competition.

Furthermore, As(V) exposure did not induce major changes in $NADH/NAD^+$ ratio (Figure 1d, e, f), apart from an increase observed in roots after around nine hours of readings and six hours after the addition of the pollutant (Figure 1f), indicating a reduction of cytosolic NAD status. Accordingly, lower ATP level (figure 1c) and higher $NADH/NAD^+$ ratio were observed in roots compared to whole seedling or leaf discs (Figure 1f).

Very pronounced changes upon As(V) exposure were observed in glutathione redox potential (E_{GSH}, Figure 1g - i) and H_2O_2 levels (Figure j – l). The E_{GSH} immediately increased, indicating an oxidation, when the As(V) was added to the leaf discs submerged in the assay medium, reaching a plateau after approximately 30 minutes and stabilizing in the subsequent

time series (Figure 1g). A similar response was also observed in E_{GSH} in seedlings and H_2O_2 levels in all tissues analyzed (Figure 1h, j – l). In roots, however, E_{GSH} increases was lower compared to leaf discs and seedlings (Figure 1j).

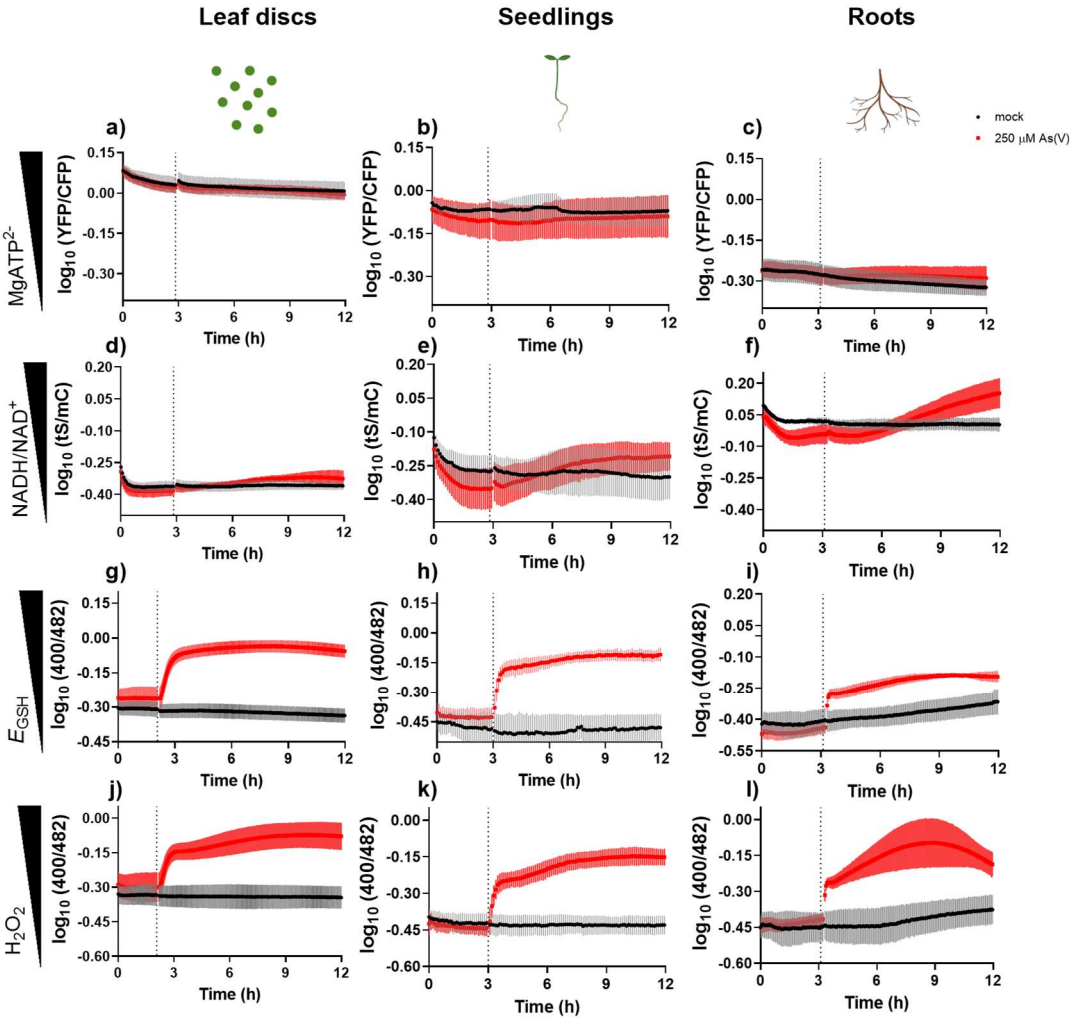

Figure 1. Monitoring the cytosolic responses to arsenic in *Arabidopsis thaliana*. Time series of five-week-old wild type Col-0 leaf discs (a, d, g, j), ten-day-old seedlings (b, e, h, k), and ten-day-old roots (c, f, I, l) expressing cytosolic ATeam1.03-nD/nA (a, b, c), Peredox-mCherry (d, e, f), Grx1-roGFP2 (g, h, i), and roGFP2-Orp1 (j, k, l) and subjected to mock (black dots) or 250 µM sodium arsenate dibasic heptahydrate (red dots) for detection of $MgATP^{2-}$, $NADH/NAD^+$ ratio, glutathione redox status, and H_2O_2, respectively. N = 6–8. Dashed line indicates application of As(V) after steady-state. Values are displayed as mean ± SD. All the fluorescence intensities were recorded from the plant material in assay medium and the autofluorescence from corresponding WT controls without sensor were used for background subtraction. ATeam: Ex = 430 ± 10 nm/Em = 480 ± 10 and 530 ± 10 nm; Peredox-mCherry: Ex = 400 ± 5 and 540 ± 20 nm/Em = 520 ± 10 and 615 ± 18 nm; reduction–oxidation-sensitive green fluorescent protein2 (roGFP2): Ex = 400 ± 5 and 482 ± 16 nm/Em = 520 ± 10 nm.

A further investigation of ATP and $NADH/NAD^+$ responses were done by performing an As(V) titration on leaf discs from plants expressing the sensors (Figure 2). Interestingly,

even higher As(V) concentrations were not able to induce changes in the overall trend of ATP sensing during the time series (Figure 2a) nor in the ATP status after 12 h of the starting point (Figure 2b). Otherwise, the increase of As(V) concentration in the medium increased the $NADH/NAD^+$ ratio (Figure 2c) in a concentration-dependent response, following a quadratic fitting model (Figure 2d).

These results led us to investigate whether an efficient reduction of As(V) to As(III), catalyzed by arsenate reductase, could avoid interference in phosphate metabolism and ATP synthesis. For this, the sensor for ATeam for cytosolic ATP was expressed in a mutant line in the High Arsenic Content 1 (*hac1-1*), necessary for the reduction of As(V) to As(III) [8,36]. These lines, along with lines without the hac1 mutation expressing the ATeam sensor, were exposed to As(V) and As(III) (Figure 2e, f). As previously observed, the addition of As in the medium of Col-0 plants expressing ATeam, in the form of As(V) or As(III), did not change the ATP response of the plants (Figure 2e). Similarly, *hac1-1* mutants had no major changes in the real-time response to As(V) or As(III) (Figure 2f). The ATP level in the steady-state in both genotypes in response to As in different forms was also similar to control (mock) plants (Figure 2g). Interestingly, at the 12h-time point from the start of the readings, the ATP status was similar in Col-0 plants, but higher in As(III) leaf discs compared to As(V) (Figure 2h). Nevertheless, in comparison to the control, $Mg\text{-}ATP^{2-}$ level remained unchanged under As(V) treatment (Figure 2h).

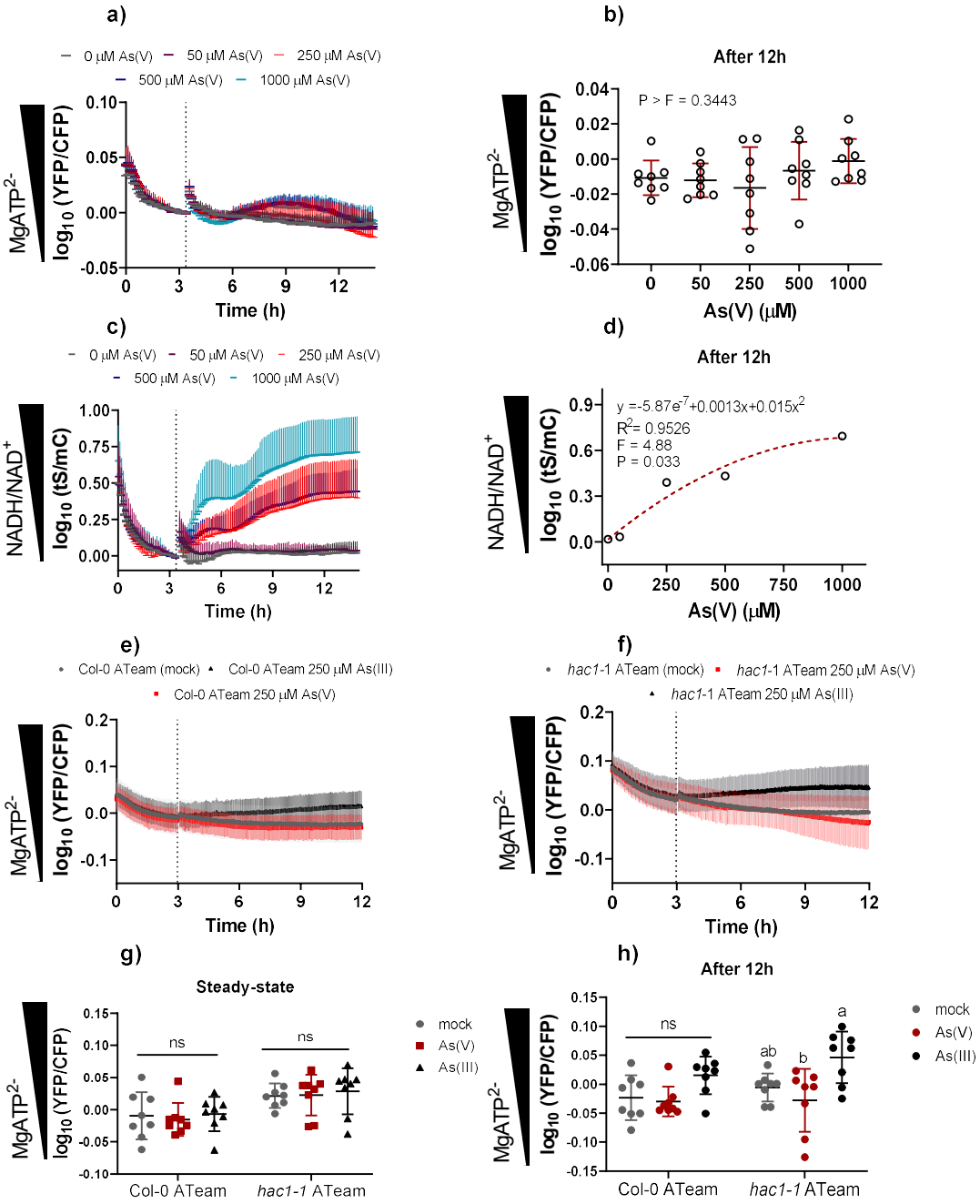

Figure 2. Exploring the status of ATP and NADH/NAD$^+$ ratio in arsenate concentration series along with the pollutant response in arsenate reductase deficient plants. Time series of five-week-old wild type Col-0 leaf discs expressing cytosolic ATeam1.03-nD/nA (**a**), and Peredox-mCherry (**c**) subjected to a range of sodium arsenate dibasic heptahydrate concentrations (0 - 1000 µM) for detection of MgATP^{2-} level and NADH/NAD$^+$ ratio. N = 6–8. Dashed line indicates application of As(V) after steady-state. Values are displayed as mean ± SD. In **b** and **d**, the values indicate the MgATP^{2-} level and NADH/NAD$^+$ ratio in the 12 h time-point from **a** and **c**. Time series of five-week-old wild type (**e**) or arsenate reductase deficient lines (*hac1-1*; **f**) in Col-0 background (leaf discs) expressing cytosolic ATeam1.03-nD/nA subjected of 250 µM sodium arsenate dibasic heptahydrate (AsV) or 250 µM sodium arsenite (AsIII). In **g** the values are from the steady-state (ten points before arsenic application), whereas in **h**, they are from the 12h time-point in **e** and **f**. All the fluorescence intensities were recorded from the plant

material in assay medium and the autofluorescence from corresponding WT controls without sensor were used for background subtraction. ATeam: Ex = 430 ± 10 nm/Em = 480 ± 10 and 530 ± 10 nm; Peredox-mCherry: Ex = 400 ± 5 and 540 ± 20 nm/Em = 520 ± 10 and 615 ± 18 nm. Different letters above the individual values in **g** and **h** indicate significant differences between mock, AsV, and AsIII, according to two-way ANOVA followed by Tukey's multiple comparisons test.

Investigation of glutathione redox potential in response to As(V)

The oxidation of E_{GSH} observed upon As(V) exposure (Figure 1e, f, g) was also further investigated with an As(V) titration assay (Figure 3). Interestingly, the response of E_{GSH} increase followed by stabilization overtime on a plateau was observed, independent of As(V) concentration (Figure 3a). On the other hand, sensor oxidation was proportional to As(V) concentration, up to 250 µM. From then on, there was saturation, with no increase in E_{GSH} with the increase in As(V) in the medium (Figure 3b, c).

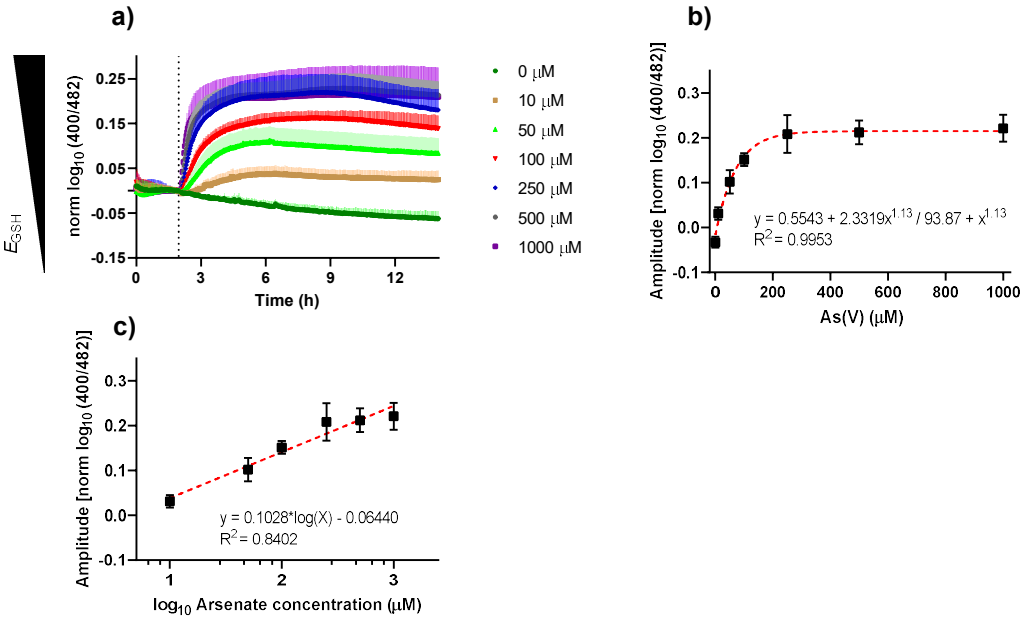

Figure 3. Arsenate concentration-dependent response of cytosolic glutathione redox status. Time series of five-week-old wild type Col-0 leaf discs expressing cytosolic Grx1-roGFP2 (**a**) subjected to a range of sodium arsenate dibasic heptahydrate concentrations (0-1000 µM; AsV) for detection of cytosolic glutathione redox status and maximum oxidation of the sensor upon AsV exposure in regular (**b**) and $\log_{10}$ (**c**) of AsV concentration. N = 6-8. Dashed line indicates application of As(V) after steady-state. Values are displayed as mean ± SD.

Over the last years, several genetic screens identified mutants with defects in GSH1 (At4g23100), the enzyme catalyzing the first step of glutathione biosynthesis, leading to the GSH depletion in the range of 20 and 40% [53]. These glutathione-biosynthesis along with glutathione reductase impaired mutants expressing Grx1-roGFP2 were included in the assays

and compared to Col-0 Grx1-roGFP2 lines to better understand the contribution of the depletion of the GSH pool and the changes in GSH/GSSG ratio in the increase of glutathione redox potential (Figure 4). In the steady-state, before As(V) treatment, all the mutant lines already have a higher E_{GSH} compared to Col-0 plants (Figure 4). Upon adding As(V) in the medium most of the mutant lines did not display additional increase of E_{GSH}, except for *rax1* line, which had similar values in the steady-state and showed an increase followed by stabilization similar to Col-0 plants after applying As(V) (Figure 4d).

To verify the fully oxidation and reduction of the probe and investigate whether As exposure or the mutations in glutathione metabolism also induce full oxidation, we performed H_2O_2 (oxidizing compound) and dithiothreitol (DTT-reducing compound) assays to have the complete range of detection (Figure 5a, b). Sensor oxidation with the application of 50 mM H_2O_2 was higher than that induced by As(V), even at higher concentrations (Figure 5a). Otherwise, the use of DTT caused the total reduction of the sensor in Col-0 plants and the *zir-1* and *gr1-1* mutant lines, while the total probe oxidation (50 mM H_2O_2) did not overcome the E_{GSH} initially presented in the mutant lines (Figure 5b). As expected, the BSO-incubated leaf discs displayed increased (more oxidized) glutathione redox potential compared to non-incubated ones, as a result of the inhibition of GSH biosynthesis (Figure 5c). Interestingly, there was no additional oxidation of E_{GSH} in leaf discs incubated with BSO and exposed to As(V) treatment (Figure 5c).

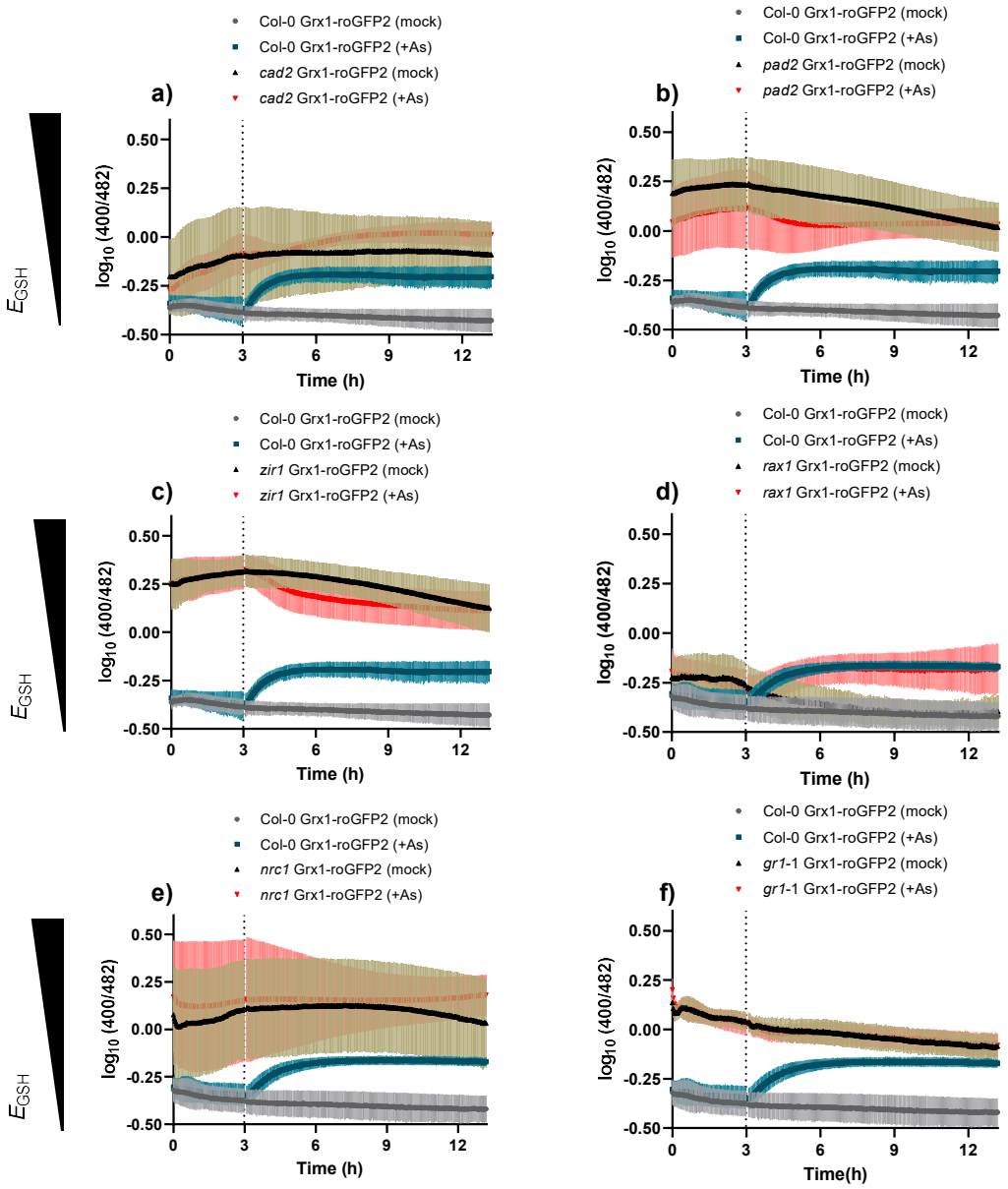

Figure 4. Arsenic-induced changes in glutathione redox status in mutant lines impaired in glutathione biosynthesis or glutathione reductase. Time series of leaf discs from five-week-old wild type, *cad-2* (**a**), *pad2* (**b**), *zir1* (**c**), *rax1* (**d**), *nrc1* (**e**), and *gr1-1* (**f**) lines in Col-0 background expressing cytosolic Grx1-roGFP2 and subjected to mock or 50 µM sodium arsenate dibasic heptahydrate for detection of glutathione redox status. N = 6–8. Dashed line indicates application of mock or As(V) after steady-state. Values are displayed as mean ± SD. All the fluorescence intensities were recorded from the plant material in assay medium and the autofluorescence from corresponding WT controls without sensor were used for background subtraction. Channel 400: excited at 400 ± 10 emission collected at 520 ± 10 nm; Channel 482: excited at 482 ± 10 emission collected at 520 ± 10 nm.

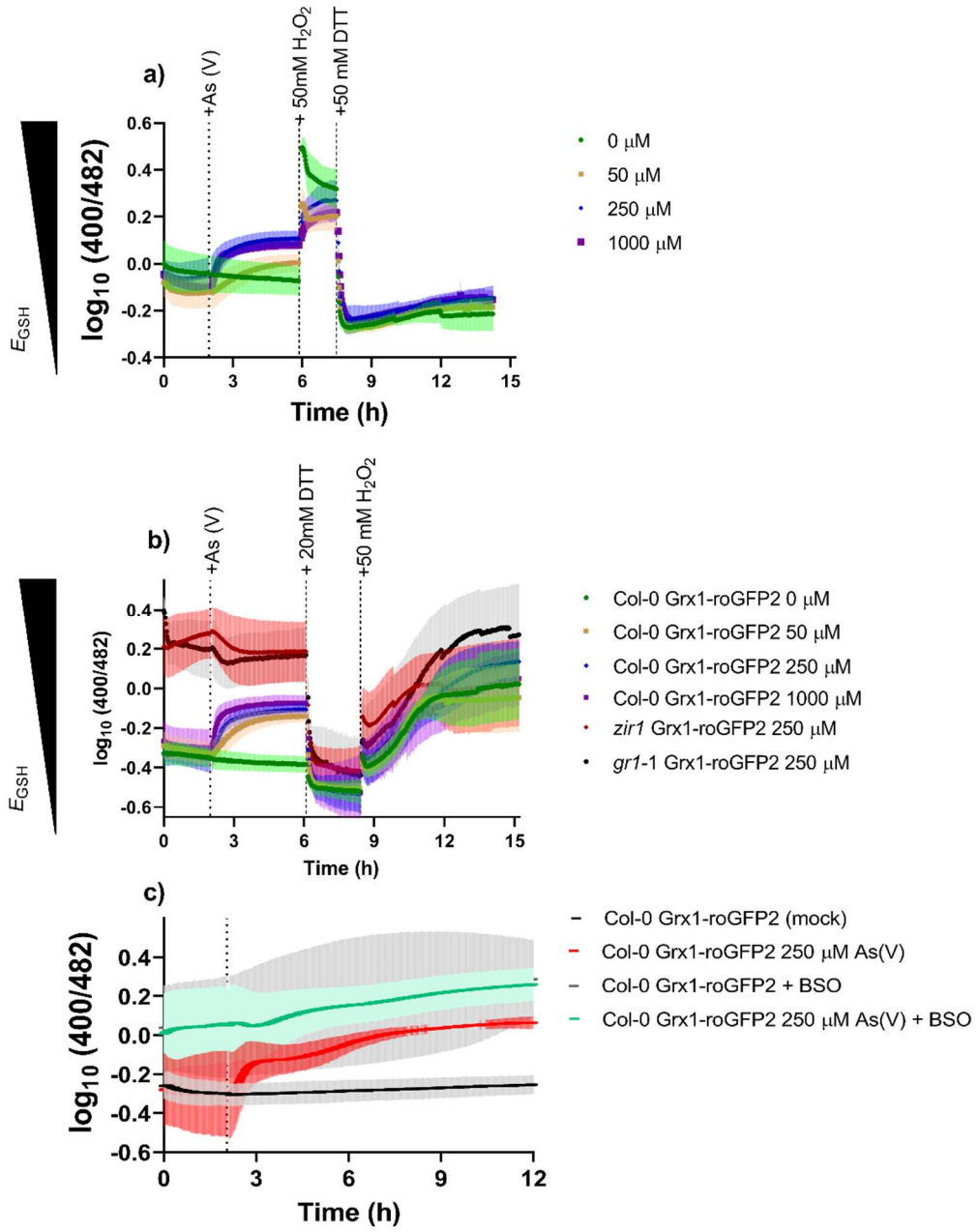

Figure 5. Monitoring maximum reduction and oxidation of E_{GSH} sensor along with the effect of glutathione depletion on the redox status. Time series of leaf discs from five-week-old wild type, *zir1* and *gr1*-1 in Col-0 background expressing cytosolic Grx1-roGFP2 and subjected to: (**a**) a range of sodium arsenate dibasic heptahydrate concentrations (0 - 1000 µM; AsV) added of 50 mM H_2O_2 and 50 mM DTT; (**b**) a range of sodium arsenate dibasic heptahydrate concentrations (0 - 1000 µM; AsV) added of 20 mM DTT and 50 mM H_2O_2; (**c**) mock or 250 µM sodium arsenate dibasic heptahydrate added of 1 mM L-Buthionine-sulfoximine (BSO – glutathione biosynthesis inhibitor). The BSO was incubated in the leaf discs 18 hours before the readings. N = 6–8. Dashed line indicates application of treatments (250 µM AsV in **c**). Values are displayed as mean ± SD. All the fluorescence intensities were recorded from the leaf discs in assay medium and the autofluorescence from corresponding WT controls without sensor were used for background subtraction. Channel 400: excited at 400 ± 10 emission collected at 520 ± 10 nm; Channel 482: excited at 482 ± 10 emission collected at 520 ± 10 nm.

Effects of depleted glutathione on As tolerance

To elucidate the role of glutathione on arsenic tolerance in plants, were transferred 5-day-old seedlings of WT and the glutathione-biosynthesis mutants *cad-2* and *zir1* to agar plates containing different concentrations of arsenate (AsV) and arsenite (AsIII) (Figure 6a). In preliminary experiments, the seedlings were exposed to the same concentrations for As(V) and As(III) – 0 to 500 μM. Nevertheless, As(III)-treated plants, including WT, displayed severe toxicity symptoms and died within five days. Therefore, the concentrations of As(III) were ten times lower than that used for As(V). Naturally, plants deficient in GSH biosynthesis have a lower growth phenotype compared to WT plants under control conditions (Figure 6a). Furthermore, the increase of arsenic in the medium induced decreases in the growth of the plants, in both forms, with a remarkable effect in GSH-mutant lines, even in the lower concentrations (Figure 6a - e). These plants with GSH depleted displayed chlorotic leaves (Figure 6a) as well as a complete impairment of root growth and fresh weight accumulation, at concentrations close to 50 μM As(V) and 5 μM As(III) (Figure 6b – e). By contrast, WT plants keep growing at concentrations of 250 μM As(V) and 10 μM As(III), although they had As-induced strong effects on fresh weight (Figure 6b, c) and root length (Figure 6d, e), compared to control plants.

The effects of As(V) and As(III) were also compared regarding the monitoring of glutathione redox potential (Figure 7). Interestingly, the overall effect was similar, with rapid increase of E_{GSH} followed by stabilization at a plateau (Figure 7a). Moreover, the maximum oxidation induced by the As forms at the same concentration was also close to each other (Figure 7b). Nevertheless, the oxidation rate, measured by the curve slope, in As(III)-treated leaf discs were strongly increased compared to As(V) in the same concentrations (Figure 7c). Interestingly, even in the lower concentration of As(III), the rate of oxidation was higher than in the higher concentration of As(V) (Figure 7c).

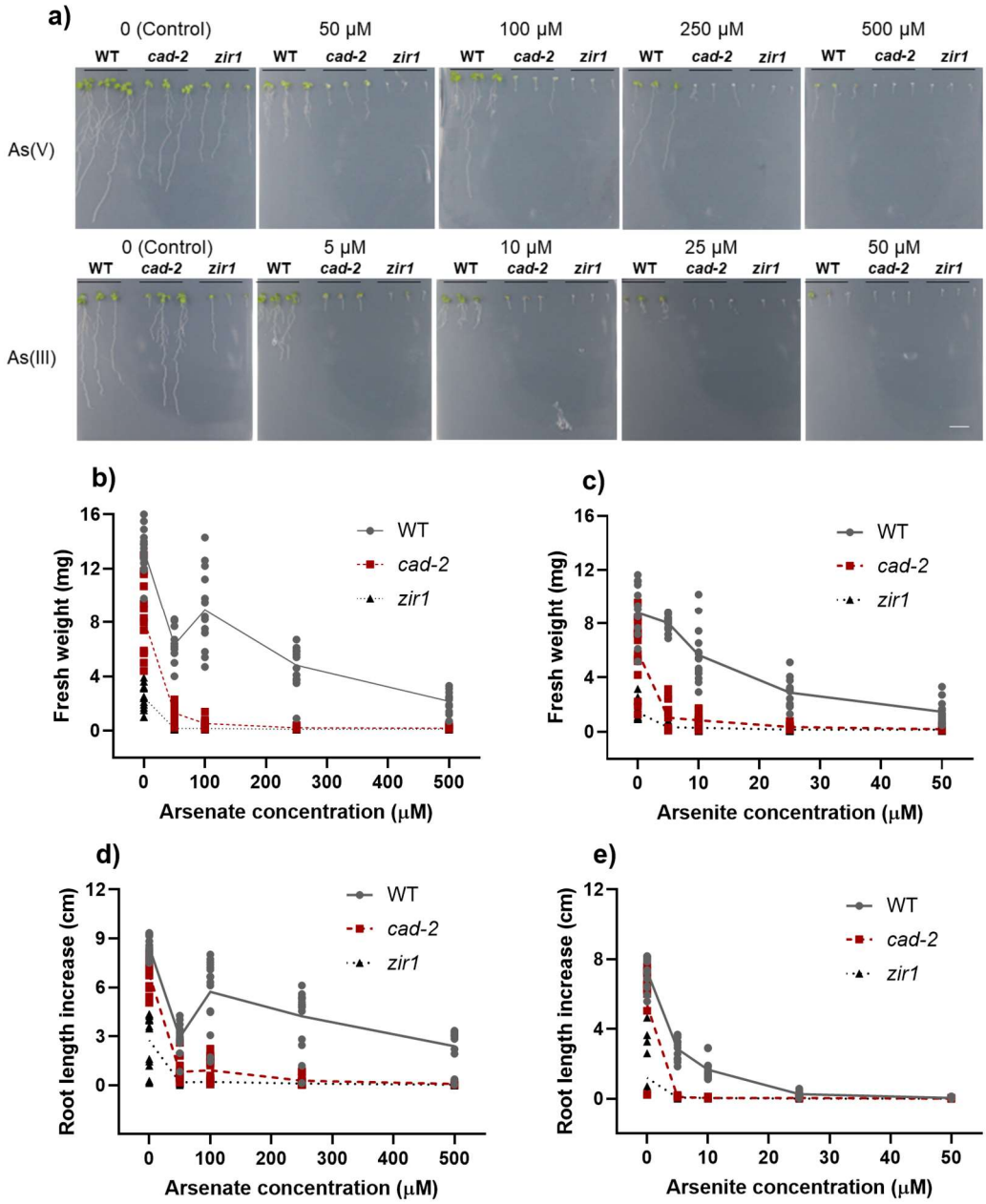

Figure 6. Impacts of depleted glutathione on plant tolerance to arsenic. (**a**) Growth of 15-day-old *Arabidopsis thaliana* wild type or mutant lines impaired in glutathione biosynthesis (*cad-2*, and *zir1*) growing for ten days in agar plates containing MS medium alone or supplied with 50; 100; 250; and 500 µM sodium arsenate dibasic heptahydrate (AsV) or 5; 10; 25; and 50 µM sodium arsenite (AsIII). Individual values (N = 15. 5 plates with 3 plants of each genotype) of fresh weight and root length of plants growing for ten days in agar plates containing MS medium alone or supplied with 50; 100; 250; and 500 µM sodium arsenate dibasic heptahydrate (AsV, **b, d**) or 5; 10; 25; and 50 µM sodium arsenite (AsIII, **c, e**).

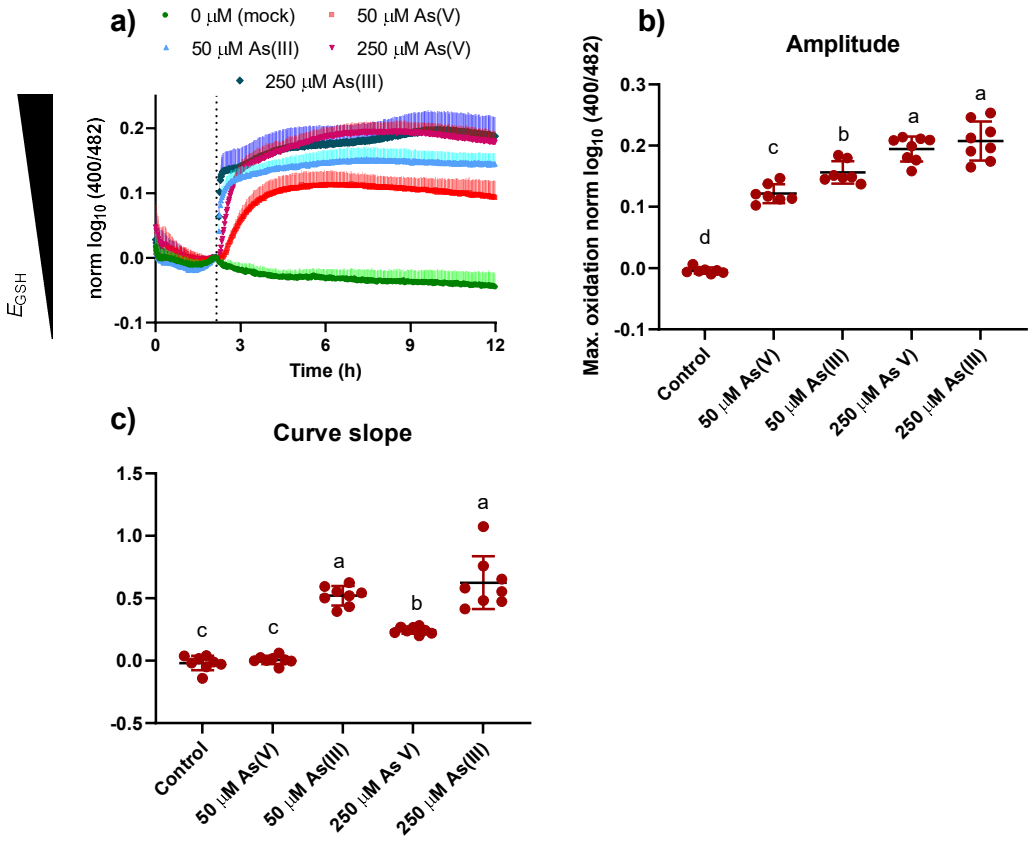

Figure 7. Comparative effect of arsenate and arsenite on glutathione redox status in Arabidopsis. (**a**) Time series of leaf discs from five-week-old wild type Col-0 expressing cytosolic Grx1-roGFP2 and subjected to mock or 50 µM and 250 µM sodium arsenate dibasic heptahydrate or sodium arsenite for detection of glutathione redox status. In **b** and **c**, the values were extracted from the maximum oxidation and curve slope of the first ten readings after applying the treatments, respectively. N = 6–8. Dashed line indicates application of mock or As(V) or As(III) after steady-state. Values are displayed as mean ± SD. All the fluorescence intensities were recorded from the plant material in assay medium and the autofluorescence from corresponding WT controls without sensor were used for background subtraction. Channel 400: excited at 400 ± 10 emission collected at 520 ± 10 nm; Channel 482: excited at 482 ± 10 emission collected at 520 ± 10 nm. Different letters above the individual values in **b** and **c** indicate significant differences between treatments, according to two-way ANOVA followed by Tukey's multiple comparisons test.

6.4. Discussion

Impairments induced by As(V) on energy metabolism are not originated from short-term ATP depletion

A well-established state-of-the-art claims that phosphorus and arsenic share critical chemical properties, including oxidative states, in which phosphate (HPO_4^{-2}) and phosphate analogues (arsenate, $HAsO_4^{-2}$) have highly similar pKa values in their most prevalent 5+(V) oxides [4]. Also due to the similarities, arsenate (AsV) mimics phosphate (Pi) to share

transporters, such as phosphate transporter 1 (PHT1) for uptake and Arabidopsis phosphate 1 (PHO1) for xylem loading and translocation [37]. As far as is known, relatively few enzymes utilize Pi (or AsV) directly as a substrate due to the irreversible nature of the majority of Pi-liberating processes [38]. Nevertheless, the primary Pi-requiring and susceptible of substitution by As(V)-reaction is the phosphorylation of ADP to ATP by the F_1F_o-type ATP synthases located in the inner membrane of mitochondria and the thylakoid membrane of plastids, both of which are essential for plant metabolism [39].

The knowledge established over decades is that mitochondrial ATP synthase uses AsV, with K_M and V_{max} values remarkably similar for Pi and AsV [39,40]. The by-product of this reaction, ADP-As, is a highly unstable AsV-ester which a rate of hydrolysis at least 10^5 greater than for the corresponding Pi-ester [40]. As a consequence of the instability of As-esters, enzymes that utilize free AsV to make AsV-esters are surrounded by ineffective reaction cycles [41]. For instance, the AsV and ADP produced in the autohydrolysis of ADP-AsV in mitochondrial and plastid ATP synthases can be utilized in the following reaction cycles. Such futile cycling is thought to decouple ATP synthesis from both photosynthetic and respiratory electron transport in chloroplast thylakoid membranes and the inner membrane of mitochondria, respectively. Therefore, these reactions have potentially severe consequences for the energy status of the cell as a result of the collapse of ATP synthesis [39,41].

Several studies confirm the AsV-induced effects on the depletion of ATP levels in different plant species [42–45]. However, most of these studies are performed on long-term As exposure and therefore the observed effects can be originated from side-effects of As on overall plant metabolism, as ROS overproduction triggers decreases in ATP contents. Thus, cytosolic genetically-encoded biosensors were used to monitor the effects of As on plant metabolism in real-time and *in vivo*.

Contrary to the AsV-replacing-Pi causing disruption of ATP synthesis dogma in plant metabolism, our results using a cytosolic ATeam sensor showed surprising stability of ATP status upon As(V) exposure, even in different plant materials or different concentrations (Figure 1a, b, c; 2a, b). Given the consistency of the aforementioned evidence of the toxic effect of AsV disrupting high-energy phosphate metabolism, we hypothesized that AsV would be efficiently reduced to As(III), thereby preventing further toxic effects. In this framework, the effects observed in the NADH/NAD+ ratio (Figure 2c, d) may be due to As(III)-induced impairments in the conversion of NADH to NADPH.

To include new insights into the investigation, mutant lines deficient in arsenate reductase *hac1-1* expressing cytosolic ATeam were generated and tested in plater reader assays (Figure 2 e, f). Even in the mutant lines, an astonishing absence of ATP-related responses to AsV (Figure 2e, f) indicates that possibly ATP synthases, have a higher affinity for Pi, maintaining the energetic status or that the AsV reduction pathway is largely redundant in plants, as thoroughly discussed by Salt et al. (2007) [46]. Further investigations are needed to elucidate AsV reduction pathways in plants, as well as compound-specific effects on phosphate metabolism, including site-specific effects.

Oxidation of E_{GSH} is likely to be related to depletion of GSH pool

According to the Nernst equation, glutathione redox potential (E_{GSH}) changes as a function of the ratio $[GSH]^2/[GSSG]$, although the usage of this parameter, which is typically based simply on the mediation of concentrations of the redox pair in the total cell extract, might lead to incorrect and ill-founded interpretations that are irrelevant in complicated biological systems [47]. However, fundamental drawbacks of invasive approaches can now be overcome by using roGFP-based genetically encoded biosensors to monitor real-time E_{GSH} *in vivo* and with subcellular resolution [24,48,49]. This approach is extremely relevant in the study of redox metabolism in plants and particularly in the response to xenobiotics and metallic elements such as Cd and As, since GSH plays a dual role in the compartmentalization of the pollutants as well as in ROS scavenging [50]. Therefore, cytosolic E_{GSH} is likely to be oxidized in plants under As stress [13]. The increase in the E_{GSH} may occur as a result of the incorporation of the tripeptide into phytochelatin molecules, which later complex AsIII and transport it to the vacuole, and/or by the oxidation of GSH to GSSG in the ascorbate-glutathione cycle or by arsenate reduction catalysis [50,51].

The increase in the redox potential of glutathione observed in the present study begins a few minutes after exposure to AsV, increasing rapidly until it reaches stabilization in a new steady-state, which remains constant during the following hours (Figure 1g, h, i). Similarly, an intense oxidative process occurred, which was monitored by the cytosolic H_2O_2 levels (Figure 1j, k, l), and this can trigger concomitant defense responses, such as the production of phytochelatins [52]. Interestingly, the E_{GSH} oxidation was found to be increased as As(V) increased in the medium, up to 250 µM, following the same pattern of rapid oxidation followed by stabilization over time (Figure 3).

These responses inspired our curiosity in attempting to decompose the effects of GSH pool depletion on phytochelatin synthesis and the changes in thiol/disulfide ratio caused by GSH oxidation to GSSG on redox potential. In the first approach, mutant lines with GSH depleted at different levels together with a glutathione reductase knockout line expressing the Grx1-roGFP2 probe were used (Figure 4). Interestingly, it was observed that all lines, except for *rax1*, which has a higher GSH content than the others [53], already had higher redox potential even before exposure to As (Figure 4). Intriguingly, there was no further E_{GSH} oxidation by adding As(V) in the mutant lines, including *gr1-1* (Figure 4f), indicating that the sensor could already be fully oxidized. To test this hypothesis, as well as to assess whether As stress itself caused complete sensor oxidation to E_{GSH}, the reversible sensor response to perfusion with H_2O_2 and DTT was investigated (Figure 5a, b).

Firstly, it was observed further increase of the E_{GSH} upon adding H_2O_2 after the stabilization of AsV-induced oxidation (Figure 5a), indicating that the observed plateau was not a methodological limitation, but a biological response. After that, we included the mutant lines *zir1* and *gr1-1* and verified that in those lines the maximum oxidation indeed corresponds to the levels observed in the steady-state (Figure 5b). Therefore, we tested leaf discs incubated in BSO, a potent inhibitor of γ-glutamyl-cysteine synthetase in glutathione biosynthesis, and again observed that no further oxidation of the sensor occurred after the addition of AsV (Figure 5c). These findings collectively indicate that the redox potential increase is subjected to control mechanisms, probably mediated by thiol switches regulation of phytochelatin synthase, maintaining basal glutathione levels for the accomplishment of other crucial metabolic functions in plants.

Role of glutathione on As tolerance: As(V) vs As(III) comparison

Plant growth impairment in GSH-deficient plants exposed to As highlighted GSH role for tolerance in a phenotype that is remarkably pronounced (Figure 6) but was overlooked in previous studies. Glutathione is an essential small peptide that plays a role in plant development including biosynthetic pathways, signaling, detoxification, redox homeostasis and antioxidant biochemistry [54] and cannot be replaced by other thiols or antioxidants. Interestingly, some mutant lines with depleted GSH content, which have impairments in the first step of the biosynthetic pathway - the GSH1 (γ-glutamylcysteine synthetase) protein, were discovered because of the susceptibility to Cd [25,28]. Several studies since then have demonstrated the

importance of GSH in various aspects of plant development, including stress tolerance [53,55–57].

Nevertheless, data on the phenotype of these lines under As stress, as presented in the current study, were still unexplored. We observed a strong phenotype of the mutant lines subjected to arsenic, including chlorosis and impaired growth at substantially lower concentrations for AsIII compared to AsV (Figure 6). To eliminate the bias of this outcome, we performed a competition assay with a series of Pi concentrations, as that the assay medium contained 625 μM of Pi [35], which could potentially compete for AsV uptake. It was verified that there was no influence on the concentrations tested (Supporting Information Figure S2), indicating that the observed phenotype was derived from the properties of the two inorganic forms and their metabolism in the plant.

The differential toxicity of the As chemical forms may come from the distinguished uptake mechanisms, in which the trivalent form (AsIII) is passively absorbed by plant membrane channels known as nodulin type 26 (NIP) [58], whereas the pentavalent forms (AsV) enter cells via PHT1-type membrane phosphate transporters [59]. For AsV uptake, it was related to an elegant mechanism through subcellular stimulus mediated by AsIII control AsV/Pi uptake depending upon the capacity of plants to detoxify AsV, minimizing plant accumulation and toxic effects [37,60]. Supporting this hypothesis, plants grown at the same concentrations of AsV and AsIII need a 4-fold increase in the pentavalent form to accumulate the same amount of total As in the tissues [18]. Our comparative assay demonstrated that As supplied as AsIII causes significantly faster oxidation of E_{GSH} compared to AsV (Figure 7a, c), also supporting the idea that differential toxicity arises from differences in the control of absorption and transport of the two forms.

6.5. Conclusion

Our results demonstrated that ATP content in the cytosol seems not to be depleted as a direct effect of short-term arsenate exposure even under decreased arsenate reduction. Furthermore, the depletion of the GSH pool, used to enable As(III) compartmentalization, is the most likely cause of E_{GSH} oxidation, although further investigation is needed to elucidate the redox control of phytochelatin synthesis and glutathione pool maintenance. We also confirm that the depletion of GSH pool abolishes arsenic tolerance in plants, and arsenite (AsIII) in lower concentrations is capable of inhibiting plant growth compared to arsenate (AsV), which seems to be related to the strict regulation of AsV transport.

Supporting information

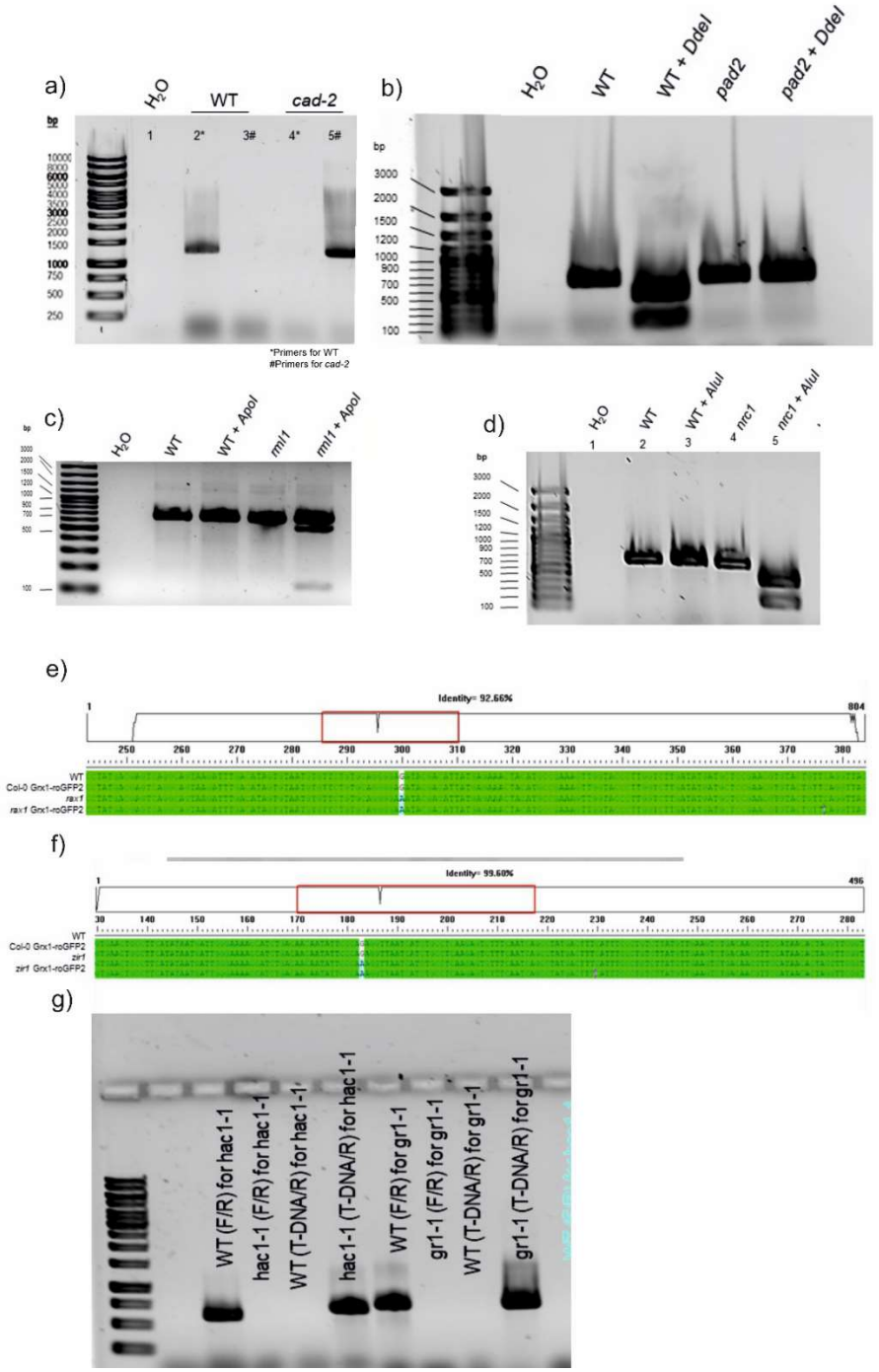

Figure S1. Genotyping of mutant lines used in the study. Gels of PCR followed by restriction enzymes for detection of *cad-2* (**a**), *pad2* (**b**), *rml1* (**c**), and *nrc1* (**d**) mutations along with the gene sequence of *rax1* (**e**) and *zir1* (**f**). Gel of PCR for detection of T-DNA insertion in *hac1*-1 and *gr1*-1 (**g**). All the lines were identified as homozygous, apart from *rml1*, which displayed a third band from heterozygous locus.

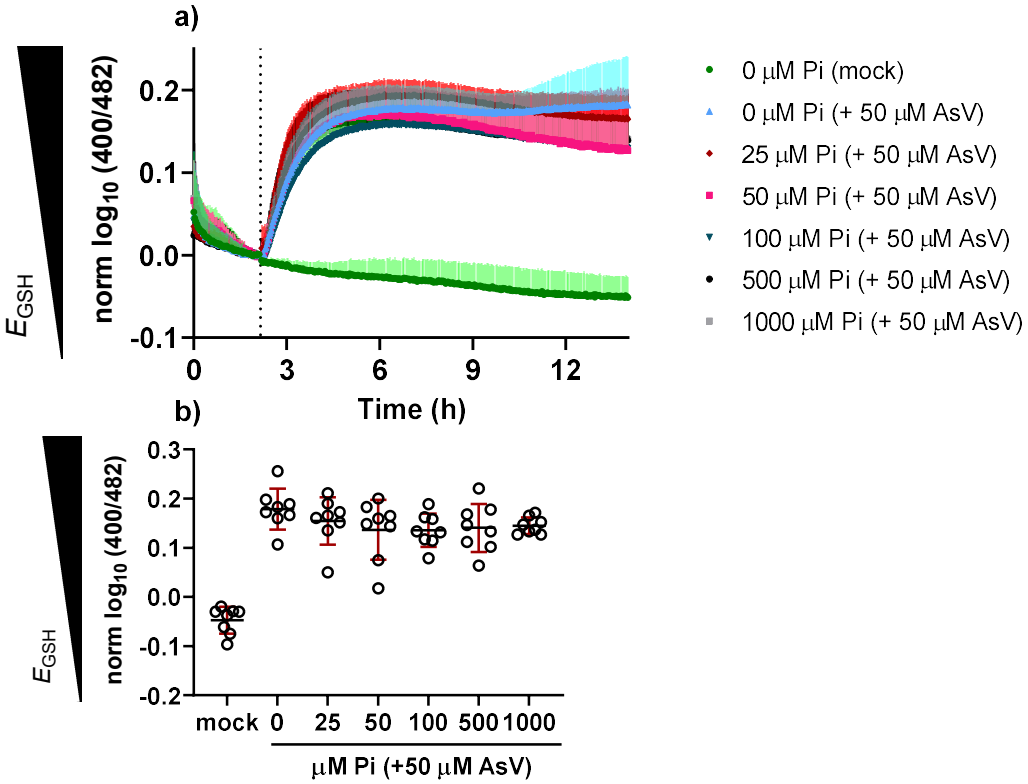

Figure S2. Phosphate/arsenate competition assay for the oxidation of E_{GSH}. (**a**) Time series of leaf discs from five-week-old wild type Col-0 expressing cytosolic Grx1-roGFP2 and subjected to mock or 50 µM sodium arsenate dibasic heptahydrate and a range of phosphate concentrations (0-1000 µM) for detection of glutathione redox status. In **b** the values were extracted from the maximum oxidation of the sensor (a) after applying the treatments. N = 8. Dashed line indicates application of mock or As(V) after steady-state. Values are displayed as mean ± SD. All the fluorescence intensities were recorded from the plant material in assay medium and the autofluorescence from corresponding WT controls without sensor were used for background subtraction. Channel 400: excited at 400 ± 10 emission collected at 520 ± 10 nm; Channel 482: excited at 482 ± 10 emission collected at 520 ± 10 nm.

References

[1] M.C. Teixeira, A.C. Santos, C.S. Fernandes, J.C. Ng, Arsenic contamination assessment in Brazil – Past, present and future concerns: A historical and critical review, Sci. Total Environ. 730 (2020) 138217. https://doi.org/10.1016/j.scitotenv.2020.138217.

[2] J. Bundschuh, M.A. Armienta, N. Morales-Simfors, M.A. Alam, D.L. López, V. Delgado Quezada, S. Dietrich, J. Schneider, J. Tapia, O. Sracek, E. Castillo, L.-M. Marco Parra, M. Altamirano Espinoza, L.R. Guimarães Guilherme, N.N. Sosa, N.K. Niazi, B. Tomaszewska, K. Lizama Allende, K. Bieger, D.L. Alonso, P.F.B. Brandão, P. Bhattacharya, M.I. Litter, A. Ahmad, Arsenic in Latin America: New findings on source, mobilization and mobility in human environments in 20 countries based on decadal research 2010-2020, Crit. Rev. Environ. Sci. Technol. 0 (2020) 1–139. https://doi.org/10.1080/10643389.2020.1770527.

[3] J.M. Abercrombie, M.D. Halfhill, P. Ranjan, M.R. Rao, A.M. Saxton, J.S. Yuan, C.N. Stewart, Transcriptional responses of Arabidopsis thaliana plants to As(V) stress, BMC Plant Biol. 8 (2008) 1–15. https://doi.org/10.1186/1471-2229-8-87.

[4] P.M. Finnegan, W. Chen, Arsenic toxicity: The effects on plant metabolism, Front. Physiol. 3 JUN (2012) 1–18. https://doi.org/10.3389/fphys.2012.00182.

[5] S.L. Winski, D.E. Carter, Arsenate toxicity in human erythrocytes: Characterization of morphologic changes and determination of the mechanism of damage, J. Toxicol. Environ. Heal. - Part A. 53 (1998) 345–355. https://doi.org/10.1080/009841098159213.

[6] G. Abbas, B. Murtaza, I. Bibi, M. Shahid, N.K. Niazi, M.I. Khan, M. Amjad, M. Hussain, Natasha, Arsenic uptake, toxicity, detoxification, and speciation in plants: Physiological, biochemical, and molecular aspects, Int. J. Environ. Res. Public Health. 15 (2018). https://doi.org/10.3390/ijerph15010059.

[7] E. Sánchez-Bermejo, G. Castrillo, B. Del Llano, C. Navarro, S. Zarco-Fernández, D.J. Martinez-Herrera, Y. Leo-Del Puerto, R. Muñoz, C. Cámara, J. Paz-Ares, C. Alonso-Blanco, A. Leyva, Natural variation in arsenate tolerance identifies an arsenate reductase in *Arabidopsis thaliana*, Nat. Commun. 5 (2014) 1–9. https://doi.org/10.1038/ncomms5617.

[8] D.Y. Chao, Y. Chen, J. Chen, S. Shi, Z. Chen, C. Wang, J.M. Danku, F.J. Zhao, D.E.

Salt, Genome-wide association mapping identifies a new arsenate reductase enzyme critical for limiting arsenic accumulation in plants, PLoS Biol. 12 (2014). https://doi.org/10.1371/journal.pbio.1002009.

[9] A. Navazas, S. Hendrix, A. Cuypers, A. González, Integrative response of arsenic uptake, speciation and detoxification by *Salix atrocinerea*, Sci. Total Environ. 689 (2019) 422–433. https://doi.org/10.1016/j.scitotenv.2019.06.279.

[10] F.V. Campos, J.A. Oliveira, A.A. Silva, C. Ribeiro, F.S. Farnese, Phytoremediation of arsenite-contaminated environments: is *Pistia stratiotes* L. a useful tool?, Ecol. Indic. 104 (2019) 794–801. https://doi.org/10.1016/j.ecolind.2019.04.048.

[11] S.S. Gill, N. Tuteja, Reactive oxygen species and antioxidant machinery in abiotic stress tolerance in crop plants, Plant Physiol. Biochem. 48 (2010) 909–930. https://doi.org/10.1016/j.plaphy.2010.08.016.

[12] S. Hayashi, M. Kuramata, T. Abe, H. Takagi, K. Ozawa, S. Ishikawa, Phytochelatin synthase OsPCS1 plays a crucial role in reducing arsenic levels in rice grains, Plant J. 91 (2017) 840–848. https://doi.org/10.1111/tpj.13612.

[13] V. Kumar, L. Vogelsang, T. Seidel, R. Schmidt, M. Weber, M. Reichelt, A. Meyer, S. Clemens, S.S. Sharma, K.J. Dietz, Interference between arsenic-induced toxicity and hypoxia, Plant Cell Environ. 42 (2019) 574–590. https://doi.org/10.1111/pce.13441.

[14] J. Deckers, S. Hendrix, E. Prinsen, J. Vangronsveld, A. Cuypers, Glutathione is required for the early alert response and subsequent acclimation in cadmium-exposed *Arabidopsis thaliana* plants, Antioxidants. 11 (2022). https://doi.org/10.3390/antiox11010006.

[15] F.S. Farnese, J.A. Oliveira, E.A.S. Paiva, P.E. Menezes-Silva, A.A. Silva, F.V. Campos, C. Ribeiro, The involvement of nitric oxide in integration of plant physiological and ultrastructural adjustments in response to arsenic, Front. Plant Sci. 8 (2017) 1–14. https://doi.org/10.3389/fpls.2017.00979.

[16] Y. Chen, C.-Y. Hua, M.-R. Jia, J.-W. Fu, X. Liu, Y.-H. Han, Y. Liu, B. Rathinasabapathi, Y. Cao, L.Q. Ma, Heterologous expression of *Pteris vittata* arsenite antiporter PvACR3;1 reduces arsenic accumulation in plant shoots, Environ. Sci. Technol. 51 (2017) 10387–10395. https://doi.org/10.1021/acs.est.7b03369.

[17] L.M.C. Forino, M. Ruffini Castiglione, G. Bartoli, M. Balestri, A. Andreucci, A.M.

Tagliasacchi, Arsenic-induced morphogenic response in roots of arsenic hyperaccumulator fern *Pteris vittata*, J. Hazard. Mater. 235–236 (2012) 271–278. https://doi.org/10.1016/j.jhazmat.2012.07.051.

[18] D.G. Coelho, C.S. Marinato, L.P. de Matos, H.M. de Andrade, V.M. da Silva, P.H. Santos-Neves, S.C. Araújo, J.A. Oliveira, Is arsenite more toxic than arsenate in plants?, Ecotoxicology. 29 (2020) 196–202. https://doi.org/10.1007/s10646-019-02152-9.

[19] N. Demircan, G. Cucun, B. Uzilday, Mitochondrial alternative oxidase (AOX1a) is required for the mitigation of arsenic-induced oxidative stress in *Arabidopsis thaliana*, Plant Biotechnol. Rep. 14 (2020) 235–245. https://doi.org/10.1007/s11816-020-00595-9.

[20] W. Chen, N.L. Taylor, Y. Chi, A.H. Millar, H. Lambers, P.M. Finnegan, The metabolic acclimation of *Arabidopsis thaliana* to arsenate is sensitized by the loss of mitochondrial LIPOAMIDE DEHYDROGENASE2, a key enzyme in oxidative metabolism, Plant, Cell Environ. 37 (2014) 684–695. https://doi.org/10.1111/pce.12187.

[21] M. Schwarzländer, T.P. Dick, A.J. Meyer, B. Morgan, Dissecting Redox Biology Using fluorescent protein sensors, Antioxid. Redox Signal. 24 (2016) 680–712. https://doi.org/10.1089/ars.2015.6266.

[22] A. Walia, R. Waadt, A.M. Jones, Genetically encoded biosensors in plants: Pathways to discovery, Annu. Rev. Plant Biol. 69 (2018) 497–524. https://doi.org/10.1146/annurev-arplant-042817-040104.

[23] T. Nietzel, M. Elsässer, C. Ruberti, J. Steinbeck, J.M. Ugalde, P. Fuchs, S. Wagner, L. Ostermann, A. Moseler, P. Lemke, M.D. Fricker, S.J. Müller-Schüssele, B.M. Moerschbacher, A. Costa, A.J. Meyer, M. Schwarzländer, The fluorescent protein sensor roGFP2-Orp1 monitors *in vivo* H_2O_2 and thiol redox integration and elucidates intracellular H_2O_2 dynamics during elicitor-induced oxidative burst in Arabidopsis, New Phytol. 221 (2019) 1649–1664. https://doi.org/10.1111/nph.15550.

[24] S. Wagner, J. Steinbeck, P. Fuchs, S. Lichtenauer, M. Elsässer, J.H.M. Schippers, T. Nietzel, C. Ruberti, O. Van Aken, A.J. Meyer, J.T. Van Dongen, R.R. Schmidt, M. Schwarzländer, Multiparametric real-time sensing of cytosolic physiology links hypoxia responses to mitochondrial electron transport, New Phytol. 224 (2019) 1668–1684. https://doi.org/10.1111/nph.16093.

[25] R. Howden, C.R. Andersen, P.B. Goldsbrough, C.S. Cobbett, A cadmium-sensitive, glutathione-deficient mutant of *Arabidopsis thaliana*, Plant Physiol. 107 (1995) 1067–1073. https://doi.org/10.1104/pp.107.4.1067.

[26] J. Glazebrook, F.M. Ausubel, Isolation of phytoalexin-deficient mutants of *Arabidopsis thaliana* and characterization of their interactions with bacterial pathogens, Proc. Natl. Acad. Sci. U. S. A. 91 (1994) 8955–8959. https://doi.org/10.1073/pnas.91.19.8955.

[27] J.C. Cheng, K.A. Seeley, Z.R. Sung, RML1 and RML2, Arabidopsis genes required for cell proliferation at the root tip, Plant Physiol. 107 (1995) 365–376. https://doi.org/10.1104/pp.107.2.365.

[28] T.O. Jobe, D.-Y. Sung, G. Akmakjian, A. Pham, E.A. Komives, D.G. Mendoza-Cózatl, J.I. Schroeder, Feedback inhibition by thiols outranks glutathione depletion: a luciferase-based screen reveals glutathione-deficient γ-ECS and glutathione synthetase mutants impaired in cadmium-induced sulfate assimilation, Plant J. 70 (2012) 783–795. https://doi.org/10.1111/j.1365-313X.2012.04924.x.

[29] L. Ball, G.P. Accotto, U. Bechtold, G. Creissen, D. Funck, A. Jimenez, B. Kular, N. Leyland, J. Mejia-Carranza, H. Reynolds, S. Karpinski, P.M. Mullineaux, Evidence for a direct link between glutathione biosynthesis and stress defense gene expression in Arabidopsis, Plant Cell. 16 (2004) 2448–2462. https://doi.org/10.1105/tpc.104.022608.

[30] V. Shanmugam, M. Tsednee, K.C. Yeh, Zinc tolerance induced by iron 1 reveals the importance of glutathione in the cross-homeostasis between zinc and iron in *Arabidopsis thaliana*, Plant J. 69 (2012) 1006–1017. https://doi.org/10.1111/j.1365-313X.2011.04850.x.

[31] L. Marty, W. Siala, M. Schwarzländer, M.D. Fricker, M. Wirtz, L.J. Sweetlove, Y. Meyer, A.J. Meyer, J.P. Reichheld, R. Hell, The NADPH-dependent thioredoxin system constitutes a functional backup for cytosolic glutathione reductase in Arabidopsis, Proc. Natl. Acad. Sci. U. S. A. 106 (2009) 9109–9114. https://doi.org/10.1073/pnas.0900206106.

[32] V. De Col, P. Fuchs, T. Nietzel, M. Elsässer, C.P. Voon, A. Candeo, I. Seeliger, M.D. Fricker, C. Grefen, I.M. Møller, A. Bassi, B.L. Lim, M. Zancani, A.J. Meyer, A. Costa, S. Wagner, M. Schwarzländer, ATP sensing in living plant cells reveals tissue gradients and stress dynamics of energy physiology, Elife. 6 (2017) 1–29.

https://doi.org/10.7554/eLife.26770.

[33] T. Nietzel, M. Elsässer, C. Ruberti, J. Steinbeck, J.M. Ugalde, P. Fuchs, S. Wagner, L. Ostermann, A. Moseler, P. Lemke, M.D. Fricker, S.J. Müller-Schüssele, B.M. Moerschbacher, A. Costa, A.J. Meyer, M. Schwarzländer, The fluorescent protein sensor roGFP2-Orp1 monitors *in vivo* H_2O_2 and thiol redox integration and elucidates intracellular H_2O_2 dynamics during elicitor-induced oxidative burst in Arabidopsis, New Phytol. 221 (2019) 1649–1664. https://doi.org/10.1111/nph.15550.

[34] S.J. Clough, A.F. Bent, Floral dip: a simplified method forAgrobacterium-mediated transformation of *Arabidopsis thaliana*, Plant J. 16 (1998) 735–743. https://doi.org/10.1046/j.1365-313x.1998.00343.x.

[35] T. Murashige, F. Skoog, A revised medium for rapid growth and bioassays with tobacco tissue cultures, Physiol. Plant. 15 (1962) 473–497. https://doi.org/10.1021/jf9040386.

[36] C. Wang, G.N. Na, E.S. Bermejo, Y. Chen, J.A. Banks, D.E. Salt, F.J. Zhao, Dissecting the components controlling root-to-shoot arsenic translocation in *Arabidopsis thaliana*, New Phytol. 217 (2018) 206–218. https://doi.org/10.1111/nph.14761.

[37] C. Navarro, C. Mateo-Elizalde, T.C. Mohan, E. Sánchez-Bermejo, O. Urrutia, M.N. Fernández-Muñiz, J.M. García-Mina, R. Muñoz, J. Paz-Ares, G. Castrillo, A. Leyva, Arsenite provides a selective signal that coordinates arsenate uptake and detoxification through the regulation of PHR1 stability in Arabidopsis, Mol. Plant. 14 (2021) 1489–1507. https://doi.org/10.1016/j.molp.2021.05.020.

[38] D.S. Tawfik, R.E. Viola, Arsenate replacing phosphate: Alternative life chemistries and ion promiscuity, Biochemistry. 50 (2011) 1128–1134. https://doi.org/10.1021/bi200002a.

[39] M.J. Gresser, ADP-arsenate. Formation by submitochondrial particles under phosphorylating conditions., J. Biol. Chem. 256 (1981) 5981–5983. https://doi.org/10.1016/s0021-9258(19)69115-5.

[40] S.A. Moore, D.M. Moennich, M.J. Gresser, Synthesis and hydrolysis of ADP-arsenate by beef heart submitochondrial particles., J. Biol. Chem. 258 (1983) 6266–6271. https://doi.org/10.1016/s0021-9258(18)32402-5.

[41] H.F. Ter Welle, E.C. Slater, Uncoupling of respiratory-chain phosphorylation by

arsenate, BBA - Bioenerg. 143 (1967) 1–17. https://doi.org/10.1016/0005-2728(67)90104-1.

[42] S. Srivastava, J.J. Akkarakaran, P. Suprasanna, S.F. D'Souza, Response of adenine and pyridine metabolism during germination and early seedling growth under arsenic stress in *Brassica juncea*, Acta Physiol. Plant. 35 (2013) 1081–1091. https://doi.org/10.1007/s11738-012-1146-0.

[43] P. Fonseca-Pereira, R. Neri-Silva, J.H.F. Cavalcanti, D.S. Brito, A.P.M. Weber, W.L. Araújo, A. Nunes-Nesi, Data-Mining bioinformatics: Connecting adenylate transport and metabolic responses to stress, Trends Plant Sci. 23 (2018) 961–974. https://doi.org/10.1016/j.tplants.2018.09.002.

[44] T. Shukla, S. Kumar, R. Khare, R.D. Tripathi, P.K. Trivedi, Natural variations in expression of regulatory and detoxification related genes under limiting phosphate and arsenate stress in *Arabidopsis thaliana*, Front. Plant Sci. 6 (2015) 1–13. https://doi.org/10.3389/fpls.2015.00898.

[45] S. Srivastava, P. Suprasanna, S.F. D'Souza, Redox state and energetic equilibrium determine the magnitude of stress in *Hydrilla verticillata* upon exposure to arsenate, Protoplasma. 248 (2011) 805–815. https://doi.org/10.1007/s00709-010-0256-z.

[46] D.E. Salt, Would the real arsenate reductase please stand up?, New Phytol. 215 (2017) 926–928. https://doi.org/10.1111/nph.14691.

[47] L. Flohé, The fairytale of the GSSG/GSH redox potential, Biochim. Biophys. Acta - Gen. Subj. 1830 (2013) 3139–3142. https://doi.org/10.1016/j.bbagen.2012.10.020.

[48] M. Schwarzländer, M.D. Fricker, C. Müller, L. Marty, T. Brach, J. Novak, L.J. Sweetlove, R. Hell, A.J. Meyer, Confocal imaging of glutathione redox potential in living plant cells, J. Microsc. 231 (2008) 299–316. https://doi.org/10.1111/j.1365-2818.2008.02030.x.

[49] M. Schwarzländer, T.P. Dick, A.J. Meyer, B. Morgan, Dissecting redox biology using fluorescent protein sensors, Antioxid. Redox Signal. 24 (2016) 680–712. https://doi.org/10.1089/ars.2015.6266.

[50] S.K. Yadav, Heavy metals toxicity in plants: An overview on the role of glutathione and phytochelatins in heavy metal stress tolerance of plants, South African J. Bot. 76 (2010)

167–179. https://doi.org/10.1016/j.sajb.2009.10.007.

[51] J.F. Briat, Arsenic tolerance in plants: "*Pas de deux*" between phytochelatin synthesis and ABCC vacuolar transporters, Proc. Natl. Acad. Sci. U. S. A. 107 (2010) 20853–20854. https://doi.org/10.1073/pnas.1016286107.

[52] A. González, D. Laporte, A. Moenne, Cadmium accumulation involves synthesis of glutathione and phytochelatins, and activation of CDPK, CaMK, CBLPK, and MAPK signaling pathways in *Ulva compressa*, Front. Plant Sci. 12 (2021) 1–14. https://doi.org/10.3389/fpls.2021.669096.

[53] S.A.K. Bangash, S.J. Müller-Schüssele, D. Solbach, M. Jansen, F. Fiorani, M. Schwarzländer, S. Kopriva, A.J. Meyer, Low-glutathione mutants are impaired in growth but do not show an increased sensitivity to moderate water deficit, PLoS One. 14 (2019) 1–19. https://doi.org/10.1371/journal.pone.0220589.

[54] G. Noctor, A. Mhamdi, S. Chaouch, Y. Han, J. Neukermans, B. Marquez-Garcia, G. Queval, C.H. Foyer, Glutathione in plants: An integrated overview, Plant, Cell Environ. 35 (2012) 454–484. https://doi.org/10.1111/j.1365-3040.2011.02400.x.

[55] T. Bashandy, J. Guilleminot, T. Vernoux, D. Caparros-Ruiz, K. Ljung, Y. Meyer, J.P. Reichheld, Interplay between the NADP-linked thioredoxin and glutathione systems in Arabidopsis auxin signaling, Plant Cell. 22 (2010) 376–391. https://doi.org/10.1105/tpc.109.071225.

[56] Y. Han, A. Mhamdi, S. Chaouch, G. Noctor, Regulation of basal and oxidative stress-triggered jasmonic acid-related gene expression by glutathione, Plant, Cell Environ. 36 (2013) 1135–1146. https://doi.org/10.1111/pce.12048.

[57] E. García-Quirós, J.D.D. Alché, B. Karpinska, C.H. Foyer, Glutathione redox state plays a key role in flower development and pollen vigour, J. Exp. Bot. 71 (2020) 730–741. https://doi.org/10.1093/jxb/erz376.

[58] Y. Chen, S.K. Sun, Z. Tang, G. Liu, K.L. Moore, F.J.M. Maathuis, A.J. Miller, S.P. McGrath, F.J. Zhao, The Nodulin 26-like intrinsic membrane protein OsNIP3;2 is involved in arsenite uptake by lateral roots in rice, J. Exp. Bot. 68 (2017) 3007–3016. https://doi.org/10.1093/jxb/erx165.

[59] S.F. Ditusa, E.B. Fontenot, R.W. Wallace, M.A. Silvers, T.N. Steele, A.H. Elnagar, K.M.

Dearman, A.P. Smith, A member of the Phosphate transporter 1 (PHT1) family from the arsenic-hyperaccumulating fern *Pteris vittata* is a high-affinity arsenate transporter, New Phytol. 209 (2016) 762–772. https://doi.org/10.1111/nph.13472.

[60] N. Kandhol, V.P. Singh, L. Herrera-Estrella, L.S.P. Tran, D.K. Tripathi, Arsenite: the umpire of arsenate perception and responses in plants, Trends Plant Sci. 27 (2022) 420–422. https://doi.org/10.1016/j.tplants.2022.02.005.

7. CONCLUDING REMARKS

The pollution by metallic elements is one of the major problems affecting natural ecosystems, human health and crop productivity. The results presented here demonstrate that an environmental disaster involving the rupture of iron ore tailings dam impacts the concentration of mineral elements in soil, as well as the accumulation and changes in nutritional homeostasis in plants.

Furthermore, our experimental data support the qualification of water lettuce as an alternative to phytoremediate aquatic habitats with Fe and Mn contamination. Also, in the combinations of these two elements or with As, the plants displayed additive toxicity symptoms without loosening bioaccumulation capacity or strong effects on metabolism. Altogether, the plants showed strong bioaccumulation and tolerance mechanisms, which maintained pollutants mostly in the apoplastic portion and worked in tandem with an effective antioxidant system and photosynthetic apparatus.

Finally, the *in vivo* monitoring of As-induced responses in *Arabidopsis thaliana* brought to light the discussion about the direct impacts of AsV on phosphate metabolism because there was no energy crisis due to ATP depletion in response to the pollutant, contradicting a widely accepted concept in the metabolism of living organisms in response to the pollutant. The investigation of the As effects also demonstrated that the depletion of the GSH pool via the production of phytochelatin appears to be the main component of the oxidation of the glutathione redox potential (E_{GSH}). The data also suggested a regulatory control of phytochelatin synthesis which could be crucial for maintaining redox homeostasis by stabilizing E_{GSH} in a new steady state.

Taken together, the results discussed here highlight the significance of continuing to monitor metal-contaminated areas, provide new information for the phytoremediation of aquatic ecosystems, and offer new information on how plants cope with toxic concentration of metallic elements.

REFERENCES

ARIF, N. *et al.* Influence of high and low levels of plant-beneficial heavy metal ions on plant growth and development. *Frontiers in Environmental Science*, v. 4, n. NOV, 2016.

BOECHAT, C. L. *et al. Transgenic plants and rhizosphere-associated microbiota in phytoremediation of heavy metals and organic pollutants*. [S.l.]: Elsevier B.V., 2021.

BREWER, G. J. Risks of copper and iron toxicity during aging in humans. *Chemical Research in Toxicology*, v. 23, n. 2, p. 319–326, 2010.

BRIFFA, J.; SINAGRA, E.; BLUNDELL, R. Heavy metal pollution in the environment and their toxicological effects on humans. *Heliyon*, v. 6, n. 9, p. e04691, 2020.

BUDINGER, D. *et al.* The role of manganese dysregulation in neurological disease: emerging evidence. *The Lancet Neurology*, v. 20, n. 11, p. 956–968, 2021.

COELHO, D. G. *et al.* Evaluation of metals in soil and tissues of economic-interest plants grown in sites affected by the Fundão dam failure in Mariana, Brazil. *Integrated Environmental Assessment and Management*, v. 16, n. 5, p. 596–607, 6 set. 2020.

FAY, R. M.; MUMTAZ, M. M. Development of a priority list of chemical mixtures occurring at 1188 hazardous waste sites, using the HazDat database. *Food and Chemical Toxicology*, v. 34, n. 11–12, p. 1163–1165, 1996.

GAUTAM, P. K. *et al.* Heavy metals in the environment: Fate, transport, toxicity and remediation technologies. *Heavy Metals: Sources, Toxicity and Remediation Techniques*. [S.l: s.n.], 2016. p. 101–130.

GUERRA, M. B. B. *et al.* Post-catastrophe analysis of the fundão tailings dam failure in the doce river system, Southeast Brazil: Potentially Toxic Elements in Affected Soils. *Water, Air, and Soil Pollution*, v. 228, n. 7, 2017.

KHALID, S. *et al.* A comparison of technologies for remediation of heavy metal contaminated soils. *Journal of Geochemical Exploration*, v. 182, p. 247–268, 2017.

LI, C. *et al.* A review on heavy metals contamination in soil: Effects, sources, and remediation techniques. *Soil and Sediment Contamination*, v. 28, n. 4, p. 380–394, 2019.

MUSZYŃSKA, E.; LABUDDA, M. Dual role of metallic trace elements in stress biology—from negative to beneficial impact on plants. *International Journal of Molecular Sciences*, v. 20, n. 13, 2019.

NABI, A. *et al.* A comprehensive review of adaptations in plants under arsenic toxicity: Physiological, metabolic and molecular interventions. *Environmental Pollution*, v. 290, n. August, p. 118029, 2021.

QUADRA, G. R. *et al.* Far-reaching cytogenotoxic effects of mine waste from the Fundão dam disaster in Brazil. *Chemosphere*, v. 215, p. 753–757, 2019.

QUARESMA, V. S. *et al.* The impact of trace metals in marine sediments after a tailing dam failure: the Fundão dam case (Brazil). *Environmental Earth Sciences*, v. 80, n. 17, 2021.

RAMAKRISHNAN, B. *et al.* Mixtures of environmental pollutants: Effects on microorganisms and their activities in soils. *Reviews of Environmental Contamination and Toxicology*. [S.l: s.n.], 2011. v. 211. p. 63–120.

ROELS, H. A. *et al.* Manganese exposure and cognitive deficits: A growing concern for manganese neurotoxicity. *NeuroToxicology*, v. 33, n. 4, p. 872–880, 2012.

SABIR, M. *et al.* Phytoremediation: Mechanisms and adaptations. *Soil Remediation and Plants: Prospects and Challenges*. [S.l.]: Elsevier Inc., 2015. p. 85–105.

SEGURA, F. R. *et al.* Potential risks of the residue from Samarco's mine dam burst (Bento Rodrigues, Brazil). *Environmental Pollution*, v. 218, p. 813–825, 2016.

VERGILIO, C. DOS S. *et al.* Metal concentrations and biological effects from one of the largest mining disasters in the world (Brumadinho, Minas Gerais, Brazil). *Scientific Reports*, v. 10, n. 1, p. 1–12, 2020.